



In the name of God

CRANFIELD UNIVERSITY

COLLEGE OF AERONAUTICS

PhD Thesis

F. Saghafi

**DEVELOPMENT OF A SIMULATION TOOL FOR FLIGHT
DYNAMICS AND CONTROL INVESTIGATIONS OF
ARTICULATED VTOL UNMANNED AIRCRAFT**

Supervisor: P. G. Thomasson

June 1996

**This thesis is submitted in partial fulfilment of the requirements for the
degree of Doctor of Philosophy**



To my mother

ABSTRACT

A simulation tool for flight dynamics and control investigations of three different Vertical Take Off and Landing (VTOL) unmanned aircraft configurations has been developed. A control concept has been proposed in order to take advantage of the fast response characteristics of the ordinary small engine/propeller propulsion systems in such aircraft, as well as replacing the complex rotors used previously in VTOL concepts for small unmanned aircraft. The simulation model has been established on the basis of the proposed concept so that it can also be used to study the feasibility of this idea. An Object-based methodology has been introduced so as to reduce the amount of aerodynamic required data for the simulation model. The equations of motion associated with the aircraft multibody system with ten degrees of freedom have been derived using the Newton-Euler method. The modelling of various subsystems including the propeller model, the airframe aerodynamics and the engine model has been carried out. A method for calculating the propellers' slipstream effects on the other components has been presented. Input data for the simulation model have been estimated, using different sources. The Advanced Continuous Simulation Language (ACSL) has been used for the programming of the mathematical model. A series of comprehensive tests have been carried out in order to demonstrate the validity of the simulation model. The ability of the simulation model to explain the aircraft modes of motion as well as to discover unknown nonlinear behaviours and to describe them has been demonstrated.

ACKNOWLEDGEMENTS

I would like to express my gratitude to the Ministry of Culture and Higher Education of the I. R. of Iran, for providing financial support during the course of this research program.

I am grateful to my supervisor Mr. Peter Thomasson for his supervision and invaluable advice. His rich knowledge of the subject has always provided confidence for the next step of the work. His comments and suggestions are therefore very much appreciated.

Finally, I would like to thank my family, father, mother, brothers (Faramarz and Farshad) and my sister (Faranak) for their love and constant support throughout my academic study. I owe a special debt to my mother who has always been wholeheartedly supportive. I thank God for providing another opportunity for me to express my gratitude by dedicating this thesis to her.

PREFACE

This thesis is submitted for the degree of Doctor of Philosophy at Cranfield University. Some of the work described in this thesis has been presented at conferences or being refereed by a journal. The supporting papers are as follows

1. Saghafi, F., Thomasson, P. G., *Development of A Mathematical Model for an Articulated Unmanned Aircraft*, 11th RPVs International Conference, Bristol, 12-14 Sept. 1994
2. Saghafi, F., Thomasson, P. G., *An Object-based Simulation of an Articulated Unmanned Aircraft*, 6th European Simulation Symposium, Istanbul 1994
3. Saghafi, F., Thomasson, P. G., *UFOs-Unmanned Flying Objects*, Aerogram, College of Aeronautics, Cranfield University, Vol. 8, No. 1, May 1995
4. Saghafi, F., Thomasson, P. G., *A Simulation Tool for Initial Design Project of Unmanned Converti-plane*, Submitted for publication in the Aeronautical Journal of Royal Aeronautical society.

TABLE OF CONTENTS

CHAPTER ONE

INTRODUCTION	1
1.1 BACKGROUND	1
1.2 THE PROPOSED CONTROL CONCEPT	2
1.3 REQUIREMENT FOR A SIMULATION TOOL	6
1.4 OBJECTIVES AND THESIS OUTLINE	8

CHAPTER TWO

RELEVANT CONCEPT OF FLIGHT SIMULATION	11
2.1 INTRODUCTION	11
2.2 MATHEMATICAL MODELLING AND SIMULATION	11
2.2.1 Basics	11
2.2.2 Mathematical Modelling Versus Stability and Control Analysis	13
2.3 MAIN ELEMENTS OF THE MODEL	13
2.4 EQUATIONS OF MOTION	14
2.4.1 The General Equations	14
2.4.2 Small Perturbation Equations	14
2.4.3 Aircraft Orientation	15
2.4.4 Axes and Frames of Reference	16
2.4.5 Axes Transformation	17
2.4.6 The Aerodynamic Angles	18
2.5 DATA PRESENTATION	18
2.6 THE STATE-SPACE FORMULATION	19
2.7 NUMERICAL SOLUTION OF THE STATE EQUATIONS	21
2.7.1 Stability, Accuracy and Stiff Systems	23

2.7.2 Choice of Integration Algorithm	24
2.8 STEADY-STATE TRIMMED FLIGHT	25
2.9 LINEARISATION	26
2.10 VERIFICATION AND VALIDATION	28
2.10.1 Internal Verification Criteria	29
2.10.2 External Validation Criteria	29
CHAPTER THREE	
GENERAL METHODOLOGY	31
3.1 INTRODUCTION	31
3.2 PROBLEM DEFINITION AND METHOD OF APPROACH	31
3.3 THE OBJECT-BASED MODELLING	34
3.4 SIMULATION MODEL	41
3.4.1 Main Objects	41
3.4.2 Secondary Objects	43
3.5 ASSESSMENT	46
CHAPTER FOUR	
EQUATIONS OF MOTION	50
4.1 INTRODUCTION	50
4.2 FORMULATION METHOD	50
4.3 VECTOR FORMULATION	52
4.4 NOTATION AND CONVENTIONS	52
4.5 DERIVATION OF THE AIRCRAFT	
EQUATIONS OF MOTION	56
4.5.1 Assumptions	56
4.5.2 Reference Frames	56
4.5.3 Equations of Motion of the Body A	58
4.5.4 Equations of motion of the Body ${}^k n p$	59
4.5.5 Equation of Motion of the Body ${}^k p$	61
4.5.6 Equations of Motion of the Aircraft Multibody System	62

4.6 AIRCRAFT ATTITUDE	67
4.7 AIRCRAFT POSITION	68
4.8 ASSEMBLING THE STATE EQUATIONS	69

CHAPTER FIVE

BUILDING THE AIRCRAFT MODEL	70
5.1 INTRODUCTION	70
5.2 MODELS OF SUBSYSTEMS	70
5.2.1 Propeller Model	70
5.2.2 Propeller Slipstream Effect	80
5.2.3 Airframe Aerodynamics	84
5.2.4 Engine Model	95
5.2.4 Servomotor Model	97
5.3 GRAVITATIONAL FORCES AND MOMENTS	97
5.4 MASS MOMENT OF INERTIA MODELLING	99

CHAPTER SIX

DATA PREPARATION	102
6.1 INTRODUCTION	102
6.2 BASELINE CONFIGURATION	102
6.3 AIRCRAFT DIMENSIONS	103
6.4 PROPELLER CHARACTERISTICS	106
6.5 ENGINE CHARACTERISTICS	108
6.6 AIRFOIL CHARACTERISTICS	110
6.7 STREAMLINE BODY CHARACTERISTICS	115
6.8 MASS ESTIMATION	120
6.9 MOMENT OF INERTIA ESTIMATION	125

CHAPTER SEVEN**COMPUTER PROGRAMMING 130****7.1 INTRODUCTION 130****7.2 SUPPORT LANGUAGES FOR MODEL SIMULATION 130**

7.2.1 General Purpose Languages 131

7.2.2 Languages Inadequate Facilities 131

7.2.3 Simulation Languages 132

7.3 ADVANCED CONTINUOUS SIMULATION LANGUAGE - ACSL 133

7.3.1 Choice of ACSL 134

7.3.2 ACSL Explicit Structure 134

7.3.3 ACSL Inconveniences 135

7.4 PROGRAM DEVELOPMENT 138

7.4.1 Simulation Program 140

7.4.2 Programming Style 141

7.4.3 Program Hierarchical Structure 143

7.5 PROGRAM TESTING 147

7.5.1 The Testing Process 147

7.5.2 Testing Strategies 148

7.5.3 Test Techniques 151

7.5.4 Component Testing 151

7.5.5 Integration Testing 152

7.5.6 User Testing 168

CHAPTER EIGHT**SIMULATION RESULTS 170****8.1 INTRODUCTION 170****8.2 RESULT PRODUCING STRATEGY 171****8.3 FINAL CONSIDERATIONS 173****8.4 WING-SUPPORTED FLIGHT 174****8.5 PROPELLER-SUPPORTED FLIGHT 185**

8.5.1 Tail-sitter Configuration 185

8.5.2 Tilt-nacelle Configuration 192

8.5.3 Tilt-wing Configuration 198

CHAPTER NINE
CONCLUSIONS AND FURTHER WORKS 209

9.1 CONCLUSIONS 209
9.2 FURTHER WORKS 209

REFERENCES 217
BIBLIOGRAPHY 224

APPENDIX A1 228
APPENDIX A2 231
APPENDIX A3 235
APPENDIX A4 236

APPENDIX B1 254
APPENDIX B2 260
APPENDIX B3 263

APPENDIX C 265

LIST OF FIGURES

Chapter one

Fig.(1.1): Rotor-tilt and Nacelle-tilt control concepts	4
Fig.(1.2): Tilt-nacelle configuration	5
Fig.(1.3): Tilt-wing configuration	5
Fig.(1.4): Tail-sitter configuration	7
Fig.(1.5): Aircraft controls	7

Chapter two

Fig.(2.1): The simulation space and the definition of models	22
Fig. (2.2): State-space models and associated software	22

Chapter three

Fig.(3.1): The structure of the object-based approach	35
Fig.(3.2): The main objects	36
Fig.(3.3): The secondary objects	36
Fig.(3.4): Definition of BOXes and UNITs	38
Fig.(3.5): The elements and sub-elements for model construction	40
Fig.(3.6): A typical airfoil	45
Fig.(3.7): A typical streamline body	45
Fig.(3.8): A typical propeller	47
Fig.(3.9): The engine model	47

Chapter four

Fig.(4.1): Aircraft multibody system	57
--	----

Chapter five

Fig. (5.1): The propeller pitch angle	73
Fig. (5.2): The propeller force and moment components	73
Fig. (5.3): Plane coordinate rotation of $X_m Y_m Z_m$ relative to $X_n Y_n Z_n$	73
Fig. (5.4): The flow model for momentum theory analysis of the propeller	79
Fig. (5.5): Vortex-ring state in vertical descent	79
Fig. (5.6): The model of the propeller slipstream effect on a typical component	81

Fig. (5.7): Inaccuracy in the calculated deflection angle	88
Fig. (5.8): Airfoil dimensions	88
Fig. (5.9): A typical lift coefficient vs angle of attack curve for an airfoil	88
Fig. (5.10): A typical drag vs angle of attack curve for an airfoil	90
Fig. (5.11): An airfoil in local flow	90
Fig. (5.12): Streamline body dimensions	96
Fig. (5.13): An streamline body in local flow	96
Fig. (5.14): A typical engine power vs rpm	96
 Chapter six	
Fig.(6.1): Three view drawing of Pointer.....	104
Fig.(6.2): C_T vs ADR for two-blade 5869-9 propeller with Clark Y section	107
Fig.(6.3): C_p vs ADR for two-blade 5869-9 propeller with C_T plotted as parameter	107
Fig.(6.4): Aerodynamic characteristic of NACA 0012 airfoil section	112
Fig.(6.5): Approximated C_L vs δ_r curve at an angle of attack α	116
Fig.(6.6): $C_{af_{Lb}}$ vs α_{af}	116
Fig.(6.7): Dimensionless coefficient of lift and pitching moment for a pair of streamline bodies, differing in fineness ratio	117
Fig.(6.8): a) C_{sb_L} vs δ_{sb} b) C_{sb_D} vs δ_{sb} c) $C_{sb_{M1}}$ vs δ_{sb}	118
Fig.(6.9): $C_{D_{wn}}$ vs Rel for a rotational symmetric streamline body	119
Fig.(6.10): Drag coefficient of a circular cylinder in a flow normal to its axis	121
Fig.(6.11): The rectangular plate used to estimate the mass moment of inertia of an airfoil	128
Fig(6.12): The circular cylinder used to estimate the mass moment of inertia of streamline body	128
Fig.(6.13): The straight bar used to estimate the mass moment of inertia of the propeller	128
 Chapter seven	
Fig.(7.1): ACSL explicit structure	136
Fig.(7.2): Simulation program procedure	136
Fig.(7.3): The data flow diagram of the simulation model	139
Fig.(7.4): The VTOLUMA simulation program hierarchical structure	144

Fig.(7.5):	Testing process, strategies and techniques	150
Fig.(7.6):	Incremental testing	150
Fig.(7.7):	Vehicle projectile like dynamics, Test 1	154
Fig.(7.8):	Vehicle projectile like dynamics, Test 2	155
Fig.(7.9):	Vehicle projectile like dynamics, Test 3	155
Fig.(7.10):	Vehicle projectile like dynamics, Test 4	156
Fig.(7.11):	Vehicle projectile like dynamics, Test 5	156
Fig.(7.12):	Vehicle projectile like dynamics, Test 6	158
Fig.(7.13):	Vehicle projectile like dynamics, Test 7	158
Fig.(7.14):	Vehicle projectile like dynamics, Test 8	159
Fig.(7.15):	Vehicle projectile like dynamics, Test 9	161
Fig.(7.16):	Vehicle projectile like dynamics, Test 10	162
Fig.(7.17):	Vehicle projectile like dynamics, Test 11.....	164
Fig.(7.18):	Vehicle projectile like dynamics, Test 12	165
Fig.(7.19):	Vehicle projectile like dynamics, Test 13	166
Fig.(7.20):	Vehicle projectile like dynamics, Test 14	167

Chapter eight

Fig.(8.1):	Different flight conditions of the VTOL aircraft	172
Fig.(8.2):	Simulated aircraft in trimmed wing-supported flight - Short period	177
Fig.(8.3):	Simulated aircraft in trimmed wing-supported flight - Long period	177
Fig.(8.4):	Excited Short-period mode	179
Fig.(8.5):	Excited Phugoid mode	179
Fig.(8.6):	Linearised system matrices for wing-supported trimmed flight	180
Fig.(8.7):	Gain matrix and closed-loop eigenvalues of controlled aircraft in wing-supported flight	184
Fig.(8.8):	Simulation of the controlled aircraft in wing-supported flight	186
Fig.(8.9):	Aircraft response to an altitude change command	186
Fig.(8.10):	Propeller-supported, Tail-sitter, simulation in trimmed condition	189
Fig.(8.11):	Uncontrolled pitching motion of a vertically-rising model in hovering flight	190
Fig.(8.12):	Linearised system matrices for propeller-supported trimmed flight, Tail-sitter configuration	191
Fig.(8.13):	Propeller-supported, Tail-sitter, controlled aircraft without δ_h	193
Fig.(8.14):	Propeller-supported, Tail-sitter, controlled aircraft with δ_h	194

Fig.(8.15): Aircraft response to a position change command	195
Fig.(8.16): Propeller-supported, Tail-sitter, aircraft trajectory	196
Fig.(8.17): Propeller-supported, Tilt-nacelle, simulation in trimmed condition	199
Fig.(8.18): The linearised system matrices for propeller-supported trimmed flight, Tilt-nacelle configuration	200
Fig.(8.19): Propeller-supported, Tilt-nacelle, controlled aircraft	202
Fig.(8.20): Propeller-supported, Tilt-nacelle, aircraft trajectory	204
Fig.(8.21): Propeller-supported, Tilt-wing, simulation in trimmed condition	205
Fig.(8.22): Propeller-supported, Tilt-wing, controlled aircraft	206
Fig.(8.23): Propeller-supported, Tilt-wing, aircraft trajectory	207

Chapter nine

Fig(9.1): Daedalus STF-9A demonstrator	214
Fig.(9.2): Slaved tandem freewing take off and landing sequence	214
Fig.(9.3): Freewing Scorpion Tilt-body UAV	215
Fig.(9.4): Alternative Tilt-body deck landing sequence	215
Fig.(9.5): Bell Eagle-Eye tilt-rotor UAV	216

Appendix B1

Fig. (B1.1): Definition of all the axes systems and position vectors	255
Fig. (B2.2): Incidence angles	255

Appendix C

Fig.(C.1): The VTOLUMA simulation program hierarchical structure	265
--	-----

LIST OF TABLES

Chapter six

Table(6.1): The propeller thrust coefficient	109
Table(6.2): The propeller power coefficient	109
Table(6.3): The original engine data	111
Table(6.4): The recalculated engine data	111
Table(6.5): Tabulated aerodynamic characteristics of NACA 0012 airfoil section...	113
Table(6.6): Vertical stabiliser lift coefficient of the Bell model 301 Tilt-rotor research aircraft	114
Table(6.7): C_{afLs} vs α_{af}	122
Table(6.8): C_{sbL} and C_{sbM1} vs γ_{sb}	122
Table(6.9): C_{sbL} vs R_{ed}	122
Table(6.10) C_{Dwet} vs R_{el}	122

Chapter eight

Table(8.1): The wing-supported flight longitudinal modes	184
Table(8.2): The wing-supported flight lateral-directional modes	184
Table(8.3): Propeller-supported, Tail-sitter, aircraft modes	201
Table(8.4): Propeller-supported, Tilt-wing, open-loop modes	201
Table (8.5): Propeller-supported, Tilt-wing, open-loop and closed-loop eigenvalues	205

NOTATIONS

<i>A</i>	: Main body
<i>AIM</i>	: Pack of information including boxes <i>A, I, M</i>
<i>AIMT</i>	: Pack of information including boxes <i>A, I, M, T</i>
<i>A</i>	: Aerodynamics characteristics box
<i>AR</i>	: Aspect ratio
<i>ADR</i>	: Advance ratio
<i>ATAN2</i>	: FORTRAN four-quadrant tangent function
<i>AC</i>	: Aerodynamic center
<i>A_b</i>	: Total aerodynamic force on the fuselage-empennage assembly
<i>A_f</i>	: Fuselage aerodynamic force vector
<i>A_h</i>	: Horizontal stabiliser aerodynamic force vector
<i>A_v</i>	: Vertical stabiliser aerodynamic force vector
<i>A_w</i>	: Wing aerodynamic force vector
<i>A_n</i>	: Nacelle aerodynamic force vector
<i>A_a</i>	: Total aerodynamic force on the body <i>A</i>
<i>A_p</i>	: Propeller aerodynamic force
<i>A_{np}</i>	: Total aerodynamic force on the body <i>np</i>
<i>b</i>	: The position vector of the center of gravity of the body <i>A</i> w.r.t. <i>O</i>
<i>conf1</i>	: Configuration code 1
<i>conf2</i>	: Configuration code 2
<i>C1...C36</i>	: Non-acceleration terms defined in Appendices A1 to A4
<i>C_T</i>	: Propeller thrust coefficient
<i>C_P</i>	: Propeller power coefficient
<i>CHORD</i>	: Wing chord
<i>C_{afL0}</i>	: Airfoil, dimensionless coefficient of lift
<i>C_{afD0}</i>	: Airfoil, dimensionless coefficient of drag
<i>C_{afM0}</i>	: Airfoil, dimensionless coefficient of pitching moment

$C_{af_{DP}}$: Airfoil, dimensionless coefficient of parasite drag
C_{af_x}	: Airfoil, dimensionless coefficient of X-force
C_{af_y}	: Airfoil, dimensionless coefficient of Y-force
C_{af_m}	: Airfoil, dimensionless coefficient of pitching moment, body axes
$C_{af_{Lb}}$: Airfoil, control surface contribution in lift
$C_{af_{Db}}$: Airfoil, control surface contribution in drag
C_{sb_L}	: Streamlinebody, dimensionless coefficient of lift
C_{sb_D}	: Streamlinebody, dimensionless coefficient of drag
$C_{sb_{M1}}$: Streamlinebody, dimensionless coefficient of pitching moment
C_{sb_x}	: Streamlinebody, dimensionless coefficient of X-force, body axes
C_{sb_y}	: Streamlinebody, dimensionless coefficient of Y-force, body axes
C_{sb_z}	: Streamlinebody, dimensionless coefficient of Z-force, body axes
$C_{D_{wet}}$: Drag coefficient based on wetted area
$C_{sb_{D1}}$: Dimensionless drag coefficient of a circular cylinder in a flow normal to its axis
$C_{L_{max}}$: Maximum lift coefficient
d	: The position vector of the joint w.r.t. the origin O
D	: Propeller diameter
DIAMETER	: Streamline body diameter
e	: The position vector of the center of gravity of the body np w.r.t. joint
f	: The position vector of the center of gravity of the body p w.r.t joint
f	: Force vector
F_a	: Total resultant force on the body A
F_{np}	: Total resultant force on the body np
F_{J_1}	: Reaction force at the joint J_2
GraAcc	: Gravitational acceleration
ga	: The center of gravity of the body A

gp	: The center of gravity of the body p
gnp	: The center of gravity of the body np
gb	: The center of gravity of the fuselage-empennage assembly
h	: Position vector described in figure B1.1
H_f	: Propeller in plane H-force
H_a	: Total angular momentum of the body A
H_{np}	: Total angular momentum of the body np
H_n	: Total angular momentum of the body n
H_p	: Total angular momentum of the body p
$[I_a]$: Mass moment of inertia matrix of the body A
$[I_{np}]$: Mass moment of inertia matrix of the body np
$[I_n]$: Mass moment of inertia matrix of the body <i>nacelle</i>
$[I_p]$: Mass moment of inertia matrix of the body p
$[I_b]$: Mass moment of inertia matrix of the fuselage-empennage
$[I_f]$: Mass moment of inertia matrix of the fuselage
$[I_h]$: Mass moment of inertia matrix of the horizontal stabiliser
$[I_v]$: Mass moment of inertia matrix of the vertical stabiliser
$[I_w]$: Mass moment of inertia matrix of the wing
I	: Inertia characteristics box
J_1	: Interaction point between bodies p and n
J_2	: Interaction point between bodies n and A
$k1$: The position vector of the center of gravity of the body n w.r.t. <i>joint</i>
$k2$: Position vector described in figure B1.1
$Ksscon1$: Slipstream contraction code 1
$Ksscon2$: Slipstream contraction code 2
Kss	: Slipstream influence code
Kar	: A constant value in the coefficient of induced drag

K_{servo}	: Torque constant
$LENGTH$: Streamline body length
L	: Position vector
LS	: Position vector w.r.t. the propeller disk center
$L1$: Position vector described in figure B1.1
$L2$: Position vector described in figure B1.1
M.O.	: Main object
M	: Mass characteristics box
$MODEL$: Model of a main object
M_s	: Output torque of servomotor
M_E	: Output torque of engine
M_y	: Propeller pitch moment
M_z	: Propeller yaw moment
m_a	: Mass of the body A
m_n	: Mass of the <i>nacelle</i>
m_p	: Mass of the body p
m_{np}	: Mass of the body np
m_w	: Wing mass
m_f	: Fuselage mass
m_h	: Horizontal stabiliser mass
m_{vu}	: Upper vertical stabiliser mass
m_{vl}	: Lower vertical stabiliser mass
m_{tot}	: Total mass
M_a	: Total resultant moment on the body A
M_{np}	: Total resultant moment on the body np
M_p	: Total resultant moment on the body p
M_s	: Output torque of the servomotor
M_E	: Output torque of the engine
M_T	: Moment of the T force
M_{w_a}	: Moment of the weight of the body A

M_{A_a}	: Total aerodynamic moment on the body A
$M_{W_{np}}$: Moment of the weight of the body np
$M_{A_{np}}$: Total aerodynamic moment on the body np
M_{A_p}	: Aerodynamic moment on the body p
M_{J_2}	: Reaction moment at the joint J_2
M_{J_1}	: Reaction moment at the joint J_1
M_{pc}	: Total moment arising from propeller rotation
M_{A_b}	: Total aerodynamic moment of the fuselage-empennage assembly
M_f	: Fuselage aerodynamic moment
M_{A_h}	: Horizontal stabiliser aerodynamic moment
M_{A_v}	: Vertical stabiliser aerodynamic moment
M_{A_w}	: Wing aerodynamic moment
M_{A_n}	: Nacelle aerodynamic moment
M_{W_p}	: Moment of the weight of the body p
np	: n & p assembly
n	: Tilting body
N	: Propeller rotational speed
OAC	: Object aerodynamic coefficients Unit
$OLAC$: Object local airflow characteristics Unit
OI	: Object inertia Unit
OM	: Object mass Unit
OTC	: Object thrust coefficients Unit
$OSPO$: Object size, position and orientation
OJR	: Object joint-reactions
OK	: Object kinematics
o	: The position vector of the fuselage-empennage assembly w.r.t. O
P_E	: Engine power
PH	: Pressure head
pc	: Propeller disk center

P_{prop}	: Propeller power
P	: Roll rate
p	: Propeller
P_a	: Total linear momentum of the body A
P_{np}	: Total linear momentum of the body np
P_n	: Total linear momentum of the body n
P_p	: Total linear momentum of the body p
P	: $(North, East, Down)^T$, Position vector
Q	: Pitch rate
q	: $(e_0, e_1, e_2, e_3)^T$, Quaternion vector
Re_d	: Reynolds number based on diameter
Re_l	: Reynolds number based on length
rpm	: Propeller rotational speed (revolution per minute)
R	: Yaw rate
$RBEOM$: Rigid body equation of motion
$RPMrdc$: Propeller rotational direction code
S.O.	: Secondary objects
S	: Reference area
$SPAN$: Airfoil span
T	: Thrust characteristics box
T	: Total force arising from propeller rotation
$Thrust$: Propeller thrust
$Torque$: Propeller torque
$THICKNESS$: Propeller blade thickness
U	: Forward velocity
V	: Slipstream velocity
V_i	: Induced velocity at the propeller disk

V_h	: Propeller induced velocity in hover
V_s	: Absolute velocity vector of the propeller slipstream
V_{AC}	: Local velocity vector at aerodynamic center
V_{pc}	: Velocity of the propeller disk center
V_o	: Absolute velocity of the point O
V_{J_1}	: Absolute velocity of the point J_1
V_{J_2}	* : Absolute velocity of the point J_2
V_{ga}	: Absolute velocity of the point ga
V_{gn}	: Absolute velocity of the point gn
V_{gp}	: Absolute velocity of the point gp
W	: Heave velocity
W_i	: Propeller velocity in far wake
W_{ind}	: Induced velocity vector
W_a	: Weight of the body A
W_{np}	: Weight of the body np
$X_m Y_m Z_m$: Local wind axes system for propeller
$X_a Y_a Z_a$: The axes system fixed to the body A (Body axes system)
$X_n Y_n Z_n$: The axes system fixed to the body n
$X_i Y_i Z_i$: Inertial axes system
Y_f	: Propeller in plane Y-force
Ω_{ai}	: Absolute angular velocity of the $X_a Y_a Z_a$ axes system
Ω_{ni}	: Absolute angular velocity of the $X_n Y_n Z_n$ axes system
Ω_{na}	: Relative angular velocity of the $X_n Y_n Z_n$ axes system w.r.t. $X_a Y_a Z_a$ axes system
Ω_{pn}	: Relative angular velocity of the body p w.r.t. $X_n Y_n Z_n$ axes system
$[\mu]$: Mass matrix

$[DCM]^j$: Direction Cosine Matrix j to i
θ_n	: Tilt angle
θ_s	: Slipstream deflection angle
θ_c	: Propeller collective pitch
θ_{nd}	: Servomotor input current
θ	: Pitch angle
ψ	: Yaw angle
ϕ	: Roll angle
ρ	: Air density
ρ_{cm}	: Mass density of a typical composite material
ζ	: State vector
ν	: Viscosity factor
α	: Angle of attack
β	: Sideslip angle
γ	: Angle of attack defined in local wind axes for bodies
σ	: Rotation angle
δ	: Control surface deflection angle
δ_t	: Throttle setting
ψ_m	: Rotation angle between $X_n Y_n Z_n$ and $X_m Y_m Z_m$ axes systems
λ_{wa}	: Wing incidence angle
λ_{ha}	: Horizontal stabiliser incidence angle
λ_{nw}	: The angle between each nacelle and its associated wing

Superscripts

On the top right hand side of the symbol indicates the axes system in which the variable is defined.

On the left hand side of the symbol indicates the side of the aircraft with which the variable is associated. It may take r or l indicating right and left side of the aircraft.

r	: right side
l	: left side
κ	: Dummy index (right, left)

v	: Dummy index (different components of the aircraft)
$\frac{d}{dt}$: Time derivative w.r.t. inertial frame
\cdot	: Time derivative w.r.t. $X_a Y_a Z_a$ axes system
\circ	: Time derivative w.r.t. $X_n Y_n Z_n$ axes system
$'$: Time derivative
a	: $X_a Y_a Z_a$ axes system
n	: $X_n Y_n Z_n$ axes system
m	: $X_m Y_m Z_m$ axes system
v	: $X_v Y_v Z_v$ axes system
h	: $X_h Y_h Z_h$ axes system
w	: $X_w Y_w Z_w$ axes system

Subscripts

On the bottom right hand side of the symbol denotes the name of the symbol

On the bottom left hand side of the symbol is reserved to indicate the reference point of the moment of a force or moment of inertia.

M	: Main object
S	: Secondary object
s	: Propeller slipstream
nr	: Right tilting part
nl	: Left tilting part
pr	: Right propeller
pl	: Left propeller
n	: Tilting part, body n
p	: Propeller, body p
b	: Fuselage-empennage assembly
fu	: Fuselage
hr	: Right horizontal stabiliser
hl	: Left horizontal stabiliser
vu	: Upper vertical stabiliser
vl	: Lower vertical stabiliser
wr	: Right wing

<i>wl</i>	: Left wing
<i>tot</i>	: Vector size
<i>x,y,z</i>	: Vector components
<i>xx,xy,xz</i>	: Matrix components
	: Dummy index (different components)
<i>af</i>	: Airfoil
<i>sb</i>	: Streamline body

CHAPTER ONE

INTRODUCTION

1.1 BACKGROUND

Pilotless aircraft is one of the most challenging areas in aeronautical science. These aircraft are called by a variety of names and acronyms. The most generic terms are Unmanned Aircraft (UMA), Unmanned Aerial Vehicle (UAV) and Remotely Piloted Vehicle (RPV). The future of UMAs seems to be very promising, mainly because they can be significantly cheaper to develop, build and can be used for a broad spectrum of applications [1].

Among the existing problems in the development of these systems, recovery has always been of much concern. Current arrangements which vary from the simple parachute to the large net-carrying recovery vehicle, are still not able to provide a safe, cheap and easy recovery for UMA customers. Each method has its own disadvantages which can cause serious performance limitations and increase service cost [2]. The application of the helicopter type UMA considerably reduces the recovery problems, however, at the expense of reductions in speed, altitude, endurance and manoeuvrability.

One solution for this problem is to combine the attribute of vertical take off and landing of a helicopter with the high speed and efficient cruise ability of fixed-wing aircraft. This is the reason for the growing interest in the Vertical Take Off and Landing (VTOL) type UMA which can fly at high speeds whilst still being able to take off and land vertically as well as hover anytime during flight.

The idea of VTOL aircraft has been a recurrent theme in full size aircraft design and research for well over sixty years [3-24]. Many VTOL concepts have been built and flown with reasonable success. However, only the concepts of *Jet Lift*

and *Tilt-rotor* have reached to the stage of production. The British VATOL aircraft *Harrier* and the American V22 Tilt-rotor aircraft *Osprey* can be quoted as examples.

In the area of VTOL unmanned aircraft, some limited studies have been reported about the possible configurations and technology assessment for VTOL UMA [25,26]. However, the number of reports on the development programs are greater. The best known previous efforts are the Naval Ship Research and Development Center's VATOL demonstration vehicle [26], and the shrouded propeller UMAs Dornier-Lippisch *Aerdyne* and Short-Brothers *Skyspy* [26,27]. The recent efforts are much more promising. These efforts are mostly focused on the open-rotor concepts (systems normally seen on propeller-driven aircraft and rotorcraft). The most famous development programs of VTOL UMA of these kind in recent years are the Bell tilt-rotor UMA *Pointer* and its next generation *Eagle Eye* [1,20,29-38], the Sky Technology tail-sitter UMA *Sparrow Hawk* [28,39], the Boeing tail-sitter UMA *Heliwing* [40], the McDonnell Douglas Stopped-rotor UMA [28], the Freewing Aircraft Tilt-body UMA [38,41] and Daedalus Research Free-wing UMA *STF-9A* [28,38]. The majority of these VTOL UMA concepts are still in the research stage and almost no detailed information about the flight dynamics of these aircraft are available.

1.2 THE PROPOSED CONTROL CONCEPT

In the existing VTOL concepts, the ability of the engines to play an important role in aircraft control seems to be ignored. This is most probably due to either the poor response characteristics of their comparatively large engines or because there has not been much advantage compared to the cost of development. However, the small engines which are commonly used in ordinary small to medium size UMAs have sufficiently fast response characteristics to be considered as an active component of the aircraft control system. This ability can be used to control the amount of thrust force delivered by the propeller. If the direction of thrust is also controlled simply by rotating the propeller axis, then the complex rotors in VTOL concepts such as Tilt-rotor aircraft may be replaced by an ordinary simple engine/propeller propulsion system. In this way, the

resulting simplicity in mechanical system leads to lower manufacturing and maintenance cost.

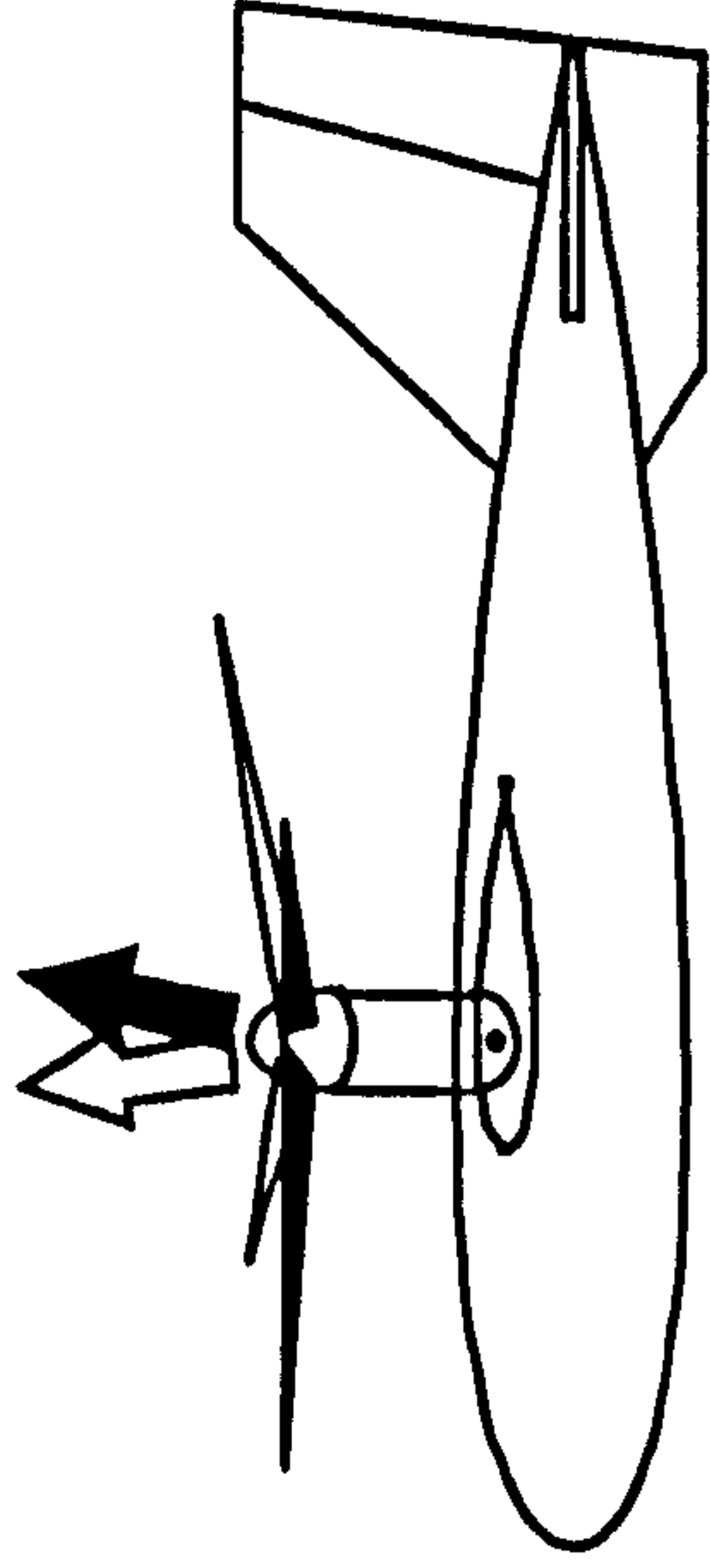
The application of this idea in a tilt-rotor configuration is shown in Figure 1.1. In this figure, the existing and the proposed concepts are respectively titled as Rotor-tilt and Nacelle-tilt control concepts. The Nacelle-tilt concept is called a Tilt-nacelle aircraft in this thesis. The main difference between the two concepts is the type of controllers which are used to control the aircraft orientation in different directions. As shown in Figure 1.1, in a Tilt-nacelle aircraft the complex rotor is eliminated and the differential collective and cyclic pitch controls are replaced by differential engine throttle settings and nacelle tilt controls.

The application of the proposed concept can also be examined using the other VTOL configurations such as Tilt-wing and Tail-sitter. The Tilt-nacelle, Tilt-wing and Tail-sitter configurations and their associated velocity diagram describing the conversion process are shown in Figures 1.2, 1.3 and 1.4.

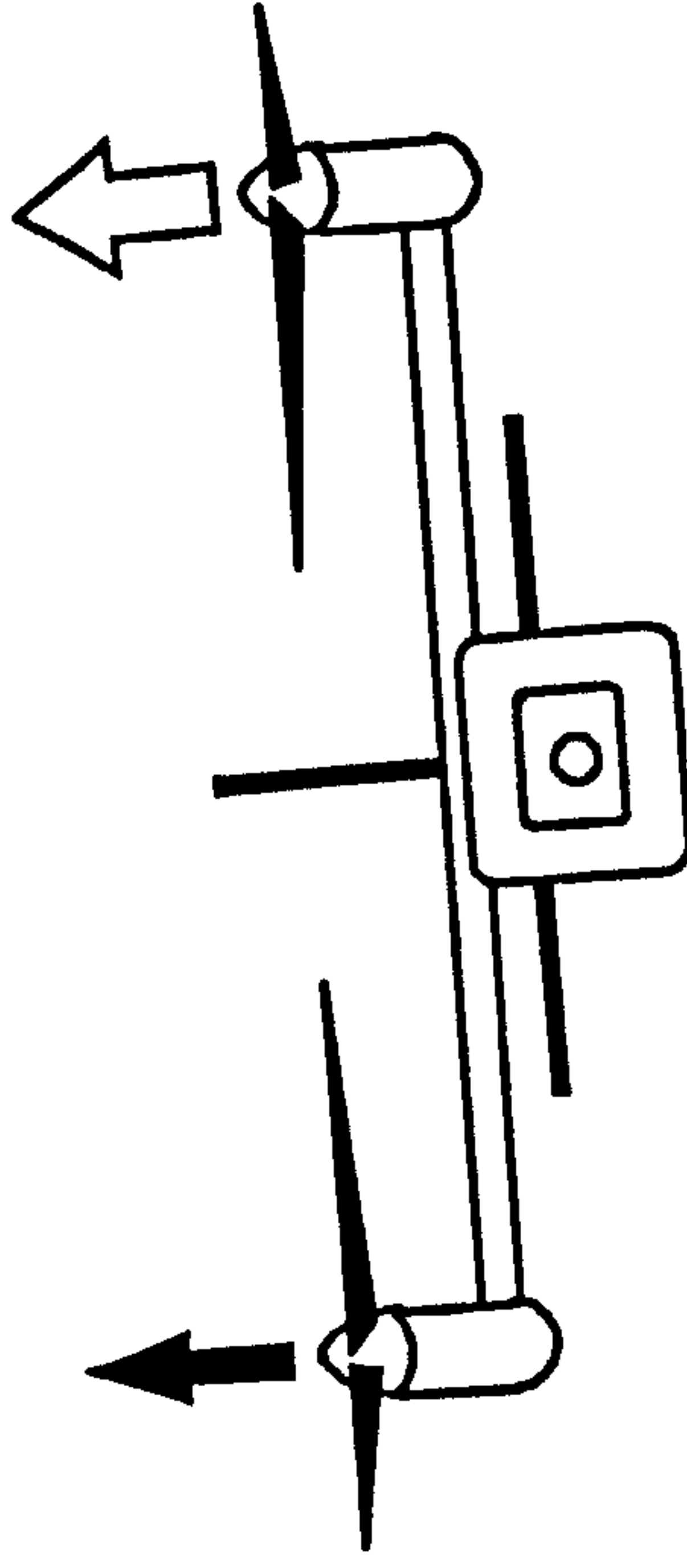
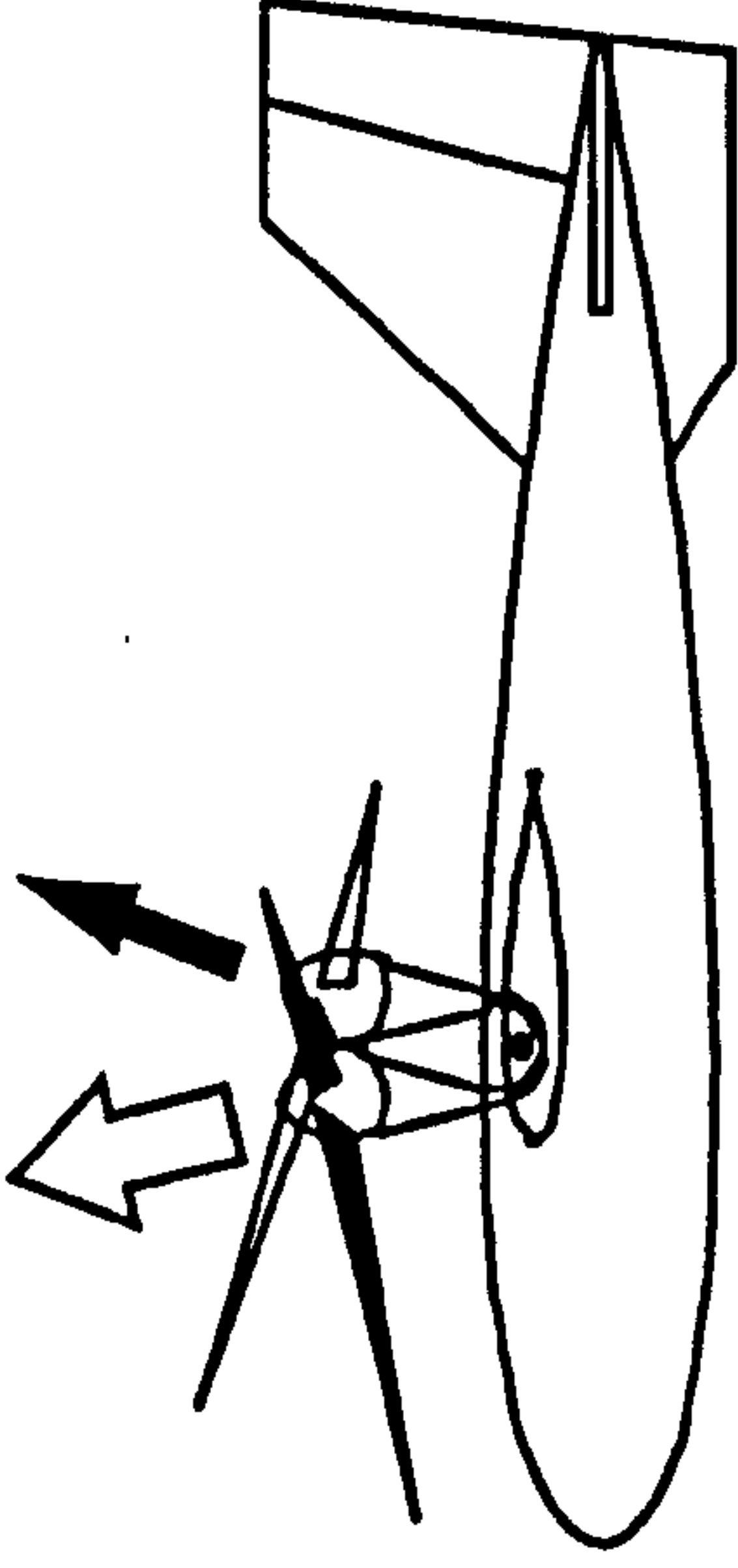
In the Tilt-nacelle configuration, the nacelles can rotate relative to the fuselage and the wing is fixed. During take off and landing, the nacelles are in the vertical position. The aircraft transition from hover to cruise or from cruise to hover can then be carried out by rotating the nacelles from the vertical to the horizontal position and vice versa. The fuselage remains in the horizontal orientation in all flight regimes. The actual airspeed over the wing (V_i) is a vector summation of the aircraft velocity and the propeller induced velocity. The wing angle of attack during the hover and the conversion process is negative.

In the Tilt-wing configuration, the nacelles are fixed to the wing. The wing is in the vertical position for VTOL type manoeuvre and is rotated approximately ninety degrees forward to enable conventional propeller-driven flight. The configuration is similar to Tilt-nacelle except that in the Tilt-wing configuration the nacelles are attached to a tilting wing. The effective angle of attack over the wing is equal to the difference between the wing angle of attack (α_w) and induced angle of attack (α_i).

Rotor-tilt control concept



Nacelle-tilt control concept



Rotor-tilt control concept		Nacelle-tilt control concept	
VTOL	Helicopter Mode	Helicopter Mode	Airplane Mode
Pitch	Collective pitch	Throttle	-----
Roll	Fore & aft cyclic	Fore & aft tilt angle	Elevator
Yaw	Differential Collective	Differential throttle	Aileron
	Differential cyclic	Differential tilt angle	Rudder

Fig.(1.1): Rotor-tilt and Nacelle-tilt control concepts

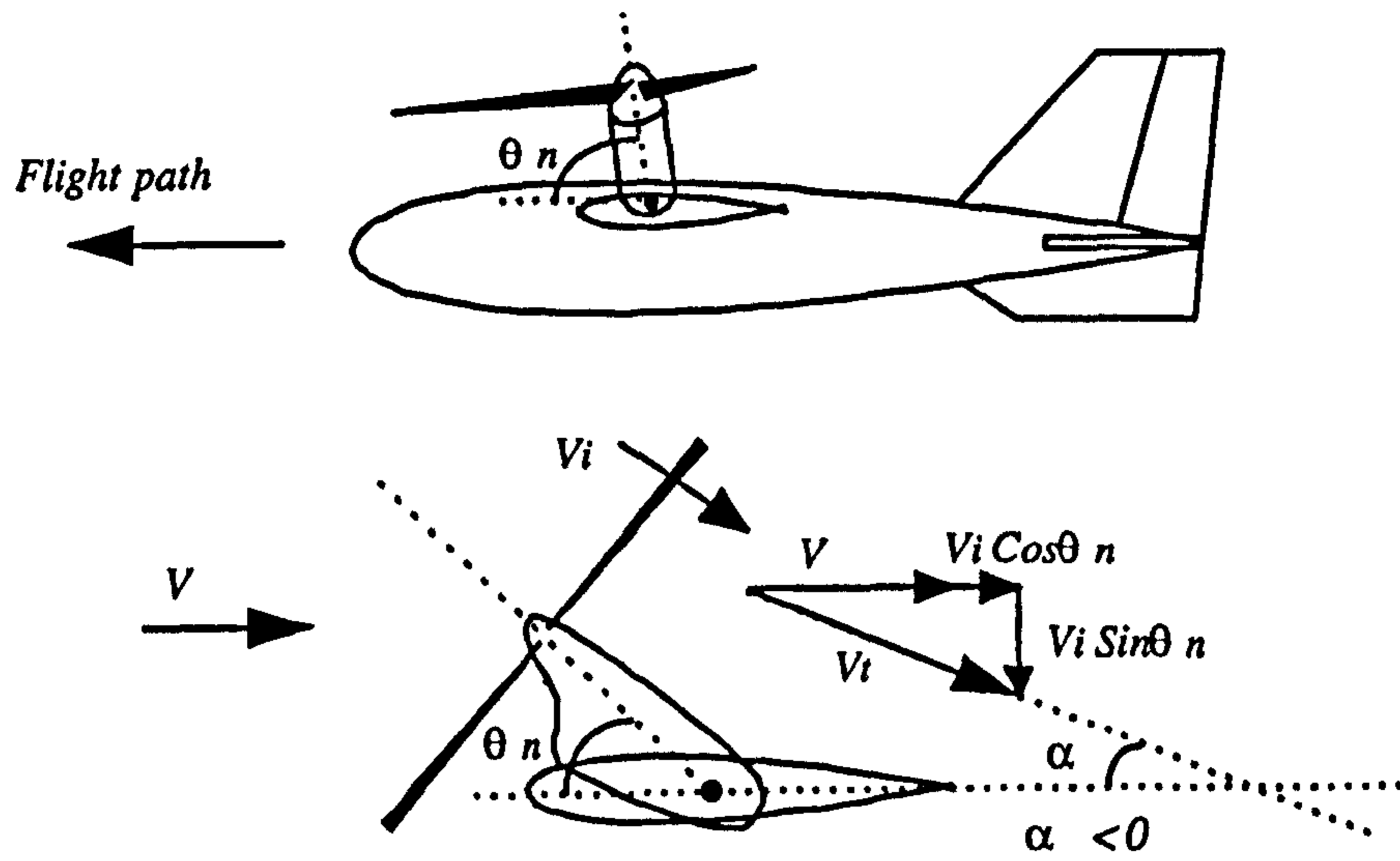


Fig.(1.2): Tilt-nacelle configuration

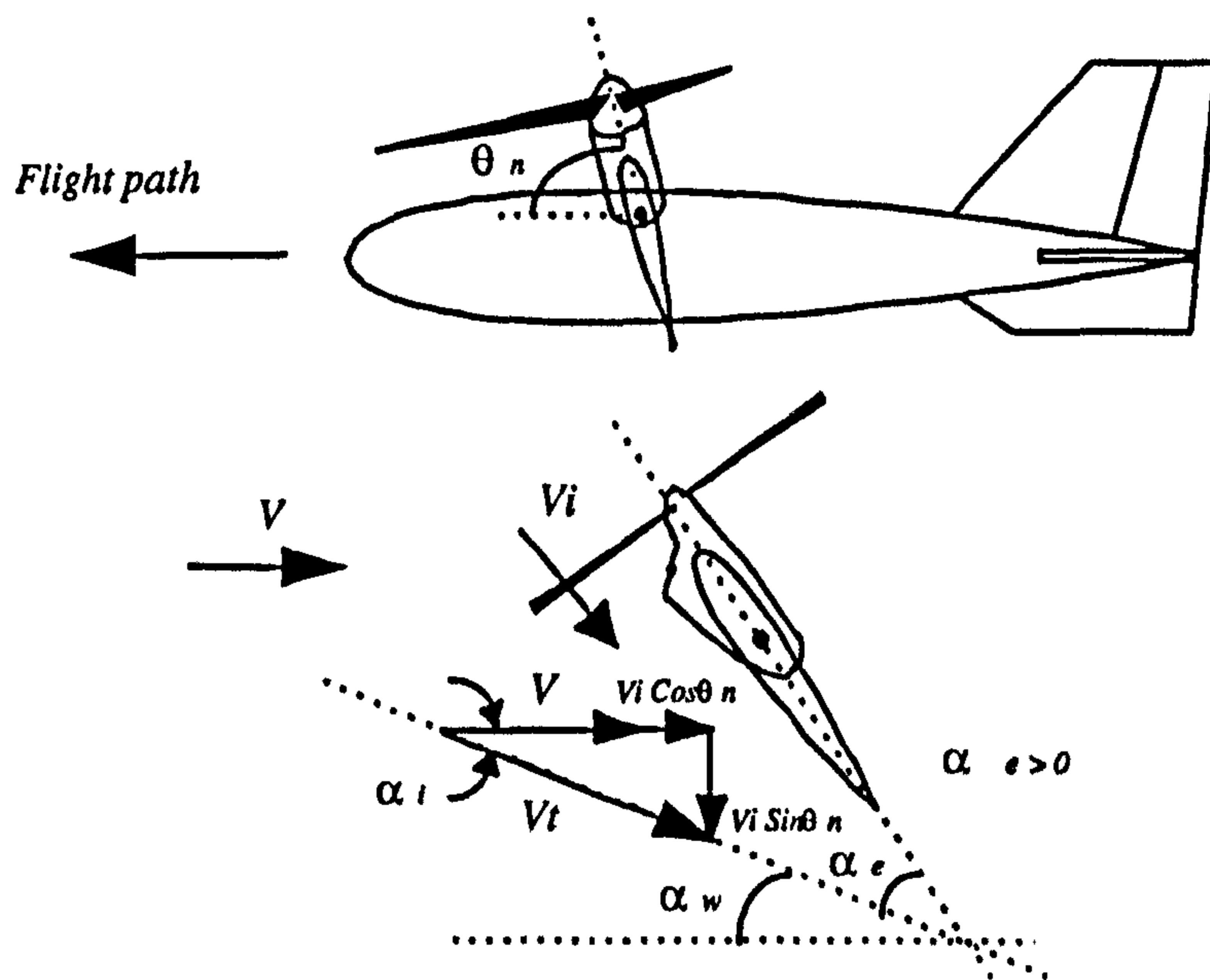


Fig.(1.3): Tilt-wing configuration

The Tail-sitter configuration has the same appearance as a conventional aircraft but with large diameter propellers. At launch, it is held in the vertical position until released for a vertical take off using the lift provided by the propellers. The aircraft then changes attitude and begins a conventional flight with the lift force being generated by the wing. In recovery, it flies to vertical position and lands vertically on its tail.

Figure 1.5 depicts the available independent controls in an aircraft with the proposed control concept. Different combinations of these controllers may be used for different configurations and in different flight phases.

1.2 REQUIREMENT FOR A SIMULATION TOOL

The transition between propeller borne and wing borne flight is a complex physical process during which the propeller and wing pass through regions that are not normally experienced by conventional aircraft. Therefore, it is by no means certain that such transitions are physically possible for previously mentioned configurations. In addition, it is not immediately obvious what the advantages and disadvantages are between the configurations with regard to this manoeuvre and their compatibility with the considered control concept. A simulation tool is therefore necessary for such investigations. This simulation model can also be used for investigations of the aircraft stability and control as well as development of suitable control strategies.

Moreover, the sizing of VTOL aircraft is very much influenced by its stability and control characteristics during flight in different regimes. Therefore, it is very important that the evaluation of the stability and control characteristics is carried out at early stage in the design process so that satisfactory flying characteristics can be obtained later with minimum need to change the aircraft sizing. A simulation model is equally useful in providing invaluable insight for conceptual design of a nearly optimised configuration, considering all factors including desired control tasks.

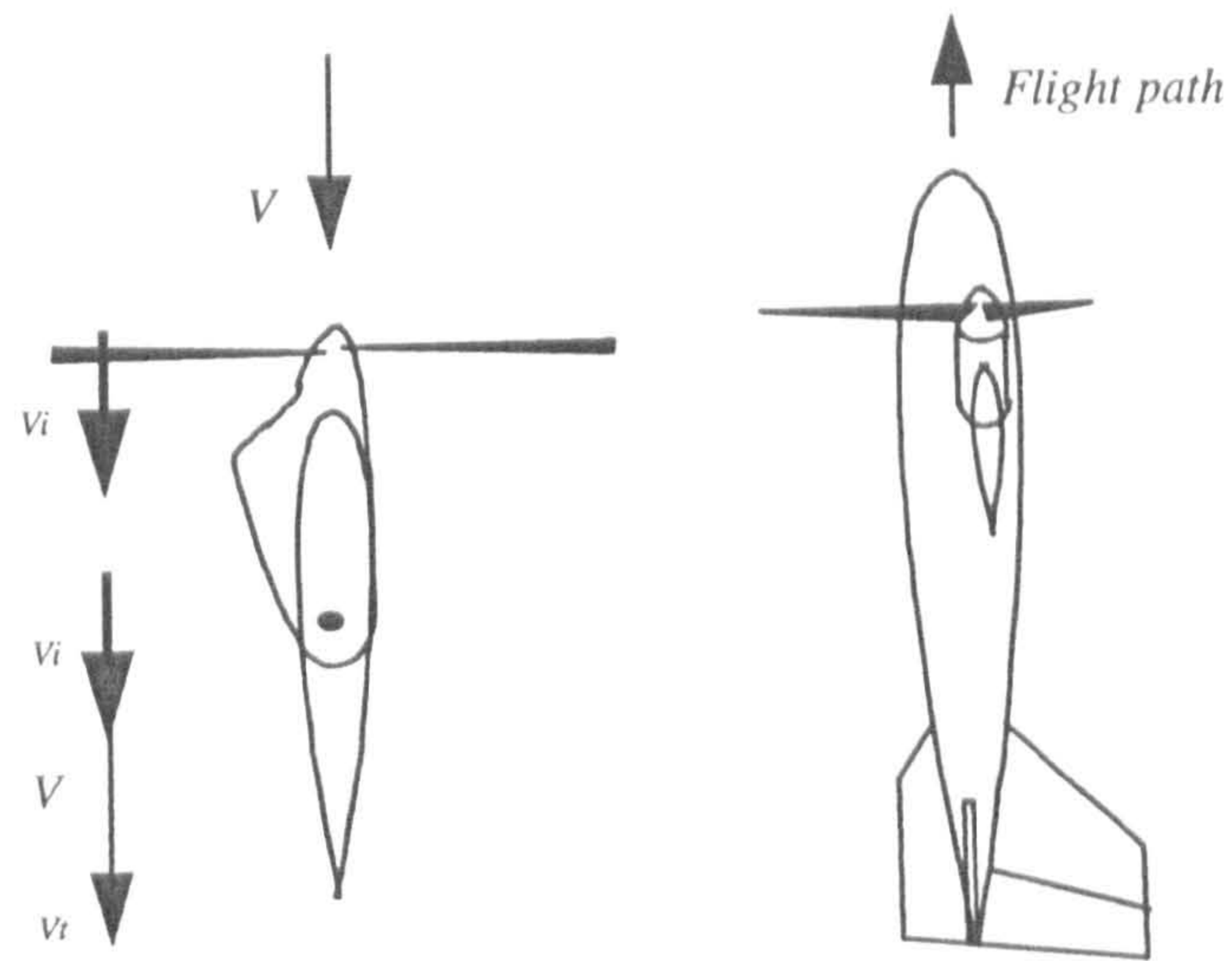


Fig.(1.4): Tail-sitter configuration

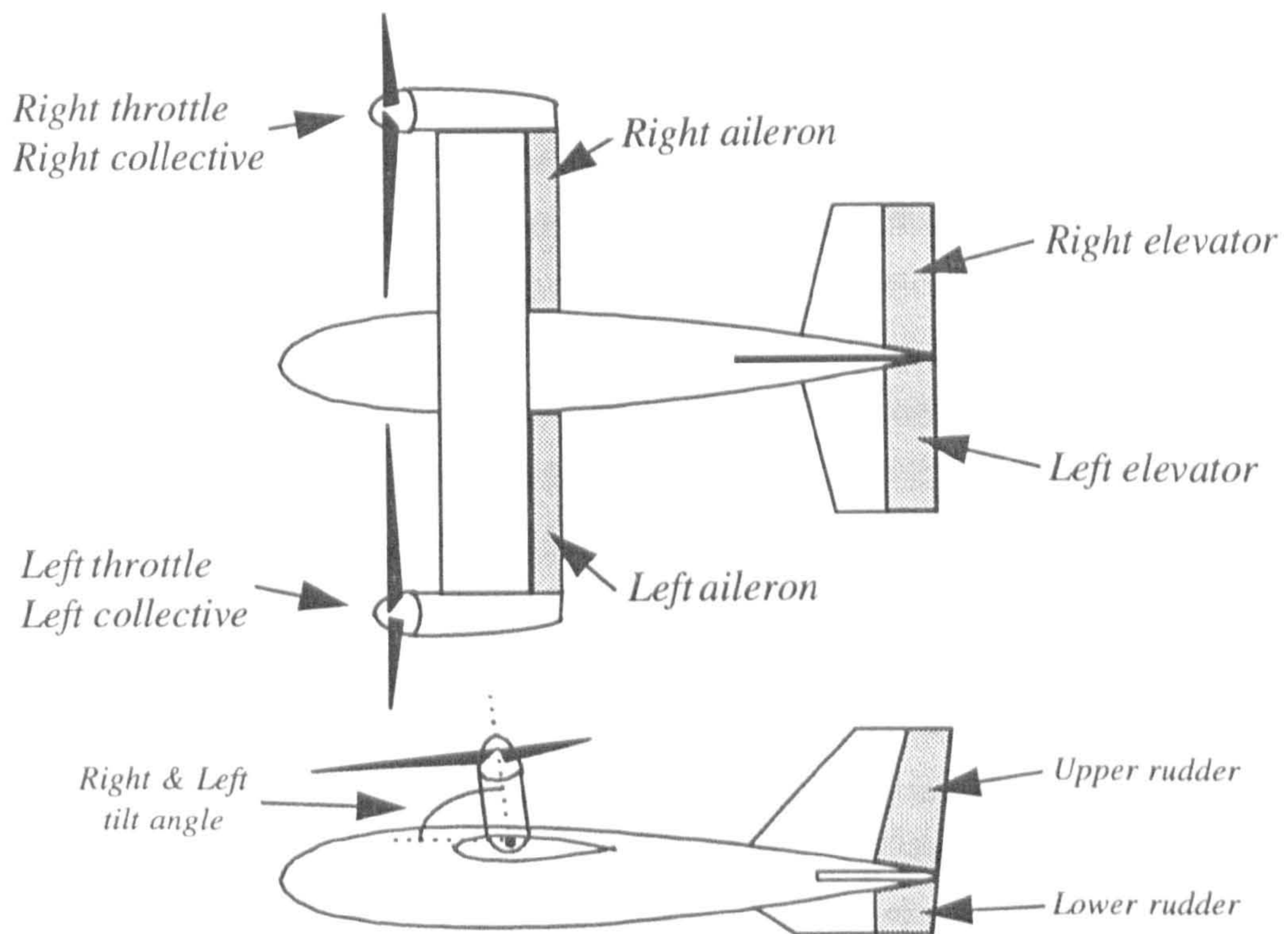


Fig.(1.5): Aircraft controls

The complex coupled dynamics associated with the proposed concept (described in Chapter 3) leads to elimination of any simplifications in the aircraft equations of motion. Therefore, the complete equations of motion of an articulated flying structure with ten degrees of freedom must be used in this simulation. In other words, the quasi-static assumptions which have been used in previous works for tilt-rotor aircraft can not be made in this work [13,21,23].

As a research tool, the simulation model should be sufficiently general and flexible to be simultaneously used for investigations of all the aspects of flight dynamics of the three different VTOL configurations. Clearly, development of such a simulation tool is a multidisciplinary task which involves different areas such as dynamics of multibody systems, flight dynamics and simulation, aerodynamics of VTOL aircraft, propeller/engine propulsion system, aircraft stability and control, computer programming and validation methods.

1.3 OBJECTIVES AND THESIS OUTLINE

As the thesis title implies, the ultimate objective of this work is to develop a simulation tool to be used when there is little specific data available. This tool can then be used for investigations of flight dynamics and control of the previously mentioned VTOL UMA configurations, together with a feasibility study of the proposed control concept. In order to achieve this ultimate goal, some prerequisite objectives had to be completed in the form of different tasks. These tasks have been carried out in a step-by-step manner and are presented in different chapters. The following thesis outline represents the process of completion of these prerequisite objectives.

In chapter one, a very brief introduction of unmanned aircraft and their recovery problems is provided. The capabilities of VTOL aircraft and recent development programs are then reviewed. The concept of using engines in aircraft control in order to reduce the mechanical complexity together with three aircraft configurations as the potential candidates are introduced. The application of the simulation tool, the objectives and the thesis outline are also described.

In chapter two, the relevant concepts of mathematical modelling and flight simulation are reviewed. This chapter provides all the basics which must be known for development of a successful flight simulation. The state-space presentation is described in order to be used for formulation of the aircraft mathematical model in the following chapters.

In chapter three, the general methodology used to establish the simulation model is described. This methodology is the baseline of all the mathematical modelling in the forthcoming chapters. The reasons for system complexity, the generality and flexibility requirements, and the kind of restrictions that led to devise such an approach are explained. An assessment about different aspects of the methodology is also provided.

In chapter four, the equations of motion of the aircraft multibody system are developed. The Newton-Euler approach has been used in this development. These equations are then integrated with navigation equations and assembled in a state-space form. An appropriate system of notations and conventions is introduced.

In chapter five, the modelling of various subsystems including propeller model, airframe aerodynamics, engine model and servomotor model has been carried out. In addition, the gravitational and inertia terms in the equations of motion are defined. A method for calculating the propellers' slipstream effect is also presented.

In chapter six, the data preparation procedure for the simulation model is discussed. As previously mentioned, since there is no specific data available, a set of reasonable input data must be approximated to be used in the validation studies. The approximation of these data for various quantities is presented in this chapter.

In chapter seven, attention is focused on programming the resulting equation on the computer. Firstly, the support languages for model simulation are reviewed. The Advanced Continuous Simulation Language (ACSL) is then introduced and its structure, advantages and inconveniences are discussed. Secondly, the

program development issues are explained, such as programming procedure, program structure, programming style, etc. A review of the testing process, strategies and techniques is then presented. This chapter finally ends by describing the comprehensive tests that have been carried out in order to prove the internal consistency and algorithmic validity of the developed model.

In chapter eight, it is aimed to show the validity of the simulation model in terms of its capabilities to provide a series of reasonable and explainable simulation results associated with the considered VTOL configurations. The wing-supported flight as a common flight phase and the propeller-supported flight phase of each individual configuration are considered. The simulation results covering aircraft trimming, aircraft modes and aircraft controls are then presented. The ability of the simulation model to predict and to explain the aircraft behaviour correctly and to be used for hypothesis testing, explanation and discovery is also discussed . The discussion includes the prediction of the unstable oscillatory mode of tailsitters.

In chapter nine, some generalised conclusions are drawn and prospects of future works are presented.

CHAPTER TWO

RELEVANT CONCEPTS OF FLIGHT SIMULATION

2.1 INTRODUCTION

In creating a successful flight simulation, it is important to have a clear understanding of what are the different steps in the development process as well as the kind of difficulties that might be encountered later. The more comprehensive the initial conception is the more elaborate the final product will be. The present chapter intends to provide such a background in order to reduce the number of unexpected problem.

2.2 AIRCRAFT MATHEMATICAL MODELLING AND SIMULATION

2.2.1 Basics

The basis for analysis, computation or simulation of the motions of flight vehicles is the mathematical model of the vehicle and its subsidiary systems, i.e. their general equations of motion. Whatever configuration a vehicle may take, its motion is governed by the generic form of Newton's second law:

$$\ddot{\mathbf{X}} = \mathbf{F} / \mathbf{M} \quad (2.1)$$

Where \ddot{X} is the acceleration of the vehicle, F is the applied force and M is the mass. The specific form of the equations of motion will be dealt with later on, but given an expression like Equation 2.1, the basic mathematical model of the vehicle is embodied in the definition of F . For a vehicle flying in air, this mathematical model is primarily the relationship between the air reactions and the motion of the aircraft relative to air. This can be called the aerodynamic model. The other external force and moment arise from engine thrust. Bearing in mind that the gravitational acceleration is already considered in the acceleration term \ddot{X} . Definition of these force and moment components is the key to a realistic description of an aircraft flight characteristic. The aircraft performance and dynamic behaviour can then be calculated for as wide a range of flight conditions as that for which F can be defined. *Simulation is fundamentally the generation of these forces and the solution of the equations of motion [42].*

The simulation space is divided into three basic elements as depicted in Figure 2.1. Starting with reality, a conceptual model, described via equations or other governing relationship, is obtained by analysis. Implementation via programming yields a computer model which, through simulation, may be related to reality. The credibility of the conceptual model is then evaluated by procedures which test the adequacy of the model to provide an acceptable level of agreement with reality, while the computer model, in the form of an operational computer program, is confirmed as an adequate representation of the conceptual model by procedures of verification. Finally, model validation demonstrates that computer model possesses a satisfactory range of accuracy in comparison with reality consistent with its intended application.

In creating or deriving mathematical models, it is important that the modeller (the person doing the modelling) has a clear idea of what the model is for, and that he states this together with his definition of his model. It is important because the purpose of the model influences its form and quality [43].

Modelling of many systems is extremely difficult, especially, when there is no 'Reality', for example when the model is going to be used as a basis for a research work on a new concept and there is no specific data available. These kind of systems may often be simplified in the interest of obtaining an applicable model and yet still retaining sufficient realism for the task at hand. An applicable model in the present context means the one

that requires minimal data but is still able to keep the generality requirement to predict all the major aspects of the vehicle flight dynamics.

2.2.2 Mathematical Modelling Versus Stability and Control Analysis

Deriving mathematical models for simulation has some similarities with basic techniques of stability and control theory but there are also some differences. Similarities include mathematical notation, system of axes and basic nomenclature. Differences, however, are significant, and include the need for a wide range of speed, aircraft configuration and manoeuvre.

The classical approach to stability and control analysis is to start with the complete equations of motion and make assumptions that enable the equations to be linearised about some local point of equilibrium (a trimmed state). Once linear equations are available, many techniques can be applied to the analysis of the system to investigate the stability of motion following a disturbance from trim. While such techniques have been, and are, invaluable in the design process, only small disturbances from the equilibrium state are permitted before the model is invalid. Many simulation tasks, demand a wide range of flight speed or require large changes in aircraft configuration in order to accomplish that task. A transition from wing-borne to rotor-borne flight of a VTOL vehicle is an example.

2.3 MAIN ELEMENTS OF THE MODEL

The concept of a mathematical model is introduced in the previous section, where the primary, or core elements of the model were defined as those which directly produce the external forces acting on the airframe, namely aerodynamic and engine thrust.

The aerodynamic model has to reproduce the dominant features of the forces and moments acting on the aircraft. These are lift and drag, the main contributors to the aircraft's performance, and moments about three axes, through which the aircraft is controlled. Mathematical models would normally consider the physical components of the vehicle, e.g. wing, body or, for a helicopter main rotor, tail rotor, body and tail-plane,

and build mathematical expressions for the contributions made by these components. Aerodynamic models are normally static or quasi-static, based on the assumption that the airflow can establish a steady condition in a time scale much shorter than that of the aircraft manoeuvre itself. This time, as such, does not appear explicitly in the mathematical model, but the aircraft's transient behaviour is, of course, a function of time [42].

An engine model must first produce the correct amount of steady thrust to correspond with the demanded value. An engine can not change its thrust instantaneously. Burning more fuel to increase thrust must first accelerate the rotating machinery of the engine and this takes time. The timescale, being in the range of a few tenths of a second to several seconds, can influence the ability of controlling the aircraft. This, especially, happens with VTOL aircraft in which, in the hover, engines play an important role to generate control forces. Thus, adequate modelling of the growth or decay of thrust with time is necessary.

2.4 EQUATIONS OF MOTION

2.4.1 The General Equations

As it was stated, the core of a mathematical model for flight simulation is the equations of motion of the aircraft. To find these equations for a conventional aircraft it is quite usual to start with the Newton's second law of motion. By applying this law, the equations of motion can be established in terms of the translational and angular accelerations which occur as a consequence of some forces and moments being applied to the aircraft. The obtained nonlinear set of equations, sometimes called "total force" or "large amplitude" equations, is sufficient to cope with general large-scale motion of an aircraft, but is not solvable in this form except by numerical techniques, and then only once all the forcing terms can be described.

2.4.2 Small Perturbation Equations

In many simulations there is no alternative to use of the large amplitude equations and fortunately modern computer techniques now permit this. It may still be desirable, however, to seek a linearised form of equations, since they then become amenable to

treatment by a wide range of analytical techniques. Such procedures are important at the design stage of a new aircraft and also in research, when experiments are conducted to establish data on the fundamental behaviour of aircraft based on simplified situations and modes. The large-amplitude equations, can be linearised by using small-disturbance theory [42]. In applying small-disturbance theory it is assumed that the aircraft deviates to only small extent from a datum, steady flight condition or trimmed state. The resulted equations are called small perturbation equations. Obviously, this theory can not be applied to problems in which large-amplitude motions are to be expected. However, in many cases small-disturbance theory yields sufficient accuracy for practical engineering purposes and can provide much valuable information and many important insights with relatively little effort. It gives sufficiently correct results for engineering purposes over surprisingly wide range of applications, including stability and control responses.

2.4.3 Aircraft Orientation

In order to describe the motion of an aircraft, it is necessary to define the aircraft orientation in space by its attitude, which may be specified in a number of ways. The conventional method is to define a sequence of three angles, known as the Euler attitude angles [44].

Equations derived in terms of Euler angles have the advantages of using physically meaningful variables and of being minimal, i.e. minimum number of first-order differential equation that can be used. They also have some significant disadvantages. First, in these equations a division by zero occurs if the pitch attitude variable reaches ± 90 deg. In digital simulation this exact number has almost zero probability of occurrence, but significant computational errors may occur in the vicinity of the singularities. Second, the Euler angles may be integrated up to the values outside the normal ± 90 deg. range of pitch, and the normal ± 180 deg. range of the bank and yaw angles. This *wraparound* problem may make it difficult to determine the attitude uniquely. Finally, the relationships involving Euler angles are linear in terms of the aircraft angular rates but nonlinear in terms of the Euler angles [44].

There are a number of other ways to represent the orientation of an aircraft. These methods involve four, five, or even six variables in place of the three Euler angles. They have all been considered for the purpose of avoiding the mathematical singularity of the

Euler angle representation and increasing the speed of computer processing. One of these methods is now used almost exclusively in all of various aircraft applications. This method referred to an quaternion four-variable or Euler parameter representation [44]. Unlike the nonlinear relationships involving the Euler angles, the quaternion parameters satisfy a set of linear differential equations, with the angular rates as their coefficients. The differential equations can be used to “propagate” the quaternion representation of attitude forward in time. In this case, Euler angles need only to be calculated when needed for feedback control and for visualisation of the attitude. They are also needed at the beginning of a simulation to initialise the quaternions.

Nowadays, the quaternion representation of attitude is widely used. It gives a unique representation of attitude and does not suffer from the singularity and wraparound problems of Euler equations. Also, the linearity of the quaternion differential equations leads to some computational advantages.

2.4.4 Axes and Frames of Reference

During the process of formulating and solving a problem in flight dynamics, a number of frames of reference (coordinate axes) must be used for specifying relative positions and velocities, components of vectors (forces, velocities, accelerations, etc.) and elements of matrices (aerodynamic derivatives, moments and products of inertia, etc.). The equations of motion may be written from the standpoint of an observer fixed in any of the reference frames, the choice being a matter of convenience and preference, and formulae must be available for transforming quantities of interest from one frame to another.

There are many possible axis systems, but for simulation they fall into broad classes, *Body* and *Earth* or *Inertial* axes. Body axes consist of an axis system fixed in the aircraft and thus move in the space and rotate with the aircraft. For a specific set of body axes it is essential to know how the orientation of the axis system is defined with respect to the aircraft.

Geometric-body axes are those axes defined such that the x-axis is aligned with a geometric feature, such as the fuselage reference line or a wing datum. Often such axes are known just as body axes. An alternative set of body axes is known as principal-body axes, defined such that the x-axis is aligned with principal inertia axis, thus making the

cross-products of inertia zero. This simplifies the lateral equations of motion but it is not particularly helpful in simulation, since the location of the principal axis could change with aircraft configuration. It is, however, sometimes useful in theoretical studies. Geometric-body axes offer sufficient advantages in giving constant moments of inertia.

Aerodynamic-body axes (sometimes known as stability axes or wind axes) have an x-axis aligned with the projection of the velocity vector, in a datum flight condition, onto the plane of symmetry. Aerodynamic-body axes are therefore at an angle relative to geometric-body axes. These axes are usually employed to define the basic aerodynamic forces, especially lift and drag, as they are the natural axes for such definitions. If the x-axis is always coincident with the projection of the velocity vector, then the axes are no longer body axes, because they are no longer fixed in the aircraft.

Flight- path and air-path axes also exist. Neither is a body axis system. For both, the x-axis is directed along the path followed by the origin O (the center of gravity), either the path relative to earth or the path related to the air-speed vector. They differ only if there are winds.

Earth or *Normal* axes comprise a set of axes defined with respect to the earth, with the origin at a suitable point, the x-axis pointing North, the y-axis East and the z-axis down. Unlike body axes, Earth axes are inertial axes. They are used as reference axes for position and attitude and for the definition of winds.

2.4.5 Axis Transformation

One of the most fundamental operations in formulation of an aircraft equations is axes transformation. Many axes systems are used in flight simulation (e.g. Body axes or Earth axes) and many vector quantities are required to be transformed between them. The basic tool is the *Direction Cosine Matrix*. This is the linear transformation from one axes system to another. The elements of the DCM are the cosines of the angles between the base vectors of each axes system. These are not all independent and six algebraic equations, usually called constraint equations, have to be satisfied as well. Once a DCM has been obtained, the axes transformation is straight forward. However, computationally it represents nine products and nine summations and if many such transformations are required this can be a major part of computer work load. The inverse

transformation between axis system is simple, since the inverse of DCM is its transpose [45].

In many parts of a simulation program, the axes are rotating relative to each other and as a result the DCM is time dependent and changes as the calculations proceed. Thus, it is a part of the simulation's job to calculate the new DCM at each calculation step. A good example is the use of body axes to express the equations of motion. In such a formulation the translational and rotational velocities are expressed as differential equations and solution of the equations provides the relevant velocities in body axes. To find the earth referenced velocities, a direction cosine matrix is needed. Since it will be time varying due to the relative velocities of the axes, it would be expected that its elements to be dependent on the angular velocities. This is indeed the case and nine differential equations can be written for the DCM elements that have angular rates as coefficients. The solution of these nine simultaneous differential equations will yield the required DCM. Since, the elements are not all independent, six algebraic constraint equations have to be satisfied as well. This is a considerable calculation problem. Many schemes have been used, all requiring a lot of computing, fortunately alternative methods are available [46].

2.4.6 The Aerodynamic Angles

The aerodynamic forces and moments on any moving object in air are produced by the relative motion with respect to the air and depend on the orientation of the aircraft with respect to the airflow. In a uniform airflow, these forces and moments are unchanged after a rotation around the free-stream velocity vector. Therefore, only two orientation angles (with respect to relative wind) are needed to specify the aerodynamic forces and moments. The angles that are used are the angle of attack (α) and sideslip angle (β). They are known as aerodynamic angles. These angles will be defined later in the following chapters.

2.5 DATA REPRESENTATION

Depending on the implied form of the model and required accuracy, the input data, such as aerodynamic, engine, propeller and so on, to the simulation program, may be

presented in a variety of ways. Sometimes a compact table of numbers is sufficient, but more often many data tables are needed, and some are two or three-dimensional. These tabulated data are discrete, whereas aircraft models require data at arbitrary values of the independent variables. This problem can be solved by using an interpolation algorithm with the data. Given a table of values of Y as a function of a set of values of X then the value of Y for any general value X is obtained by interpolation between adjacent coordinate axes. Special action has to be taken if X is either less than the lowest X -value in the table or greater than the highest X value. One action would be to set Y to the nearest end-point value. An alternative would be to extend the slope of the final segment. Which of these procedures is adopted depends on the problem and the nature of the data.

2.6 THE STATE-SPACE FORMULATION

The aircraft mathematical model can be built from a set of simultaneous ordinary differential equations of various orders. In this case, if we wish to examine the dynamic behaviour starting from some point on a trajectory, the initial values of the derivatives of various orders are needed to be known. As an alternative, the aircraft mathematical model can be expressed by a set of first-order differential equations that governs the dynamics of the aircraft. These are represented in the state-space form as the vector equations

$$\dot{\mathbf{X}} = f(\mathbf{X}, \mathbf{U}) \quad (2.2)$$

where \mathbf{X} is the $(n \times 1)$ *state vector*, \mathbf{U} is the $(m \times 1)$ *control vector*, and f is a vector-valued nonlinear (in general) function of the state and control vectors. In addition to the state Equation 2.2, an output equations of the general form:

$$\mathbf{Y} = g(\mathbf{X}, \mathbf{U}) \quad (2.3)$$

is also required, where \mathbf{Y} is a $(p \times 1)$ *output vector* and g represents a set of nonlinear equations which are functions of the state and control vectors. The state variables can be any set of variables that completely describe the system. The state is an indication of the stored energy of a system (i.e., potential and kinetic of the aircraft) and its distribution. We normally choose a minimal set of state variables (i.e. independent set of variables)

and use the obvious orthogonal component of position and velocity (translational and angular) for this purpose . The output variable, Y , usually correspond to physical quantities for which measurement sensors have been supplied.

For much of the analysis and design, the nonlinear model is approximated by a linear model. For the linear case, the Equations 2.2, 2.3 can be rewritten as:

$$\dot{\mathbf{x}} = \mathbf{A}\mathbf{x} + \mathbf{B}\mathbf{u} \quad (2.4)$$

$$\mathbf{y} = \mathbf{C}\mathbf{x} + \mathbf{D}\mathbf{u} \quad (2.5)$$

where, for an n th-order system, A is an $(n \times n)$ *system matrix*, B is an $(n \times m)$ *input matrix*, C is a $(p \times n)$ matrix referred to as the output matrix and D is a $(p \times n)$ *direct matrix* [44].

Note, that the uppercase symbols are used in Equations 2.2, 2.3 for the state, control and output vectors because they represent the actual values of aircraft variables. However, in Equations 2.4, 2.5, the lowercase symbols indicate that the state, control and output vectors are deviations from some nominal values (the steady-state flight condition). The steady-state condition and the linearization process will be discussed later in this chapter.

Because of particular form of state equations, all of the necessary initial-condition information is carried by the state vector. In fact, the state variables can be defined as a set of variables such that the knowledge of the state vector at a particular time, and the control vector after this time, completely defines the motion (state trajectory) from that time on. This concept of state implies our earlier definition that the state vector defines the energy stored in the dynamics of each instant of time. This property will be useful when one wants to choose a set of state variables. Obviously, reduction of equations of motion to state-space form may include simply redefining the derivatives of some state variables as state variables in their own right.

The advantages of state-space formulation will become evident if one gets involved with the development of analytical tools and numerical algorithms. Here, it should be pointed out that the vector function f can not in general be represented analytically, because they encompass a number of nonlinear effects, in the form of large body of tabular

aerodynamic data. Despite this, there is no difficulty involved in computing a trajectory. This is because the expression for the derivative vector, and starting value for the state-vector, constitute an initial value problem in the mathematical theory of ordinary differential equations. The theory and algorithms for numerical integration of this type of problems were developed long time ago by mathematicians. The numerical algorithms developed based on the state space formulation can readily be turned into software tools. The software tools will provide the capability to trim aircraft models for steady-state flight, perform digital flight simulation, extract linear state-space and transfer functions descriptions of aircraft models, and perform operations on the linear equations. These linear equations allow us, to design aircraft flight control systems. Figure 2.2 shows how the software tools fit together and emphasises the central core of the nonlinear state-space model [44].

2.7 NUMERICAL SOLUTION OF THE STATE EQUATIONS

To simulate a flight using an aircraft model, the governing differential equations must be solved. These equations are nonlinear, depend on experimental data, and are subjected to arbitrary input signals. Therefore, an analytical solution is out of the question, and numerical methods must be used to calculate an aircraft trajectory.

In general, a trajectory mean the motion of the tip of the state vector in the state coordinate as time evolves, in a more limited sense it also means the motion of the aircraft in some three-dimensional coordinate frame as time evolves. The state trajectory will change in a continuous manner because the state variables describe the energy stored in a physical system, and an instantaneous change in energy would require infinite power. This continuous variation of the state makes numerical integration possible, although state derivatives can often change discontinuously, and this may cause difficulties with a particular integration algorithm.

Numerical evaluation of continuous trajectory implies calculating discrete sequential values of the state:

$$\mathbf{X}(t_0 + kT) , \quad k = 0,1,2,\dots \quad (2.6)$$

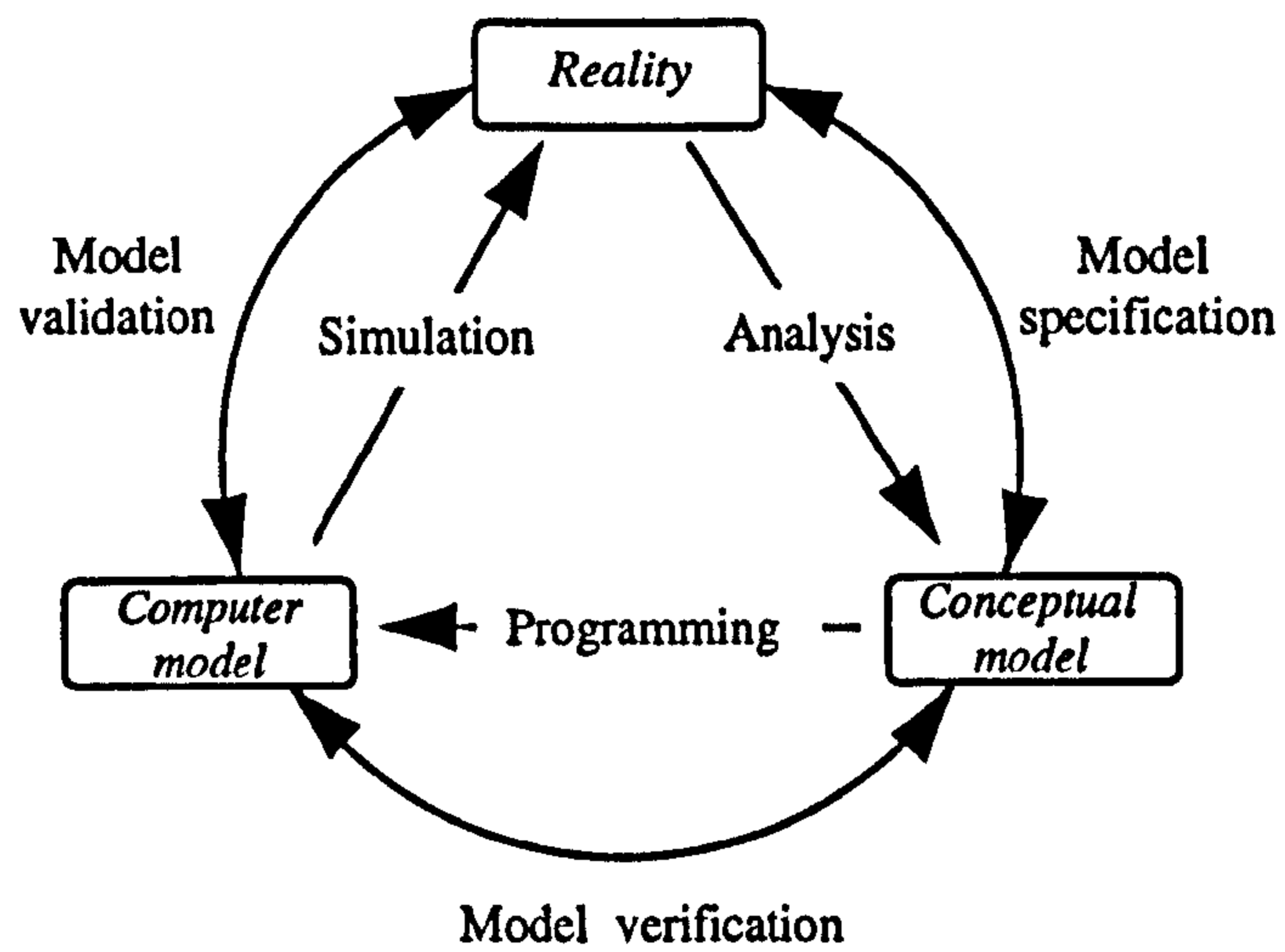


Fig. (2.1): The simulation space and the definition of models [42].

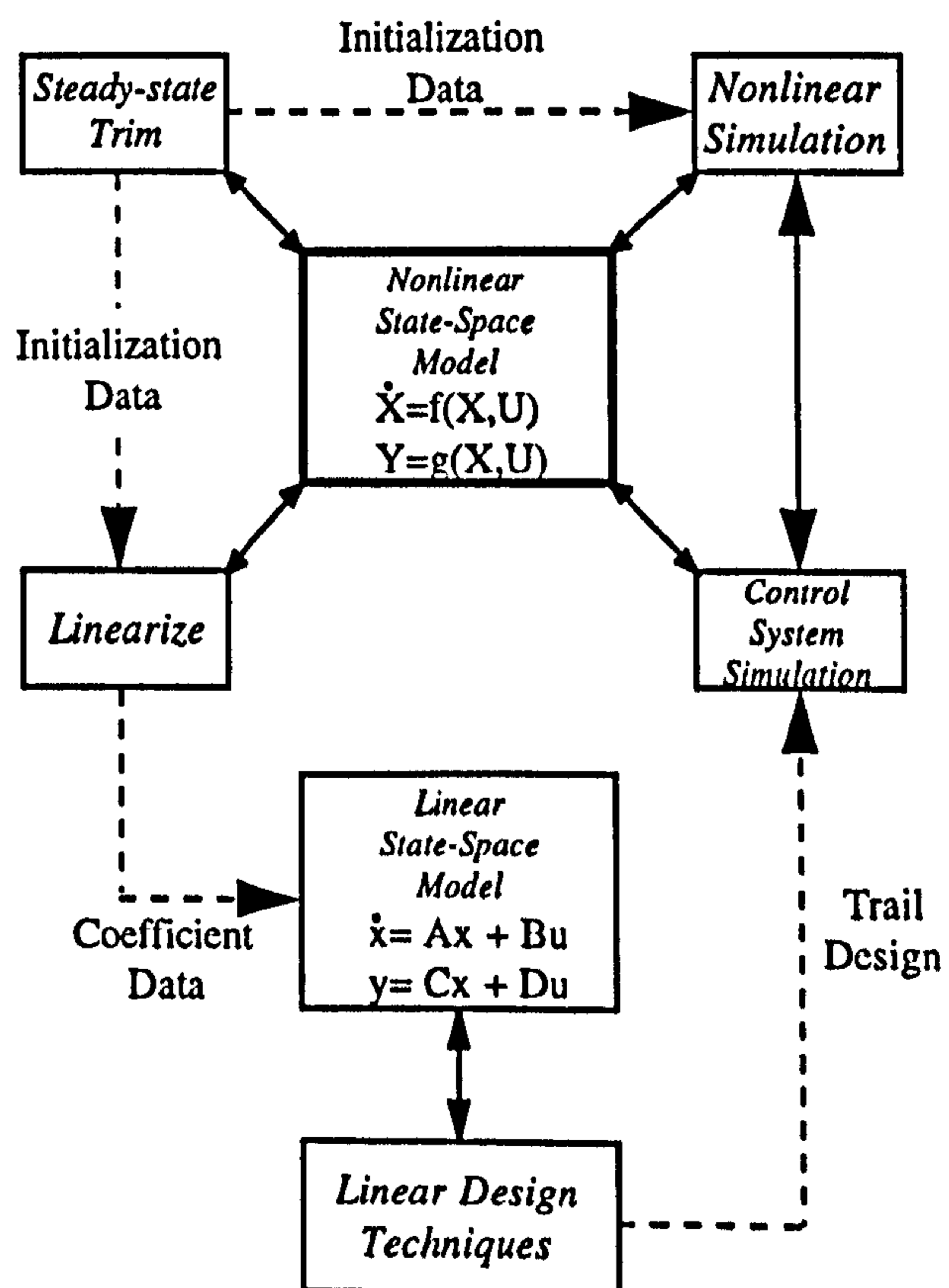


Fig. (2.2): State-space models and associated software [44].

that satisfy the state equations:

$$\dot{\mathbf{X}}(t) = f(\mathbf{X}(t), \mathbf{U}(t)) \quad (2.7)$$

where t_0 is the initial time and T is the *time step*. It is convenient to use a fixed basic time step for a given simulation, but the integration algorithm may internally subdivide the basic time step as it attempts to obtain an accurate solution.

Next, we must consider the fact that the state equations are not autonomous since the control input is an external input. In order to use standard numerical integration algorithms, it is necessary to assume that the time step is so small that the control input remains constant within the sample interval kT to $(k+1)T$.

Numerical integration of the continuous state equations is an initial-value problem. The initial value $\mathbf{X}(t_0)$ is given and the *future* values given by Equation 2.6 must be calculated. This can also be called *prediction* of future states based on current values of the first derivative. It is therefore intimately related to the Taylor series, which links prediction to knowledge of the derivatives of the orders. By using Taylor series some basic algorithms can be derived. One class of algorithms, that is called *Runge-Kutta algorithms*, directly solves the initial-value problem. They use the set of continuous state equations to predict the state derivative within the sample interval, at time instants beyond the current time.

Another class, called *linear multistep methods*, requires past values of the state. They are therefore not self-starting and do not directly solve the initial-value problem. However, they do not require values of the state derivatives within the sample interval and are therefore useful for integrating the discrete-time signals in combined continuous-discrete simulations.

2.7.1 Stability, Accuracy and Stiff Systems

In developing numerical algorithms it is always necessary to consider how computational errors are magnified. If, in pursuit of greater accuracy, one blindly attempts to create higher-order linear multistep method formulae, it is quite possible that the algorithm will

be unstable and errors will grow with time, stability can be determined by analysing a finite-difference equation associated with the integration algorithm.

The Runge-Kutta properties are different from those of the linear multistep methods. In the case of the Runge-Kutta algorithms, a reduction in step size will eventually eliminate an instability, although the required step size may be unrealistically small. When a set of state equations is being integrated, the required step size will be determined by the smallest time constant (i.e. the fastest component) of the solution function. A system with a very wide spread of time constants is known as *stiff system*, and a very large number of Runge-Kutta steps may be necessary to yield only a small part of the complete solution. Indeed they may be so many that rounding errors become a problem. Other techniques are required for stiff systems [44].

2.7.2 Choice of Integration Algorithm

The most important feature of the Runge-Kutta methods is that they directly solve the initial value problem. In other words, no past values are needed to start the integration. This, of course, exactly matches the philosophy of the state-space formulation in which all of the information describing the *state* of the system is contained in the state vector at any time instant. The full significance of these facts can only be appreciated when a simulation containing discrete events is considered. This is a common practical engineering situation. For instance, at a given time a new subsystem may be activated, or at a certain value of some variables, the equations of motion may change because limiting or saturation behaviour occurs. Consequently, previous states are less relevant, the information they carry may now apply to only a part of the complete system. This favours the Runge-Kutta methods over the multistep methods. The disadvantages of the Runge-Kutta methods are that the error expressions are complex, they are inefficient when dealing with stiff systems, and more derivative evaluations are required for a given order than is the case with linear multistep methods. The tremendous increases in computing power in recent years have made these disadvantages much less significant for small to medium-sized simulations. Such simulations are commonly run with a fixed time step that has been found to be adequate for the required accuracy and is also determined by other discrete event considerations.

The important features of linear multistep methods are that higher-order methods are obtained for a given number of derivative evaluation, and an accurate expression for the integration error can usually be obtained. These methods come into their own on very large systems of equations, large stiff systems, and when there is no hard-limiting behaviour or topological changes due to switching [44].

2.8 STEADY-STATE TRIMMED FLIGHT

The concept of a singular point, or equilibrium, of an autonomous (no external control inputs) time-invariant system is introduced in the theory of nonlinear systems [44]. According to this theory the coordinate of the singular point of a nonlinear state equations are given by the solution vector, \mathbf{X}_e , which satisfies:

$$\dot{\mathbf{X}} = f(\mathbf{X}, \mathbf{U}) \quad \text{with} \quad \dot{\mathbf{X}} = \mathbf{0} ; \quad \mathbf{U} = \mathbf{0} \text{ or constant} \quad . \quad (2.8)$$

This idea has a strong intuitive appeal, the system is a *at rest* when all of the derivatives are identically zero, and then one may examine the behaviour of the system near the singular point by slightly perturbing some of the variables. If, in the case of an aircraft model, the state trajectory departs rapidly from the singular point in response to a small perturbation in, for example, pitch attitude, then the aircraft is unlikely to be controlled.

To find the steady-state flight condition, the simultaneous nonlinear Equation 2.8 must be solved. Then the values of the state and control vectors that satisfies these equations can be calculated. In general, because of nonlinearity, a steady-state solution can only be found by using a numerical algorithm on a digital computer which iteratively adjusts the independent variables until some solution criterion is met. The solution will be approximate but can be made arbitrarily close to the exact solution by tightening up the criterion. Multiple solutions may exist, and a feasible solution will emerge only when practical constraints are placed on the variables.

The trim algorithm communicates with state-space model only through its proper inputs and outputs. This means, we don't work within the model to balance forces and moments separately. It has the important advantage of separating the method from

supporting software, and promoting modular software with standard mathematical algorithms. Figure 2.2 illustrates this idea, the generic trim program links to any nonlinear model and produces a file containing the steady-state values of the control and state vectors for use by the time-history and linearization programs.

One of the first issues that must be decided is how to specify the steady-state condition, how many of the state and control variables may be chosen independently, and what constraints exist on the remaining variables. A computer program can then be written so that the specified variables are entered from the keyboard, and the independent variables are adjusted by the numerical algorithm which solve the nonlinear equations, while the remaining variables are determined from the constraint equations.

2.9 LINEARIZATION

When we perform a computer simulation to evaluate the performance of an aircraft with its control systems, we almost always deal with nonlinear equations. Such equations are much more difficult to solve than linear ones, and the kinds of possible motions resulting from a nonlinear model are much more difficult to categorise than those resulting from a linear model. It is therefore useful to linearize models in order to gain access to linear analysis methods. It may be that the linear models and linear analysis are used only for the design of the control system (whose function may be to maintain the system in the linear region). Once a control system is synthesised and shown to have desirable performance based on linear analysis, it is then prudent to carry out an accurate numerical simulation of the system with all the nonlinearities in order to validate the performance.

By definition, *Linearisation* is the process of finding a linear model that approximate a nonlinear one. Fortunately, as Lyapanov proved over 100 years ago, if a small-signal linear model is valid near a equilibrium and is stable, then there is a region (which may be small, of course) containing the equilibrium within which the nonlinear system is stable [44]. Thus, we can safely make a linear model and design a linear control for it so that , at least in the neighbourhood of the equilibrium, our design will be stable. Since a very

important role of feedback is to maintain the process variable near equilibrium, such small-signal linear models are a frequent starting point for control models.

Starting with a nonlinear equation and considering small perturbations from the steady-state condition X_e , U_e , linear-coefficient state equations can be derived by expanding the nonlinear state equation in a *Taylor Series* about the equilibrium point (X_e, U_e) . Approximating by the first-order terms, the perturbations in the state, state derivative, and control vectors must satisfy:

$$\frac{\partial f}{\partial \dot{x}} \delta \dot{x} = \frac{\partial f}{\partial x} \delta x + \frac{\partial f}{\partial u} \delta u \quad (2.9)$$

Equation 2.9 can then be rewritten in an implicit linear state-variable form as follows:

$$E \dot{x} = Fx + Gu \quad (2.10)$$

where

$$E = \frac{\partial f}{\partial \dot{x}} \Big|_{x_e, u_e}; \quad F = \frac{\partial f}{\partial x} \Big|_{x_e, u_e}; \quad G = \frac{\partial f}{\partial u} \Big|_{x_e, u_e} \quad (2.11)$$

Lowercase notation has been used to indicate that x and u are perturbations from the equilibrium values of the state and control vectors. By premultiplying the Equation 2.10 by E^{-1} then:

$$\dot{x} = E^{-1}Fx + E^{-1}Gu \quad (2.12)$$

or

$$\dot{x} = Ax + Bu \quad (2.13)$$

where

$$A = E^{-1}F \quad ; \quad B = E^{-1}G \quad (2.14)$$

The coefficient matrices A and B are called *Jacobian* and must be calculated at the equilibrium point. Obviously, for a given flight condition, A and B are time invariant and the resulting state equations are referred to as LTI (Linear-Time-Invariant) state equations.

For the aircraft dynamic and control analysis, usually, equations are needed to be linearised in different steady-state conditions. Therefore, algebraic linearisation is not a convenient way of doing this, because, different steady-state flight conditions may have significantly different dynamics and a linearised equation about one equilibrium point that has been done with certain approximation and assumptions may not be applicable for the other one and it needs another set of linearised equations. This makes considerable inconvenience. As an alternative method of deriving LTI equation from our aircraft model, numerical linearisation can be used. Since a nonlinear simulation model is established in state-space form, it is convenient to use the aerodynamic data and calculate the Jacobian matrices for the LTI equations directly from the nonlinear model. This is done by perturbing the state and control variables from the steady-state condition, and numerically evaluating the partial derivatives in the Jacobian matrices. The Jacobian matrices may therefore be determined for any steady-state flight condition. Figure 2.2 illustrated how this idea fits into the software environment.

2.10 VERIFICATION AND VALIDATION

The very important parts of the process of developing a useful computer simulation are verification and validation of the underlying mathematical description. According to Reference [48], *verification* is defined as being concerned with proving that a computer based description is consistent with the underlying mathematical or conceptual model to a specified degree of accuracy. *Validation*, on the other hand, is concerned with demonstrating that the mathematical or conceptual model has a satisfactory accuracy over the range of conditions relevant for the intended application. Since these two words are often confused and used interchangeably, it is useful to use the words *internal* and *external*, respectively, when discussing verification and validation. The processes of 'internal verification' and 'external validation' are then clearly and distinctly separated. This gives emphasis to the fact that the processes leading to model verification should provide proof of the internal consistency of the model and the associated software whereas the assessment of external validity of the model involves questions of judgement to a greater extent.

2.10.1 Internal Verification [48]

The criteria for internal verification may be summarised as follows:

- a. Internal consistency of the model and the associated computer program in that they can be shown to involve no logical, mathematical or conceptual contradictions.
- b. Algorithmic validity of the computer-based model such that the algorithms and associated programs can be shown to be appropriate and leads to solutions with a specified numerical accuracy.

Internal verification processes are important at every stage of model development. All proposed changes within an established model must also be subjected to careful assessment in terms of these internal verification criteria.

2.10.2 External Validation Criteria [48]

Criteria for external validation are concerned with assessment of the suitability and accuracy of the model in the context of its intended application and include the following issues.

- a. Theoretical validity in that model is consistent with currently accepted theories or based upon some sound theoretical foundation.
- b. Empirical validity in terms of agreement between the behaviour of the model and all of the available data concerning the real system.
- c. Pragmatic validity in terms of the extent to which the model satisfies the requirements of the intended application.
- d) Heuristic validity in terms of the potential of the model for hypothesis testing, explanation and discovery.

The most important of these four criteria in practical modelling applications are usually the empirical and theoretical criteria. These should be considered at every state of model

development and evaluation. Empirical validity is especially important and has to be assessed not only during model development but also throughout the subsequent application. If at any stage the model does not satisfy this criteria it is essential to return to the theory and to the data which form the basis of the mathematical description. Additional tests on the real system may be necessary as part of this process of model refinement.

CHAPTER THREE GENERAL METHODOLOGY

3.1 INTRODUCTION

Having discussed the requirement of a simulation model in Chapter 1, the next step is to develop the vehicle mathematical model. The mathematical model of the considered VTOL configurations is a combination of multibody dynamics and VTOL aerodynamics which are both fundamentally complicated phenomena. Therefore, the existing well-established methods for mathematical modelling of the conventional aircraft are not applicable to this case. In addition, as it is also pointed out in Chapter 1, there is no specific data available. What should actually be investigated by the simulation model is the feasibility of the concepts. This, in turn, demands a high level of generality and flexibility for the mathematical model. In the following sections, it is intended to explain the important issues and the kind of restrictions that were faced at the beginning of the model construction. Considering the issues, an ad hoc methodology was devised to meet all the requirements.

3.2 PROBLEM DEFINITION AND METHOD OF APPROACH

Dynamic Complexity

The dynamics of the mentioned VTOL configurations is much more complicated than conventional aircraft, principally due to the relative movement of several massive parts such as propellers, nacelles, wings and fuselage. These vehicles

have ten degrees of freedom instead of six degrees of freedom associated with conventional aircraft. In fact, they can be considered as articulated flying structures.

In these vehicles the c.g. and mass moment of inertia are not fixed. They change during transition or anytime that tilt angle controls are active. These changes may happen unsymmetrically, for example in yaw control during hover. Therefore, unlike conventional aircraft, the usual assumptions such as fixed c.g. location, fixed mass moment of inertia and aircraft symmetry can not be made in mathematical modelling of the aircraft. The time rate of change of inertia and c.g. position are the issues that must be considered in the derivation of the aircraft equations of motion.

The other important features of a VTOL vehicle is to have large diameter propellers, needed to produce sufficient lift in the helicopter phase. The considerable mass and inertia of these kind of propellers together with high rotational speed may cause significant gyroscopic effects whenever the propeller axis experiences an angular velocity in space. It may happen either due to the control system action (active tilt angle control) or when transition takes place, or even, when the aircraft flies on a curvilinear trajectory.

Aerodynamic Complexity

A VTOL aircraft typically flies in three different regimes including, low speed flight, transition flight and cruising flight. Because of flying in different conditions the aircraft aerodynamics is more complicated than the aerodynamics of a conventional aircraft. This complexity is principally due to three facts.

First, the wide range of angle of attack and sideslip that aircraft is subjected to. In low speed flight, aircraft is capable of flying rearward and sideward as well as forward. In addition, it ascends and descends vertically, therefore, it experiences angles of attack in the range of -180 to $+180$ deg. and sideslip angle from -90 to $+90$ degree. Moreover, due to the different flight conditions, propellers have to operate at angle of attack within -90 to $+90$ deg.

The second fact is the considerable aerodynamic effect of the propellers slipstream on the other components, in particular wings that in the considered configurations are fully immersed in the propeller's slipstream. The propeller slipstream influences the local velocity vector acting on the vehicle airframe. When the aircraft is operating at low speed the velocity of the propeller induced flow is at its maximum, as transition takes place the vehicle accelerate and the velocity of the induced flow reduces until it reaches its minimum in aeroplane mode. Consequently, the slipstream effect is in its most severe condition during low speed flight in helicopter mode.

The direction and the strength of the propeller slipstream are not constant. They depend on airspeed, propeller induced velocity and tilt angle. Thus, they change in terms of flight condition. It means that if one component is immersed in the propeller slipstream for a certain flight condition, it may not still be located in there if the flight condition changes. When calculating the aerodynamics of the aircraft it is important to specify which parts of the aircraft are affected by the propellers slipstream at the time. It should be pointed out that the components primarily influenced by the propeller flow field are horizontal and vertical stabilisers, wing and nacelles.

Different Configurations

As pointed out in Chapter 1, there were three different VTOL concepts to be simulated. The concepts had similarities in multibody system and baseline shape. Therefore, it was decided to take benefit of having these similarities and avoiding development of separate simulation model for each of them. As a consequence, the need for generality was further increased.

Lack of Data

The shortage of any specific data was the other important problem in the development of the simulation model including mass, inertia, engine and aerodynamics. Due to the mentioned aerodynamic complexity, a huge number of data over a wide range of angle of attack and sideslip angle was required to entirely cover the flight envelope associated with VTOL flight. The estimation of these data for three different configuration was not possible by using existing data sheets which are limited to small aerodynamic angles.

Flexibility Requirement

In order to be used as a research tool, the simulation model had to be sufficiently general and flexible so that the user has a large amount of freedom in specifying the components' characteristics individually. In this way, there is no need for re-estimating the aircraft characteristics for every single change in the components' specifications during research work.

Method of Approach

Regarding the mentioned requirements, difficulties and restrictions, the only way which could lead to development of a simulation model was to consider the aircraft as a combination of a number of the separated elements. The aircraft modelling could then be carried out by integrating the model of these individual components. This method is called the Object-based approach in the present work and is explained in the following section. An assessment of the approach is also provided at the end of this chapter.

3.3 THE OBJECT-BASED MODELLING

The structure of the approach which has been used to develop the simulation model of an articulated aircraft is shown in Figure 3.1. In this approach the aircraft is considered to be composed of several elements grouped as 'MAIN' and 'SECONDARY' objects (M.O. and S.O.). The first group is in fact the multibody system which is used to derive the general equations of motion of the vehicle. It includes five main objects A , $'n$, $'n$, $'p$ and $'p$. In Figure 3.2 a better representation is given. The second group is the group of objects of which the dynamics of the aircraft is a result of their characteristics, i.e. mass, inertia, size, position and aerodynamics. This group includes fuselage, vertical and horizontal stabilisers, wings, nacelles, engines, servomotors and propellers. The location of each of these objects in the real aircraft is shown in Figure 3.3.

The chart in Figure 3.1 shows, how different elements are related to each other and what kind of information is needed to build up the simulation model. In this chart, fixed connections are shown by the solid lines. Those lines that are ended

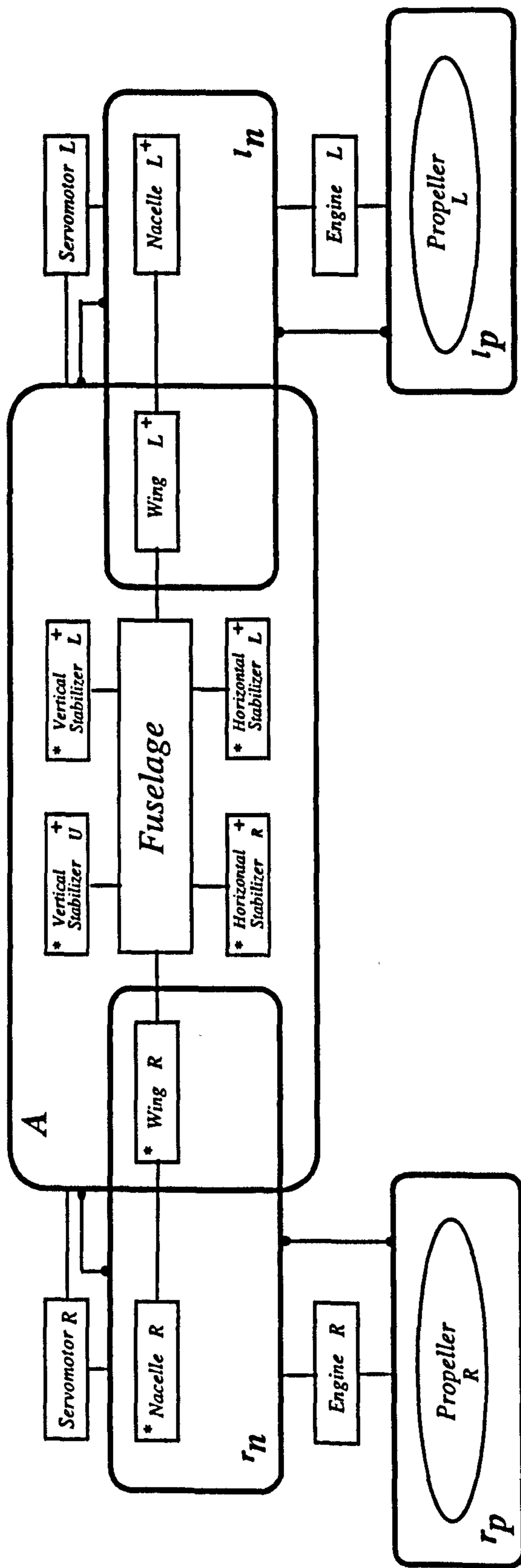


Fig. (3.1): The structure of the object-based approach

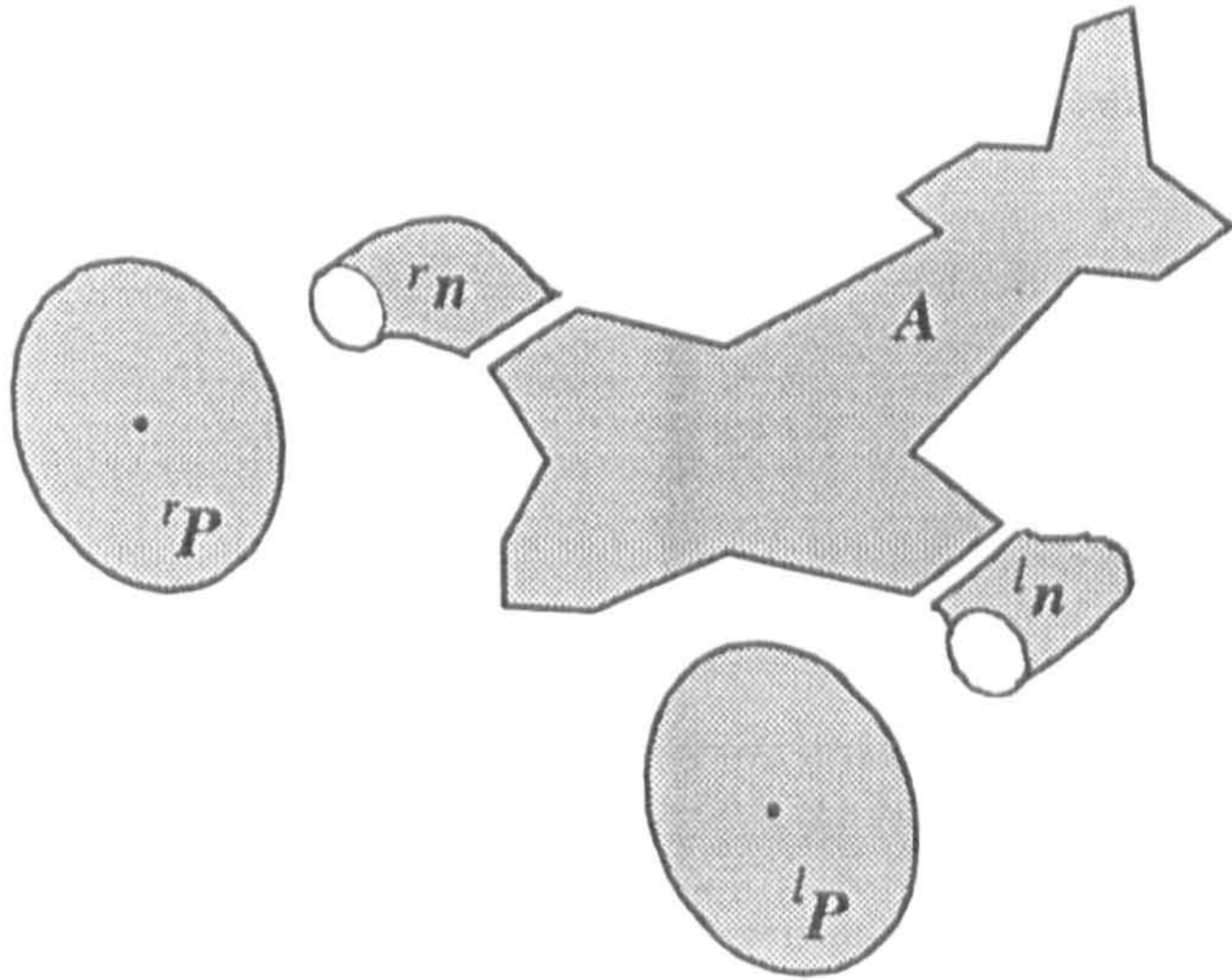


Fig. (3.2): The main objects

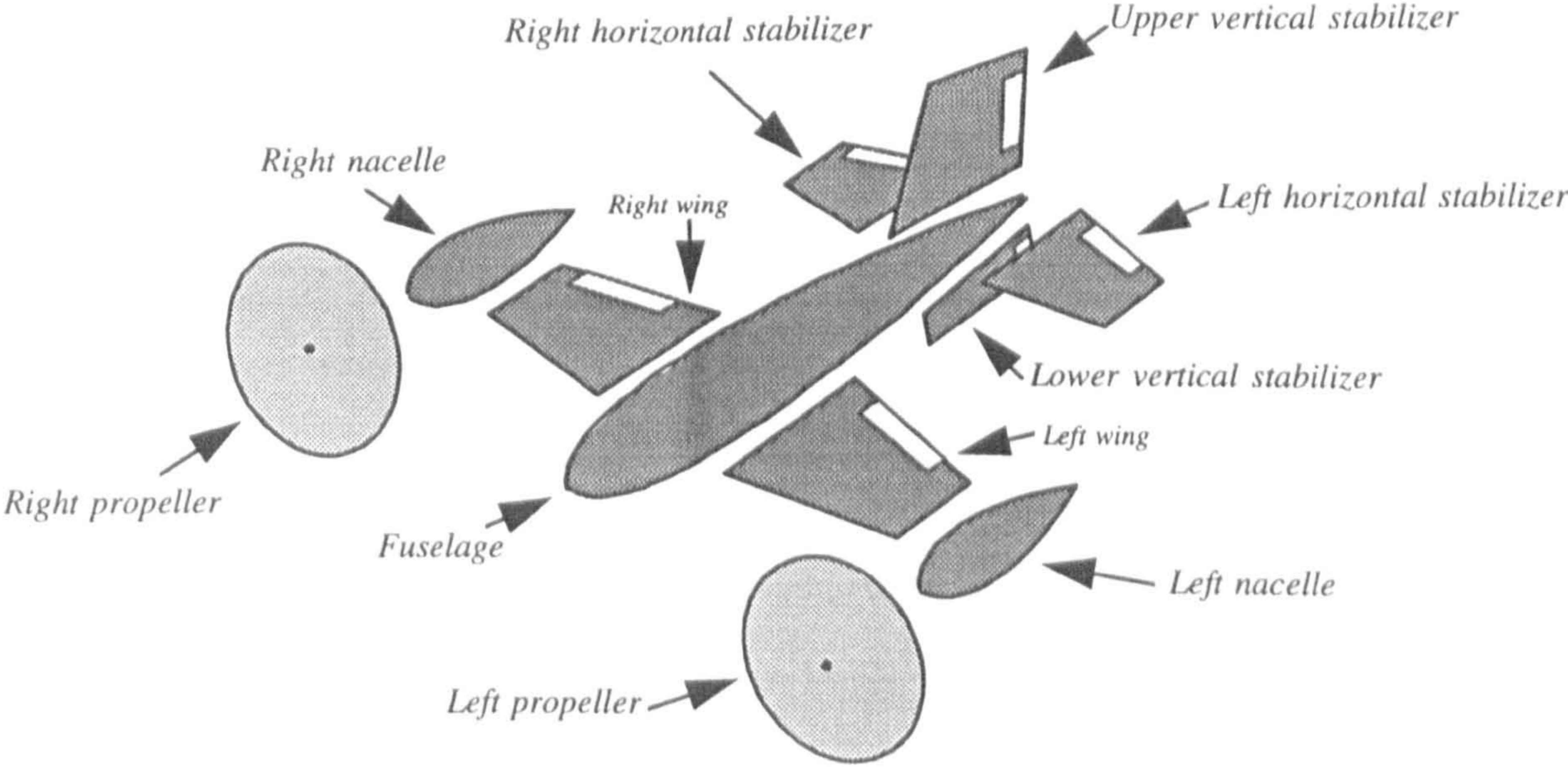


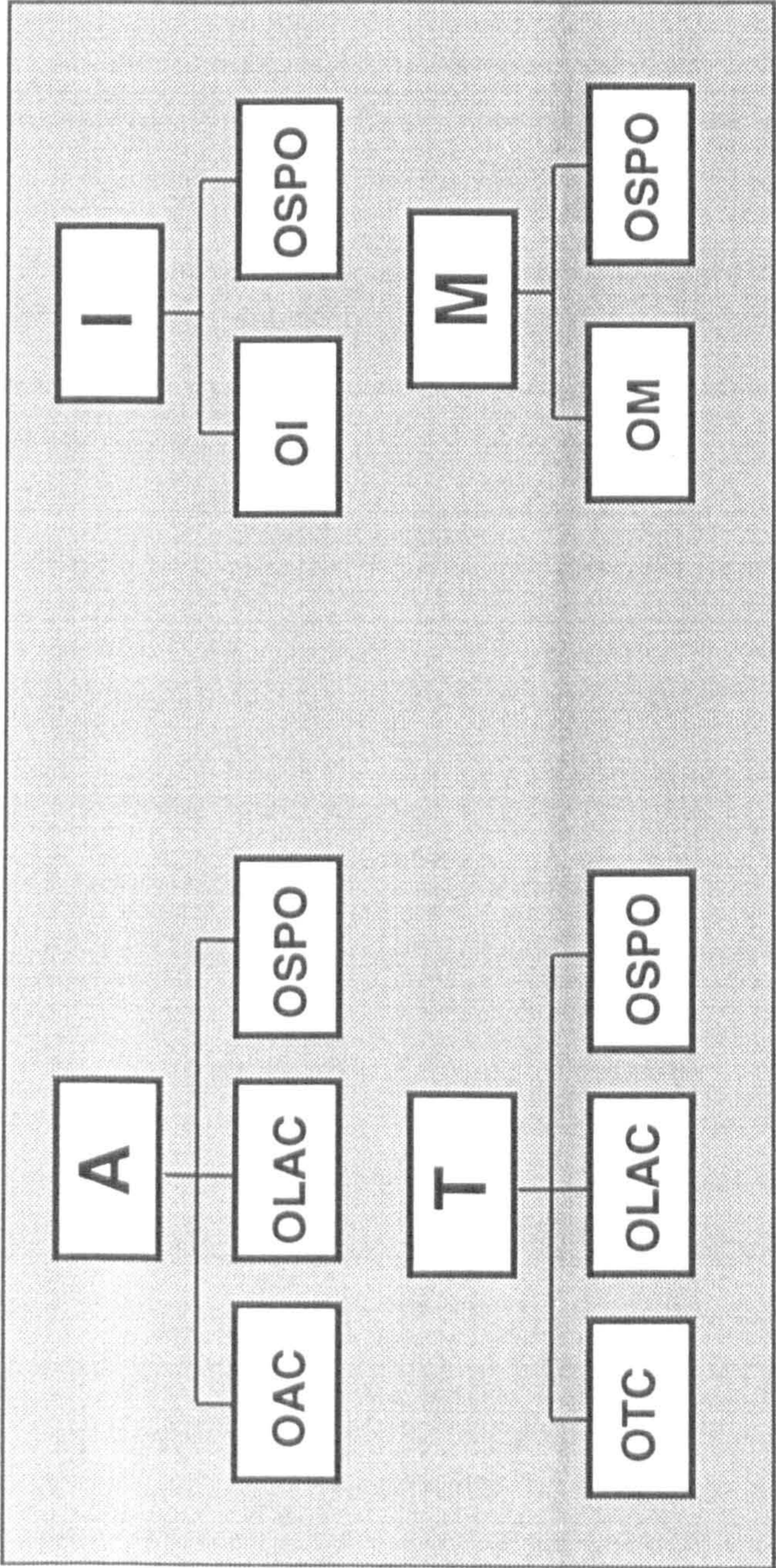
Fig. (3.3): The secondary objects

by the small filled circles indicate that two objects are connected through revolute joints. The signs '*' and '+' indicate that the S.O. may be affected by the right and left propeller's slipstream, respectively.

The primary information to build up the model are aerodynamic forces and moments, inertia, mass and thrust characteristics of each object. For a secondary object, these kind of characteristics are shown by a number of BOXes which are titled by A , I , M and T . An A box contains all the necessary information to establish the aerodynamic model of the corresponding object. In other words, it provides aerodynamic forces and moments generated by that object. The boxes I and M contain inertia and mass characteristics, respectively, and T is a box to represent generated thrust forces and moments by the object.

Each of these boxes can be divided into the smaller internal parts of information which are called UNITS as shown in Figure 3.4. A 'UNIT' can be considered as the smallest independent pack of information which should be available at any time during simulation. The information inside the units OAC , OI , OM , OTC should be given as the inputs to the simulation model. Note that, the T box only appears for the main objects $'p$ and $'l$. It should be pointed out that the propeller slipstream effect will be manifested by changing the local flow characteristics over the other parts of the aircraft. Therefore, these effects have automatically been considered in the $OLAC$ unit of an object. The $OSPO$ unit is an essential part of each box. It is useful for transformation of values from a data defined axes system to a main axes system.

An M.O. is a single rigid body which is connected to other parts by revolute joints. It moves in space while subjected to external aerodynamic loads and reaction forces and moments at the joints. The dynamics of an M.O. can be expressed by the equations of motion of a single rigid body. Each main object can be a collection of the secondary objects which are fixed together and have the same velocity and acceleration as the main object. The aerodynamic forces and moments, inertia and mass of a main object can be determined by a summation of all the partial values of its secondary objects as follows:



BOXes:

- A** : Aerodynamic characteristics
- I** : Inertia characteristics
- M** : Mass characteristics
- T** : Thrust characteristics

UNITS:

- OAC** : Object Aerodynamic Coefficients
- OLAC** : Object Local Airflow Characteristics
- OI** : Object Inertia
- OM** : Object Mass
- OTC** : Object Thrust Coefficients
- OSPO** : Object Size, Position and Orientation

Fig. (3.4): Definition of BOXes and UNITS

$$\begin{aligned}
 A_M &= \sum_i (A_S)_i \\
 I_M &= \sum_i (I_S)_i \\
 M_M &= \sum_i (M_S)_i
 \end{aligned}
 \tag{3.1}$$

A bigger pack of information can also be defined for an object. This pack is built by a set of the boxes A , I and M , and is called the AIM of an object. Using the above relationships, the AIM of a main object can be defined in terms of the $AIMs$ of its secondary objects as follows:

$$AIM_M = \sum_i (AIM_S)_i
 \tag{3.2}$$

It should be pointed out that due to the nature of the thrust producer objects $'p$ and $'p$, the relevant pack includes an additional box T and it is specially called $AIMT$.

Having established the AIM of a M.O., two other essential parts are needed to complete the model of the M.O. .These two are reactions at the joints and the object kinematics. The OJR , *Object Joint Reactions*, which in fact expresses the boundary conditions of a M.O. can be broken down into the two parts as 'KNOWN' and 'UNKNOWN' joint reactions. The known reactions are those which are produced by servomotor and engine output torque. The unknown reactions are the internal structural force and moment reactions. They will be eliminated from the equations as shown in the following section. The OK , *Object Kinematics*, represents the kinematics of the main objects and contains all the velocities and accelerations.

Relating all of these parts by the single *Rigid Body Equations Of Motion (RBEOM)*, the model of a M.O. will be completed. Figure 3.5 shows all the elements and sub-elements necessary to build up the model of a main object. This model can be demonstrated briefly by the following relationship:

$$MODEL = RBEQM(AIM, OJR, OK)
 \tag{3.3}$$

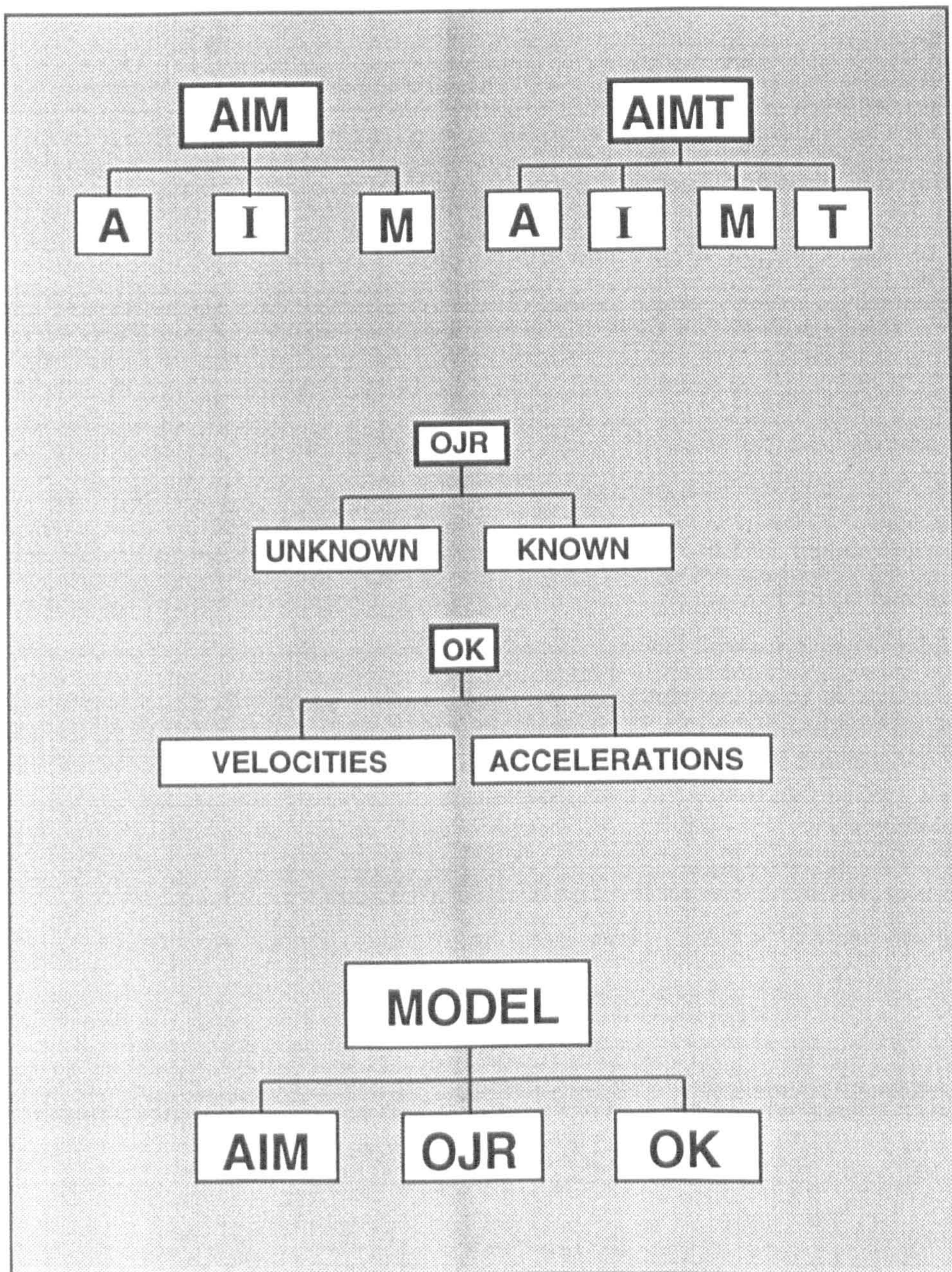


Fig. (3.5): The elements and subelements for model construction

3.4 SIMULATION MODEL

3.4.1 Main Objects

As it is shown in Figure 3.1, the aircraft is composed of five main objects A , $'n$, $'n$, $'p$ and $'p$. The object A represents the fuselage-empennage assembly. Dependant on configuration type, the object n may represent nacelle or nacelle-wing assembly. The former for Tilt-nacelle and the latter for Tilt-wing aircraft. The objects $'n$, $'n$ can rotate relative to the object A through revoluted joints. The objects $'p$ and $'p$ are the right and left propellers which rotate relative to objects $'n$ and $'n$, respectively. The multi-object model contains ten degrees of freedom. Three translation and three rotational degrees of freedom are associated with the object A . Two rotational degrees of freedom are associated with tilting objects $'n$ and $'n$, and the last two rotational degrees of freedom are associated with the objects $'p$ and $'p$. The total mass of the system is:

$$m = m_a + m_{nr} + m_{nl} + m_{pr} + m_{pl} \quad (3.4)$$

Equations of motion

The kinematic similarity of the Tilt-nacelle and Tilt-wing provides the capability of deriving one set of equations of motion for both of them, using the mentioned multi-object system. In addition, when the objects $'n$ and $'n$ are fixed at zero tilt angle, the model can also represent the dynamics of a Tail-sitter. According to Equation 3.3, the model of all main objects can be demonstrated as follows:

$$\begin{aligned} \text{MODEL } A &= \text{RBEQM}_A (\text{AIM}_A, \text{OJR}_A, \text{OK}_A) \\ \text{MODEL } 'n &= \text{RBEQM}_n (\text{AIM}_{nr}, \text{OJR}_{nr}, \text{OK}_{nr}) \\ \text{MODEL } 'n &= \text{RBEQM}_n (\text{AIM}_{nl}, \text{OJR}_{nl}, \text{OK}_{nl}) \\ \text{MODEL } 'p &= \text{RBEQM}_p (\text{AIMT}_{pr}, \text{OJR}_{pr}, \text{OK}_{pr}) \\ \text{MODEL } 'p &= \text{RBEQM}_p (\text{AIMT}_{pl}, \text{OJR}_{pl}, \text{OK}_{pl}) \end{aligned} \quad (3.5)$$

It should be noticed that, due to the similarity of the right and left sides of the aircraft, the same set of equations of motion are used for each pair of objects $'n$, $'n$ and $'p$, $'p$. Using relation 3.2, then:

$$\begin{aligned}
 AIM_A &= AIM_b + conf1 \cdot (AIM_{wr} + AIM_{wl}) \\
 AIM_{'n} &= AIM_{nr} + conf2 \cdot AIM_{wr} \\
 AIM_{'n} &= AIM_{nl} + conf2 \cdot AIM_{wl} \\
 AIMT_{'p} &= AIMT_{pr} \\
 AIMT_{'p} &= AIMT_{pl}
 \end{aligned} \tag{3.6}$$

Where, the subscript b denotes the fuselage-empennage assembly. Therefore

$$AIM_b = AIM_{fu} + AIM_{hr} + AIM_{hl} + AIM_{vu} + AIM_{vl} \tag{3.7}$$

By eliminating the unknown part of OJR between each two connected main objects, the general equations of motion can be determined in the matrix form as follows,

$$M_{10 \times 10} \cdot \ddot{S}_{10 \times 1} = F_{10 \times 1} \tag{3.8}$$

In this equation, M is the mass matrix, \ddot{S} is the acceleration vector and F is the force vector.

Various configurations

In terms of the aircraft configuration, the right and left wing can be contributed as a part of main body A or as a part of tilting body $'n$ or $'n$. Thus, two codes $conf1$ and $conf2$, presented in Equation 3.6, have been considered to express the kind of contribution that a wing can make. These codes are defined as:

$$\begin{aligned}
 \text{Tilt-nacelle: } & conf1 = 1.0 ; conf2 = 0.0 \\
 \text{Tilt-wing } & : conf1 = 0.0 ; conf2 = 1.0
 \end{aligned} \tag{3.9}$$

For a Tail-sitter aircraft, tilt angle movement is not primarily used as a controller input. Thus, the objects $'n$ and $'n$ are considered fixed to the main body. Therefore, no matter which set of the $conf$ codes is selected, the same result

will be obtained. However, if attempt is made to use tilt angle control as a complementary controller for the Tail-sitter configuration then a decision must be made whether the aircraft is a Tilt-nacelle tail-sitter or a Tilt-wing tail sitter. Having specified the type of the aircraft, the appropriate set of *conf* codes should be selected. It should be pointed out that when tilting objects ' n ' and ' n ' are fixed to the main body, the equations of motion must be rearranged to consider the change in system degrees of freedom. This issue is discussed in the following section.

Transition

The transition is a process during which the flight mode is changed from helicopter to aeroplane or vice versa. Whenever transition takes place the degrees of freedom of the system will be changed since in aeroplane mode tilting objects are fixed. Therefore, two degrees of freedom are absent from the system and the order of the governing system of equations reduces to eight. This causes discontinuities in the simulation model whenever transition occurs. However, using the same system of equations, the discontinuities can be managed by substituting a value of zero for all non-diagonal terms of the rows and columns corresponding to right and left relative angular accelerations in the mass matrix and the total force vector. In other words, the relative angular velocities and accelerations between the tilting objects and the main object A are forced to be zero during wing-borne flight. As soon as, the system becomes unlocked, the full order system will be applied again.

3.4.2 Secondary Objects

As shown in Figures 3.1 and 3.2, the vehicle is composed of fifteen secondary objects. In terms of characteristics, these objects can be grouped as 'Airfoils' , 'Bodies' , 'Propellers' , 'Engines' and 'Servomotors' .

The airfoils and bodies are the major drag and lift producers in the aircraft. Due to the aerodynamic complexity and nonexistence of a real sized aircraft, the estimation of the aircraft aerodynamic forces and moments acting on the airframe for three VTOL configurations, regarding the associated range of angle of attack and sideslip is impossible. Therefore, it seems to be most convenient to consider

the constituent parts of the vehicle separately and evaluate the corresponding force and moment contributions for each of them. The individual contributions are then summed up to produce the overall forces and moments acting on the vehicle. This idea is well-matched with the concept of object-based modelling. Using this concept, it is possible to express the force and moment contribution of each airfoil or body separately, using local airspeed, angle of attack and sideslip. The aerodynamic data is now much easier to estimate for each separate element, although it is less accurate.

The group of airfoils contains, the right & left wings, the right & left horizontal stabilisers and the upper & lower vertical stabilisers. Each airfoil is considered to be rectangle with a control surface centered at the middle of the length. A typical airfoil is shown in Figure 3.6. For simplicity of data preparation, the same airfoil section is considered for all the airfoils. In Figure 3.6, intention is to show all the necessary information required to built up the *AIM* of an airfoil. Having aerodynamic dimensionless coefficients of the selected airfoil section (C), mass & inertia (M&I), local absolute velocity vector (V), size (a,b), position (L) and orientation (λ) of each member of the group, the associated *AIM* can be constructed.

The group of bodies includes the fuselage and the right & left nacelles. Again, for the sake of simplicity the same streamline shape for all the bodies is considered. A typical streamline body is shown in Figure 3.7. Same as airfoils, by having similar set of information, the *AIM* of all members in this group can be established.

The group of propellers has two members which are the right and the left propellers. These components are the thrust producer elements in the aircraft. Therefore, as stated before, modelling of these objects needs some extra information about their thrust characteristics. This characteristics are provided by associated T box. As shown in Figure 3.8, to build up the *AIM* of a propeller, information about the aerodynamic coefficient (C), mass (M), inertia (I), size (D), position (L), pitch angle (θ_p), orientation (θ_n), speed (N), local velocity (V), and the thrust and power coefficients (C_t , C_p), are needed.

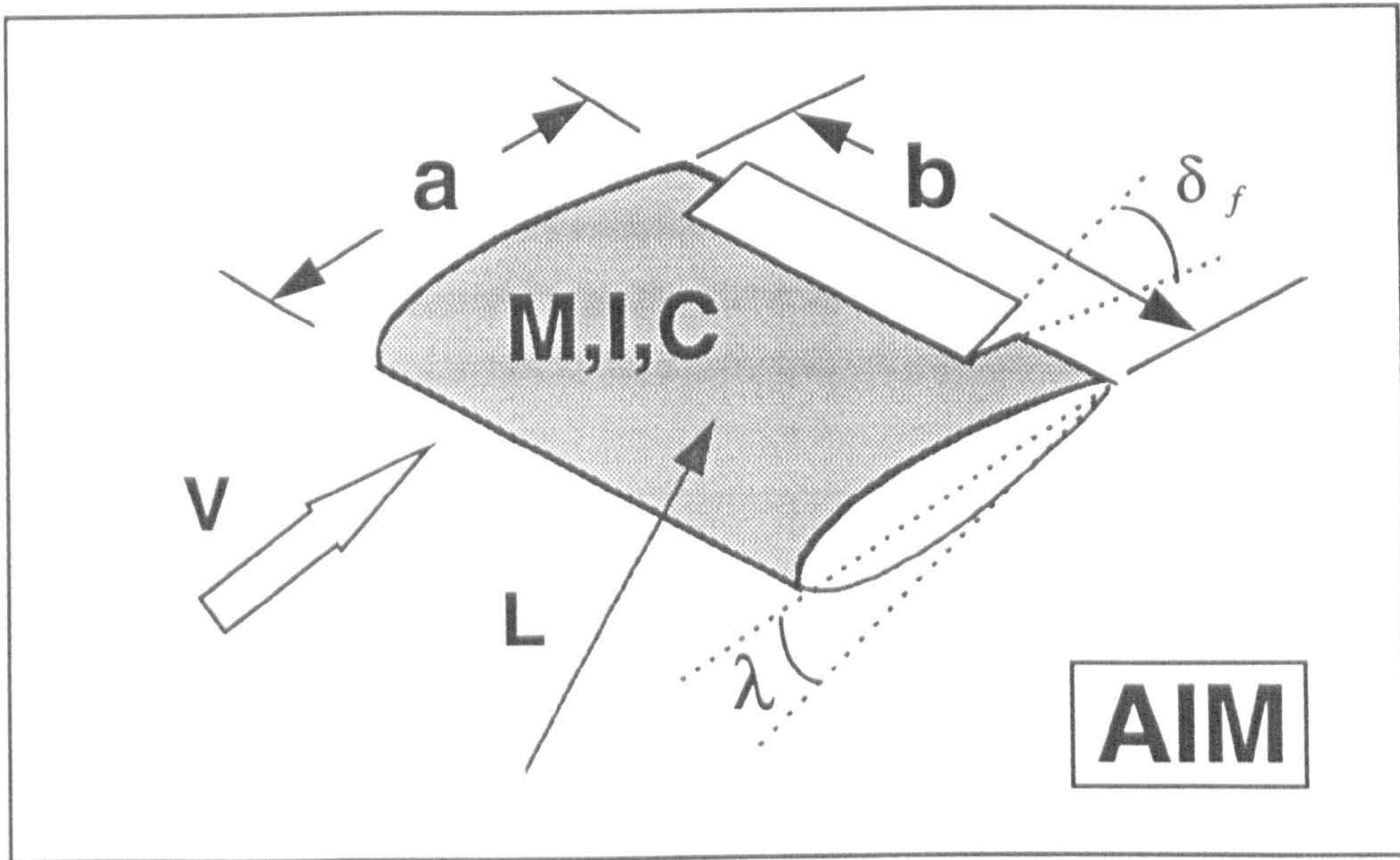


Fig. (3.6): A typical airfoil

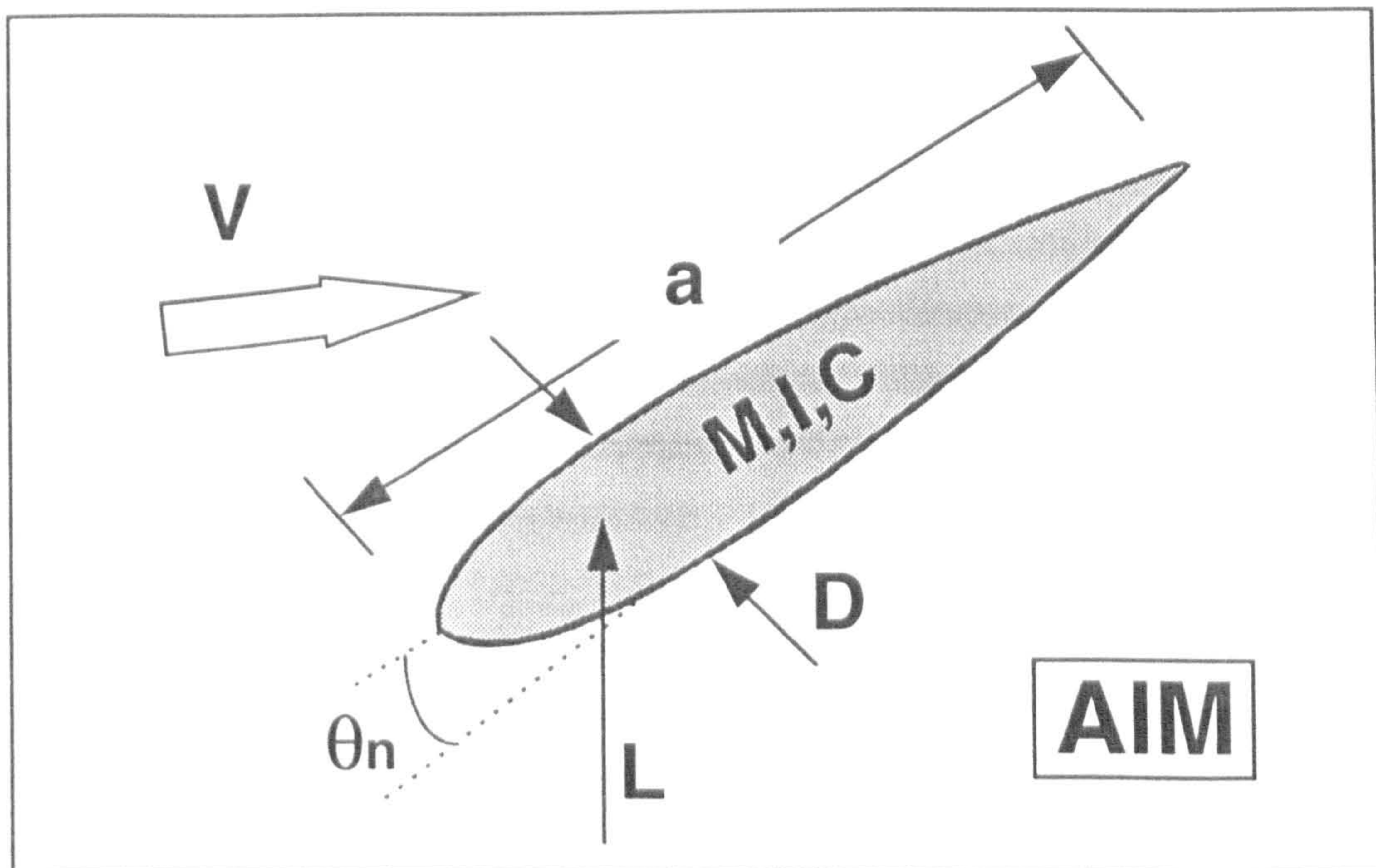


Fig. (3.7): A typical streamline body

The engines and servomotors are supposed to be placed in the fuselage. Hence, there are no independent *AIM* associated with these objects. The modelling of these objects can be carried out in terms of their output power and torque characteristics. As shown in Figure 3.9, engines may be modelled by a function which expresses the engine output power in terms of the rpm and throttle setting. The model of the servomotors can be expressed in terms of a relationship between the output torque and the input command. The level of complexity of the servo model is arbitrary and depends on the desired accuracy.

3.5 ASSESSMENT

The previously presented methodology is the foundation of all the mathematical modelling in the following chapters. Therefore, it is worthwhile having an overall assessment about the different features of the methodology which is the subject of this section.

The nature of the approach is to consider the main bodies as separate elements. Then, the single body equations of motion is used to integrate all the related parameters of each element including reactions with the other components. This procedure is well-matched with the methods commonly used to derive the equations of motion of multibody systems. Its major benefit is to simplify the derivation of the complex equations associated with multibody structures. Using the object-based approach, the general equations of motion of the aircraft articulated structure can be derived straightforwardly without explicitly dealing with the rate of change of inertia and center of gravity position.

In this methodology, all the similarities between components, e.g. the similarity of being an airfoil or streamline body, and configurations, e.g. having kinematic similarity, are well used to keep the simplicity and modularity of the simulation model. This has been one of the main priorities throughout the model construction. As a result, the existing model has a modular structure that simplifies modification tasks. One benefit of it, is that the model improvement

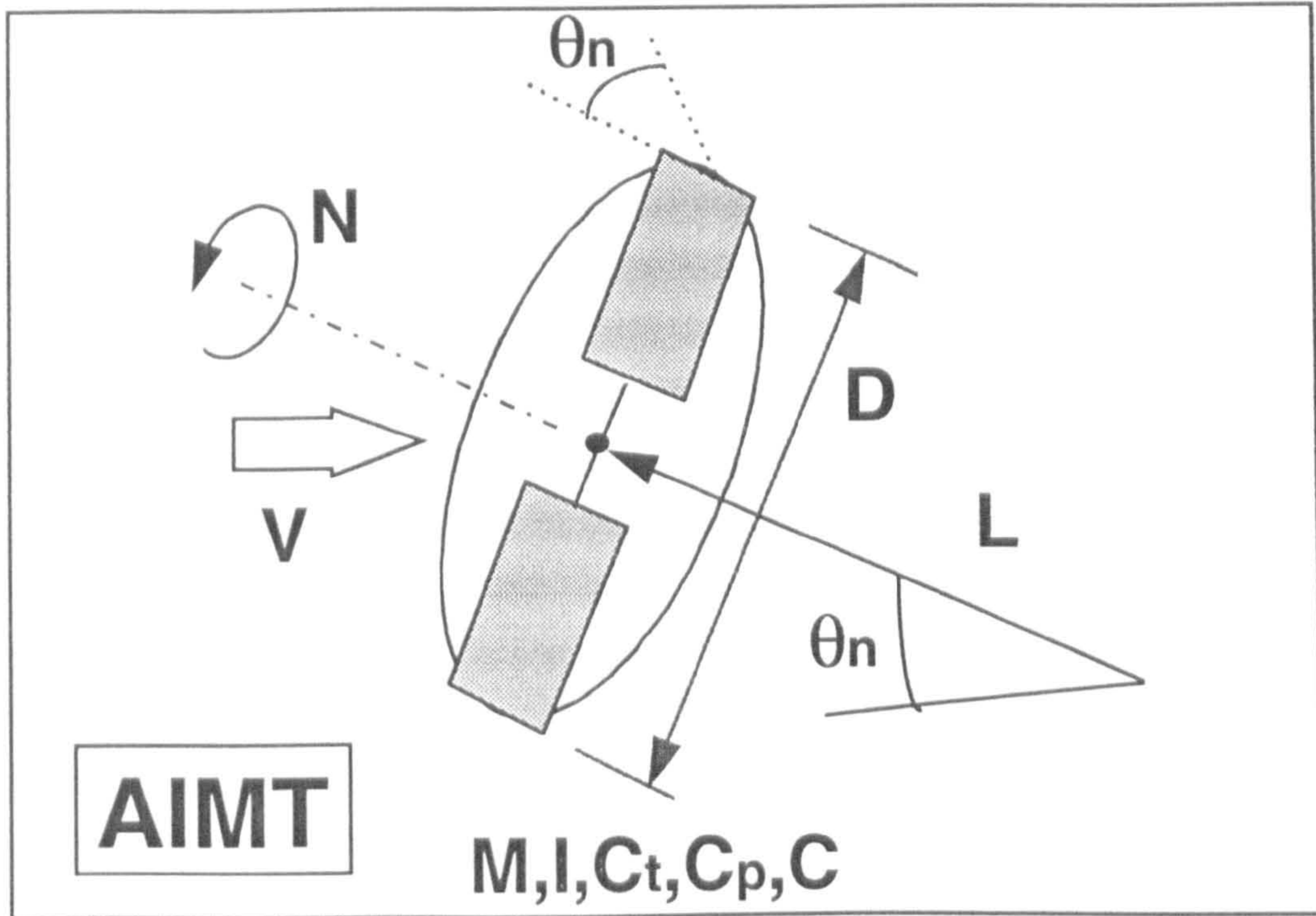


Fig. (3.8): A typical propeller

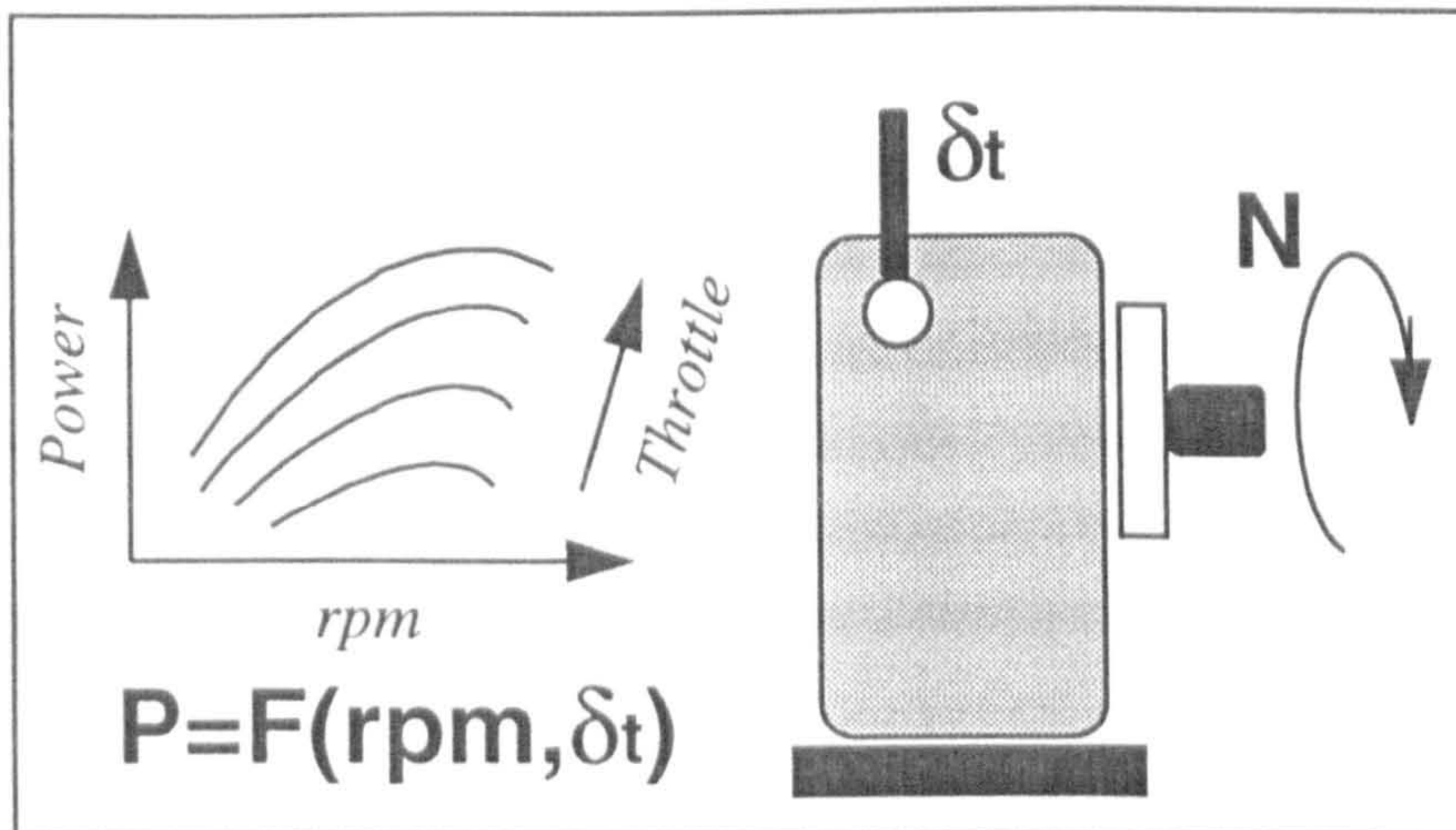


Fig. (3.9): The engine model

may be made at subsystems level while maintaining the integrity of the rest of the model.

Investigation of the effects of many different factors, such as mass and inertia distribution, aerodynamics of different parts and the characteristics of the propellers, engines and servomotors, etc. on the flight dynamics of the vehicle is quickly and easily achievable by exchanging the relevant *UNITs* in the simulation model. For example, the effect of different set of wing airfoil data on the performance of the system can be examined simply by exchanging the *OAC* unit of the wing. In the same way, the effect of mass distribution can be investigated by exchanging the *OM* and *OSPO* units of different objects. The simulation model is therefore provided the capability of being a suitable research tool. It can also be used as a tool for the initial sizing of the aircraft, considering all factors, including desired control tasks.

Due to the modular nature of the model, the control surface of each airfoil can be considered to be activated independently. Therefore, the available number of control surfaces are now more than those for a conventional aircraft. Hence, the possibility of using all these independent control surfaces which are probably necessary to manage the complex control tasks can be investigated. In particular case, the conventional control surfaces, i.e. elevator, aileron and rudder can be formed by appropriate surfaces being forced to be deflected together.

As discussed previously, if the modelling of the aircraft had been carried out in the usual way the amount of required aerodynamic data would have been huge. One of the most important features of the object-based modelling is the reduction in the amount and the variety of the required aerodynamic data. In the present simulation model the required aerodynamic data is limited to only two sets of data associated with a simple airfoil and streamline body.

It should be pointed out that the accuracy of the estimated data in considering three dimensional effects and the aerodynamic interaction between components has direct influence on the accuracy of the aerodynamic model. The better the estimation, the more accurate the aerodynamic model. However, even in the less accurate case the generality of the model to predict all the main aspects of a

VTOL flight is still satisfactory. Since the aerodynamic interaction is minimum when the angles of attack and sideslip are small, the aerodynamic model is in its most accurate time in this condition.

It may seem that the accuracy of the aerodynamics is somewhat sacrificed in favour of the generality. However, regarding the objectives and the amount of the available data, it is a good achievement to be able to develop the simulation tool. In fact, the object-based approach introduces a trade-off between generality, flexibility and accuracy requirements.

The other important benefit of using this approach is the development of one simulation model for all configurations and for three different flight conditions, helicopter, transition and aeroplane. This approach also provides the facility of accounting for the influence of the propellers slipstream on different parts of the airframe.

It should be emphasised that the reduction in the computational time has never been an objective in the current object-based modelling. Therefore, there is no claim that the resulted computer program is going to have a satisfactory run time characteristics or can ever be used for real time computing. Instead, due to the well-provided modularity, relatively easy debugging, verification and testing of computer program was expected and observed.

CHAPTER FOUR

EQUATIONS OF MOTION

4.1 INTRODUCTION

The baseline of the model development was established in the previous chapter. In this chapter, the equations of motion of the aircraft multibody system will be derived. The derivation of these equations will be started from very basic forms of the Newton's second law and will be ended by a state-space form. To be referred, almost all details are presented, mainly in the complementary appendices.

4.2 FORMULATION METHOD

Probably the most commonly used method to derive the equations of motion of a multibody system are Newton-Euler and Lagrangian methods. In the use of the Newton-Euler method the free-body diagrams of each body of the system are examined. Force and moment balances then leads to the governing equations. Thus, the equations contain interactive and constraint forces acting between the bodies. To find the general form of the equations of motion the unknown constraint reactions should be eliminated from the dynamical equations. This can be carried out by consideration of the geometrical and kinematical equations describing the nature of the constraint. When the system consists of more than one body, the need to account individually for the constraints associated with each connection substantially enhances the level of difficulty. However, the

procedure is comprehensive in that all forces and kinematic variables are included in the analysis. Due to the vectorial nature of the equations, it is also called vectorial mechanics.

Another approach for formulating the dynamic equations of motion is Lagrange's method. While vector quantities are used in Newtonian mechanics, scalar quantities such as kinetic energy, potential energy and work done by the forces acting on the systems are used in Lagrangian dynamics. In Lagrangian dynamics the concepts of the virtual work and virtual displacement are important. The system equations of motion are expressed in terms of a set of generalised coordinate and associated generalised forces. Using Lagrange's method the differential equations of motion expressed in the independent coordinate's of the problem can be obtained by a differentiation of the energy written in these same generalised coordinates. The method has the advantage of not involving the forces of constraint which do no work and which often complicate the formulation of the equations of motion. In other words, non-working interactive and constraint forces are automatically eliminated from the analysis. However, a disadvantage of using Lagrange equations is that scalar energy function needs to be differentiated. This does not usually present any difficulty for small multibody systems. However, for large multibody system, the differentiation are extremely cumbersome and unwieldy.

According to Reference[49], it is not clear that a completely objective answer can be given to the question of whether a Lagrangian type or Eulerian type formulation is the best for multibody dynamic analysis. The various routes lead to the same place, in principal, but they may differ in the degree to which they satisfy the criteria for general purpose computer simulation for a specific problem. Therefore, each problem seems to require its own particular insight. For aerospace vehicles dynamic analysis, vectorial mechanics has always been used as the method of derivation of the equations of motion. This method is the best-known and most physically direct method. On the other hand, there is no demonstrable advantage of the Lagrange method over the Newton-Euler method. Particularly for the present work where knowledge of the internal reactions is important. The Newton-Euler method is therefore used to derive the equations of motion associated with aircraft multibody system.

4.3 VECTOR FORMULATION

As stated earlier, the starting point for the derivation of the aircraft equations of motion will be the vector form of Newton's second law of motion. The magnitude and direction of the three dimensional vectors used in the dynamic analysis are in general independent of the coordinate system in which they are expressed, but components are not. Many mechanics texts treat vector quantities at a very abstract level and routinely use vectors defined relative to different coordinate systems in expressions. The clearest example is that of addition of vectors which are given or known relative to different reference systems. This is often very convenient and leads to compact and somewhat elegant formulas. However, unless these vectors are expressed with respect to a common coordinate system, they can not be summed, and so while elegant, the formulae have hidden much of the work of the computation. Therefore, it is common practice to use superscript and subscript on a vector symbol to indicate both the nature of the vector and the frame in which it is expressed. In this way, all the necessary information is carried with the vector notation and expressions may be applied directly to actual numerical computation.

In the development of the equations of motion, a given vector may be needed to be expressed in several different coordinate frames. When a vector is specified in a new coordinate frame its magnitude and direction are unchanged and only the coordinates of the vector are changed. This simply means that the vector is resolved along the instantaneous directions of the coordinate axes as if it emanated from the coordinate origin.

4.4 NOTATIONS AND CONVENTIONS

The number and variety of variables used in this thesis are quite large. Therefore, a general and consistent system of notation and convention is needed to avoid any possible error in the development of the mathematical modelling and its resulted computer program. This system of notation is explained in this section.

Generally, in terms of the type of variables, they are classified as *vectors*, *matrices* or *scalars*. Each variable, regardless of its type, is represented by a symbol usually

accompanied by leading and trailing superscripts and subscripts. The necessary definitions are given in the following. It should be pointed out that despite the apparent complexity, when reader becomes familiar with the notations and conventions, it should be easy to read and follow the text. In addition, it has the advantage of having all the related information being carried with the symbol at the same time.

Vectors

A vector will be denoted by a boldface symbol. The following symbols are considered for some of the main variables.

- V** : Linear velocity
- $\dot{\mathbf{V}}$: Linear acceleration
- $\mathbf{\Omega}$: Angular velocity
- $\dot{\mathbf{\Omega}}$: Angular acceleration
- A** : Aerodynamic force
- F** : Reaction force
- T** : Thrust force
- M** : Moment

Matrices

Matrix quantities are represented in brackets.

Symbol $[\text{DCM}]^{ij}$ denote the Direction Cosine Matrix between two typical axes system i and j.

The components of a typical vector **S** can then be transformed from j to i axes system by:

$$\mathbf{S}^i = [\text{DCM}]^{ij} \mathbf{S}^j \quad (4.1)$$

Transformation of a typical mass moment of inertia matrix **[I]** from frame j to i can be carried out by using the following relationship [46]:

$$[\mathbf{I}]^i = [\text{DCM}]^{ij} [\mathbf{I}]^j [\text{DCM}]^{ji} \quad (4.2)$$

For a typical vector **S** enclosed by brackets:

$$[\mathbf{S}] = \begin{bmatrix} 0 & -S_z & S_y \\ S_z & 0 & -S_x \\ -S_y & S_x & 0 \end{bmatrix} \quad (4.3)$$

This will be used to denote the cross-product matrix corresponding to the $(\mathbf{S} \times)$. A cross-product matrix is a skew-symmetric that is:

$$[\mathbf{S}]^T = -[\mathbf{S}] \quad (4.4)$$

Scalars

Normal non-boldface symbols are used to represent scalar quantities. As well as the other symbols they may have superscripts or subscripts.

Superscripts

On the top right hand side of the symbol indicates the axes system in which the variable is defined.

On the left hand side of the symbol indicates the side of the aircraft with which the variable is associated. It may take r or l indicating right and left side of the aircraft.

Subscripts

On the bottom right hand side of the symbol denotes the name of the symbol. It is not subjected to any strict convention. Nevertheless, the majority of the symbols may not be identified if they are not accompanied by it.

On the bottom left hand side of the symbol is reserved to indicate the reference point of the moment of a force or moment of inertia.

To indicate the components of a vector or a matrix (i.e x,y,z or xx,xy,xz, \dots), they will be added to the bottom right hand side subscript of the symbol.

\mathcal{K} : A dummy index indicating different sides of the aircraft

\mathcal{U} : A dummy index indicating different parts of the aircraft

$\frac{d}{dt}$: This operator indicates the time derivative w.r.t. inertial frame

• : A dot on the top of a symbol indicates the time derivative w.r.t. $X_a Y_a Z_a$ frame

- : An small circle on the top of a symbol indicates the time derivative w.r.t. ${}^n X_n {}^n Y_n {}^n Z_n$ axes.
- ' : A prime indicate time derivative of a symbol irrespective of the axes system

The following fundamental relationships for relative rotation between two coordinate frames are proved in Reference [44,46,49] and will be used later in the derivation of the equations of motion.

If frame j rotate with an angular velocity Ω^j w.r.t. frame i, then :

$$\begin{aligned}
 \text{a) } & \Omega_{ij}^i = -\Omega_{ji}^i \quad ; \quad \Omega_{ij}^j = -\Omega_{ji}^j \\
 \text{b) } & [DCM]^{ji} = -[\Omega^j][DCM]^{ji} \\
 \text{c) } & [\Omega_{ij}^i][DCM]^{ij} = -[DCM]^{ij}[\Omega_{ji}^j]
 \end{aligned} \tag{4.5}$$

At the same time the following relationships are valid for the rate of change of a typical vector \mathbf{S} :

$$\begin{aligned}
 \text{a) } & \frac{d^i}{dt}(\mathbf{S}^j) = \frac{d^j}{dt}(\mathbf{S}^j) + \Omega_{ji}^j \times \mathbf{S}^j \\
 \text{b) } & \frac{d^i}{dt}(\mathbf{S}^i) = \frac{d^i}{dt}([DCM]^{ij}\mathbf{S}^j) = \frac{d^i}{dt}([DCM]^{ij})\mathbf{S}^j + [DCM]^{ij} \frac{d^j}{dt}(\mathbf{S}^j)
 \end{aligned} \tag{4.6}$$

Finally, we may have occasions to use the derivative of a cross product. The following rule will be useful. For typical vectors \mathbf{S} and \mathbf{P} :

$$\begin{aligned}
 \frac{d}{dt}(\mathbf{S} \times \mathbf{P}) &= \frac{d}{dt}(\mathbf{S}) \times \mathbf{P} + \mathbf{S} \times \frac{d}{dt}(\mathbf{P}) \\
 \mathbf{S} \times \mathbf{P} &= -(\mathbf{P} \times \mathbf{S}) \\
 a(\mathbf{S} \times \mathbf{P}) &= (a\mathbf{S}) \times \mathbf{P} = \mathbf{S} \times (a\mathbf{P}) \\
 \mathbf{S} \times (\mathbf{P} + \mathbf{T}) &= (\mathbf{S} \times \mathbf{P}) + (\mathbf{S} \times \mathbf{T})
 \end{aligned} \tag{4.7}$$

4.5 DERIVATION OF THE EQUATIONS OF MOTION

In this section the equations of motion of the aircraft will be derived and expressed in the state-space form. The selected states are the linear and angular velocities of the main body A , relative angular velocity of the bodies ${}^r n$ and ${}^l n$ w.r.t. the body A , and relative angular velocity of the bodies ${}^k p$ w.r.t. the body ${}^k n$. To keep the brevity, only the highlights of the derivation of the equations are represented. The complete procedure is presented in Appendices A1, A2, A3 and A4. Having defined all the variables in the list of symbols and using extensive set of subscripts and superscripts, no attempt is made to define every single variable during the process of derivation of the equations. The variables whose names are started by C are used to simplify the equations. These variables include non-acceleration terms. The definition of these variables are presented in Appendices A1 to A4.

4.5.1 Assumptions

The aircraft is a multi-rigid-body system. The total mass of the system is constant, however, the location of the center of gravity is subjected to change. Apart from the relative motion of the components, any deformation of the structure are not taken into account. The earth is flat and fixed in space. This assumption is particularly valid for an unmanned aircraft since the flight time and the distance covered for each operation are generally small. The atmosphere is assumed still and not moving with respect to earth.

4.5.2 Reference Frames

In order to formulate the equations of motion for describing the aircraft motion, suitable coordinate systems are required. Figure 4.1 depicts the multibody and the system of reference frames which are used to derive the equations of motion of the aircraft. As shown in this figure, four main right-hand orthogonal axes system are considered. The $X_i Y_i Z_i$ set is fixed to the earth and can be considered to be an inertial coordinate system. The positive X_i is aligned with North direction, positive Y_i with East and positive Z_i points downwards to the center of the Earth. The $X_a Y_a Z_a$ set is fixed to the body A and moves as it translates and rotates. The origin of the set is located at an arbitrary point O . The positive X_a axis is aligned forward along the fuselage, the

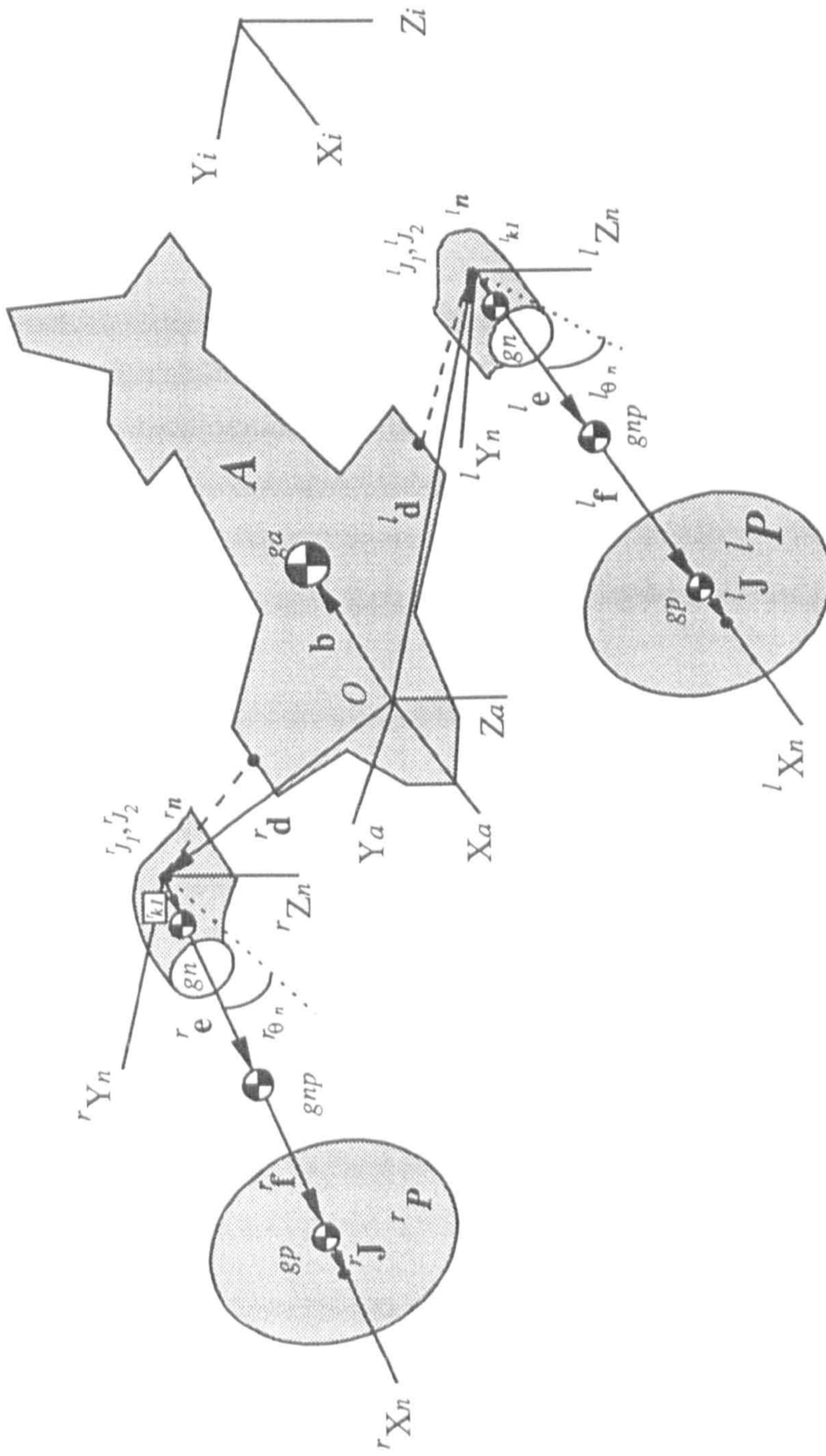


Fig.(4.1): Aircraft multibody system

positive Y_i axis along the right wing and the positive Z_i axis downward. Such a set of axes is referred to as *body axes*. The equations of motion will be derived with respect to this axes. Two other frames $'X_n 'Y_n 'Z_n$ and $'X_n 'Y_n 'Z_n$ are fixed to the bodies $'n$ and $'n$ with their origins located at the joints $'J$ and $'J$, respectively. Each of the bodies $'p$ and $'p$ is considered to have an axis of inertia symmetry whose mass center is on this axis. The positive $'X_n$ and $'X_n$ are aligned with the axes of symmetry of the bodies $'p$ and $'p$. The planes $X_a Z_a$, $'X_n 'Z_n$ and $'X_n 'Z_n$ are always parallel.

It should be emphasised that the term *joint* is considered here to represent the entity of interaction between two bodies. By definition, a joint is an arbitrarily designated point where the effects of all interactions can be represented by a single interaction force and a single interaction torque applied at that point. Therefore this term doesn't imply a physical joint. Meanwhile, in each side of the aircraft we have two joints J_1 and J_2 between bodies $'p$ & $'n$ and $'n$ & A , respectively. These joints are coincident.

4.5.3 Equations of Motion of the Body A

The Newton's second laws for the translational motion and angular rotation of the body A, as an isolated body, take the forms obtained in Appendix A1, Equations A1.6 and A1.18 that are repeated here:

$$\mathbf{F}_a^a = \frac{d}{dt} (m_a \mathbf{V}_o^a + m_a \boldsymbol{\Omega}_{ai}^a \times \mathbf{b}^a) \quad (4.8)$$

$${}_o \mathbf{M}_a^a = \frac{d}{dt} \left\{ [{}_o \mathbf{I}_a^a] \boldsymbol{\Omega}_{ai}^a \right\} + m_a \mathbf{b}^a \times \frac{d}{dt} (\mathbf{V}_o^a) \quad (4.9)$$

\mathbf{F}_a^a and ${}_o \mathbf{M}_a^a$ are the summations of all the external forces and moments acting on the body A, respectively. In terms of the aerodynamic, gravitational and joint reaction forces and moments they can be expressed as follows:

$$\mathbf{F}_a^a = \mathbf{W}_a^a + \mathbf{A}_a^a - {}' \mathbf{F}_{j_1}^a - {}' \mathbf{F}_{j_2}^a \quad (4.10)$$

$${}_o \mathbf{M}_a^a = {}_o \mathbf{M}_{w_a}^a + {}_o \mathbf{M}_{A_a}^a - {}' \mathbf{M}_{j_1}^a - {}' \mathbf{M}_{j_2}^a - {}' \mathbf{d}^a \times {}' \mathbf{F}_{j_1}^a - {}' \mathbf{d}^a \times {}' \mathbf{F}_{j_2}^a \quad (4.11)$$

In these equations the effect of the bodies ${}^r n$ and ${}^l n$ on the body A are represented by force and moment vectors $-{}^r F_{J_i}^a$, $-{}^l F_{J_i}^a$, $-{}^r M_{J_i}^a$ and $-{}^l M_{J_i}^a$.

Expanding the time derivatives in Equations 4.8 and 4.9 in terms of the time derivative in $X_a Y_a Z_a$ axes system by using Equation 4.6a, then:

$$\mathbf{F}_a^a = m_a \dot{\mathbf{V}}_o^a + m_a \boldsymbol{\Omega}_{ai}^a \times \mathbf{V}_o^a + m_a (\dot{\boldsymbol{\Omega}}_{ai}^a \times \mathbf{b}^a + \boldsymbol{\Omega}_{ai}^a \times \dot{\mathbf{b}}^a) + m_a \boldsymbol{\Omega}_{ai}^a \times (\boldsymbol{\Omega}_{ai}^a \times \mathbf{b}^a) \quad (4.12)$$

$${}^o \mathbf{M}_a^a = [{}^o \mathbf{I}_a^a] \dot{\boldsymbol{\Omega}}_{ai}^a + \boldsymbol{\Omega}_{ai}^a \times ([{}^o \mathbf{I}_a^a] \boldsymbol{\Omega}_{ai}^a) + m_a \mathbf{b}^a \times \dot{\mathbf{V}}_o^a + m_a \mathbf{b}^a \times (\boldsymbol{\Omega}_{ai}^a \times \mathbf{V}_o^a) \quad (4.13)$$

Considering the fact that $\dot{\mathbf{b}}^a = \mathbf{0}$, then after substituting \mathbf{F}_a^a and ${}^o \mathbf{M}_a^a$ from Equations 4.10 and 4.11 and using the matrix form of cross-product, the equations of motion of the body A can be expressed as follows:

$$\mathbf{W}_a^a + \mathbf{A}_a^a -{}^r \mathbf{F}_{J_i}^a -{}^l \mathbf{F}_{J_i}^a = m_a \dot{\mathbf{V}}_o^a - m_a [\mathbf{b}^a] \dot{\boldsymbol{\Omega}}_{ai}^a + \mathbf{C25} \quad (4.14)$$

$${}^o \mathbf{M}_{W_a}^a + {}^o \mathbf{M}_{A_a}^a -{}^r \mathbf{M}_{J_i}^a -{}^l \mathbf{M}_{J_i}^a - [{}^r \mathbf{d}^a] {}^r \mathbf{F}_{J_i}^a - [{}^l \mathbf{d}^a] {}^l \mathbf{F}_{J_i}^a = [{}^o \mathbf{I}_a^a] \dot{\boldsymbol{\Omega}}_{ai}^a + m_a [\mathbf{b}^a] \dot{\mathbf{V}}_o^a + \mathbf{C26} \quad (4.15)$$

4.5.4 Equations of Motion of the Body ${}^k np$

As stated in chapter three, due to the similarity of the bodies np at right and left side of the aircraft, one set of equations can be used for both sides. Starting with Equations A2.12 and A2.29, we have:

$${}^k \mathbf{F}_{np}^n = \frac{d}{dt} (m_{np} {}^k \mathbf{V}_{J_i}^n + m_{np} {}^k \boldsymbol{\Omega}_{ni}^n \times {}^k \mathbf{e}^n) \quad (4.16)$$

$${}^k \mathbf{M}_{np}^n = \frac{d}{dt} \left\{ [{}^k \mathbf{I}_{np}^n] {}^k \boldsymbol{\Omega}_{ni}^n + [{}^k \mathbf{I}_p^n] {}^k \boldsymbol{\Omega}_{pn}^n \right\} + m_{np} {}^k \mathbf{e}^n \times \frac{d}{dt} ({}^k \mathbf{V}_{J_i}^n) \quad (4.17)$$

${}^{\kappa}F_{np}^n$ and ${}_{J_1}^{\kappa}M_{np}^n$ are the summation of all the external forces and moments acting on the body ${}^{\kappa}np$, respectively. In terms of the aerodynamic, gravitational and joint reaction forces and moments, they can be expressed as follows:

$${}^{\kappa}F_{np}^n = {}^{\kappa}T^n + {}^{\kappa}W_{np}^n + {}^{\kappa}A_{np}^n + {}^{\kappa}F_{J_1}^n \quad (4.18)$$

$${}_{J_1}^{\kappa}M_{np}^n = {}^{\kappa}M_{pc}^n + {}_{J_1}^{\kappa}M_T^n + {}_{J_1}^{\kappa}M_{W_{np}}^n + {}_{J_1}^{\kappa}M_{A_{np}}^n + {}^{\kappa}M_{J_1}^n \quad (4.19)$$

In these equations the effect of the body A on the body ${}^{\kappa}np$ are represented by the force and moment vectors ${}^{\kappa}F_{J_1}$ and ${}^{\kappa}M_{J_1}$.

Expanding the time derivatives in Equations 4.16 and 4.17 in terms of the time derivatives in ${}^{\kappa}X_n {}^{\kappa}Y_n {}^{\kappa}Z_n$ axes system, these equations take the following forms:

$$\begin{aligned} {}^{\kappa}F_{np}^n &= m_{np} \dot{{}^{\kappa}V_{J_1}^n} + m_{np} {}^{\kappa}\Omega_{ni}^n \times {}^{\kappa}V_{J_1}^n + m_{np} ({}^{\kappa}\dot{\Omega}_{ni}^n \times {}^{\kappa}e^n + {}^{\kappa}\Omega_{ni}^n \times \dot{{}^{\kappa}e}^n) \\ &\quad + m_{np} {}^{\kappa}\Omega_{ni}^n \times ({}^{\kappa}\dot{\Omega}_{ni}^n \times {}^{\kappa}e^n) \end{aligned} \quad (4.20)$$

$$\begin{aligned} {}_{J_1}^{\kappa}M_{np}^n &= [{}_{J_1}^{\kappa}I_{np}^n] {}^{\kappa}\dot{\Omega}_{ni}^n + [{}_{gp}^{\kappa}I_p^n] {}^{\kappa}\dot{\Omega}_{pn}^n + {}^{\kappa}\Omega_{ni}^n \times ([{}_{J_1}^{\kappa}I_{np}^n] {}^{\kappa}\Omega_{ni}^n) + {}^{\kappa}\Omega_{ni}^n \times ([{}_{gp}^{\kappa}I_{np}^n] {}^{\kappa}\Omega_{pn}^n) \\ &\quad + m_{np} {}^{\kappa}e^n \times ({}^{\kappa}\dot{V}_{J_1}^n + {}^{\kappa}\Omega_{ni}^n \times {}^{\kappa}V_{J_1}^n) \end{aligned} \quad (4.21)$$

Considering the fact that $\dot{{}^{\kappa}e}^n = 0$, then after substituting ${}^{\kappa}F_{np}^n$ and ${}_{J_1}^{\kappa}M_{np}^n$ from Equations 4.18 and 4.19 and using the matrix form of cross-product, the joint reactions ${}^{\kappa}F_{J_1}^n$ and ${}^{\kappa}M_{J_1}^n$ can be expressed as follows:

$${}^{\kappa}F_{J_1}^n = m_{np} \dot{{}^{\kappa}V_{J_1}^n} - m_{np} [{}^{\kappa}e^n] {}^{\kappa}\dot{\Omega}_{ni}^n + {}^{\kappa}C3 \quad (4.22)$$

$${}^{\kappa}M_{J_1}^n = [{}_{J_1}^{\kappa}I_{np}^n] {}^{\kappa}\dot{\Omega}_{ni}^n + [{}_{gp}^{\kappa}I_p^n] {}^{\kappa}\dot{\Omega}_{pn}^n + m_{np} [{}^{\kappa}e^n] {}^{\kappa}\dot{V}_{J_1}^n + {}^{\kappa}C4 \quad (4.23)$$

Using the following relationships obtained in Appendix A4, Equations A4.6 and A4.13,

$${}^{\kappa}\dot{\Omega}_{ni}^n = {}^{\kappa}C1 + {}^{\kappa}[DCM]^{na} \dot{\Omega}_{ai}^a + {}^{\kappa}\dot{\Omega}_{na}^n \quad (4.24)$$

$${}^{\kappa}\dot{V}_{j_i}^n = {}^{\kappa}C2 + {}^{\kappa}[DCM]^{na}\dot{V}_o^a - {}^{\kappa}[DCM]^{na}[\kappa d^a]\dot{\Omega}_{ai}^a \quad (4.25)$$

to substitute ${}^{\kappa}\dot{\Omega}_{ni}^n$ and ${}^{\kappa}\dot{V}_{j_i}^n$ in Equations 4.22 and 4.23, then :

$${}^{\kappa}F_{j_i}^n = {}^{\kappa}C5 + [{}^{\kappa}C6]\dot{V}_o^a + [{}^{\kappa}C7]\dot{\Omega}_{ai}^a + [{}^{\kappa}C8]{}^{\kappa}\dot{\Omega}_{na}^n \quad (4.26)$$

$${}^{\kappa}M_{j_i}^n = {}^{\kappa}C9 + [{}^{\kappa}C10]\dot{V}_o^a + [{}^{\kappa}C11]\dot{\Omega}_{ai}^a + [{}^{\kappa}I_{j_i np}^n]{}^{\kappa}\dot{\Omega}_{na}^n + [{}^{\kappa}I_{gp p}^n]{}^{\kappa}\dot{\Omega}_{pn}^n \quad (4.27)$$

In above equations the joint reactions are expressed in terms of the time derivatives of the selected state variables.

4.5.5 Equations of Motion of the Body ${}^{\kappa}p$

Similar to the body ${}^{\kappa}np$, one set of equations can be used for both ${}^{\prime}p$ and ${}^l p$. For this body, only the angular equation of motion is needed. Therefore, starting with Equation A3.3, we have:

$${}^{\kappa}M_{gp p}^n = \frac{d}{dt} \left\{ [{}^{\kappa}I_{gp p}^n] ({}^{\kappa}\Omega_{ni}^n + {}^{\kappa}\Omega_{pn}^n) \right\} \quad (4.28)$$

${}^{\kappa}M_{gp p}^n$ is the summation of all the external moments acting on the body ${}^{\kappa}p$. In terms of aerodynamic, gravitational and joint reaction moments, it can be expressed as follows:

$${}^{\kappa}M_{gp p}^n = {}^{\kappa}M_{pc}^n + {}^{\kappa}M_{gp T}^n + {}^{\kappa}M_{gp W_p}^n + {}^{\kappa}M_{gp A_p}^n + {}^{\kappa}M_{j_i}^n \quad (4.29)$$

In this equation the effect of the body ${}^{\kappa}n$ on the body ${}^{\kappa}p$ are expressed by the moment ${}^{\kappa}M_{j_i}^n$.

Expanding the time derivative in Equation 4.28 in terms of the time derivative in ${}^{\kappa}X_n {}^{\kappa}Y_n {}^{\kappa}Z_n$ axes system and substituting ${}^{\kappa}M_{gp p}^n$ from Equation 4.29, and using matrix representation of cross-product, Equation 4.28 takes the following form:

$${}^{\kappa}M_{j_i}^n = \begin{bmatrix} \kappa I_p^n \\ \kappa I_p^n \end{bmatrix} \dot{\Omega}_{ni}^n + \begin{bmatrix} \kappa I_p^n \\ \kappa I_p^n \end{bmatrix} \dot{\Omega}_{pn}^n + C34 \quad (4.30)$$

Now, using Equation 4.24 to substitute $\dot{\Omega}_{ni}^n$, then :

$${}^{\kappa}M_{j_i}^n = C35 + [C36] \dot{Q}_{ai}^a + \begin{bmatrix} \kappa I_p^n \\ \kappa I_p^n \end{bmatrix} \dot{\Omega}_{na}^n + \begin{bmatrix} \kappa I_p^n \\ \kappa I_p^n \end{bmatrix} \dot{\Omega}_{pn}^n \quad (4.31)$$

In above equation the reaction moment is expressed in terms of the derivative of the selected state variables.

4.5.6 Equations of Motion of the Aircraft Multibody System

To find the general form of the aircraft equations of motion, the equations of individual elements must be combined. Therefore, using the following relations:

$${}^{\kappa}F_{j_i}^a = {}^{\kappa}[DCM]^{na} {}^{\kappa}F_{j_i}^n \quad (4.32)$$

$${}^{\kappa}M_{j_i}^a = {}^{\kappa}[DCM]^{na} {}^{\kappa}M_{j_i}^n \quad (4.33)$$

The joint reaction force and moments between body A and ${}^{\kappa}np$, obtained in Equations 4.26 and 4.27 can be transformed from ${}^{\kappa}X_n {}^{\kappa}Y_n {}^{\kappa}Z_n$ frame of reference to $X_a Y_a Z_a$ reference frame as follows:

$${}^{\kappa}F_{j_i}^a = C12 + [C13] \dot{V}_o^a + [C14] \dot{Q}_{ai}^a + [C15] \dot{\Omega}_{na}^n \quad (4.34)$$

$${}^{\kappa}M_{j_i}^a = C16 + [C17] \dot{V}_o^a + [C18] \dot{Q}_{ai}^a + [C19] \dot{\Omega}_{na}^n + [C20] \dot{\Omega}_{pn}^n \quad (4.35)$$

Now, they can be substituted in Equations 4.14 and 4.15. After re-arranging terms these equations will take the following forms:

$$[C27] \dot{V}_o^a + [C28] \dot{Q}_{ai}^a + [{}^{\prime}C15] {}^{\prime} \dot{\Omega}_{na}^n + [{}^{\prime}C15] {}^{\prime} \dot{\Omega}_{na}^n = C29 \quad (4.36)$$

$$[C30]\dot{V}_o^a + [C31]\dot{\Omega}_{ai}^a + [{}^rC32]{}^r\dot{\Omega}_{na}^n + [{}^lC32]{}^l\dot{\Omega}_{na}^n + [{}^rC20]{}^r\dot{\Omega}_{pn}^n + [{}^lC20]{}^l\dot{\Omega}_{pn}^n = C33 \quad (4.37)$$

Now, using Equations 4.36, 4.37, 4.27 (for right and left side) and 4.31 (for right and left side), then the general equations of motion of the aircraft multibody system can be expressed in matrix form as follows:

$$\begin{array}{c}
 3 \times 3 \\
 3 \times 3 \\
 3 \times 3 \\
 1 \times 3 \\
 1 \times 3 \\
 1 \times 3
 \end{array}
 \begin{array}{c}
 3 \times 3 \\
 3 \times 3 \\
 3 \times 1 \\
 3 \times 1 \\
 3 \times 1 \\
 3 \times 1
 \end{array}
 \begin{array}{c}
 [C27] \\
 [C30] \\
 [{}^rC10] \\
 [{}^lC10] \\
 [0] \\
 [0]
 \end{array}
 \begin{array}{c}
 [C28] \\
 [C31] \\
 [{}^rC11] \\
 [{}^lC11] \\
 [{}^rC36] \\
 [{}^lC36]
 \end{array}
 \begin{array}{c}
 [{}^rC15] \\
 [{}^rC32] \\
 [{}^rI_{np}^n] \\
 [0] \\
 [{}^rI_p^n] \\
 [0]
 \end{array}
 \begin{array}{c}
 [{}^lC15] \\
 [{}^lC32] \\
 [0] \\
 [{}^lI_{np}^n] \\
 [0] \\
 [{}^lI_p^n]
 \end{array}
 \begin{array}{c}
 [0] \\
 [{}^rC20] \\
 [{}^rI_p^n] \\
 [0] \\
 [{}^rI_p^n] \\
 [0]
 \end{array}
 \begin{array}{c}
 [0] \\
 [{}^lC20] \\
 [0] \\
 [{}^lI_p^n] \\
 [0] \\
 [{}^lI_p^n]
 \end{array}
 \begin{array}{c}
 \dot{V}_o^a \\
 \dot{\Omega}_{ai}^a \\
 \dot{\Omega}_{na}^n \\
 \dot{\Omega}_{na}^n \\
 \dot{\Omega}_{pn}^n \\
 \dot{\Omega}_{pn}^n
 \end{array}
 =
 \begin{array}{c}
 C29 \\
 C33 \\
 -{}^rC9 + {}^rM_{J_z}^n \\
 -{}^lC9 + {}^lM_{J_z}^n \\
 -{}^rC35 + {}^rM_{J_z}^n \\
 -{}^lC35 + {}^lM_{J_z}^n
 \end{array}
 \quad (4.38)$$

Equation 4.38 represents the conventional form of the governing equation of a dynamical system. It can be simplified as follows:

$$MS'' = F \quad (4.39)$$

In this equation M is the mass matrix, S' is the state vector and F is the force vector. For the present dynamical system, mass matrix must be symmetric. The following conditions which are necessary for the mass matrix to be symmetric are proved in Appendix A4.

$$\left. \begin{array}{c}
 [C27] \\
 [C31] \\
 [{}^rI_{np}^n] \\
 [{}^lI_{np}^n] \\
 [{}^rI_p^n] \\
 [{}^lI_p^n]
 \end{array} \right\} : \text{Symmetric} \quad (4.40)$$

$$\begin{aligned}
[C30] &= [C28]^T \\
[{}^{\kappa}C10] &= [{}^{\kappa}C15]^T \\
[{}^{\kappa}C11] &= [{}^{\kappa}C32]^T \\
[{}^{\kappa}C36] &= [{}^{\kappa}C20]^T
\end{aligned}$$

Equation 4.38 is a system of eighteen equations with thirty unknown which are the components of the vectors \dot{V}_o^a , $\dot{\Omega}_{ai}^a$, ${}^r\dot{\Omega}_{na}^n$, ${}^l\dot{\Omega}_{na}^n$, ${}^r\dot{\Omega}_{pn}^n$, ${}^l\dot{\Omega}_{pn}^n$, ${}^rM_{J_i}^n$, ${}^lM_{J_i}^n$, ${}^rM_{J_i}^n$ and ${}^lM_{J_i}^n$. Obviously such a system can not be solved. It should be noticed that the equations are derived with the assumption of the universal joints in all the connections. However, the joints are actually revolutes joints (one degree of freedom) which impose some constraints on the system. These constraints can be implemented by eliminating the unnecessary equations which are not related to the actual relative motion of the two bodies. These are the equations associated with X and Z directions of the vectorial form 4.27 and Y and Z directions of the vectorial form 4.31. Considering this fact and defining the following vectors:

$$\begin{aligned}
\dot{\Omega}_{ai}^a &= \begin{Bmatrix} \dot{P} \\ \dot{Q} \\ \dot{R} \end{Bmatrix} ; \dot{V}_o^a = \begin{Bmatrix} \dot{U} \\ \dot{V} \\ \dot{W} \end{Bmatrix} \\
{}^r\dot{\Omega}_{na}^n &= \begin{Bmatrix} 0 \\ \infty \\ {}^r\theta_n \\ 0 \end{Bmatrix} ; {}^l\dot{\Omega}_{na}^n = \begin{Bmatrix} 0 \\ \infty \\ {}^l\theta_n \\ 0 \end{Bmatrix} ; {}^r\dot{\Omega}_{pn}^n = \begin{Bmatrix} {}^{\circ}rN \\ 0 \\ 0 \end{Bmatrix} ; {}^l\dot{\Omega}_{pn}^n = \begin{Bmatrix} {}^{\circ}lN \\ 0 \\ 0 \end{Bmatrix}
\end{aligned} \tag{4.41}$$

the final expanded, tenth order system of equations can then be expressed in the form shown in Equation 4.42. It should be noticed that the column of mass matrix associated with the eliminated states are also omitted.

$$\begin{aligned}
 & \begin{bmatrix} C27_{11} & C27_{12} & C27_{13} & C28_{11} & C28_{12} & C28_{13} & {}^rC15_{12} & {}^rC15_{12} & {}^rC32_{12} & {}^rC20_{11} & 0 & 0 & C29_x \\ C27_{21} & C27_{22} & C27_{23} & C28_{21} & C28_{22} & C28_{23} & {}^rC15_{22} & {}^rC15_{22} & {}^rC32_{22} & {}^rC20_{21} & 0 & 0 & C29_y \\ C27_{31} & C27_{32} & C27_{33} & C28_{31} & C28_{32} & C28_{33} & {}^rC15_{32} & {}^rC15_{32} & {}^rC32_{32} & {}^rC20_{31} & 0 & 0 & C29_z \\ C30_{11} & C30_{12} & C30_{13} & C31_{11} & C31_{12} & C31_{13} & {}^rC32_{12} & {}^rC32_{12} & {}^rC32_{32} & {}^rC20_{11} & {}^rC20_{21} & {}^rC20_{31} & C33_x \\ C30_{21} & C30_{22} & C30_{23} & C31_{21} & C31_{22} & C31_{23} & {}^rC32_{22} & {}^rC32_{22} & {}^rC32_{32} & {}^rC20_{21} & {}^rC20_{31} & & C33_y \\ C30_{31} & C30_{23} & C30_{33} & C31_{31} & C31_{32} & C31_{33} & {}^rC32_{32} & {}^rC32_{32} & & {}^rC20_{31} & & & C33_z \\ {}^rC10_{21} & {}^rC10_{22} & {}^rC10_{23} & {}^rC11_{21} & {}^rC11_{22} & {}^rC11_{23} & 0 & 0 & 0 & 0 & 0 & 0 & -{}^rC9_y + {}^rM_{J_y}^n \\ {}^rC10_{21} & {}^rC10_{22} & {}^rC10_{23} & {}^rC11_{21} & {}^rC11_{22} & {}^rC11_{23} & {}^rI_{J_z}^{np\eta} & {}^rI_{J_z}^{np\eta} & 0 & 0 & 0 & 0 & -{}^rC9_y + {}^rM_{J_y}^n \\ 0 & 0 & 0 & {}^rC36_{11} & {}^rC36_{12} & {}^rC36_{13} & 0 & 0 & 0 & {}^rI_{SP}^n & 0 & 0 & -{}^rC35_x + {}^rM_{J_x}^n \\ 0 & 0 & 0 & {}^rC36_{11} & {}^rC36_{12} & {}^rC36_{13} & 0 & 0 & 0 & {}^rI_{SP}^n & 0 & 0 & -{}^rC35_x + {}^rM_{J_x}^n \end{bmatrix} \\
 & = \\
 & \begin{bmatrix} \dot{U} \\ \dot{V} \\ \dot{W} \\ \dot{P} \\ \dot{Q} \\ \dot{R}_\infty \\ {}^r\theta_\infty^n \\ {}^r\theta_\infty^n \\ {}^rN_\infty^n \\ {}^rN_\infty^n \end{bmatrix}
 \end{aligned}
 \tag{4.42}$$

In this equation

$${}^{\kappa}M_{J_y}^n = {}^{\kappa}M_S \quad (4.43)$$

$${}^{\kappa}M_{J_x}^n = {}^{\kappa}M_E \quad (4.44)$$

where ${}^{\kappa}M_S$ is the output torque of the servomotor driving the body ${}^{\kappa}np$ w.r.t. body A and ${}^{\kappa}M_E$ is the output torque of the engine. ${}^{\kappa}M_E$ can be expressed in terms of the engine output power and engine angular velocity as follows:

$${}^{\kappa}M_E = \frac{{}^{\kappa}P_E}{{}^{\kappa}N} \quad (4.45)$$

The right side of the Equation 4.42 can be broken down into the two parts as shown in Equation 4.46,

$$\begin{bmatrix} C29_x \\ C29_y \\ C29_z \\ C33_x \\ C33_y \\ C33_z \\ -{}^rC9_y + {}^rM_{J_y}^n \\ -{}^lC9_y + {}^lM_{J_y}^n \\ -{}^rC35_x + {}^rM_{J_x}^n \\ -{}^lC35_x + {}^lM_{J_x}^n \end{bmatrix} = \begin{bmatrix} C29A_x \\ C29A_y \\ C29A_z \\ C33A_x \\ C33A_y \\ C33A_z \\ -{}^rC9A_y \\ -{}^lC9A_y \\ -{}^rC35A_x \\ -{}^lC35A_x \end{bmatrix} + \begin{bmatrix} C29B_x \\ C29B_y \\ C29B_z \\ C33B_x \\ C33B_y \\ C33B_z \\ -{}^rC9B_y + {}^rM_{J_y}^n \\ -{}^lC9B_y + {}^lM_{J_y}^n \\ -{}^rC35B_x + {}^rM_{J_x}^n \\ -{}^lC35B_x + {}^lM_{J_x}^n \end{bmatrix} \quad (4.46)$$

The first term in the right side of Equation 4.46 is called the dynamic vector. It contains the products of the components of linear and angular velocities. The second term is the vector summation of all the aerodynamic, gravitational and thrust forces and moments.

If Equation 4.42 is abstracted as follows:

$$[\mu]\zeta' = f \quad (4.47)$$

then the state-space form of the equation will be

$$\zeta' = [\mu]^{-1} f \quad (4.48)$$

4.6 AIRCRAFT ATTITUDE

In order to describe the motion of the aircraft with respect to the earth or inertial frame, it is necessary to be able to specify the orientation of $X_a Y_a Z_a$ axes system with respect to $X_i Y_i Z_i$ axes system. In the present work the Euler symmetric parameters or quaternions are used to calculate the body-to-earth Direction Cosine Matrix and Euler angles θ , ψ and ϕ . Quaternions are related to the Euler angles by [44,46]:

$$\begin{aligned} e_0 &= \pm(\cos(\phi/2)\cos(\theta/2)\cos(\psi/2) + \sin(\phi/2)\sin(\theta/2)\sin(\psi/2)) \\ e_1 &= \pm(\sin(\phi/2)\cos(\theta/2)\cos(\psi/2) - \cos(\phi/2)\sin(\theta/2)\sin(\psi/2)) \\ e_2 &= \pm(\cos(\phi/2)\sin(\theta/2)\cos(\psi/2) + \sin(\phi/2)\cos(\theta/2)\sin(\psi/2)) \\ e_3 &= \pm(\cos(\phi/2)\cos(\theta/2)\sin(\psi/2) - \sin(\phi/2)\sin(\theta/2)\cos(\psi/2)) \end{aligned} \quad (4.49)$$

whichever sign is chosen in Equation 4.49, the same choice must be used for all. The constraint equation is:

$$e_0^2 + e_1^2 + e_2^2 + e_3^2 = 1 \quad (4.50)$$

The following differential equation can be written for the quaternion parameters: [44]

$$\mathbf{q}' = -\frac{1}{2}\omega\mathbf{q} \quad (4.51)$$

where

$$\mathbf{q} = \begin{Bmatrix} e_0 \\ e_1 \\ e_2 \\ e_3 \end{Bmatrix} \quad (4.52)$$

$$\omega = \begin{bmatrix} 0 & P & Q & R \\ -P & 0 & -R & Q \\ -Q & R & 0 & -P \\ -R & -Q & P & 0 \end{bmatrix} \quad (4.53)$$

The body-to-earth DCM can be expressed in terms of the quaternions as follows:

$$[DCM]^{ia} = \begin{bmatrix} e_0^2 + e_1^2 - e_2^2 - e_3^2 & 2(e_1e_2 - e_0e_3) & 2(e_0e_2 + e_1e_3) \\ 2(e_0e_3 + e_1e_2) & e_0^2 - e_1^2 + e_2^2 - e_3^2 & 2(e_2e_3 - e_0e_1) \\ 2(e_1e_3 - e_0e_2) & 2(e_0e_1 - e_2e_3) & e_0^2 - e_1^2 - e_2^2 + e_3^2 \end{bmatrix} \quad (4.54)$$

The relationships between Euler angles and the elements of the $[DCM]^{ia}$ are:

$$\begin{aligned} \theta &= -\sin^{-1}(DCM_{31}^{ia}) \\ \psi &= \text{ATAN2}(DCM_{21}^{ia}, DCM_{11}^{ia}) \\ \phi &= \text{ATAN2}(DCM_{32}^{ia}, DCM_{33}^{ia}) \end{aligned} \quad (4.55)$$

ATAN2 is the FORTRAN four-quadrant inverse tangent function. The inverse transformation between $X_i Y_i Z_i$ and $X_a Y_a Z_a$ axes systems is straightforward, since the inverse of the DCM is its transpose.

4.7 AIRCRAFT POSITION

The following state equation is needed to calculate the aircraft position in inertial axes system:

$$\mathbf{p}' = [DCM]^{ia} \mathbf{V}_0^a \quad (4.56)$$

where \mathbf{p} is the position vector defined as follows:

$$\mathbf{p} = \begin{Bmatrix} \text{North} \\ \text{East} \\ \text{Down} \end{Bmatrix} = \begin{Bmatrix} \text{North} \\ \text{East} \\ -\text{Height} \end{Bmatrix} \quad (4.57)$$

4.8 ASSEMBLING THE STATE EQUATIONS

For the complete state model, the relevant state equations are 4.48, 4.51 and 4.56. These are now assembled in matrix form as shown in Equations 4.58.

$$\begin{bmatrix} \zeta' \\ \mathbf{q}' \\ \mathbf{p}' \end{bmatrix} = \begin{bmatrix} [\mu]^{-1} & 0 & 0 \\ 0 & -\frac{1}{2}\omega & 0 \\ 0 & 0 & [DCM]^{ia} \end{bmatrix} \begin{bmatrix} f \\ \mathbf{q} \\ \mathbf{V}_o^a \end{bmatrix} \quad (4.58)$$

This is the way in which the equations will be programmed for computer purposes. The state vector contains seventeen elements. Three position coordinates, three translational velocity coordinates, three angular velocity coordinates, four quaternion variables, two engines angular velocities and two relative velocities of the tilting bodies.

CHAPTER FIVE

BUILDING THE AIRCRAFT MODEL

5.1 INTRODUCTION

The multi-body equations of motion which were derived in Chapter 4, establish the structure of the aircraft model. In these equations, there are many terms that must be expressed in terms of the characteristics of the secondary objects. This task can be carried out via an appropriate modelling of various subsystems and a clear definition of gravitational and inertia terms. The calculated terms will then be incorporated into the aircraft state-space model. In the process of model building presented in this chapter, the important objective is to gain the maximum flexibility in data changing for the final mathematical model. In the mean time, it is desirable to make the input data as simple as possible. By the end of this chapter the mathematical model will be completed. The required data will then be estimated in the following chapter.

5.2 MODELS OF SUBSYSTEMS

In this section the mathematical models of the aircraft components, i.e. , the propellers, the airframe, the engines and the servomotors are described.

5.2.1 Propeller Model

A propeller usually consists of two or more rotating airfoil-shaped blades. A propeller blade may be considered as a strongly twisted wing. This large twist of the blade is necessary in order to ensure that each blade element operates at a favourable angle of attack. The cross sections of the blade are of the same shape as those of a wing, with a well-rounded leading edge and a sharp trailing edge. Propeller sections, however, particularly those near the hub have usually a greater relative thickness than wing

sections. Structural considerations are responsible for increasing the thickness of the profiles towards the hub.

The angle that the chords of the blade sections form with a plane perpendicular to the axis of the propeller is called the *Pitch Angle*. This angle is much greater for the sections near the hub than those near the blade tip. Since, the outer half of the propeller does most of the work, the pitch angle usually specified to characterise the entire propeller is that at three-fourths of the tip radius, Figure 5.1.

Among the parameters determining the shape of a propeller, pitch angle has the most influence on its characteristics and it must be carefully selected. Usually, for a certain airspeed the best performance can be achieved only at a certain pitch angle. Therefore, if a wider range of airspeed has to be covered, the pitch angle must be adjustable. A propeller whose blades can be rotated simultaneously through the same angle about their longitudinal axes, i.e. axes running along the blades and perpendicular to the propeller axis, is called a *Variable-Pitch* propeller [51]. The effect of such rotation consists in changing the pitch angle of all blade sections by the angle through which the blade has been rotated.

Consider a propeller operating at the velocity V_{pc} (velocity of the propeller disk center), with angle of attack α_p between the free stream velocity and the propeller disk. Figure 5.2 summarises the quantities defining the force and moment components acting on the propeller. The $X_m Y_m Z_m$ axes system is chosen so that the free stream velocity V_{pc} always lies in the $X_m Z_m$ plane. Thus, this axes system rotates with V_{pc} as it changes direction. The force component along the propeller axis, X_m , is usually called *Thrust*. The component perpendicular to this axis and pointing along the positive Z_m direction is called the *in plane H-force* and the third component is the *in plane Y-force*. Also, there are three moment components. The X-component is called the *torque* and two others are the pitch moment M_y^m and the yaw moment M_z^m .

The velocity vector V_{pc}^n can be expressed in terms of the previously calculated linear and angular velocities $V_{J_2}^n$ and Ω_{ni}^n (Chapter 4) as follows:

$$\mathbf{V}_{pc}^n = \mathbf{V}_{j_2}^n + \boldsymbol{\Omega}_{ni}^n \times (\mathbf{f}^n + \mathbf{j}^n) \quad (5.1)$$

The position vectors \mathbf{f} and \mathbf{j} are shown in Figure 4.1. Since

$$V_{pc_x}^m = V_{pc_x}^n \quad (5.2)$$

then

$$\alpha_p = \text{Sin}^{-1} \left(\frac{V_{pc_x}^m}{V_{pc_{tot}}^m} \right) = \text{Sin}^{-1} \left(\frac{V_{pc_x}^n}{V_{pc_{tot}}^n} \right) \quad (5.3)$$

where

$$V_{pc_{tot}}^n = \left((V_{pc_x}^n)^2 + (V_{pc_y}^n)^2 + (V_{pc_z}^n)^2 \right)^{1/2} \quad (5.4)$$

Consider Figure 5.3 in which the frame $X_m Y_m Z_m$ has been rotated relative to the frame $X_n Y_n Z_n$. The rotation is a left-handed rotation about the X_n axis, through an angle ψ_m . This angle can be expressed in the following form:

$$\psi_m = \text{ATAN2}(V_{pc_y}^n, V_{pc_z}^n) \quad (5.5)$$

ATAN2 is the FORTRAN four-quadrant inverse tangent function. Having calculated ψ_m , then:

$$[DCM]^{nm} = \begin{bmatrix} 1 & 0 & 0 \\ 0 & \text{Cos}\psi_m & \text{Sin}\psi_m \\ 0 & -\text{Sin}\psi_m & \text{Cos}\psi_m \end{bmatrix} \quad (5.6)$$

The above results will be used later in this section.

Generally, two types of approach, the blade element and momentum theories, may be used to model the propeller. The first method is aimed at treating each propeller blade as a wing and introducing the usual lift and drag specifications as used for fixed wing analysis. In this approach the increment of force and moment on a typical element of the blade are calculated and then integrated along the blade to find the total force and moment. In this method it is usually assumed rather arbitrarily that each blade element

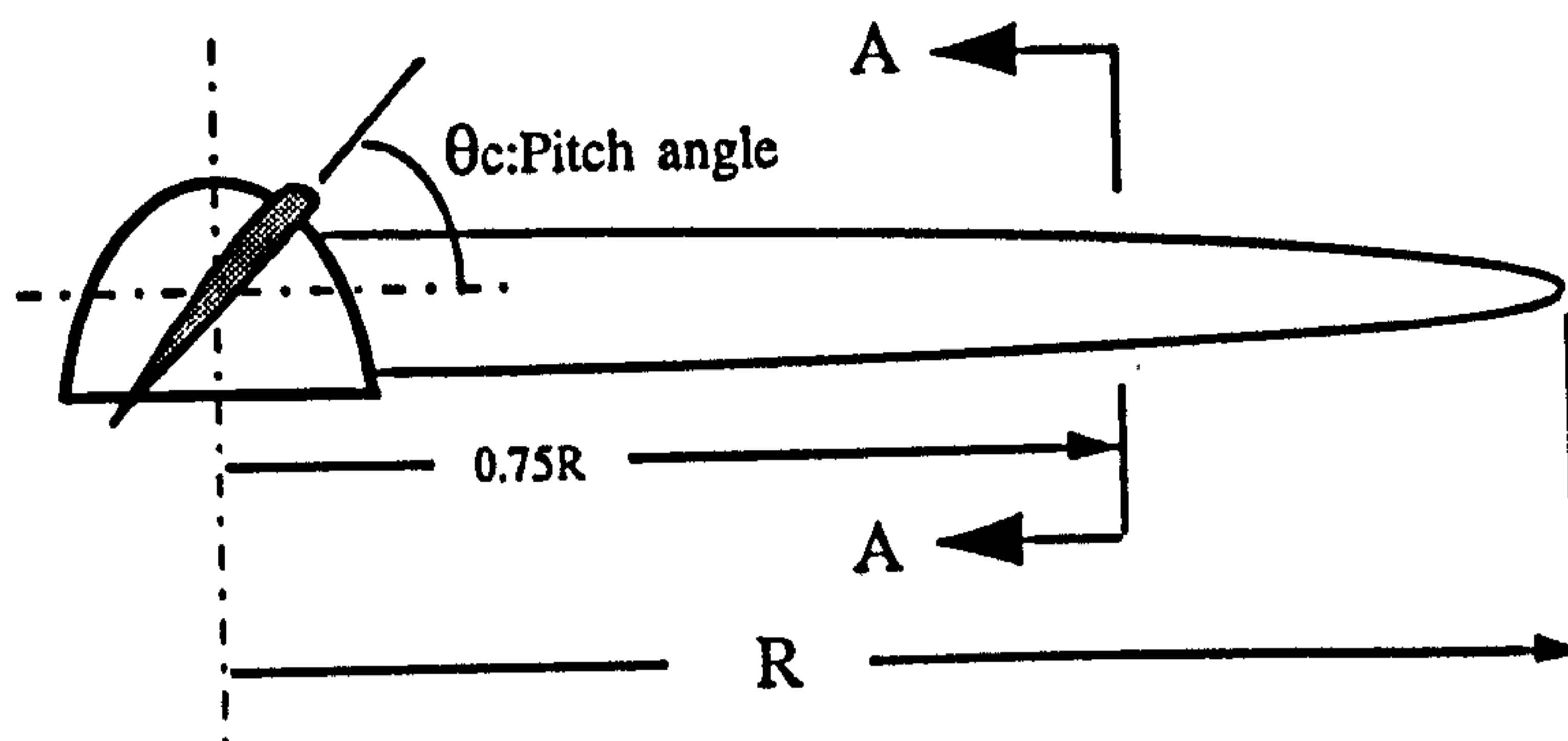


Fig. (5.1): The propeller pitch angle

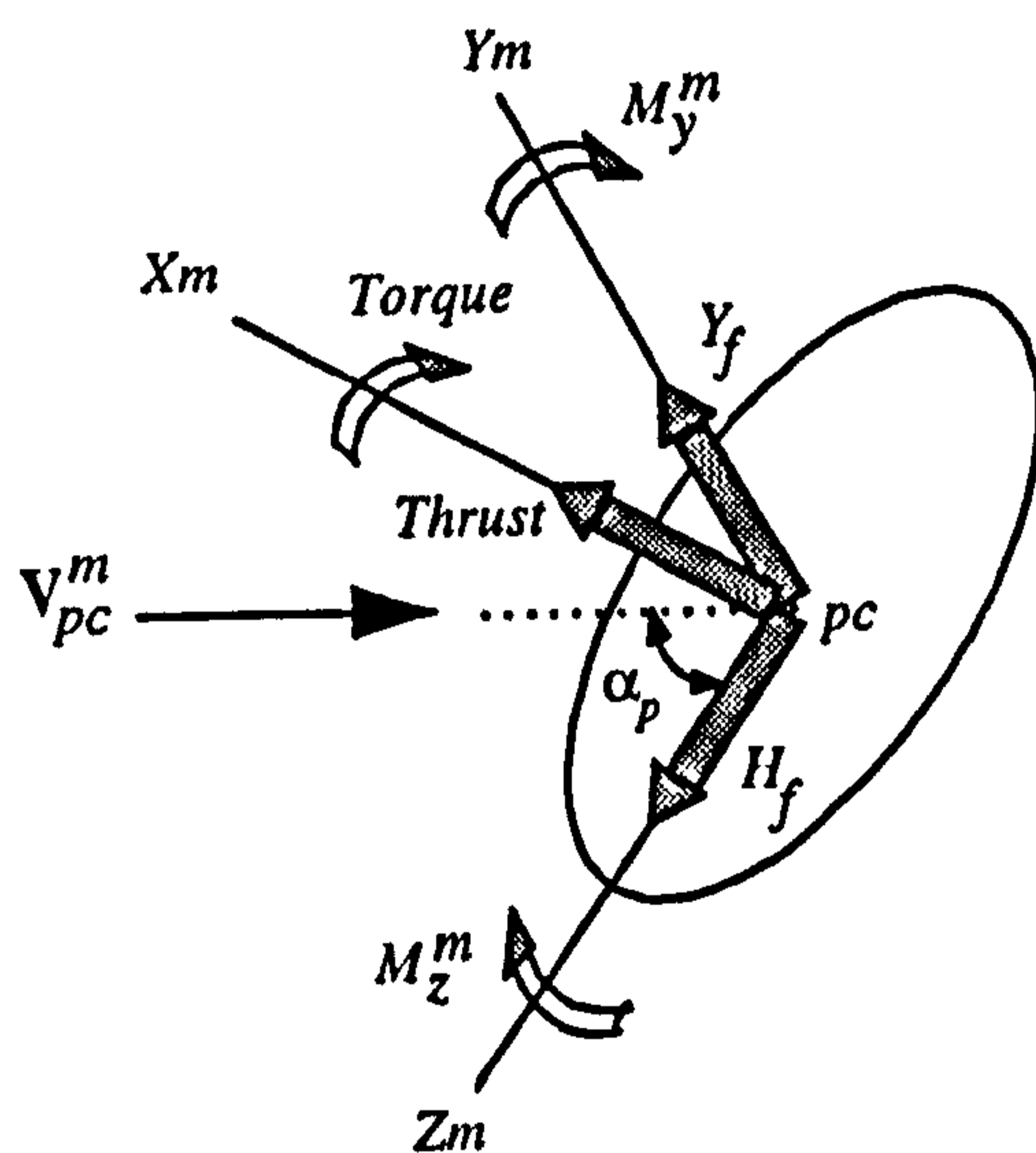


Fig. (5.2): The propeller force and moment components

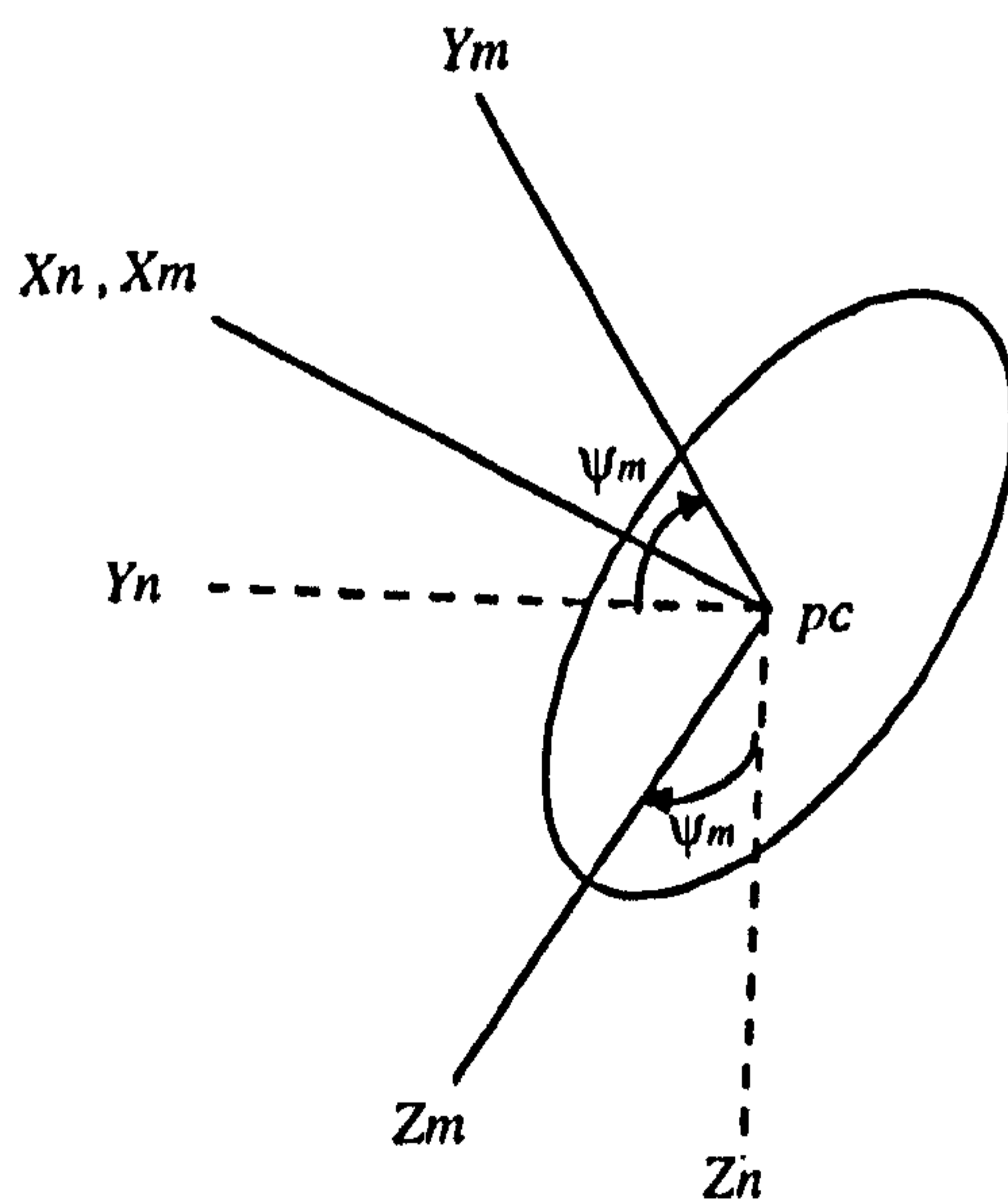


Fig. (5.3): Plane coordinate rotation of $X_m Y_m Z_m$ relative to $X_n Y_n Z_n$

operates independently of all the other elements as if it were an element of an airfoil of infinite span engaged in a uniform rectilinear motion. It is obvious that this simple form of the theory can not give more than a rough approximation. However, using this method, calculation of all the forces and components are possible.

Due to the unnecessary complication and possible numerical difficulties associated with the highly nonlinear equations derived by using the blade element theory [51], it was decided not to use this method in the current version of the simulation model. However, using the derived equations, it has been proved, at least theoretically, that the Y-force and M_y^m moment are both zero for a propeller [52].

In the second method, typified by the *actuator disk*, the realities of the propeller blades are ignored and the propeller is treated as a single entity obtaining thrust by setting up a uniform mass flow of air over its whole plan area and imparting a change of momentum to it. This is a simplistic view of the problem but highlights some important general facts about the performance of the propeller. What the momentum theory achieves is to furnish one relation between the three variables C_T , C_P and ADR which are called the *thrust coefficient*, the *power coefficient* and the *advance ratio*, respectively (will be defined later in this section). This relation is supposed to be valid for any propeller independent of the number of blades, their profiles, etc. No account whatever is taken of the shape of the propeller body. The theory replaces this body by an ideal mechanism, the so-called *actuator disk*. The action that this disk is supposed to exert on the fluid represents the main features of the action exerted by the propeller. One drawback of this method is that the Y and Z components of the force and moment can not be calculated. However, as mentioned earlier, the Y components are theoretically zero and the Z components are relatively small and can be neglected. [53]

A combined momentum and blade-element theory is also possible. Interested readers are referred to the materials in which propellers or helicopter rotors have been analysed [51,53-57].

In the present work, a combination of the momentum theory and empirical data is used in mathematical modelling of the propeller. Since, the momentum theory is well-known and widely-used method, sufficient discussion about this theory can be obtained in the relevant books, e.g. [51,53-55]. Therefore, in this work, a detailed description of the

method is avoided and only the obtained results will be used. It should be pointed out that in spite of neglecting the Y and Z components of the force and moment acting on the propeller, the process of modelling will be carried out with the complete set of the components. This simplifies any possible change of the propeller model in the final computer program. Obviously, in the current mathematical model, a value of zero should be considered for the mentioned components.

The characteristics of a variable-pitch propeller of various blade settings can be empirically represented by using a type of diagram which is called a *propeller chart* [51]. The curves on this chart show the dimensionless coefficient of thrust and power defined by:

$$C_T = \frac{\text{Thrust}}{\rho \left(\frac{\text{rpm}}{60} \right)^2 D^4} \quad (5.7)$$

$$C_P = \frac{P_{prop}}{\rho \left(\frac{\text{rpm}}{60} \right)^3 D^5} \quad (5.8)$$

as a function of advance ratio, a dimensionless term defined by:

$$ADR = \frac{V_{pc_{1\alpha}} \text{Sin}(\alpha_p)}{\left(\frac{\text{rpm}}{60} \right) D} \quad (5.9)$$

, for various blade angles θ_c . The points on these curves are obtained by experimental results. Having abstracted these curves by the following functions:

$$C_T = CTG(ADR, \theta_c) \quad (5.10)$$

$$C_P = CPG(ADR, \theta_c) \quad (5.11)$$

the generated thrust and torque and absorbed power by the propeller can then be calculated by using the Equations 5.7 and 5.8 as follows:

$$Thrust = C_T \cdot \rho \left(\frac{rpm}{60} \right)^2 D^4 \quad (5.12)$$

$$P_{prop} = C_P \cdot \rho \left(\frac{rpm}{60} \right)^3 D^5 \quad (5.13)$$

$$Torque = \frac{P_{prop}}{\left(\frac{rpm}{60} \right)} \quad (5.14)$$

As mentioned earlier, in the current propeller model

$$\begin{aligned} Y_f^m &= 0. \\ H_f^m &= 0. \\ M_y^m &= 0. \\ M_z^m &= 0. \end{aligned} \quad (5.15)$$

Now, the components of the force and moment vectors \mathbf{T}^m and \mathbf{M}_{pc}^m can be expressed as follows:

$$\begin{aligned} T_x^m &= Thrust \\ T_y^m &= RPMrdc \cdot Y_f^m \\ T_z^m &= H_f^m \end{aligned} \quad (5.16)$$

$$\begin{aligned} M_{pc_x}^m &= -RPMrdc \cdot Torque \\ M_{pc_y}^m &= M_y^m \\ M_{pc_z}^m &= RPMrdc \cdot M_z^m \end{aligned} \quad (5.17)$$

The term RPMrdc is called the *Rotational Direction Code*. This term is implemented to consider the effect of the direction of the propeller angular velocity on the sign of the calculated forces and moments and it is defined as follows:

$$\begin{aligned} RPMrdc=1 & \quad \text{For positive angular velocity} \\ RPMrdc=-1 & \quad \text{For negative angular velocity} \end{aligned} \quad (5.18)$$

Therefore, in all the above equations, the variable rpm represents the absolute value of the propeller angular velocity. For the implementation in the equations of motion the force and moment vectors \mathbf{T}^m and \mathbf{M}_{pc}^m should be transformed to the $X_n Y_n Z_n$ axes system, therefore:

$$\mathbf{T}^n = [DCM]^{nm} \mathbf{T}^m \quad (5.19)$$

$$\mathbf{M}_{pc}^n = [DCM]^{nm} \mathbf{M}_{pc}^m \quad (5.20)$$

Also, two other related vectors can be calculated as follows:

$$J_z \mathbf{M}_T^n = (\mathbf{f}^n + \mathbf{j}^n) \times \mathbf{T}^n \quad (5.21)$$

$${}_{gp} \mathbf{M}_T^n = \mathbf{j}^n \times \mathbf{T}^n \quad (5.22)$$

The flow model for the momentum theory analysis of the propeller at an angle of attack α_p is shown in Figure 5.4. This is indeed the projection of the $X_m Z_m$ plane shown in Figure 5.2. In this model, a circular jet of air of velocity V_{pc} having the same diameter as the propeller, is assumed to impinge upon the propeller and being deflected downwards so that it finally has a downward component W_i [53]. The induced velocities at the disk V_i and in the far wake W_i are assumed to be parallel to the propeller thrust.

According to Gluart's hypothesis and momentum theory results [54], the following expression can be written for induced velocity.

$$V_i = \frac{(V_h)^2}{\left[(V_{pc} \cos \alpha_p)^2 + (V_{pc} \sin \alpha_p + V_i)^2 \right]^{1/2}} \quad (5.23)$$

and

$$W_i = 2V_i \quad (5.24)$$

where V_h is the induced velocity in hover and it can be expressed as follows:

$$V_h = \left(\frac{\text{Thrust}}{(\rho\pi D^2/2)} \right)^{1/2} \quad (5.25)$$

The value of W_i will be used in the calculation of the local velocity vector over the components which are influenced by the propeller slipstream. To have control over this value, a coefficient called the *slipstream contraction code 2* is considered as follows.

$$W_i = \frac{1}{K_{sscon2}} V_i \quad 0.5 \leq K_{sscon2} \leq 1 \quad (5.26)$$

Using this coefficient, the strength of the propeller slipstream can be freely set up. This is considered as a useful capability from the research point of view. Obviously, for the value of $K_{sscon2} = 0.5$, Equation 5.24 is determined.

Nonlinear Equation 5.23 can be solved by an iterative approach. The iteration can be a simple, straight substitution as expressed by the equation itself. However, in or near to hover, if a bad choice of starting value is taken, a very slow convergence takes place and in the worst situation, hover, can result in no convergence at all when the iteration will oscillate between two results. For this reason, a modification to the expression can be made to collect both terms on one side of the equation and then to invoke the Newton-Raphson technique to determine the solution. This results in a more complicated iterative expression, but the method rapidly converges at all flight conditions and for this reason is generally more robust, [55]

The Equation 5.24 is derived based on the assumption of a definite flow through the propeller with a well-defined slipstream. However, for a negative angle of attack, e.g. in vertical descent, it is clear that the relative upward flow will, if it becomes large enough, prevent a slipstream from forming, and some of the air will recirculate through the propeller in what is known as the *vortex-ring* state, shown Figure 5.5. At small rate of descent the flow in the vicinity of the disk is still reasonably well represented by the momentum theory model. However, at descent rate beyond $V_{p_{crit}} \sin\alpha_p = -V_h/2$ the flow near the propeller disk becomes highly unsteady and turbulent [54]. In this region the momentum theory is no longer valid. To avoid this situation, the following constraint is considered in the propeller model.

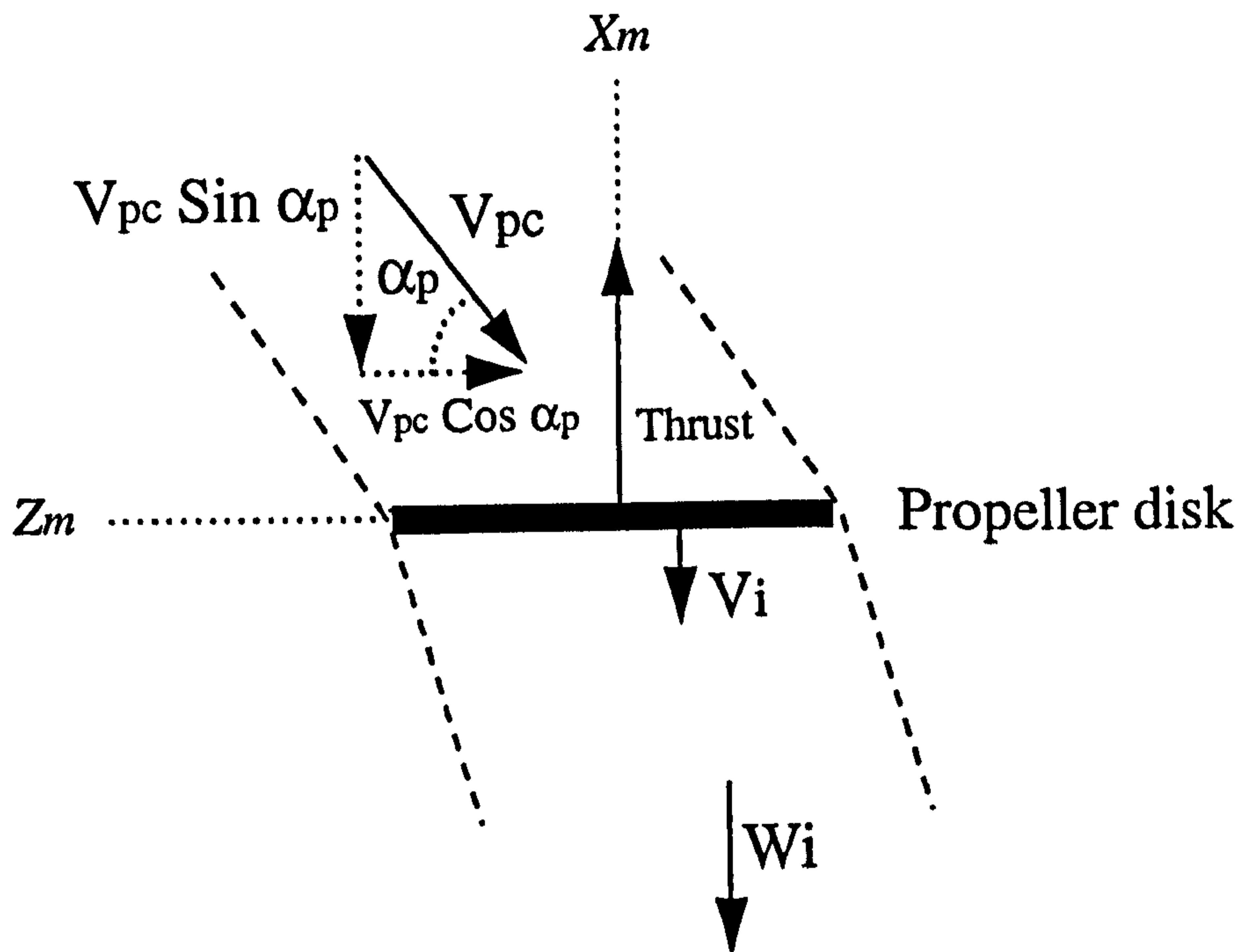


Fig. (5.4): The flow model for momentum theory analysis of propeller

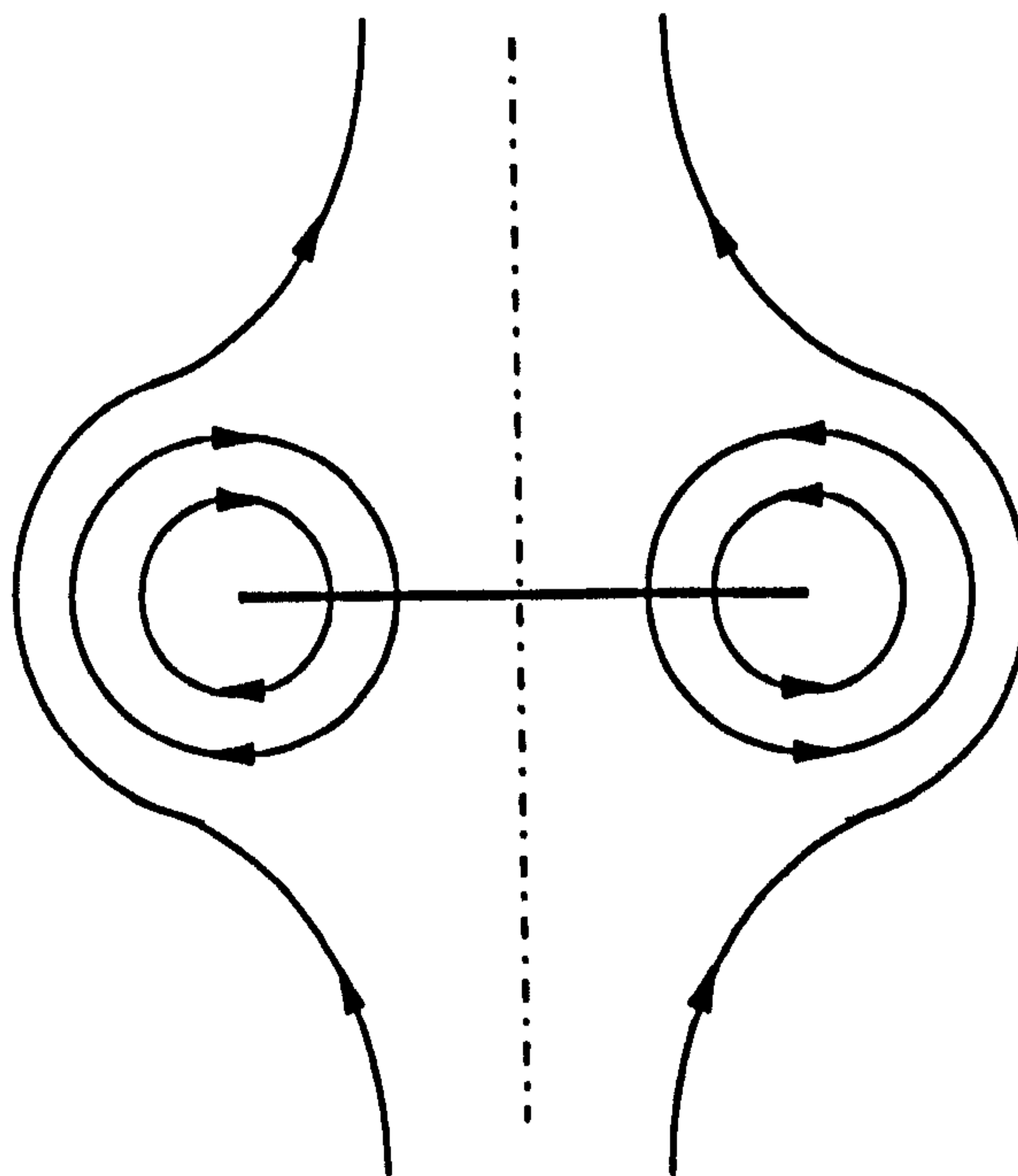


Fig. (5.5): Vortex-ring state in vertical descent [54]

$$\frac{V_{p_{c_{\alpha}}} \sin \alpha_p}{V_h} > -\frac{1}{2} \quad (5.27)$$

Finally, it should be pointed out that the propeller model has been developed based on a variable blade angle assumption. Therefore, the propeller is adjustable for various forward speeds and , in the case, this flexibility can be used for thrust controlling as a complementary option.

5.2.2 Propeller Slipstream Effect

As stated in Chapter 3, when calculating the aerodynamics of the aircraft, it is important to specify which components are affected by the propellers slipstream at the time. Therefore, continuous investigation must be carried out during simulation time to find out if a new component has located in the propellers' slipstream or an already affected part has gone out of the propellers' slipstream. Having checked that, the propeller slipstream effect will then be taken into account in aerodynamics calculations that is the subject of the next section. In this section, the method used for such an investigation is presented.

Figure 5.6 shows the model of the propeller slipstream effect on the typical component v . This component is considered to be influenced by the propeller when its aerodynamic center, AC_v , is inside the propeller streamtube. This seems to be a reasonable criterion for the normal flight conditions, although, it may not be perfect for the situations in which a component is partly immersed in the streamtube. However it is sufficiently correct for investigation of the fundamental characteristics of such effects on the flight dynamics of the aircraft.

As shown in Figure 5.6, the aerodynamic center AC_v is positioned w.r.t. the propeller disk center by the vector LS_v . The calculation of this vector for different components is the subject of the Appendix B1. In this section, the general procedure will be discussed.

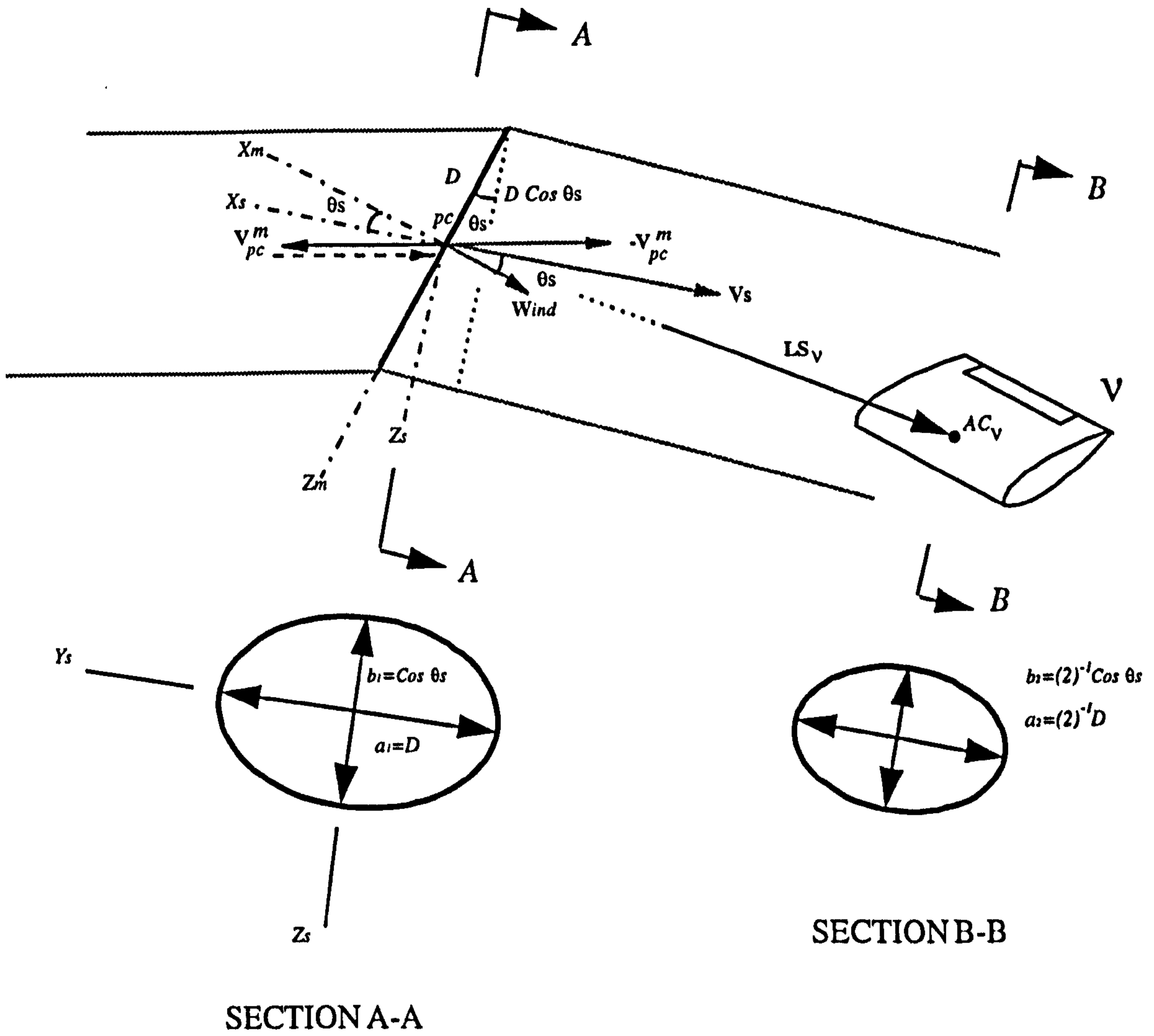


Fig. (5.6): The model of the propeller slipstream effect on a typical component

In terms of the components, the induced velocity vector ${}^{\kappa}W_{ind}$ can be written as follows:

$${}^{\kappa}W_{ind}^m = {}^{\kappa}W_{ind}^n = \begin{Bmatrix} {}^{\kappa}W_i \\ 0 \\ 0 \end{Bmatrix} \quad (5.28)$$

The absolute velocity vector of the propeller slipstream, ${}^{\kappa}V_s^m$, can then be expressed as a summation of ${}^{\kappa}V_{pc}^m$ and ${}^{\kappa}W_{ind}^m$ by

$${}^{\kappa}V_s^m = {}^{\kappa}V_{pc}^m + {}^{\kappa}W_{ind}^m \quad (5.29)$$

where

$${}^{\kappa}V_{pc}^m = [DCM]^{mn} {}^{\kappa}V_{pc}^n \quad (5.30)$$

${}^{\kappa}V_{pc}^n$ is calculated in Equation 5.1. The deflection angle ${}^{\kappa}\theta_s$ can then be defined as:

$${}^{\kappa}\theta_s = \text{Sin}^{-1} \left(\frac{-{}^{\kappa}V_{s_x}^m}{{}^{\kappa}V_{s_{tot}}^m} \right) \quad (5.31)$$

where

$${}^{\kappa}V_{s_{tot}}^m = \left[({}^{\kappa}V_{s_x}^m)^2 + ({}^{\kappa}V_{s_y}^m)^2 + ({}^{\kappa}V_{s_z}^m)^2 \right]^{1/2} \quad (5.32)$$

Changing K_{sscon2} with K_{sscon1} which is called the *slipstream contraction code 1* in Equation 5.26 yields:

$${}^{\kappa}W_i = \frac{1}{K_{sscon1}} {}^{\kappa}V_i \quad (5.33)$$

The two slipstream contraction codes 1 and 2 are actually the same. However, as it will be seen later, using two different codes provides better flexibility to the mathematical model. The elliptical cross section at ${}^{\kappa}PC$ and AC_v are geometrically identical. Therefore, using Equation 5.33 and the principal of mass conservation along the propeller slipstream, the following relations will then be obtained.

$$\begin{aligned} {}^\kappa a_2 &= (K_{sscon1})^{-1/2} a_1 = (K_{sscon1})^{-1/2} D \\ {}^\kappa b_2 &= (K_{sscon1})^{-1/2} b_1 = (K_{sscon1})^{-1/2} D \cos {}^\kappa \theta_s \end{aligned} \quad (5.34)$$

Substituting into the general form of the equation of an ellipse, then

$$\frac{({}^\kappa Y^s)^2}{(1/2 {}^\kappa a_2)^2} + \frac{({}^\kappa Z^s)^2}{(1/2 {}^\kappa b_2)^2} = 1 \quad (5.35)$$

The equation of the elliptical cross section at AC_v can then be given by

$$({}^\kappa Y^s)^2 (\cos {}^\kappa \theta_s)^2 + ({}^\kappa Z^s)^2 = 0.25 K_{sscon1} D^2 (\cos {}^\kappa \theta_s)^2 \quad (5.36)$$

For those points located inside the ellipse

$$({}^\kappa Y^s)^2 (\cos {}^\kappa \theta_s)^2 + ({}^\kappa Z^s)^2 \leq 0.25 K_{sscon1} D^2 (\cos {}^\kappa \theta_s)^2 \quad (5.37)$$

Therefore, AC_v will be located in the propeller slipstream if the Y and Z components of LS_v satisfy the above criterion, i.e.

$$({}^\kappa LS_{v,y}^s)^2 (\cos {}^\kappa \theta_s)^2 + ({}^\kappa LS_{v,z}^s)^2 \leq 0.25 K_{sscon1} D^2 (\cos {}^\kappa \theta_s)^2 \quad (5.38)$$

The following codes can then be set up as follows

$$\begin{aligned} {}^\kappa K_{ssv} &= 1.0 & AC_v & \text{ is in the propeller slipstream} \\ {}^\kappa K_{ssv} &= 0.0 & AC_v & \text{ is out of the propeller slipstream} \end{aligned} \quad (5.39)$$

The values of ${}^\kappa K_{ssv}$ will be used in the aerodynamics calculations in the next section. Detailed description associated with each individual component may be found in the Appendix B1.

Finally, it should be noticed that in the derivation of the deflection angle ${}^{\kappa}\theta_s$, the value of the induced velocity ${}^{\kappa}W_i$ is used. In other words, it is assumed that the induced velocity increases to the value ${}^{\kappa}W_i$ immediately behind the propeller disk. However, practically, it happens somewhere at a distance behind the propeller disk and the slipstream continues to deflect in the course of travelling this distance, Figure 5.7. The longer the distance, the less accurate the deflection angle. Unfortunately, the momentum theory doesn't give any clue about the length and the variation of the induced velocity along this distance. However, the possible error in the criterion 5.38, imposed by inaccuracy in the deflection angle ${}^{\kappa}\theta_s$, may be compensated by appropriately selecting the value of the coefficient K_{sscon1} . Moreover, application of the two different slipstream contraction codes K_{sscon1} and K_{sscon2} provides the capability of dealing with the value of W_i and the criterion 5.38 more independently and arbitrarily. This advantage has been experienced during the computer simulation.

5.2.3 Airframe Aerodynamics

As mentioned in Chapter 3, to follow the general methodology in considering the constituent parts of the vehicle separately when evaluating aerodynamic forces and moments, the airframe is broken down into the airfoils and streamline bodies. Therefore, the airframe aerodynamic modelling is limited to only the models of a simple airfoil and a streamline body.

To calculate the aerodynamic forces and moments acting on a component, the local velocity vector at its aerodynamic center is needed. For a typical component v of the main body A , this velocity vector can be expressed by

$$\mathbf{V}_{AC_v}^v = \mathbf{V}_O^v + {}^{\kappa}\boldsymbol{\Omega}_{ai}^v \times \mathbf{L}_{v_{ai}}^v - {}^{\kappa}K_{ssv} \cdot {}^{\kappa}\mathbf{W}_{ind}^v - {}^{\kappa}K_{ssv} \cdot {}^{\kappa}\mathbf{W}_{ind}^v \quad (5.40)$$

where, $\mathbf{L}_{v_{ai}}^v$ is the position vector of the component aerodynamic center w.r.t. the origin O . Similarly, for a component of the tilting part ${}^{\kappa}np$

$$\mathbf{V}_{AC_v}^v = {}^{\kappa}\mathbf{V}_{J_2}^v + {}^{\kappa}\boldsymbol{\Omega}_{ni}^v \times \mathbf{L}_{v_{ai}}^v - {}^{\kappa}K_{ssv} \cdot {}^{\kappa}\mathbf{W}_{ind}^v \quad (5.41)$$

where, $\mathbf{L}_{v_i}^v$ is the position vector of the component's aerodynamic center w.r.t. the point *J_2 . Definitions of ${}^*K_{ss_v}$ and ${}^*W_{ind}$ were given in the previous section. As it can be seen, the aircraft freestream velocity, aircraft angular velocity and propellers' slipstream velocity are contributed in the evaluation of the local velocity vector. The calculation of the V_{AC} for every individual element is presented in Appendix B1.

The local angle of attack and sideslip can then be calculated as follows

$$\alpha_v = ATAN2(V_{v_x}^v, V_{v_z}^v) \quad (5.42)$$

$$\beta_v = Sin^{-1}\left(\frac{V_{AC_{vy}}^v}{V_{AC_{tot}}^v}\right) \quad (5.43)$$

where

$$V_{AC_{tot}}^v = \left[(V_{AC_{ux}}^v)^2 + (V_{AC_{vy}}^v)^2 + (V_{AC_{uz}}^v)^2 \right]^{1/2} \quad (5.44)$$

For streamline bodies, two other angles must be calculated which are

$$\gamma_v = ATAN2\left(\left(V_{AC_{vy}}^v \sin(\gamma_{v1}) + V_{AC_{uz}}^v \cos(\gamma_{v1})\right), V_{AC_{ux}}^v\right) \quad (5.45)$$

$$\sigma_v = ATAN2\left(-V_{AC_{vy}}^v \cdot V_{AC_{uz}}^v, V_{AC_{uz}}^v \cdot V_{AC_{ux}}^v\right) \quad (5.46)$$

where

$$\gamma_{v1} = ATAN2\left(V_{AC_{vy}}^v, V_{AC_{uz}}^v\right) \quad (5.47)$$

The angle σ_v will be used in calculation of the Direction Cosine Matrix between the local body axes and the local wind axes systems, Equation 5.65. The angle γ_v is the true angle of attack (the angle between the local velocity vector and the body longitudinal axis). This angle will be used to find the lift, the drag and pitching moment coefficients for a streamline body later in this chapter.

Airfoils

In the present work, the term *airfoil* is used to designate a lifting surface of rectangular shape. As shown in Figure 5.8, one of the sides of the rectangle is the *Span* and the other side is the *Chord* of the airfoil. The ratio *Span/Chord* is called the aspect ratio and can be shown by

$$AR = \frac{SPAN}{CHORD} \quad (5.48)$$

Consider an airfoil moving through the air with a constant velocity. The forces exerted by the air on the airfoil will then depend on its shape, size, orientation, the velocity of motion, and the density and viscosity of the air. The shape of the airfoil can be defined by giving the shape of the profile and the aspect ratio AR . The size can be defined by giving the chord length. Finally, the orientation can be determined by giving the angle of attack.

The magnitude, direction, and line of action of the resultant force that the air exerts on an airfoil are completely determined when its components, *Drag* and *Lift*, parallel and perpendicular to the velocity, and pitching moment with respect to an arbitrarily chosen point are known. The lift, drag and pitching moment of an airfoil can be written as

$$\begin{aligned} Lift_{af} &= \frac{1}{2} \rho (V_{AC_{af}})^2 S_{af} C_{af_{L0}} \\ Drag_{af} &= \frac{1}{2} \rho (V_{AC_{af}})^2 S_{af} C_{af_{D0}} \\ Moment_{af} &= \frac{1}{2} \rho (V_{AC_{af}})^2 S_{af} C_{af_{M0}} \end{aligned} \quad (5.49)$$

$C_{af_{L0}}$, $C_{af_{D0}}$ and $C_{af_{M0}}$ are the dimensionless coefficients of lift, drag and moment. For an airfoil of given profile these coefficients depends on Reynolds number (Re), the aspect ratio AR , and the angle of attack α_{af} . The influence of Reynolds number is comparatively small. The curves showing the coefficients $C_{af_{L0}}$, $C_{af_{D0}}$ and $C_{af_{M0}}$ as functions of the angle of attack α_{af} are known as the *characteristic curves* of an airfoil [51]. The forms of these curves depend on the shape of the profile, the aspect ratio of the airfoil, and, to a certain extent, the Reynolds number. Before going into the details, some issues concerning the general form of these characteristic curves which are of prime importance in aerodynamic modelling of the aircraft should be discussed.

For each profile there is a certain direction of velocity in which the lift and accordingly, the lift coefficient are zero. This direction is called *zero lift direction* of the profile. In this work, the angle of attack of an airfoil is measured from this zero lift line. For small values of the angle of attack the lift coefficient is proportional to α_{af} . In Figure 5.9 a typical C_{afL0} vs α_{af} curve is shown. For angles of attack up to a certain value the curve is almost a straight line. For higher angles of attack, the character of curve changes abruptly. The range of values of C_{afL0} within which the curve remain linear depends on the shape of the profile and on the value of the Reynolds number. The upper end point of the approximately straight portion of the C_{afL0} vs α_{af} curve is called the *stalling point* [51]. At the stalling point the C_{afL0} vs α_{af} curve, shows a sharp bend. If the angle of attack is increased further, then C_{afL0} drops to nearly zero for $\alpha_{af} = 90^\circ$. It is obvious that at $\alpha_{af} = 90^\circ$ the problem is rather that of the motion past a rectangular plate opposed to the direction of flow.

Contrary to the C_{afL0} vs α_{af} curve, the C_{afD0} vs α_{af} curve, is of parabolic character, Figure 5.10. It has a minimum close to $\alpha_{af} = 0^\circ$. This minimum value of the drag coefficient depends on the shape of the profile and on the value of the Reynolds number. For the values of α_{af} different from zero, the drag coefficient increases proportional to α_{af}^2 at a rate that depends mainly on the aspect ratio. Since within the range of linearly increasing C_{afL0} the lift coefficient is proportional to the angle of attack α_{af} , the main character of the C_{afD0} vs α_{af} curve can be stated as follows: *Within the range of linearly increasing C_{afL0} the drag coefficient follows the parabolic law* [51,57]

$$C_{afD0} = C_{afDP} + \frac{1}{Kar \cdot AR} C_{afL0}^2 \quad (5.50)$$

where C_{afDP} depends mainly on the shape of the profile. This term is often called the *coefficient of parasite or profile drag*. The second term is known as the coefficient of *induced drag*.

The pitching moment and the pitching moment coefficient depend on the position of the point with respect to which the moment is taken. The outstanding fact concerning the

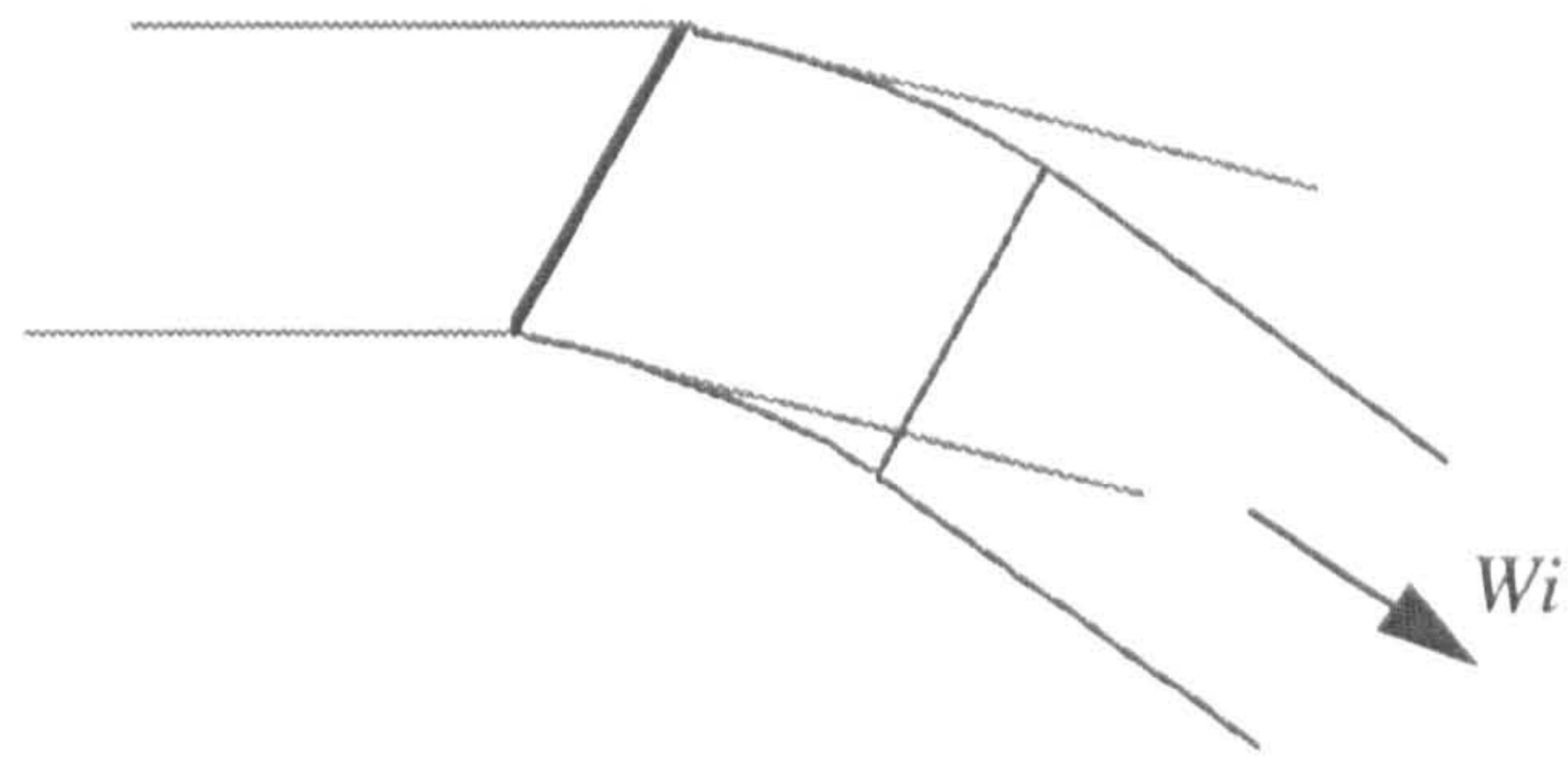


Fig. (5.7): Inaccuracy in the calculated deflection angle

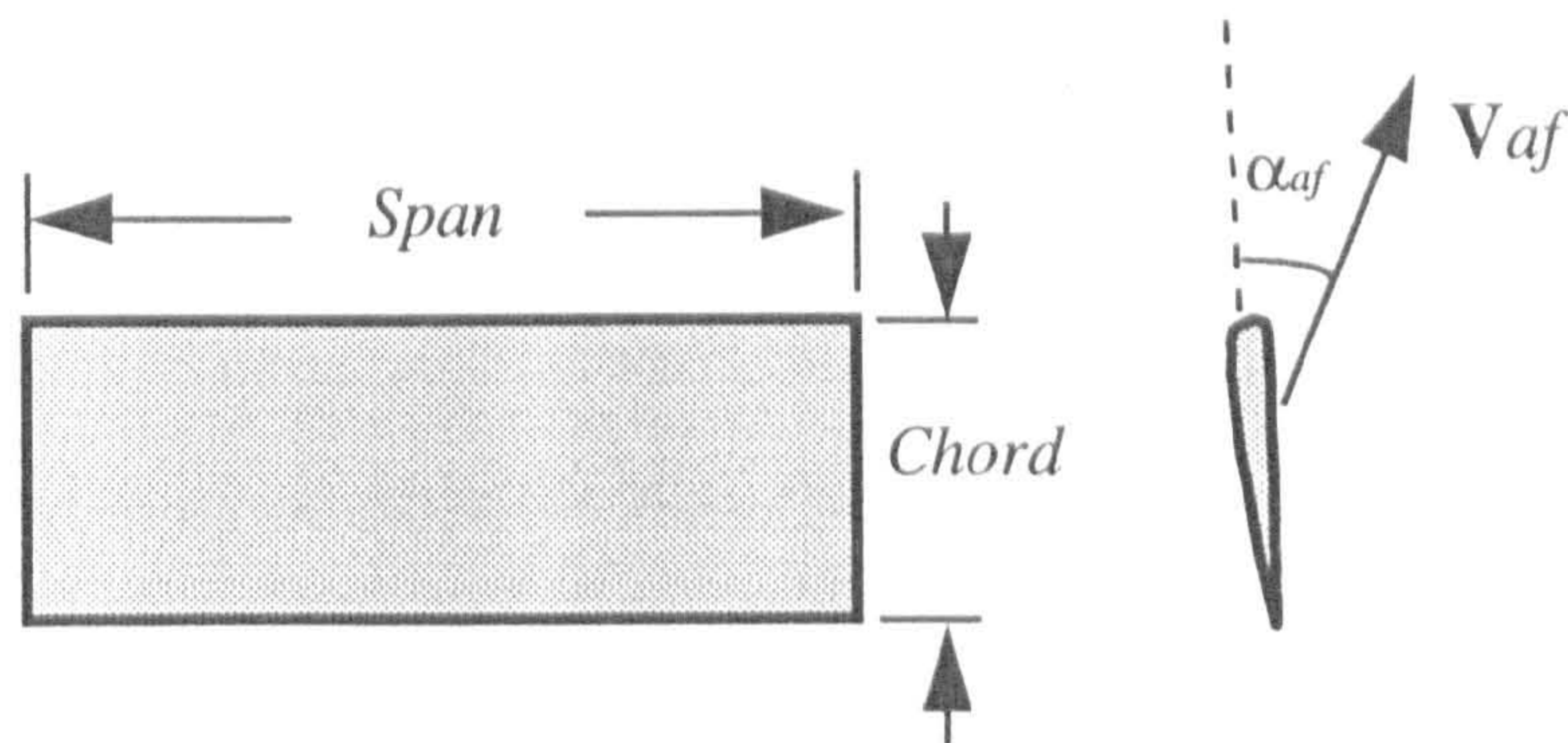


Fig. (5.8): Airfoil dimensions

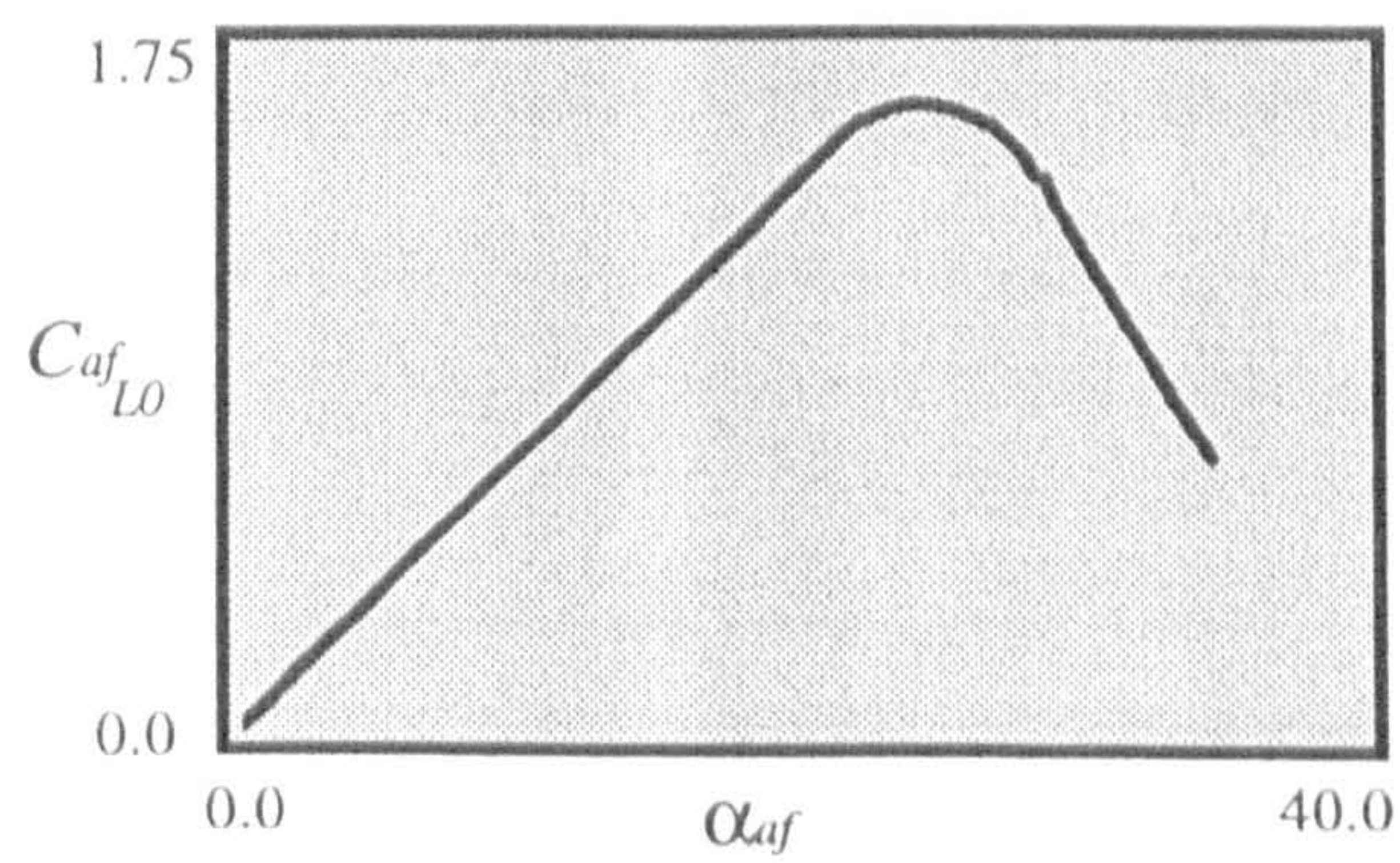


Fig. (5.9): A typical lift vs angle of attack for an airfoil [51]

variation of the moment coefficient with the range of angle of attack can be stated as follows: *For any given profile there is a certain point with respect to which the pitching moment and the pitching moment coefficient have a practically constant value as long as the angle of attack does not exceed the range of linearly varying $C_{af_{L0}}$* [51]. The constant value of the pitching moment coefficient depends on the shape of the profile but is practically independent of the aspect ratio. This point is known as the *aerodynamic center (A.C.)*. For the usual profiles it lies near the chord line, about a quarter chord length aft the leading edge, in accordance to two dimensional airfoil theory [51]. It should be pointed out that the pitching moment is counted positive if it tends to raise the leading edge of the profile.

The values of the coefficient $C_{af_{DP}}$, Kar , $C_{af_{L0}}$ and $C_{af_{M0}}$ for a selected profile are given in Chapter 6.

A general view has been given about the fundamental characteristics of an airfoil in the last few paragraphs. As it might be noticed, the symbols used are slightly different with the usual symbols of aerodynamic dimensionless coefficients. This is done to make them compatible with the overall trend of the aerodynamic modelling explanation.

Now, the components of aerodynamic force and moment acting on a typical airfoil af , shown in Figure 5.11, in terms of the aerodynamic dimensionless coefficients in local body axes system are considered to be

$$\mathbf{A}_{af}^{af} = PH_{af} \cdot S_{af} \begin{Bmatrix} C_{af_x} \\ 0 \\ C_{af_z} \end{Bmatrix} \quad (5.51)$$

$$\mathbf{M}_{af}^{af} = PH_{af} \cdot S_{af} \cdot CHORD_{af} \begin{Bmatrix} 0 \\ C_{af_m} \\ 0 \end{Bmatrix} \quad (5.52)$$

where, the local pressure head and airfoil reference area are given as follows

$$PH_{af} = \frac{1}{2} \rho V_{AC_{af_{ref}}}^2 \quad (5.53)$$

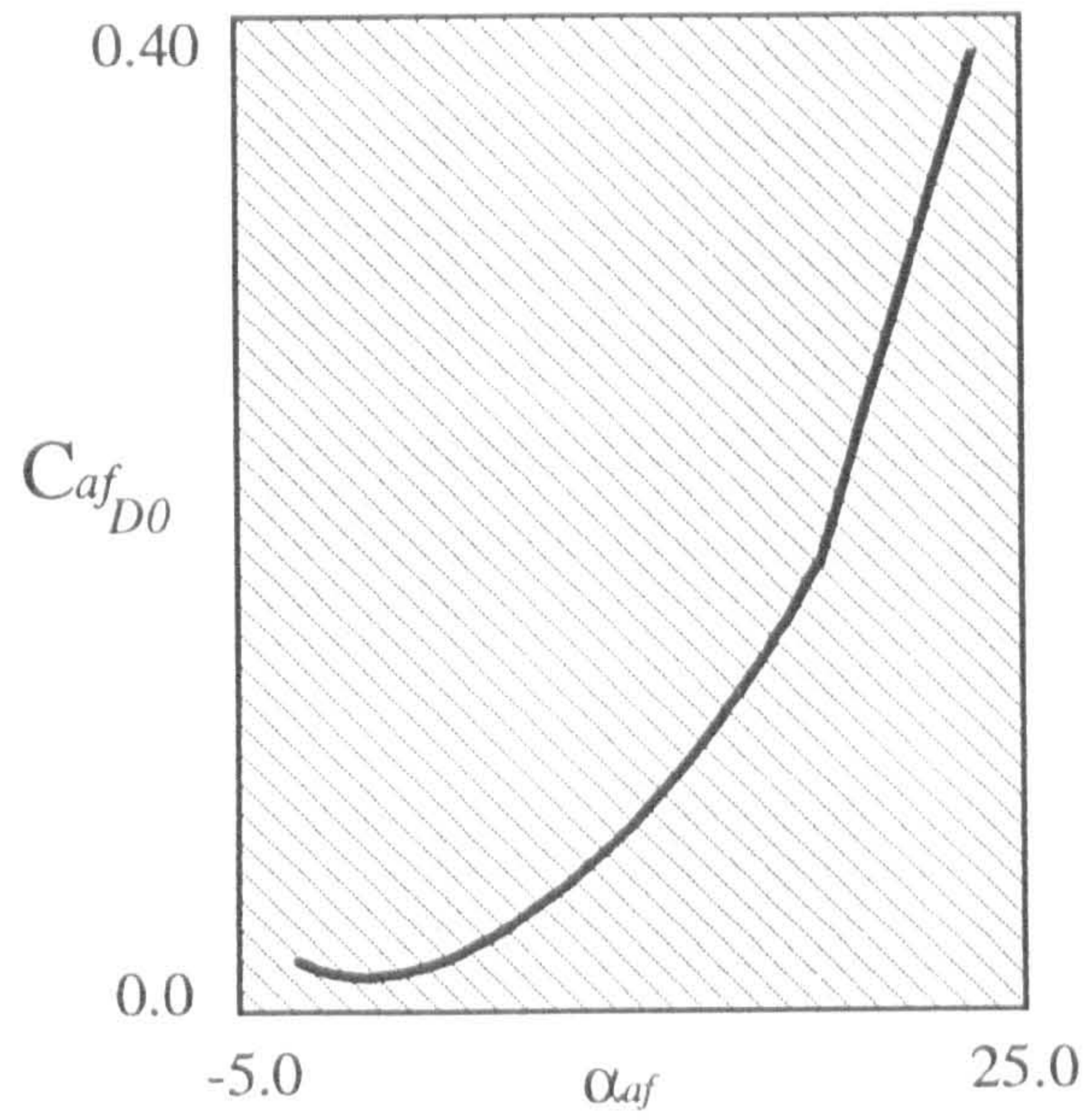


Fig. (5.10): A typical drag coefficient vs angle of attack for an airfoil [51]

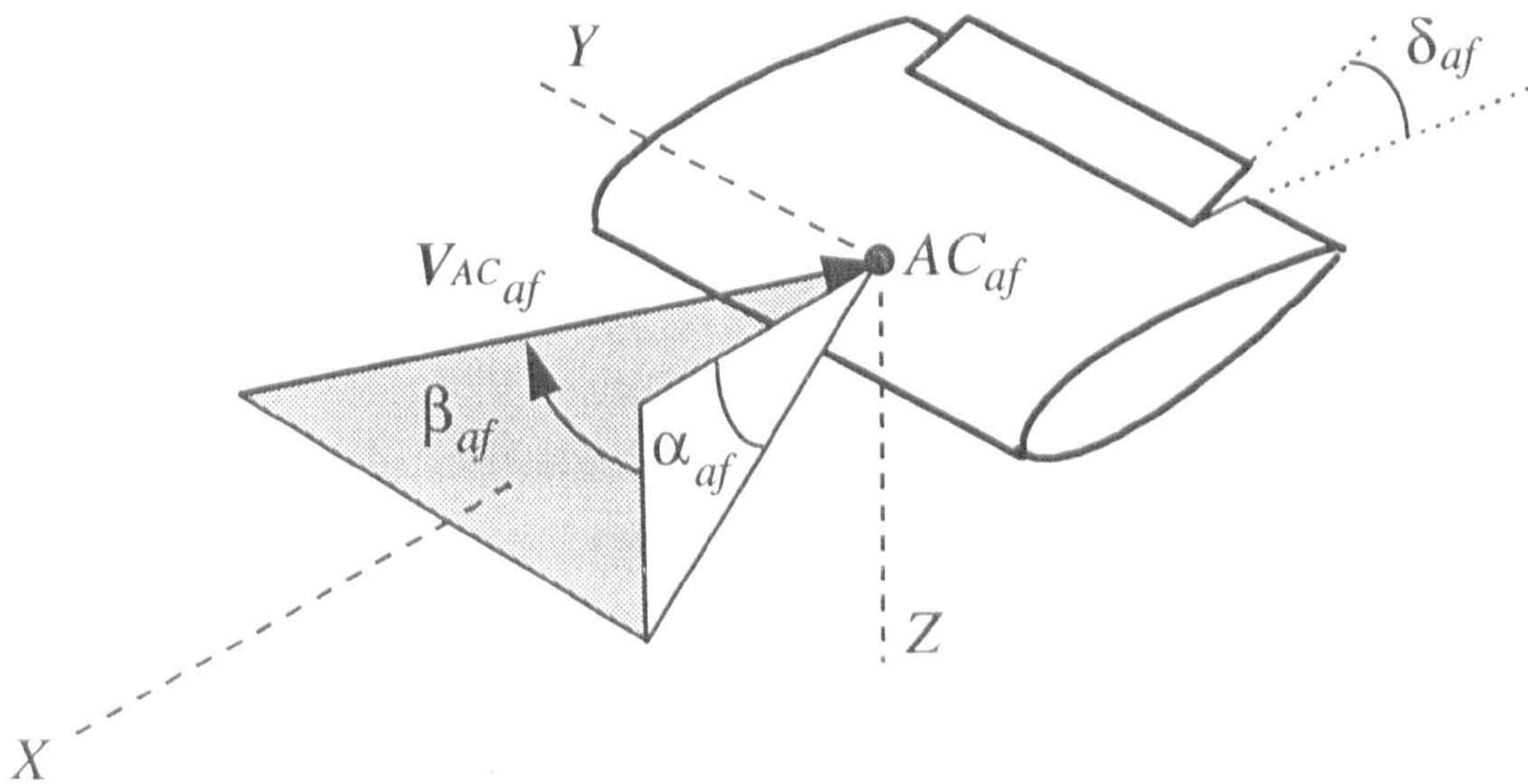


Fig. (5.11): An airfoil in local flow

$$S_{af} = CHORD_{af} \cdot SPAN_{af} \quad (5.54)$$

The aerodynamic dimensionless coefficients associated with x , z and m directions are approximated in terms of the airfoil and control surface contributions at the known angles α_{af} and β_{af} as follows:

$$\begin{aligned} C_{af_x} &= \left(C_{af_{x0}}(\alpha_{af}) + C_{af_{x\delta}}(\alpha_{af}) \delta_{af} \right) \cos(\beta_{af}) \\ C_{af_z} &= \left(C_{af_{z0}}(\alpha_{af}) + C_{af_{z\delta}}(\alpha_{af}) \delta_{af} \right) \cos(\beta_{af}) \\ C_{af_m} &= \left(C_{af_{m0}}(\alpha_{af}) + C_{af_{m\delta}}(\alpha_{af}) \delta_{af} \right) \cos(\beta_{af}) \end{aligned} \quad (5.55)$$

The symbol δ denotes the control surface deflection angle. Also, we have

$$\begin{Bmatrix} C_{af_{x0}}(\alpha_{af}) \\ C_{af_{z0}}(\alpha_{af}) \end{Bmatrix} = \begin{bmatrix} \cos\alpha_{af} & -\sin\alpha_{af} \\ \sin\alpha_{af} & \cos\alpha_{af} \end{bmatrix} \begin{Bmatrix} -C_{af_{D0}}(\alpha_{af}) \\ -C_{af_{L0}}(\alpha_{af}) \end{Bmatrix} \quad (5.56)$$

$$\begin{Bmatrix} C_{af_{x\delta}}(\alpha_{af}) \\ C_{af_{z\delta}}(\alpha_{af}) \end{Bmatrix} = \begin{bmatrix} \cos\alpha_{af} & -\sin\alpha_{af} \\ \sin\alpha_{af} & \cos\alpha_{af} \end{bmatrix} \begin{Bmatrix} -C_{af_{D\delta}}(\alpha_{af}) \\ -C_{af_{L\delta}}(\alpha_{af}) \end{Bmatrix} \quad (5.57)$$

The functions $C_{af_{L\delta}}$, $C_{af_{D\delta}}$ and $C_{af_{m\delta}}$ are the aerodynamic input data. These data will be estimated in the next chapter.

Streamline bodies

A body is called *streamline* if the flow passing it is free (or practically free) of discontinuity surfaces separating a dead-air region from the stream, [51]. There are many different type of streamline bodies. However, in this thesis, the term *streamline body* is applied to bodies of revolution, shown in Figure 5.12. This type of body is symmetric and it has a thicker front part than the rear part. The streamline bodies are used wherever the drag must be kept to a minimum. They are therefore used for the aircraft fuselage and engine nacelles.

Due to the symmetrical shape, of a streamline body, the only nonzero components of aerodynamic force and moment in its wind axes system are lift, drag and pitching moment. In other words, the lateral force, roll moment and yaw moment are theoretically zero. The non-zero components can be expressed as follows

$$\begin{aligned} \text{Lift}_{sb} &= \frac{1}{2} \rho (V_{AC_{sb}})^2 S_{sb} C_{sb_L} \\ \text{Drag}_{sb} &= \frac{1}{2} \rho (V_{AC_{sb}})^2 S_{sb} C_{sb_D} \\ \text{Moment}_{sb} &= \frac{1}{2} \rho (V_{AC_{sb}})^2 S_{sb} C_{sb_{M1}} \end{aligned} \quad (5.58)$$

where C_{sb_L} , C_{sb_D} and $C_{sb_{M1}}$ are dimensionless coefficient of lift, drag and moment. These coefficients depend on Reynolds number and true angle of attack γ_{sb} (the angle of attack between the local velocity vector and the body longitudinal axes). They will be estimated in Chapter 6 for a selected profile.

Now, the components of the aerodynamic force and moment acting on a typical streamline body sb , shown in Figure 5.13, in terms of the dimensionless coefficients in local body axes system are

$$\mathbf{A}_{sb}^{sb} = PH_{sb} \cdot S_{sb} \begin{Bmatrix} C_{sb_x} \\ C_{sb_y} \\ C_{sb_z} \end{Bmatrix} \quad (5.59)$$

$$\mathbf{M}_{A_{sb}}^{sb} = PH_{sb} \cdot S_{sb} \cdot \text{LENGTH}_{sb} \begin{Bmatrix} C_{sb_l} \\ C_{sb_m} \\ C_{sb_n} \end{Bmatrix} \quad (5.60)$$

where

$$PH_{sb} = \frac{1}{2} \rho V_{AC_{sb_{tot}}}^2 \quad (5.61)$$

$$S_{sb} = \text{LENGTH}_{sb} \cdot \text{DIAMETER}_{sb} \quad (5.62)$$

and

$$\begin{Bmatrix} C_{sb_x} \\ C_{sb_y} \\ C_{sb_z} \end{Bmatrix} = [DCM]^{sbw} \begin{Bmatrix} -C_{sb_D} \\ 0 \\ -C_{sb_L} \end{Bmatrix} \quad (5.63)$$

$$\begin{Bmatrix} C_{sb_t} \\ C_{sb_m} \\ C_{sb_n} \end{Bmatrix} = [DCM]^{sbw} \begin{Bmatrix} 0 \\ C_{sb_{m1}} \\ 0 \end{Bmatrix} \quad (5.64)$$

where,[52]

$$[DCM]^{sbw} = \begin{bmatrix} \cos\alpha_{sb} \cdot \cos\beta_{sb} & 0 & \sin\beta_{sb} \cdot \cos\alpha_{sb} \cdot \sin\alpha_{sb} \\ \sin\beta_{sb} & \cos\beta_{sb} \cdot \cos\sigma_{sb} & -\sin\alpha_{sb} \cdot \cos\sigma_{sb} \\ \sin\alpha_{sb} \cdot \cos\beta_{sb} & -\sin\alpha_{sb} \sin\beta_{sb} \cos\sigma_{sb} & -\sin\sigma_{sb} \cdot \cos\beta_{sb} \\ & +\sin\sigma_{sb} \cos\alpha_{sb} & \sin\alpha_{sb} \sin\beta_{sb} \sin\sigma_{sb} \\ & & +\cos\alpha_{sb} \cos\sigma_{sb} \end{bmatrix} \quad (5.65)$$

is the Direction Cosine Matrix from the local wind axes system to the local body axes system.

Propellers

For a propeller the main aerodynamic forces and moments are those which are generated due to the propeller rotation. These were calculated in Section 5.2.1. However, some small quantities of force and moment may be produced by the propeller body. These quantities are neglected in the present model but for the sake of completeness, the associated term are left in the equations. Thus

$${}^{\kappa} \mathbf{A}_p^n = \mathbf{0} \quad (5.66)$$

$${}^{\kappa} \mathbf{M}_{A_p}^n = \mathbf{0} \quad (5.67)$$

Having calculated the aerodynamic forces and moments of each individual component in its local axes system, they should then be transformed into the main reference frames $X_a Y_a Z_a$ and ${}^k X_n {}^k Y_n {}^k Z_n$. Starting with the components of the fuselage-empennage assembly, designated by b in Chapter 3, we have

$$\mathbf{A}_v^a = [DCM]^{vu} \mathbf{A}_v^u \quad (5.68)$$

$${}_{gb} \mathbf{M}_{\Lambda_v}^a = [DCM]^{vu} \mathbf{M}_{\Lambda_v}^u + \mathbf{L}_{v_{a2}}^a \times \mathbf{A}_v^a \quad (5.69)$$

where, $\mathbf{L}_{v_{a2}}$ is the position vector of the component aerodynamic center w.r.t. the center of gravity of the body b . The above transformation associated with each individual element is presented in Appendix B2.

Having expressed all vectors in the same axes system and w.r.t. the same reference point, then

$$\mathbf{A}_b^a = \mathbf{A}_f^a + {}^r \mathbf{A}_h^a + {}^l \mathbf{A}_h^a + {}^u \mathbf{A}_v^a + {}^l \mathbf{A}_v^a \quad (5.70)$$

and

$${}_{gb} \mathbf{M}_{\Lambda_b}^a = {}_{gb} \mathbf{M}_f^a + {}^r \mathbf{M}_{\Lambda_h}^a + {}^l \mathbf{M}_{\Lambda_h}^a + {}^u \mathbf{M}_{\Lambda_v}^a + {}^l \mathbf{M}_{\Lambda_v}^a \quad (5.71)$$

The resultant aerodynamic forces and moment acting on the body A will then be expressed as follows

$$\mathbf{A}_a^a = \mathbf{A}_b^a + \text{Conf}2({}^r \mathbf{A}_w^a + {}^l \mathbf{A}_w^a) \quad (5.72)$$

$${}_o \mathbf{M}_{\Lambda_a}^a = {}_o \mathbf{M}_{\Lambda_b}^a + \text{Conf}2({}_o \mathbf{M}_{\Lambda_w}^a + {}_o \mathbf{M}_{\Lambda_w}^a) \quad (5.73)$$

The terms ${}^r \mathbf{M}_{\Lambda_w}^a$ and ${}^l \mathbf{M}_{\Lambda_w}^a$ are defined in Appendix B2, Equation B2.13. In a similar way, for the components of the tilting body ${}^k np$

$$\mathbf{A}_v^n = [DCM]^{nv} \mathbf{A}_v^v \quad (5.74)$$

$${}_{J_2} \mathbf{M}_{A_v}^n = [DCM]^{nv} \mathbf{M}_{A_v}^v + \mathbf{L}_{v,n_2}^n \times \mathbf{A}_v^n \quad (5.75)$$

where, \mathbf{L}_{v,n_2} is the position vector of the component aerodynamic center w.r.t. the joint J_2 . The above transformation associated with each individual element is presented in Appendix B3. Since, there is no definition of the aerodynamic center for a propeller, this vector represents the position of any point at which the propeller aerodynamic forces and moments are defined. In the present study, the propeller center of gravity is chosen.

The resultant aerodynamic force and moment vector on the tilting body ${}^k np$ will also be expressed as follows.

$${}^k \mathbf{A}_{np}^n = {}^k \mathbf{A}_n^n + {}^k \mathbf{A}_p^n + Conf1. {}^k \mathbf{A}_w^n \quad (5.76)$$

$${}_{J_2}^k \mathbf{M}_{A_{np}}^n = {}_{J_2}^k \mathbf{M}_{A_n}^n + {}_{J_2}^k \mathbf{M}_{A_p}^n + Conf1. {}_{J_2}^k \mathbf{M}_{A_w}^n \quad (5.77)$$

5.2.4 Engine model

Small and medium size unmanned aircraft have historically been powered by piston engines. These engines convert the thermal energy produced by burning fuel into mechanical work. This work is done by rotating the propeller against the resisting aerodynamic torque moment. The propeller is driven either directly on the engine shaft or indirectly by means of a reduction gear.

The power output of an engine depends on two operation variables, the speed (rpm) and the throttle setting (δ_i) which controls the manifold pressure. A complete picture of the operation condition needed in connection with engine modelling is given by the family of curves P_E vs rpm for different throttle settings. Figure 5.14 shows a typical set of such curves. As seen, the output power increases with the throttle setting. For a constant throttle, the output power has a maximum value at a specific rpm. In mathematical terms, these curves can also be represented by

$$P_E = F_E(rpm, \delta_i) \quad (5.78)$$

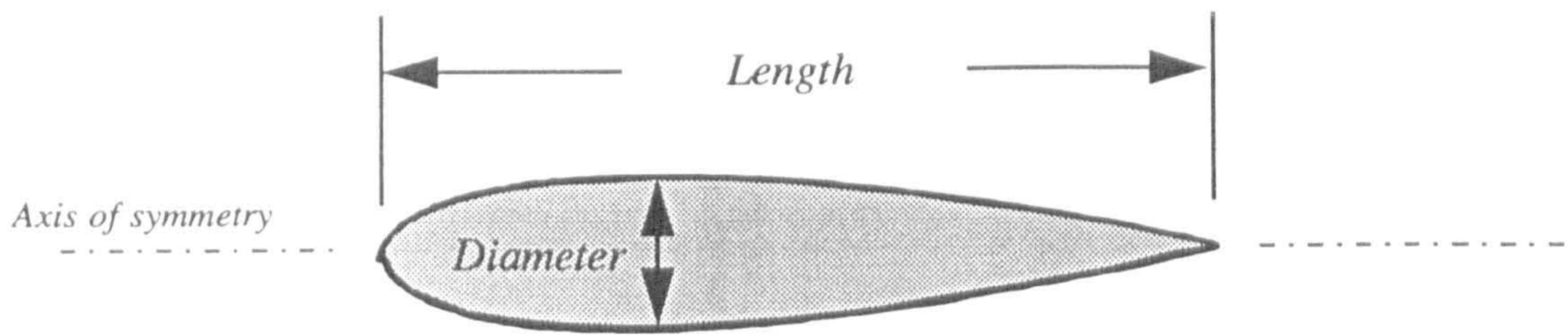


Fig. (5.12): Streamline body dimensions

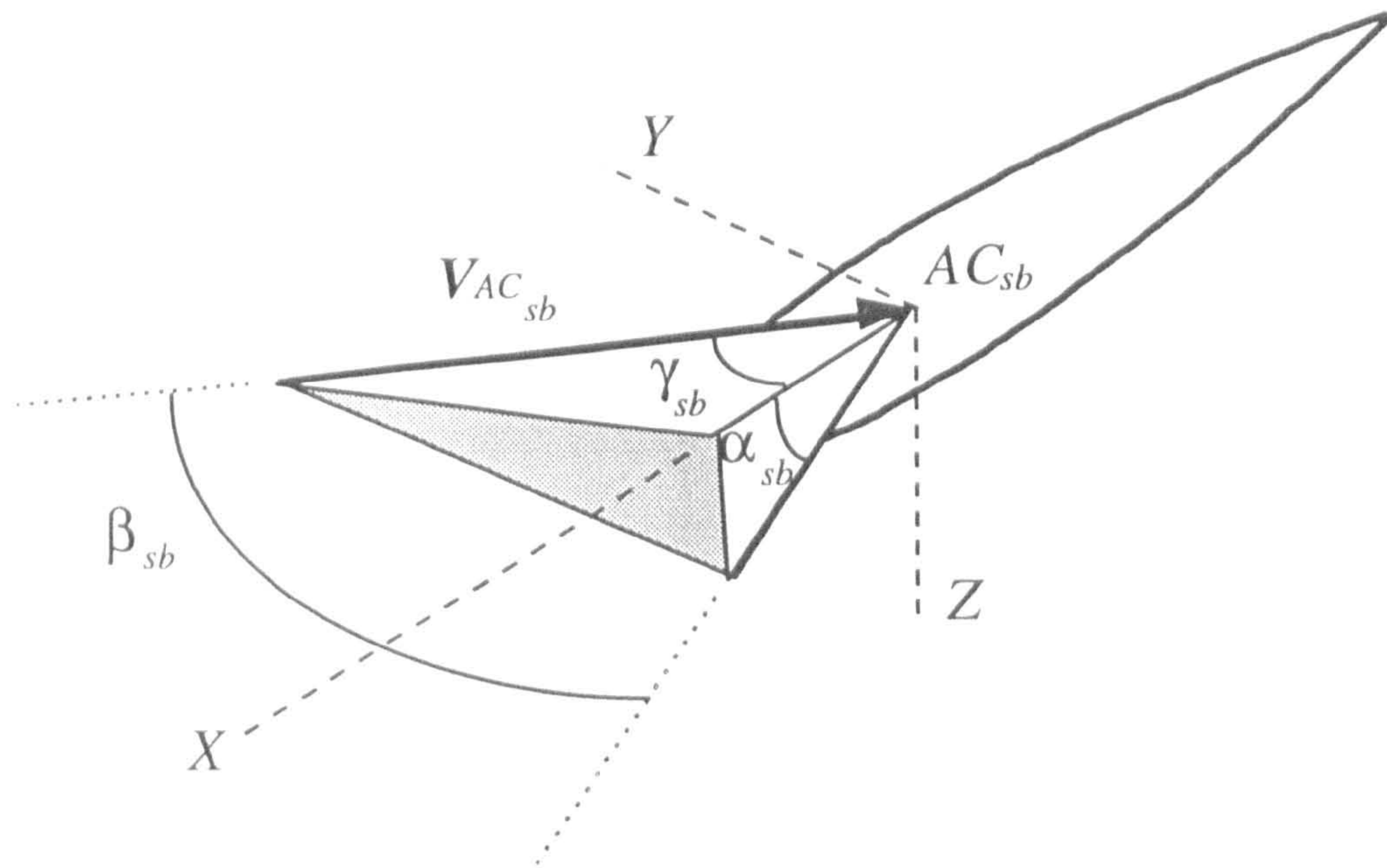


Fig. (5.13): An streamline body in local flow

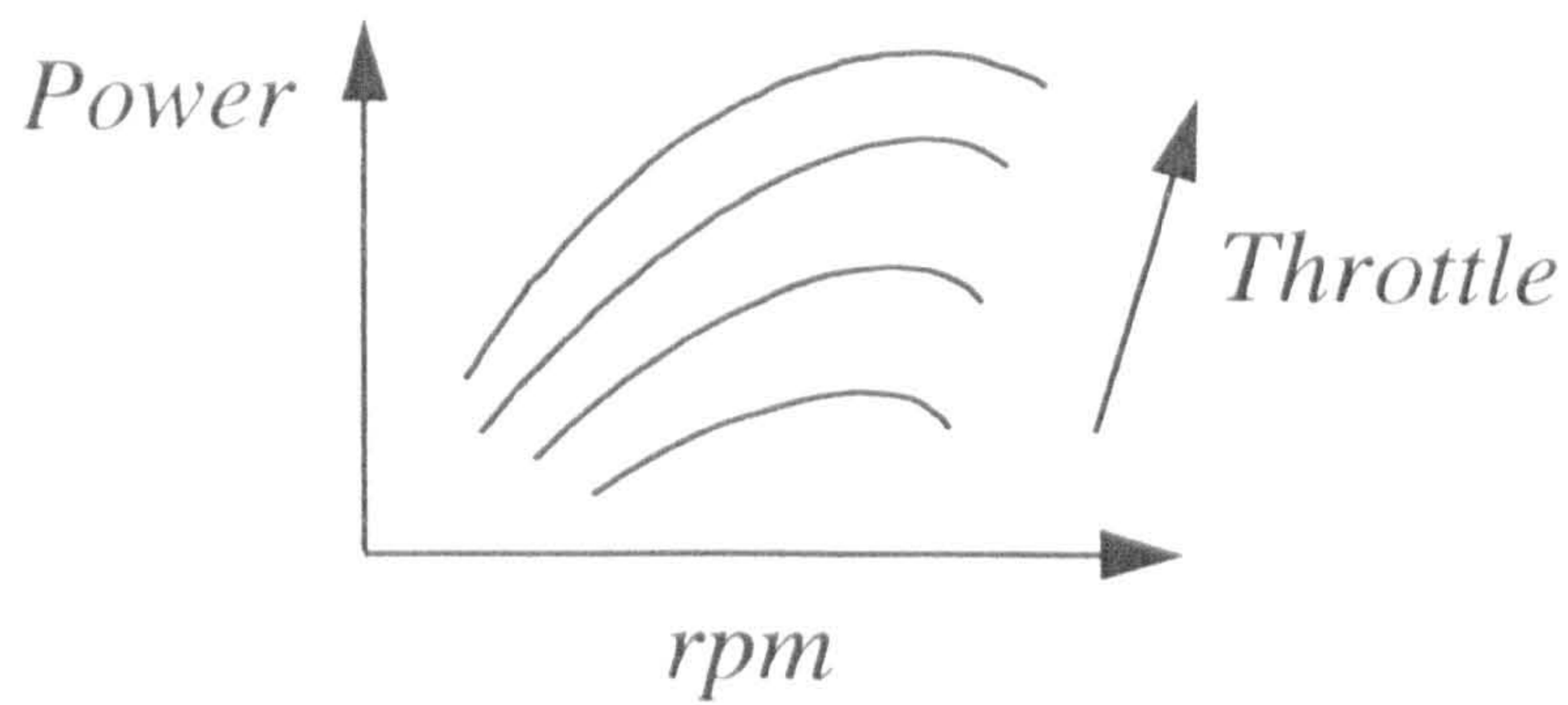


Fig. (5.14): A typical engine power vs rpm

The function F_E is obtained by using experimental data provided by manufacturers or obtained from tests. Therefore, in the present mathematical model, a real engine characteristic is considered. This is important from the point of view of establishing the validity of the control concept. Having calculated the output power, the output torque can then be obtained as follows

$$M_E = \frac{P_E}{\frac{2\pi(\text{rpm})}{60}} \quad (5.79)$$

5.2.5 Servomotor Model

One servomotor has been considered for each of the tilting bodies. A servomotor is a common actuator in control systems which directly provides rotary motion. It is standard to relate the output torque of a servomotor in terms of its armature current [47]. Using the symbols M_s as the output torque and θ_{n_d} as the input current, the servomotors can be simply modelled by the following relation.

$$M_s = K_{Servo} \theta_{n_d} \quad (5.80)$$

The term K_{Servo} is called torque constant. The above model can be easily changed by more complex models relating the output torque to input current.

5.3 GRAVITATIONAL FORCES AND MOMENTS

The objective of this section is to determine all the related terms in the equations of motion associated with gravitational forces and moments. In the first place, the mass of the main objects should be calculated in terms of the mass of the secondary objects which are considered as input data. Therefore

$$m_{np} = m_n + m_p + Conf1.m_w \quad (5.81)$$

$$m_a = m_b + Conf2.(2m_w) \quad (5.82)$$

where

$$m_b = m_f + 2m_h + m_{vu} + m_{vl} \quad (5.83)$$

As it might be noticed, similar components at the right and the left side of the aircraft are considered to have the same mass. The center of gravity location for bodies A and ${}^{\kappa}np$ can then be calculated as follows

$${}^{\kappa}e^n = \frac{m_n {}^{\kappa}k1^n + m_p f^n + Conf1.m_w {}^{\kappa}h^n}{m_{np}} \quad (5.84)$$

$$b^a = \frac{m_b o^a + Conf2(m_w {}^rL1_w^a + m_w {}^lL1_w^a)}{m_a} \quad (5.85)$$

where

$$o^a = \frac{m_f L1_f^a + m_h {}^rL1_h^a + m_h {}^lL1_h^a + m_{vu} {}^uL1_v^a + m_{vl} {}^lL1_v^a}{m_b} \quad (5.86)$$

The weight of each part can be calculated by multiplying its mass by the gravitational acceleration. Therefore

$$\begin{aligned} Weight_a &= m_a \cdot GraAcc \\ Weight_n &= m_n \cdot GraAcc \\ Weight_p &= m_p \cdot GraAcc \\ Weight_w &= m_w \cdot GraAcc \\ Weight_b &= m_b \cdot GraAcc \\ Weight_f &= m_f \cdot GraAcc \\ Weight_{np} &= m_{np} \cdot GraAcc \end{aligned} \quad (5.87)$$

The following vectors can then be defined

$$W_{np}^i = \left\{ \begin{array}{c} 0 \\ 0 \\ Weight_{np} \end{array} \right\} \quad (5.88)$$

$$\mathbf{W}_a^i = \begin{Bmatrix} 0 \\ 0 \\ \text{Weight}_a \end{Bmatrix} \quad (5.89)$$

Now, the associated gravitational forces and moments appeared in the equations of motion can be expressed as follows

$${}^{\kappa} \mathbf{W}_{np}^n = {}^{\kappa} [\mathit{DCM}]^{na} [\mathit{DCM}]^{ai} \mathbf{W}_{np}^i \quad (5.90)$$

$$\mathbf{W}_a^a = [\mathit{DCM}]^{ai} \mathbf{W}_a^i \quad (5.91)$$

$${}_{J_2}^{\kappa} \mathbf{M}_{W_{np}}^n = {}^{\kappa} \mathbf{e}^n \times {}^{\kappa} \mathbf{W}_{np}^n = [{}^{\kappa} \mathbf{e}^n] {}^{\kappa} \mathbf{W}_{np}^n \quad (5.92)$$

$${}_o \mathbf{M}_{W_a}^a = \mathbf{b}^a \times \mathbf{W}_a^a = [\mathbf{b}^a] \mathbf{W}_a^a \quad (5.93)$$

Obviously

$${}_{gp}^{\kappa} \mathbf{M}_{W_p}^n = 0 \quad (5.94)$$

5.4 MASS MOMENT OF INERTIA MODELLING

Having obtained the previously mentioned terms, the only remaining ones are the mass moments of inertia associated with the main objects. Therefore, in the following, the method of calculating these quantities in terms of the mass moment of inertia of the secondary objects is presented. The following definition is needed for the rest of the calculations.

For a typical position vector \mathbf{S}

$$\{S\} = \begin{bmatrix} S_y^2 + S_z^2 & -S_y S_x & -S_z S_x \\ -S_x S_y & S_x^2 + S_z^2 & -S_z S_y \\ -S_x S_z & -S_y S_z & S_x^2 + S_y^2 \end{bmatrix} \quad (5.95)$$

Let's start with the components of the fuselage-empennage assembly (body b). For a typical component v according to parallel axes theorem [46]

$$[{}_{gb}I_v^a] = [{}_{gv}I_v^a] + m_v \{L_{v,g}^a\} \quad (5.96)$$

where, $L_{v,g}$ is the position vector of the component center of gravity w.r.t. the center of gravity of the fuselage-empennage assembly b , and

$$[{}_{gv}I_v^a] = [DCM]^{gv} [{}_{gv}I_v^v] [DCM]^{va} \quad (5.97)$$

The expanded form of the above equations for different components is given in the Appendix B3. Having expressed all the inertia matrices in the same axes and w.r.t. the same reference point, then

$$[{}_{gb}I_b^a] = [{}_{gb}I_f^a] + [{}_{gb}^r I_h^a] + [{}_{gb}^l I_h^a] + [{}_{gb}^u I_v^a] + [{}_{gb}^l I_v^a] \quad (5.98)$$

and

$$[{}_o I_b^a] = [{}_{gb}I_b^a] + m_b \{o^a\} \quad (5.99)$$

The mass moment of inertia of the body A w.r.t. the point O can then be expressed as follows

$$[{}_o I_a^a] = [{}_o I_b^a] + Conf2. \left([{}_o^r I_w^a] + [{}_o^l I_w^a] \right) \quad (5.100)$$

In a similar way, for the components of the tilting body ${}^k np$

$$[{}_j I_v^a] = [{}_{gv}I_v^a] + m_v \{L_{v,g}^a\} \quad (5.101)$$

where, $\mathbf{L}_{v_{a3}}$ is the position vector of the component center of gravity w.r.t. the joints ${}^{\kappa}J_2$, and

$$[{}_{sv}I_v^n] = [DCM]^{sv} [{}_{sv}I_v^v] [DCM]^{va} \quad (5.102)$$

For more detail about each individual component refer to Appendix B3

The moment of inertia of the body ${}^{\kappa}np$ w.r.t. the point ${}^{\kappa}J_2$ can then be expressed as follows

$$[{}_{J_2}I_{np}^{\kappa}] = [{}_{J_2}I_n^{\kappa}] + [{}_{J_2}I_p^{\kappa}] + Conf1. [{}_{J_2}I_w^{\kappa}] \quad (5.103)$$

CHAPTER SIX

DATA PREPARATION

6.1 INTRODUCTION

In the last three chapters, the aircraft mathematical model has been developed. The next step is computer programming and validation of this mathematical model which are the subjects of the following chapters. However, since there is no specific data available, a set of reasonable input data must be approximated in the first place. The approximation of this data must be carried out carefully and based on the realistic assumptions. The data estimation procedures and associated issues were sufficiently important to form a complete chapter.

6.2 BASELINE CONFIGURATION

Since the beginning of the mathematical modelling the baseline configuration has been known. This configuration is shown in Figure 1.5. However, for the sake of model testing, the geometric proportion between the aircraft components are needed. These could be determined via a conceptual design phase if there were a defined mission and a set of requirements to be satisfied, but there are not. Therefore, the best choice was to use an already existing VTOL aircraft as the baseline configuration. The geometry of the Bell Tilt-rotor unmanned aircraft known as *Pointer* [34] was therefore selected for such an analysis. Having fixed the geometry, the size of the aircraft could then be arbitrarily selected.

In this study, in order to use the existing experimentally obtained characteristic curves of a small two-stroke engine used with a 20 inch propeller on the XRAE-2 unmanned aircraft [58], it was decided to size the aircraft so that the above combination could be used as the propulsion system. Therefore, using the Pointer configuration, the aircraft dimensions were scaled to match with the selected propeller size. Also, the total weight of the aircraft at take off was calculated in terms of the available engine power at $\delta_i = 0.64$ and $rpm = 6000.0$. Further discussion of this is presented later.

6.3 AIRCRAFT DIMENSIONS

The three view drawing of the Bell Tilt-rotor unmanned aircraft Pointer and the equivalent panels corresponding to the wings and stabilisers is shown in Figure 6.1. The dimensions of the panels are determined in terms of the average chord and span of their corresponding lifting surfaces. The position of the aircraft center of gravity is to be located as close as possible to the direction of the thrust line to prevent any unnecessary pitching moment in hover. Therefore, the joints and the wings' center of gravity are assumed to be coincident in the $X_a Z_a$ plane. In addition, the location of the fuselage center of gravity is chosen so as to ensure that the center of gravity of the whole fuselage-empennage assembly is located along the thrust line. As seen in Figure 6.1, the origin O is considered to be on the longitudinal axis of the aircraft fuselage and exactly below the joints in the $X_a Z_a$ plane. Regarding such considerations, all the required dimensions can be approximated as follows:

All dimensions are in meter

Propeller diameter=0.522

$$\begin{array}{ll}
 CHORD_w = 0.18326 & SPAN_w = 0.3318 \\
 CHORD_h = 0.1222 & SPAN_h = 0.1777 \\
 CHORD_{vu} = 0.1777 & SPAN_{vu} = 0.19436 \\
 CHORD_{vl} = 0.18326 & SPAN_{vl} = 0.0777
 \end{array} \tag{6.1}$$

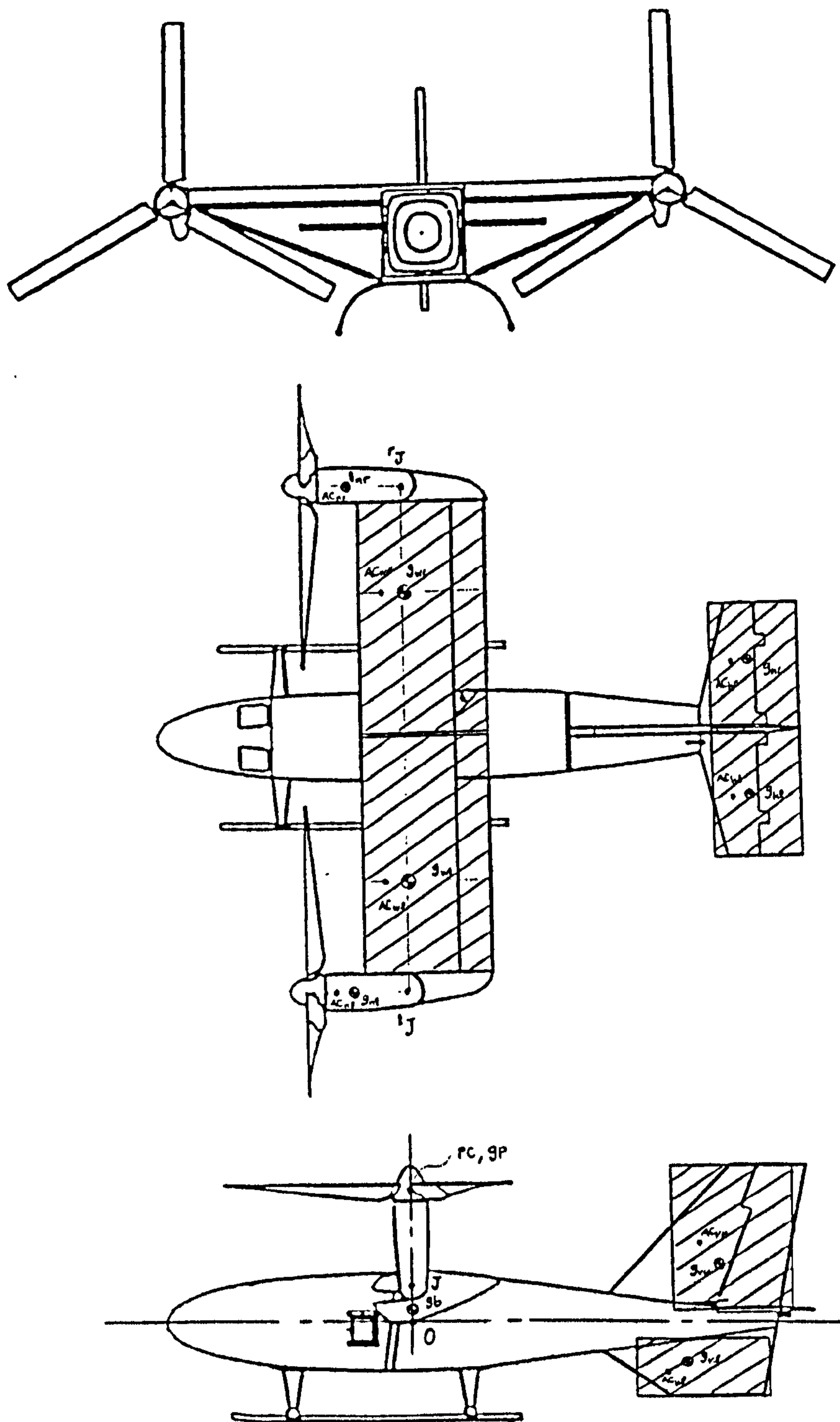


Fig.(6.1): Three drawing view of the pointer [34]

$$\begin{aligned} \text{LENGTH}_f &= 0.8552 & \text{DIA}_f &= 0.1305 \\ \text{LENGTH}_n &= 0.18326 & \text{DIA}_n &= 0.0555 \end{aligned} \quad (6.2)$$

$${}^r\mathbf{d}^a = \begin{Bmatrix} 0.0 \\ 0.35 \\ -0.05 \end{Bmatrix} ; \quad {}^l\mathbf{d}^a = \begin{Bmatrix} 0.0 \\ -0.35 \\ -0.05 \end{Bmatrix} \quad (6.3)$$

$${}^r\mathbf{k1}^n = \begin{Bmatrix} 0.0944 \\ 0.0 \\ 0.0 \end{Bmatrix} ; \quad {}^l\mathbf{k1}^n = \begin{Bmatrix} 0.0944 \\ 0.0 \\ 0.0 \end{Bmatrix} \quad (6.4)$$

$${}^r\mathbf{k2}^n = \begin{Bmatrix} 0.1133 \\ 0.0 \\ 0.0 \end{Bmatrix} ; \quad {}^l\mathbf{k2}^n = \begin{Bmatrix} 0.1133 \\ 0.0 \\ 0.0 \end{Bmatrix} \quad (6.5)$$

$$\mathbf{f}^n = \begin{Bmatrix} 0.1583 \\ 0.0 \\ 0.0 \end{Bmatrix} ; \quad \mathbf{j}^n = \begin{Bmatrix} 0.0 \\ 0.0 \\ 0.0 \end{Bmatrix} \quad (6.6)$$

$${}^r\mathbf{h}^w = \begin{Bmatrix} 0.0 \\ -0.1555 \\ 0.0 \end{Bmatrix} ; \quad {}^l\mathbf{h}^w = \begin{Bmatrix} 0.0 \\ 0.1555 \\ 0.0 \end{Bmatrix} \quad (6.7)$$

$${}^r\mathbf{L1}_h^a = \begin{Bmatrix} -0.4774 \\ 0.0889 \\ -0.0111 \end{Bmatrix} ; \quad {}^l\mathbf{L1}_h^a = \begin{Bmatrix} -0.4774 \\ -0.0889 \\ -0.0111 \end{Bmatrix} \quad (6.8)$$

$${}^r\mathbf{L1}_v^a = \begin{Bmatrix} -0.4108 \\ 0.0 \\ -0.0833 \end{Bmatrix} ; \quad {}^l\mathbf{L1}_v^a = \begin{Bmatrix} -0.3719 \\ 0.0 \\ 0.0555 \end{Bmatrix} \quad (6.9)$$

$$\mathbf{L1}_f^a = \begin{Bmatrix} 0.006714 \\ 0.0 \\ 0.0 \end{Bmatrix} ; \quad \mathbf{L2}_f^a = \begin{Bmatrix} 0.0012 \\ 0.0 \\ 0.0 \end{Bmatrix} \quad (6.10)$$

$${}^w\mathbf{L2}_w^w = \begin{Bmatrix} 0.01666 \\ 0.0 \\ 0.0 \end{Bmatrix} ; \quad {}^w\mathbf{L2}_w^w = \begin{Bmatrix} 0.01666 \\ 0.0 \\ 0.0 \end{Bmatrix} \quad (6.11)$$

$${}^h\mathbf{L2}_h^h = \begin{Bmatrix} 0.01452 \\ 0.0 \\ 0.0 \end{Bmatrix} ; \quad {}^h\mathbf{L2}_h^h = \begin{Bmatrix} 0.01452 \\ 0.0 \\ 0.0 \end{Bmatrix} \quad (6.12)$$

$${}^v\mathbf{L2}_v^v = \begin{Bmatrix} 0.01944 \\ 0.03054 \\ 0.0 \end{Bmatrix} ; \quad {}^v\mathbf{L2}_v^v = \begin{Bmatrix} 0.01666 \\ -0.01666 \\ 0.0 \end{Bmatrix} \quad (6.13)$$

6.4 PROPELLER CHARACTERISTICS

In the process of modelling the propeller in Section 5.2.1, it was pointed out that the propeller characteristics are usually represented by propeller charts. Unfortunately, for the selected propeller size, such data is very rarely obtained. Normally, these kind of propellers are two-bladed with a fixed-pitch and are constructed from a single piece of laminated wood or composite material. They are generally used in small unmanned or model aircraft. No aerodynamic data is provided by manufacturers for this type of propeller. The only data obtained, is reported in [59] which is limited to the range of the pitch angles between 12 to 18.75 deg. There is a good agreement between this data and the data provided in Reference [57] for a two-blade 5869-9 propeller which, of course, covers a much wider range of pitch angle up to 45 deg., Figure 6.2 and 6.3. Therefore, it was decided to use the charts in these figures as propeller characteristics in the present work.

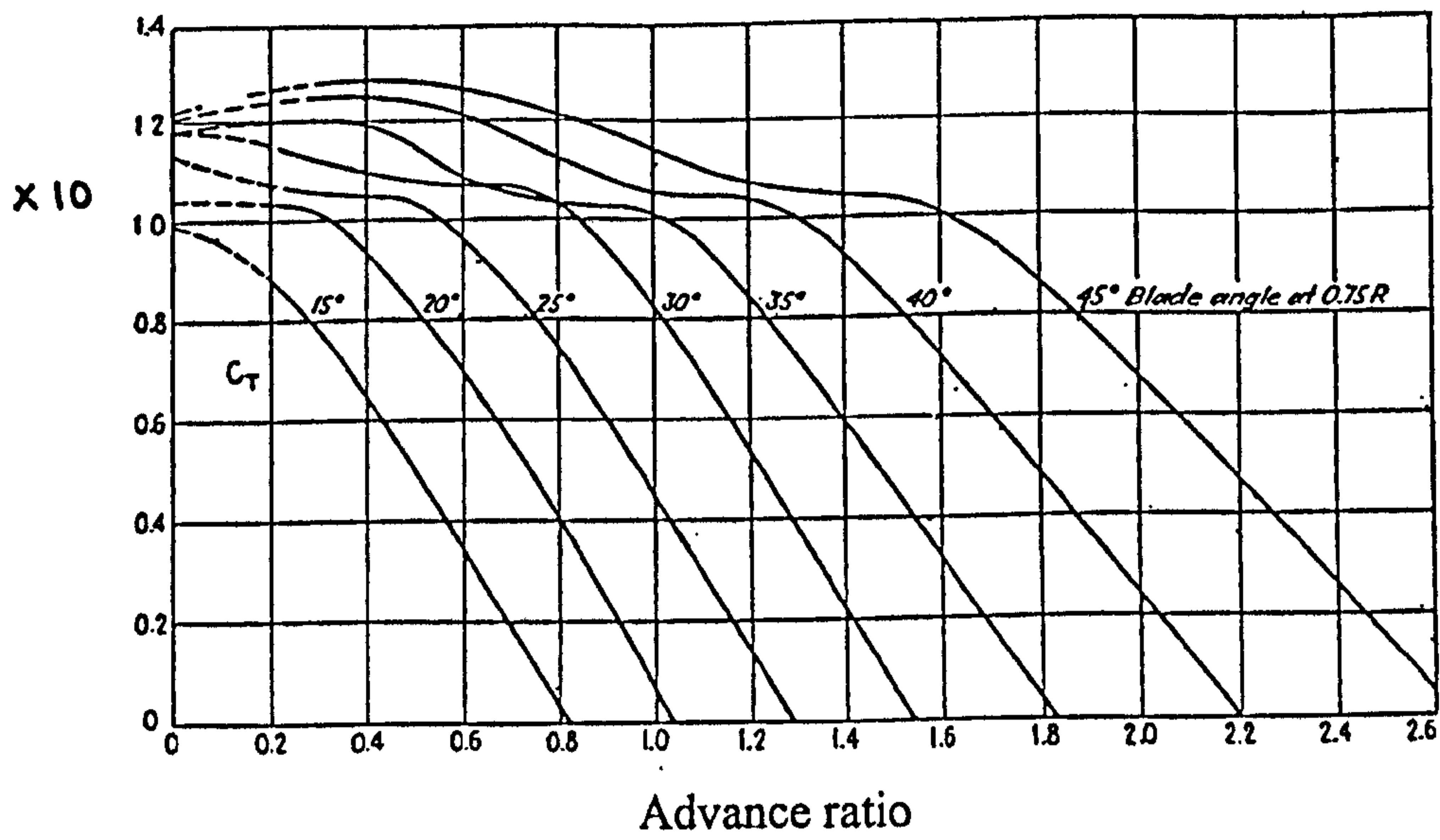


Fig.(6.2): C_T vs ADR for two-blade 5869-9 propeller with Clark Y section [57]

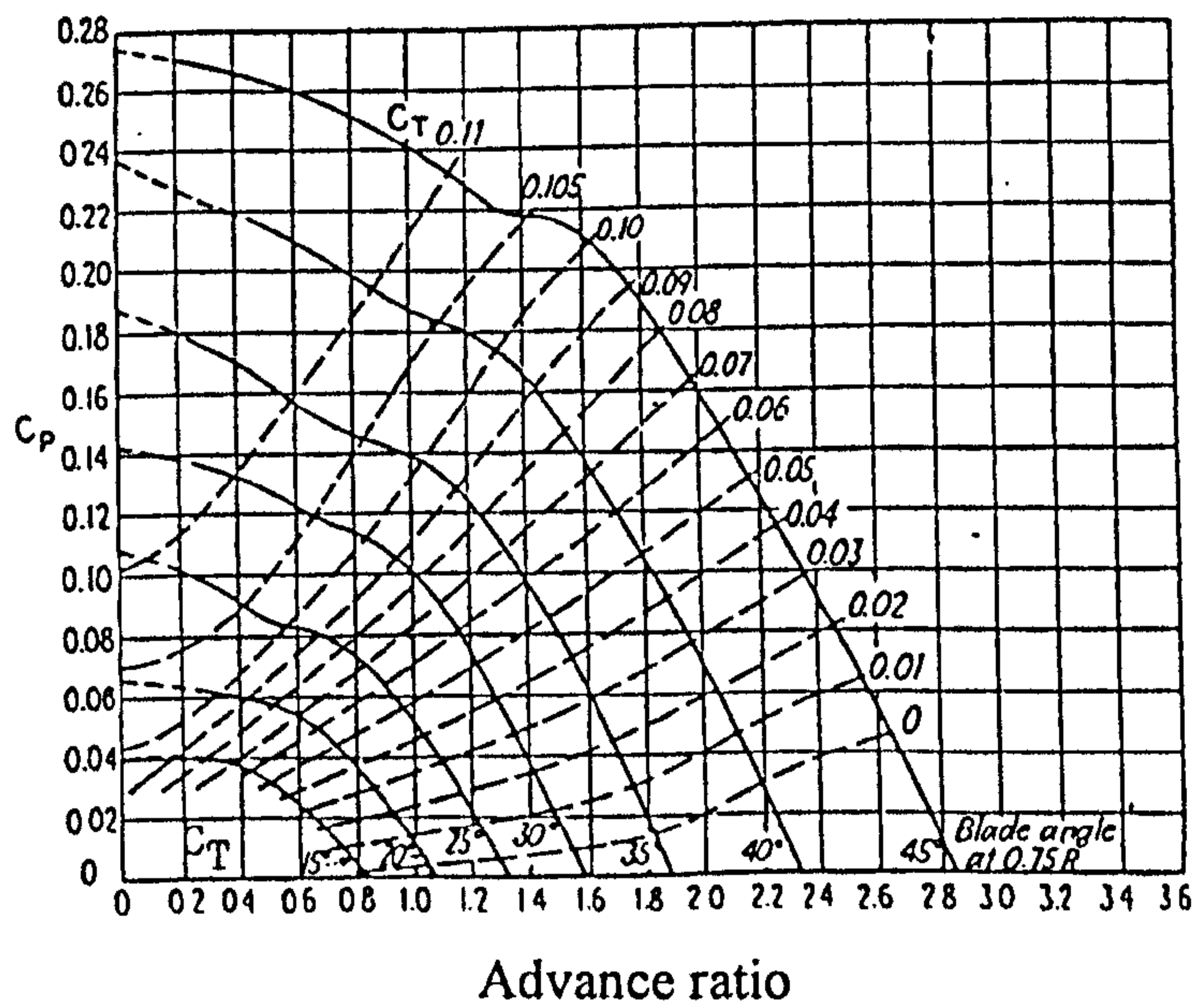


Fig.(6.3): C_p vs ADR for two-blade 5869-9 propeller with C_T plotted as parameter [57]

The lines on these charts represent tests run at a fixed blade angle at $0.75R$. For any given blade angle, there is a value of *advance ratio (ADR)* that will give zero mean effective angle of attack on the propeller blade and zero C_T . As the advance ratio is reduced from the zero thrust value, the angle of attack on all elements of the propeller blade increases. This gives an increase in C_T almost in direct proportion to the reduction in advance ratio until an angle of attack is reached where the most of the elements of the propeller blade begin to stall. Further reductions of advance ratio below the stalling value yields no increase in C_T . For different blade angles the values of advance ratio at zero thrust and stalling point are different, but the maximum C_T at stall is approximately the same.

It might be noticed in Figures 6.2 and 6.3 that the values of advance ratio corresponding to $C_T = 0.0$ and $C_p = 0.0$ are not coincident. There is always some small value of C_p when $C_T = 0.0$, corresponding to the power necessary to turn the propeller when it is delivering no thrust. This is mainly due to skin friction. As thrust coefficient increases, an induced drag is developed on the propeller blade elements, which increases the power required to turn the propeller.

For computer implementation, the C_T and C_p charts are tabulated in Tables 6.1 and 6.2. Since, there is no data for the negative values of advanced ratio, each curve is extended by a horizontal line, corresponding to its value at $ADR=0.0$, to the left up to $ADR=-0.6$. In order to use the TABLE statement available in Advanced Continuous Simulation Language (ACSL) [60], the same number of data points for all curves is needed. Therefore, a negative value -0.1 is considered wherever it is necessary in the tables.

Finally, it should be pointed out that the propeller charts in Figures 6.2 and 6.3 are determined experimentally for a propeller in axial flow, i.e. zero angle of attack. To be able to use these charts for all flight conditions, the advance ratio is defined in terms of the component of the air velocity vector normal to the propeller disk, Equation 5.9.

6.5 ENGINE CHARACTERISTICS

The engine characteristics associated with a two-stroke ML88.MCD engine which is used in XRAE-2 unmanned aircraft are tabulated in Table 6.3, [61]. In order to use the

Table (6.1): The propeller thrust coefficient

ADR	-0.6	-0.4	-0.2	0.0	0.2	0.4	0.6	0.8	1.0
θ_c	Thrust coefficient								
15	0.1	0.1	0.1	0.1	0.088	0.065	0.035	0.004	-0.03
20	0.104	0.104	0.104	0.104	0.104	0.094	0.07	0.04	0.007
25	0.113	0.113	0.113	0.113	0.108	0.105	0.096	0.075	0.045
30	0.117	0.117	0.117	0.117	0.115	0.11	0.107	0.104	0.093
35	0.117	0.117	0.117	0.117	0.120	0.119	0.109	0.104	0.102
40	0.120	0.120	0.120	0.120	0.124	0.126	0.122	0.114	0.106
45	0.122	0.122	0.122	0.122	0.126	0.129	0.126	0.122	0.115

ADR	1.2	1.4	1.6	1.8	2.0	2.2	2.4	2.6	2.8
θ_c	Thrust coefficient								
15	-0.1	-0.1	-0.1	-0.1	-0.1	-0.1	-0.1	-0.1	-0.1
20	-0.027	-0.1	-0.1	-0.1	-0.1	-0.1	-0.1	-0.1	-0.1
25	0.014	-0.017	-0.046	-0.1	-0.1	-0.1	-0.1	-0.1	-0.1
30	0.054	0.023	-0.008	-0.04	-0.1	-0.1	-0.1	-0.1	-0.1
35	0.084	0.06	0.032	0.004	-0.023	-0.1	-0.1	-0.1	-0.1
40	0.104	0.093	0.073	0.049	0.024	0.0	-0.023	-0.1	-0.1
45	0.107	0.104	0.100	0.087	0.068	0.047	0.026	0.006	-0.015

Table (6.2): The propeller power coefficient

ADR	-0.6	-0.4	-0.2	0.0	0.2	0.4	0.6	0.8	1.0
θ_c	Power coefficient								
15	0.04	0.04	0.04	0.04	0.04	0.037	0.025	0.004	-0.015
20	0.075	0.072	0.07	0.067	0.063	0.06	0.055	0.037	0.01
25	0.12	0.115	0.112	0.109	0.1	0.092	0.083	0.075	0.053
30	0.16	0.152	0.147	0.143	0.139	0.133	0.122	0.115	0.1
35	0.21	0.201	0.195	0.188	0.18	0.17	0.157	0.146	0.14
40	0.263	0.255	0.245	0.237	0.227	0.22	0.21	0.198	0.188
45	0.283	0.28	0.278	0.275	0.27	0.265	0.26	0.252	0.24

ADR	1.2	1.4	1.6	1.8	2.0	2.2	2.4	2.6	2.8
θ_c	Power coefficient								
15	-0.04	-0.1	-0.1	-0.1	-0.1	-0.1	-0.1	-0.1	-0.1
20	-0.02	-0.1	-0.1	-0.1	-0.1	-0.1	-0.1	-0.1	-0.1
25	0.022	-0.015	-0.047	-0.1	-0.1	-0.1	-0.1	-0.1	-0.1
30	0.075	0.04	-0.003	-0.04	-0.1	-0.1	-0.1	-0.1	-0.1
35	0.125	0.100	0.06	0.02	-0.025	-0.1	-0.1	-0.1	-0.1
40	0.18	0.165	0.138	0.105	0.07	0.028	-0.012	-0.06	-0.1
45	0.23	0.218	0.212	0.19	0.16	0.125	0.09	0.055	0.01

ACSL TABLE statement, the engine power should be recalculated in terms of the same specific rpms for all throttle settings. Having done this, the final form of engine data is represented in Table 6.4.

6.6 AIRFOIL CHARACTERISTICS

The only available data that covers the angles of attack from -180 to 180 degrees was associated with a NACA 0012 airfoil section [62]. This airfoil section is commonly used as a rotor-blade section in helicopters and it may not be suitable for an aircraft wing at all. However, due to the shortage of any other source of data, the characteristics of this airfoil, shown in Figure 6.4 are used. The graphs in this figure are tabulated in Table 6.5. It should be pointed out that only the attached flow characteristics would change significantly with a change of section.

The effect of the control surface deflection angle δ on the resultant drag force and pitching moment are neglected. Thus

$$\begin{aligned} C_{af_{D\delta}} &= 0.0 \\ C_{af_{M\delta}} &= 0.0 \end{aligned} \quad (6.14)$$

However, this effect on the resultant lift force can not be ignored. Therefore, $C_{af_{L\delta}}$ should be approximated for a range of angles of attack from -180 to 180 deg. Unfortunately, there is no source of data to be directly used for such an approximation over this range. However, the vertical stabiliser lift coefficient of the Bell model 301 Tilt-rotor research aircraft [63], was available in terms of the local angle of attack and rudder deflection angle in the range of -90 to 90 deg. and -20 to 20 deg., respectively, Table 6.6. Using this data, the variation of lift coefficient with rudder deflection at an angle of attack α can then be approximated by the slope of the line shown in Figure 6.5 as follows.

$$C_{L\delta}(\alpha) = \frac{C_L(20^\circ) - C_L(-20^\circ)}{\frac{\pi}{180}(20 - (-20))} = 1.424(C_L(20^\circ) - C_L(-20^\circ)) \quad (6.15)$$

Table (6.3): The original engine data [61]

Throttle setting									
$\delta t = 0.41$		$\delta t = 0.53$		$\delta t = 0.64$		$\delta t = 0.81$		$\delta t = 1.0$	
rpm	P (kw)	rpm	P (kw)	rpm	P (kw)	rpm	P (kw)	rpm	P (kw)
4700	1.92	4400	2.4	4600	2.65	4700	2.85	4900	3.06
5300	1.95	4850	2.62	5100	3.02	5200	3.15	5300	3.3
5650	2.1	5300	2.65	5550	3.02	5700	3.35	5820	3.6
6600	2.24	5760	2.62	6200	3.28	6400	3.62	6520	3.88
6700	2.24	6400	2.88	6700	3.33	7100	3.95	7260	4.28
		6760	2.72	7250	3.42	7600	4.05	7850	4.5
		7000	2.9	7600	3.5	8050	4.25	8300	4.7

Table (6.4): The recalculated engine data

rpm	4000	4500	5000	5500	6000	6500	7000	7500	8000	8500
δt	Power (KW)									
1	2.52	2.82	3.12	3.415	3.672	3.872	4.139	4.369	4.567	4.79
.81	2.43	2.73	3.03	3.27	3.466	3.667	3.903	4.03	4.228	4.45
.64	2.206	2.576	2.946	3.02	3.2	3.31	3.379	3.477	3.591	3.706
.53	2.204	2.449	2.63	2.637	2.72	2.836	2.9	2.94	2.97	3.0
.41	1.885	1.91	1.935	2.036	2.15	2.225	2.24	2.24	2.24	2.24

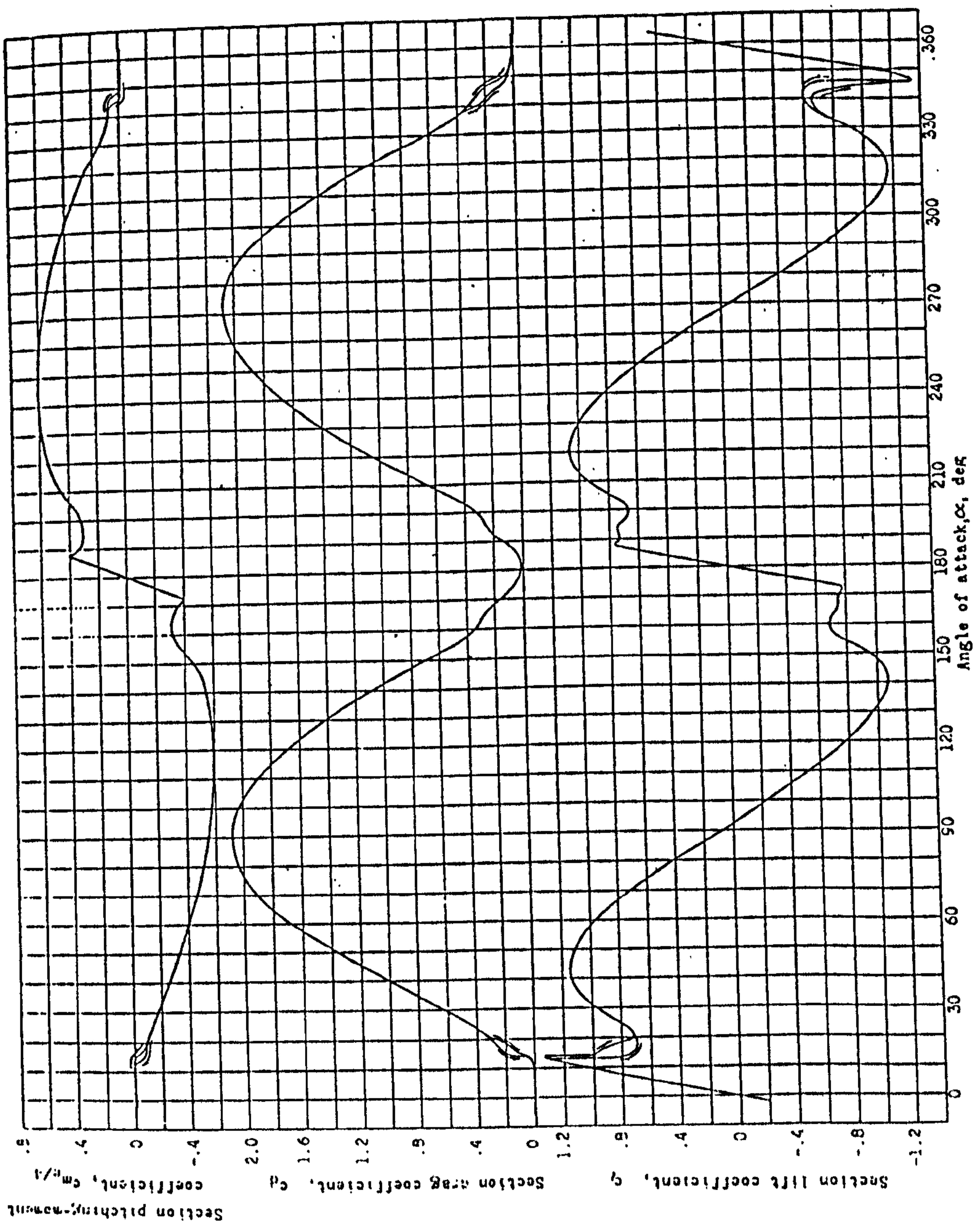


Fig.(6.4): Aerodynamic characteristics of NACA 0012 airfoil section [62]

Table (6.5): The tabulated aerodynamic characteristics of NACA 0012 airfoil section

α_{af}	-180	-175	-173	-170	-165	-160	-155	-150	-145	-140	-135	-130	-125	-120	-115	-110
C_{afLO}	0.0	0.5	0.78	0.75	0.75	0.7	0.76	0.95	1.05	1.07	1.05	0.97	0.88	0.8	0.67	0.53
C_{afDO}	0.01	0.03	0.1	0.14	0.25	0.32	0.46	0.65	0.83	1.05	1.22	1.4	1.53	1.67	1.78	1.88
C_{afm0}	0.0	0.27	0.4	0.33	0.3	0.32	0.38	0.45	0.51	0.55	0.57	0.58	0.59	0.6	0.6	0.6

α_{af}	-105	-100	-95	-90	-85	-80	-75	-70	-65	-60	-55	-50	-45	-40	-35	-30
C_{afLO}	0.38	0.23	0.1	-0.07	-0.23	-0.4	-0.55	-0.71	-0.85	-0.95	-1.05	-1.1	-1.13	-1.13	-1.08	-0.98
C_{afDO}	1.95	2.0	2.05	2.07	2.06	2.05	2.0	1.95	1.82	1.72	1.55	1.4	1.22	1.05	0.81	0.62
C_{afm0}	0.6	0.6	0.58	0.57	0.56	0.54	0.52	0.5	0.46	0.43	0.38	0.35	0.32	0.28	0.2	0.15

α_{af}	-25	-20	-15	-13	-10	-5	0.0	5	10	13	15	20	25	30	35	40
C_{afLO}	-0.8	-0.71	-0.98	-1.32	-1.02	-0.53	0.0	0.53	1.02	1.32	0.98	0.71	0.8	0.98	1.08	1.13
C_{afDO}	0.43	0.27	0.1	0.07	0.05	0.02	0.0	0.02	0.05	0.07	0.1	0.27	0.43	0.62	0.81	1.05
C_{afm0}	0.12	0.1	0.0	0.0	0.0	0.0	0.0	0.0	0.0	0.0	0.0	-0.1	-0.12	-0.15	-0.2	-0.28

α_{af}	45	50	55	60	65	70	75	80	85	90	95	100	105	110	115	125
C_{afLO}	1.13	1.1	1.05	0.95	0.85	0.71	0.55	0.4	0.23	0.07	-0.1	-0.23	-0.38	-0.53	-0.67	-0.88
C_{afDO}	1.22	1.4	1.55	1.72	1.82	1.95	2.0	2.05	2.06	2.07	2.05	2.0	1.95	1.88	1.78	1.53
C_{afm0}	-0.32	-0.35	-0.38	-0.43	-0.46	-0.5	-0.52	-0.54	-0.56	-0.57	-0.58	-0.6	-0.6	-0.6	-0.6	-0.59

α_{af}	130	135	140	145	150	155	160	165	170	173	175	180
C_{afLO}	-0.97	-1.05	-1.07	-1.05	-0.95	-0.76	-0.7	-0.75	-0.75	-0.78	-0.5	0.0
C_{afDO}	1.4	1.22	1.05	0.83	0.65	0.46	0.32	0.25	0.14	0.1	0.03	0.01
C_{afm0}	-0.58	-0.57	-0.55	-0.51	-0.45	-0.38	-0.32	-0.3	-0.33	-0.4	-0.27	0.0

Table(6.6): Vertical stabiliser lift coefficient of the Bell model 301
Tilt-rotor research aircraft [63]

 BELL
HELICOPTER COMPANY

Use or disclosure of data on this page is
subject to the restriction on the title page.

TABLE VI VERTICAL STABILIZER LIFT COEFFICIENT (C_{Y_V})

RUDDER ANGLE	0°	10°	20°	-10°	-20°
MACH NUMBER	$M_N = 0 - .2$				
β_V					
-90	0	0	0	0	0
-40	-1.0	-.96	-.92	-1.07	-1.11
-32	-.93	-.84	-.82	-1.02	-1.12
-28	-.94	-.90	-.87	-1.02	-1.09
-26	-.98	-.93	-.91	-1.07	-1.11
-24	-1.03	-.98	-.92	-1.11	-1.15
-22	-1.05	-.98	-.85	-1.14	-1.19
-20	-1.05	-.88	-.74	-1.15	-1.22
-18	-.96	-.77	-.64	-1.14	-1.24
-16	-.86	-.66	-.52	-1.05	-1.18
-12	-.635	-.45	-.30	-.84	-.99
-8	-.425	-.225	-.09	-.63	-.76
8	.425	.625	.76	.23	.10
12	.635	.84	.99	.44	.31
16	.86	1.05	1.18	.66	.52
18	.96	1.14	1.24	.77	.64
20	1.05	1.15	1.22	.88	.74
22	1.05	1.14	1.19	.98	.85
24	1.03	1.11	1.15	.98	.92
26	.98	1.07	1.11	.93	.91
28	.94	1.02	1.09	.90	.87
32	.93	1.02	1.12	.84	.82
40	1.0	1.07	1.11	.96	.92
90	0	0	0	0	0

Having calculated the above value over the entire range of 0 to 90 deg. angle of attack, the same variation of C_L vs α is assumed for our airfoil and extended over the entire range -180 to 180 degrees as shown in Figure 6.6. This curve is tabulated in Table 6.7.

To complete the airfoil related data, the value of Kar in Equation 5.50 also needs to be estimated. According to reference [51] for an airfoil of the usual type and an aspect ratio of 2 or more, Kar is approximately equal to 3. However, in our case, due to the fact that the aspect ratio of all the airfoils is less than 2, the value of $Kar=3.0$ may not be valid. Therefore, it was decided to calculate the drag force of an airfoil with the same chord but a span twice as much as that of the real airfoil and then divide it by two. By equating the obtained result with the drag force which can normally be calculated for the real size airfoil, it is concluded that Equation (5.50) can still be used if the parameter Kar takes the value of 6.0 [52]. In fact two times of the suggested value for a usual size wing.

6.7 STREAMLINE BODY CHARACTERISTICS

As it was expected, no data that covers the entire range -180 to 180 deg. angle of attack for a streamline body was found. However, some data was available for a shorter range of 0 to 30 degrees but only for the dimensionless coefficients of lift and pitching moment, shown in Figure 6.7 [64]. In this figure, thick lines are the approximated curves for the value of thickness ratio 0.15 corresponding to our streamline bodies. These curves can then be extended approximately over the entire range of angle of attack as shown in Figures 6.8 a,c. In these figure, the estimated portions are drawn by thinner lines. As it might be noticed, to produce these curves, it is assumed that the streamline body is also symmetric w.r.t. a plane perpendicular to its longitudinal axis. For the dimensionless coefficient of drag, the only data available was at zero angle of attack and as a function of Reynolds number [65], shown in Figure 6.9. Using this value, the drag coefficient over the entire range of angle of attack is approximated by a sinusoidal function as follows, shown in Figure 6.8 b.

$$C_{sb_D} = C_{sb_{D0}}(Re_l) + (C_{sb_{D1}}(Re_d) - C_{sb_{D0}}(Re_l))\sin(\gamma_{sb}) \quad (6.16)$$

Where, γ_{sb} is defined in Section 5.2.3, Equation 5.44 and

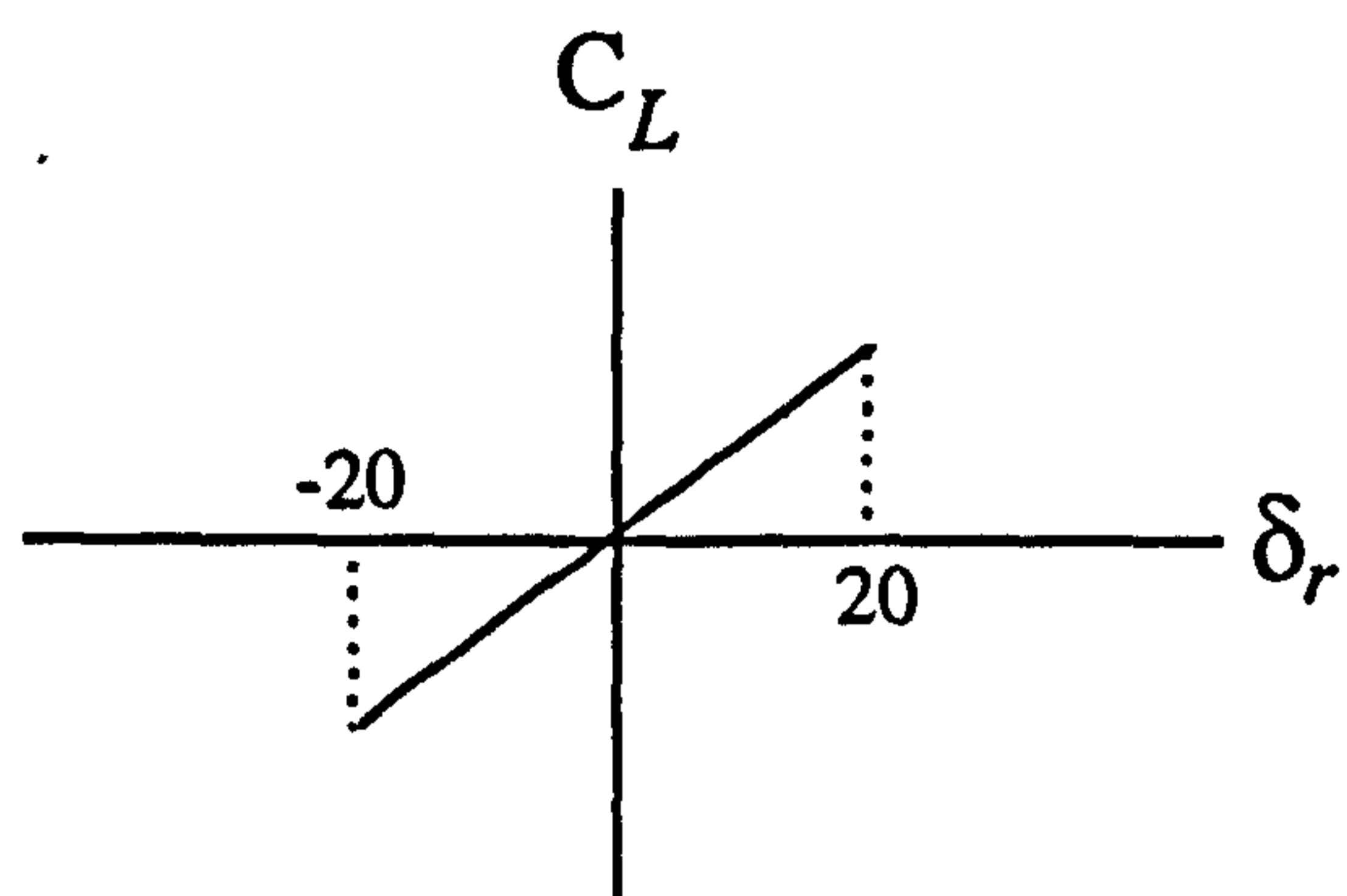
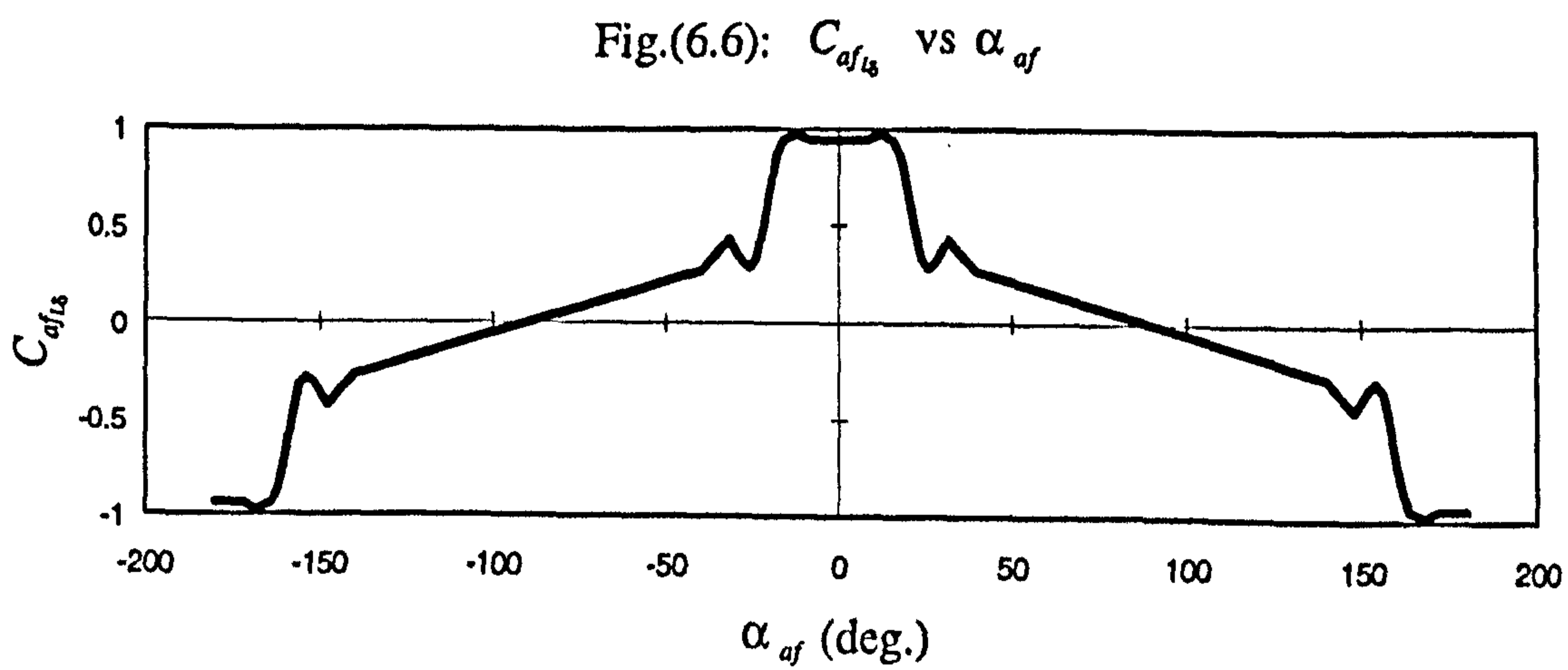


Fig. (6.5): Approximated C_L vs δ_r curve at an angle of attack α



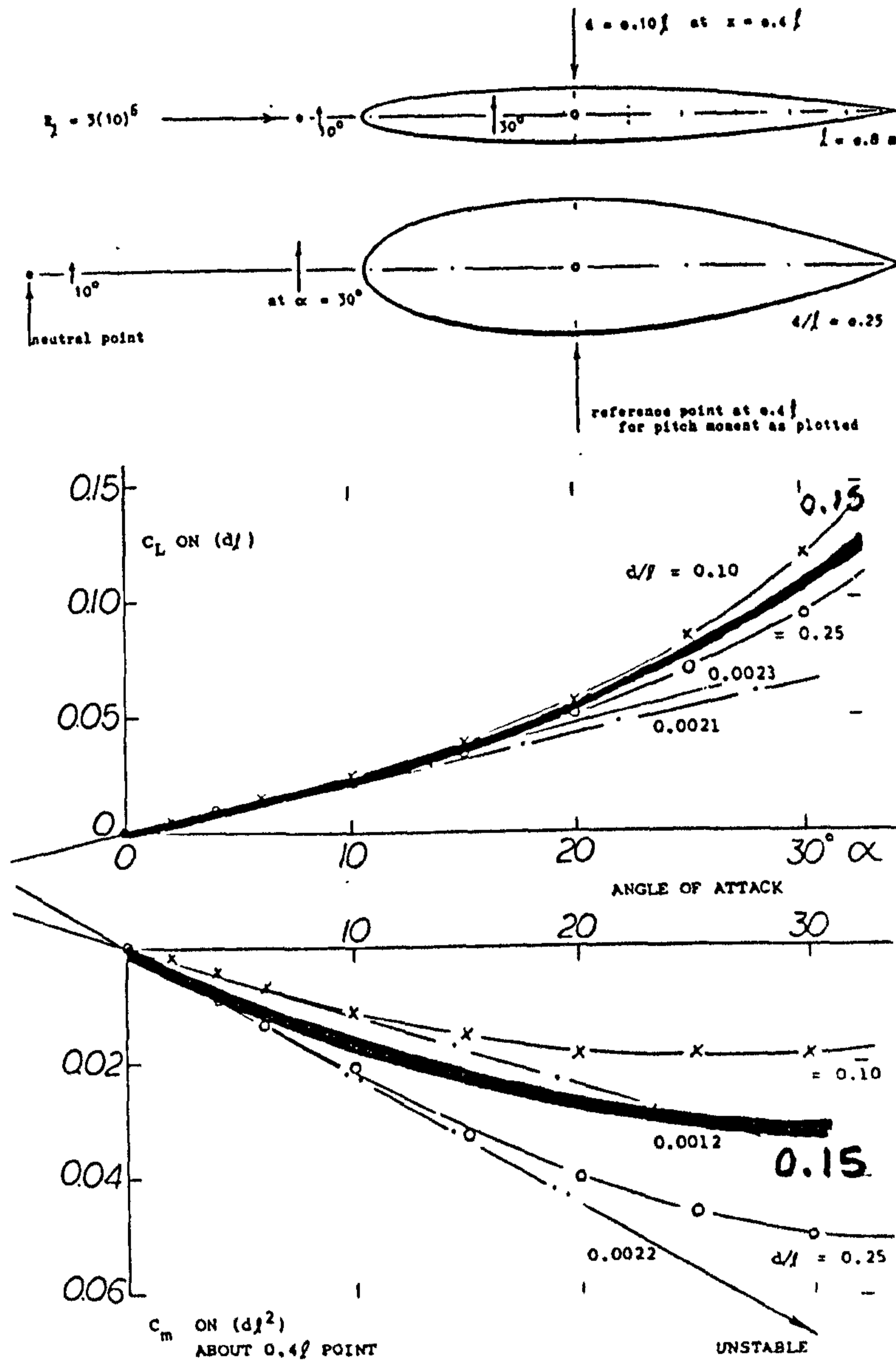


Fig.(6.7): Dimensionless coefficient of lift and pitching moment for a pair of streamline bodies, differing in fineness ratio [64]

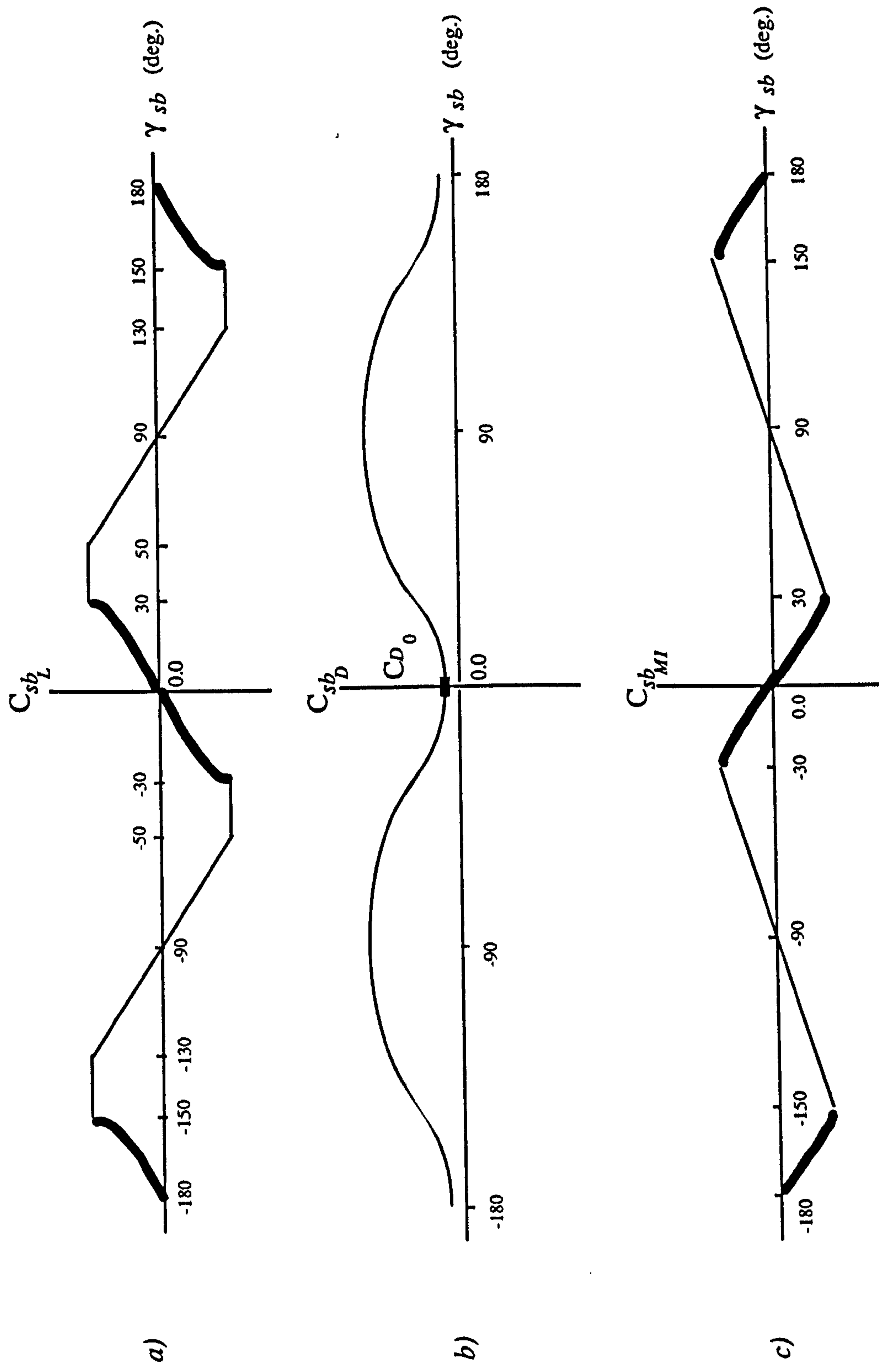


Fig.(6.8): a) C_{sbL} vs γ_{sb} b) C_{sbD} vs γ_{sb} c) C_{sbMI} vs γ_{sb}

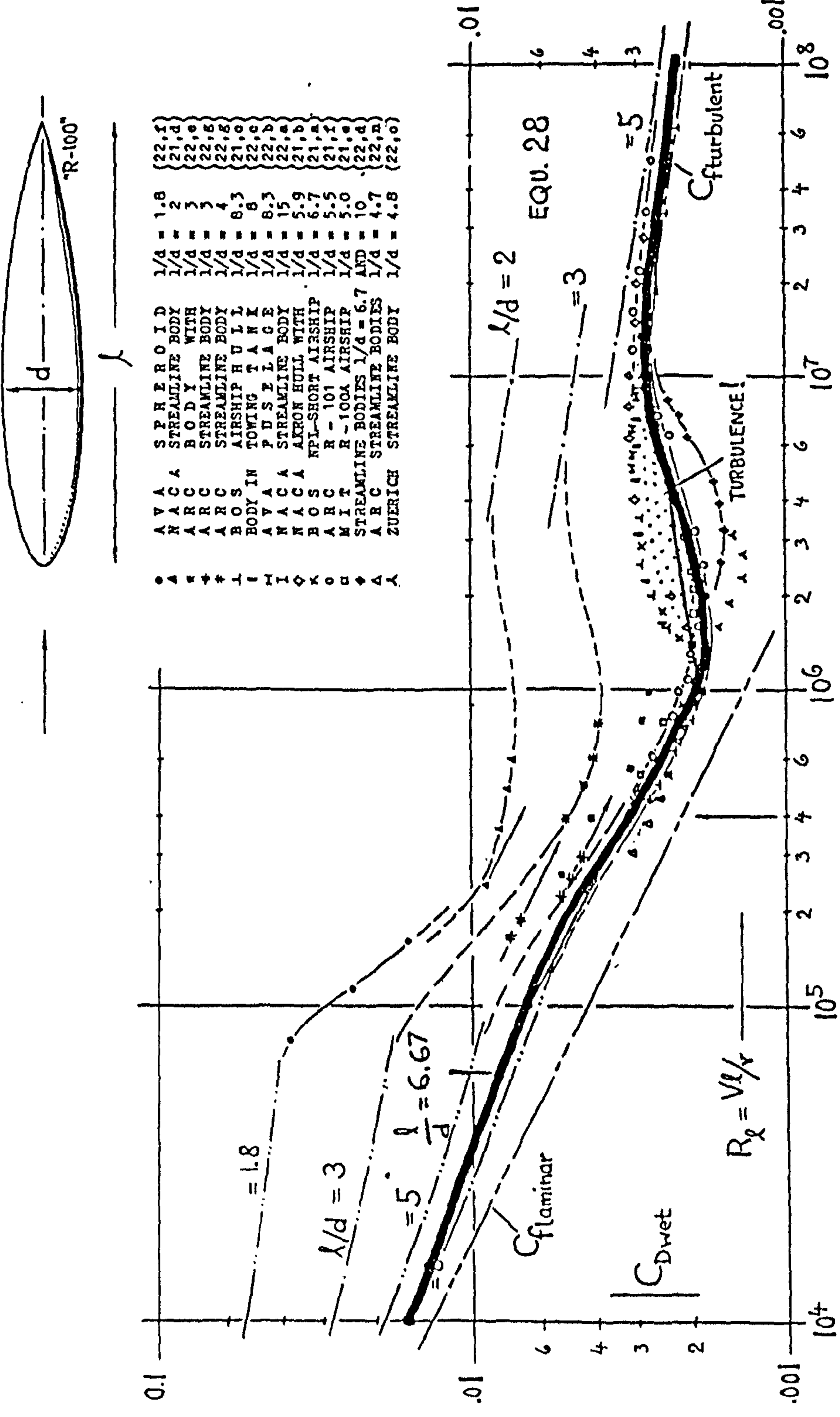


Fig.(6.9): $C_{D_{wet}}$ vs Re_l for a rotationally symmetric streamline body [65]

$$Re_d = \frac{V_{sb} \cdot DIA_{sb}}{v} \quad (6.17)$$

$$Re_l = \frac{V_{sb} \cdot LENGTH_{sb}}{v} \quad (6.18)$$

$C_{sb_{D0}}$ is the drag coefficient at zero angle of attack which can be expressed as follows

$$C_{sb_{D0}}(Re_l) = \frac{3.0 \cdot LENGTH}{DIA_{sb}} C_{D_{wei}}(Re_l) \quad (6.19)$$

The variation of $C_{D_{wei}}$ with Reynolds number is shown in Figure 6.9. In this figure, the thick line indicates the estimated curve for the value of inverse thickness ratio 6.67 corresponding to our streamline bodies. Also, $C_{sb_{D1}}$ is the drag coefficient of a circular cylinder in a flow normal to its axis, shown in Figure 6.10 [65]. The curves in figures 6.8 a,c, 6.9 and 6.10 are tabulated in Tables 6.8, 6.9 and 6.10.

6.8 MASS ESTIMATION

Since mass estimation of the structure and the other components was very difficult, it was decided to set the thrust force equal to weight for the sake of simplicity. As mentioned in Section 6.2, the net power generated by engines for the values $\delta_i = 0.64$ and $rpm = 6000.0$ is considered as the available power at take off. At this condition, the airspeed velocity and in turn the advance ratio are both zero. Selecting a propeller pitch angle equal to 20 degree and using Table 6.1 and Equation 5.12, the total thrust produced by the propulsion system can be calculated as follows

$$\begin{aligned} Thrust_{tot} &= 2 \left(\rho \left(\frac{rpm}{60} \right)^2 \cdot D^4 \cdot C_T(ADR, \theta_c) \right) \\ &= 2 \left(1.23 \left(\frac{6000}{60} \right)^2 \times 0.522^4 \times C_T(0.0, 20^\circ) \right) \quad (6.20) \\ &= 189.95 \text{ n.m} \end{aligned}$$

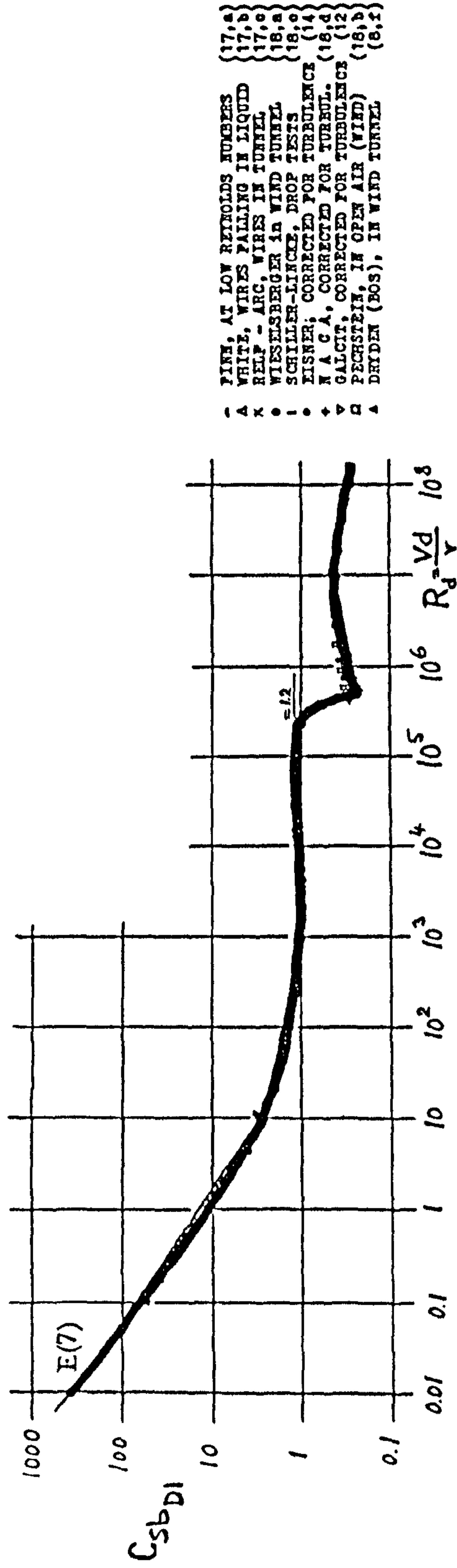


Fig. (6.10): Drag coefficient of a circular cylinder in flow normal to its axis [65]

Table (6.7): $C_{afL\delta}$ vs α_{af}

α_{af}	-180	-172	-168	-164	-162	-160	-158	-156	-154	-152	-148	-140
$C_{afL\delta}$	-0.945	-0.945	-0.974	-0.945	-0.859	-0.687	-0.487	-0.329	-0.286	-0.315	-0.43	-0.272

α_{af}	-90	-40	-32	-28	-26	-24	-22	-20	-18	-16	-12	-8
$C_{afL\delta}$	0.0	0.272	0.43	0.315	0.286	0.329	0.487	0.687	0.859	0.945	0.974	0.945

α_{af}	8	12	16	18	20	22	24	26	28	32	40	90
$C_{afL\delta}$	0.945	0.974	0.945	0.859	0.687	0.487	0.329	0.286	0.315	0.43	0.272	0.0

α_{af}	140	148	152	154	156	158	160	162	164	168	172	180
$C_{afL\delta}$	-0.272	-0.43	-0.315	-0.286	-0.329	-0.487	-0.687	-0.859	-0.945	-0.974	-0.945	-0.945

Table (6.8): $(C_{sbL} \text{ \& } C_{sbM1})$ vs γ_{sb}

γ_{sb}	-180	-175	-170	-165	-160	-155	-150	-130	-90	-50	-30
C_{sbL}	0.0	0.0125	0.022	0.035	0.05	0.075	0.1	0.1	0.0	-0.1	-0.1
C_{sbM1}	0.0	-0.008	-0.015	-0.02	-0.025	-0.028	-0.028	-	0.0	-	0.028

γ_{sb}	-25	-20	-15	-10	-5	0.0	5	10	15	20	25
C_{sbL}	-0.075	-0.05	-0.035	-0.022	-0.0125	0.0	0.0125	0.022	0.035	0.05	0.075
C_{sbM1}	0.028	0.025	0.02	0.015	0.008	0.0	-0.008	-0.015	-0.02	-0.025	-0.028

γ_{sb}	30	50	90	130	150	155	160	165	170	175	180
C_{sbL}	0.1	0.1	0.0	-0.1	-0.1	-0.075	-0.05	-0.035	-0.022	-0.0125	0.0
C_{sbM1}	-0.028	-	0.0	-	0.028	0.028	0.025	0.02	0.015	0.008	0.0

Table (6.9): C_{sbD1} vs Re_d

Re_d	0.01	10.0	1000.0	2.5e05	6.0e05	1.0e07	1.0e08
C_{sbD1}	4.0e02	3.0	1.0	1.0	0.25	0.5	0.3

Table (6.10): CD_{wet} vs Re_l

Re_l	1.0e04	1.0e05	1.0e06	1.0e07	1.0e08
CD_{wet}	0.015	0.0062	0.002	0.003	0.002

The gross weight of the aircraft is then given by dividing the above value by the gravitational acceleration (9.81). Thus

$$m_{tot} = 19.36 \text{ kg} \quad (6.21)$$

This is considered as the total mass of the aircraft and should then be broken down into the mass of the different components.

Therefore, the next step is to estimate a reasonable value for the mass of the different secondary objects. Unfortunately, there is no already given comment about it. The formulas given in Reference [66] seem not to be fully applicable in this case because they do not provide a sensible value for the mass of some of the aircraft components, e.g. wing. This is predictable because the figures given in this reference are obtained for the ordinary fixed wing unmanned aircraft. Using the hypothetically defined mass density [52] for the wing of the XRAE-1 unmanned aircraft [67] in calculating the mass of our airfoils was also not quite satisfactory. Therefore, what follows is the result of a pre-estimation by employing the above approaches which is then finalised by rather arbitrary personal judgement.

The mass of each airfoil was then considered to be

$$\begin{aligned} m_w &= 1.0 \text{ kg} \\ m_h &= 0.05 \text{ kg} \\ m_{vu} &= 0.1 \text{ kg} \\ m_{vl} &= 0.05 \text{ kg} \end{aligned} \quad (6.22)$$

The engines are considered to be located inside the fuselage. Therefore, there is no need to calculate the engine mass separately. However, to gain an idea, the following equation presented in Reference [68] is used to estimate the mass of each engine. Therefore

$$\begin{aligned} m_E &= 1.15 P_{\max} - 3.49 \\ &= 1.15 \times 5 - 3.49 \\ &\approx 3.0 \text{ kg} \end{aligned} \quad (6.23)$$

The mass of the body n is given by

$$m_n = m_{nacelle} + m_{pylon} + m_{gearbox} \quad (6.24)$$

where, according to Reference [66]

$$\begin{aligned} m_{nacelle} &= 0.015m_{tot} = 0.3 \text{ kg} \\ m_{pylon} &= 0.085m_E = 0.25 \text{ kg} \end{aligned} \quad (6.25)$$

Gearbox transfers the engine power to the propeller and it is placed inside the body n .
The gearbox mass is assumed to be

$$m_{gearbox} = 0.1 \quad (6.26)$$

Consequently,

$$m_n = 0.3 + 0.25 + 0.1 = 0.65 \text{ kg} \quad (6.27)$$

The following average values are assumed as the dimensions of each propeller blade

$$\begin{aligned} CHORD_b &= 0.03 \text{ kg} \\ SPAN_b &= 0.261 \text{ kg} \\ THICKNESS_b &= 0.035 \text{ kg} \end{aligned} \quad (6.28)$$

The total propeller mass can then be calculated by

$$m_p = 2(\rho_{CM} \cdot CHORD_b \cdot SPAN_b \cdot THICKNESS_b) \quad (6.29)$$

where, $\rho_{CM} = 1.5 \text{ gr/cm}^3$ is the mass density of an ordinary composite material [61].
Thus,

$$m_p \approx 0.08 \text{ kg} \quad (6.30)$$

Finally, the fuselage mass is given by

$$m_f = m_{tot} - 2m_w - 2m_h - m_{vu} - m_{vl} - 2m_p - 2m_n \approx 16.0 \text{ kg} \quad (6.31)$$

6.9 MOMENT OF INERTIA ESTIMATION

The calculation of an airfoil mass moment of inertia in its local axes system is carried out by approximating the airfoil with a rectangular flat plate which has the same width and length as the airfoil chord and span, respectively, and an average thickness corresponding to the airfoil thickness at one-quarter chord aft of the leading edge, Figure 6.11. Also, it is assumed that the mass is uniformly distributed. In terms of the dimensions, the associated mass moment of inertia is given by: [70]

$$[{}_{cg} I_{plate}] = \begin{bmatrix} \frac{1}{12} m(b^2 + t^2) & 0 & 0 \\ 0 & \frac{1}{12} m(h^2 + t^2) & 0 \\ 0 & 0 & \frac{1}{12} m(b^2 + h^2) \end{bmatrix} \quad (6.32)$$

Substituting the dimensions of different airfoils, we have

$$[{}_{gw} I_w^w] = \begin{bmatrix} 0.006 & 0 & 0 \\ 0 & 0.003 & 0 \\ 0 & 0 & 0.009 \end{bmatrix} \quad \begin{array}{l} b_w = 0.26655 \text{ m} \\ h_w = 0.18325 \text{ m} \\ t_w = 0.02 \text{ m} \\ m_w = 1.0 \text{ kg} \end{array} \quad (6.33)$$

$$[{}_{gh} I_h^h] = \begin{bmatrix} 0.00013 & 0 & 0 \\ 0 & 0.00006 & 0 \\ 0 & 0 & 0.002 \end{bmatrix} \quad \begin{array}{l} b_h = 0.1777 \text{ m} \\ h_h = 0.1222 \text{ m} \\ t_h = 0.01466 \text{ m} \\ m_h = 0.05 \text{ kg} \end{array} \quad (6.34)$$

$$\begin{bmatrix} {}^u_{g^v} I_v^v \end{bmatrix} = \begin{bmatrix} 0.0003 & 0 & 0 \\ 0 & 0.00026 & 0 \\ 0 & 0 & 0.00057 \end{bmatrix} \quad \begin{array}{l} b_{vu} = 0.19436 \text{ m} \\ h_{vu} = 0.1749 \text{ m} \\ t_{vu} = 0.021 \text{ m} \\ m_{vu} = 0.1 \text{ kg} \end{array} \quad (6.35)$$

$$\begin{bmatrix} {}^l_{g^v} I_v^v \end{bmatrix} = \begin{bmatrix} 0.000027 & 0 & 0 \\ 0 & 0.00014 & 0 \\ 0 & 0 & 0.000165 \end{bmatrix} \quad \begin{array}{l} b_{vl} = 0.07775 \text{ m} \\ h_{vl} = 0.1833 \text{ m} \\ t_{vl} = 0.022 \text{ m} \\ m_{vl} = 0.05 \text{ m} \end{array} \quad (6.36)$$

Similarly, each streamline body is approximated by a circular cylinder shown in Figure 6.12. Again, the mass of the body is assumed to be uniformly distributed. The mass moment of inertia matrix for this shape is given by:[70]

$$\begin{bmatrix} {}_{cg} I_{cylinder} \end{bmatrix} = \begin{bmatrix} \frac{1}{2} mr^2 & 0 & 0 \\ 0 & \frac{1}{4} mr^2 + \frac{1}{12} ml^2 & 0 \\ 0 & 0 & \frac{1}{4} mr^2 + \frac{1}{12} ml^2 \end{bmatrix} \quad (6.37)$$

In the following, the above matrix is calculated for each streamline bodies. It should be pointed out that in calculation of the fuselage inertia matrix, a shorter length than the actual value is used because, it is assumed that in a VTOL aircraft the mass of the fuselage is more likely to be concentrated near the center of gravity or the direction of thrust line at take off in order to have less longitudinal inertia and in turn better control in hover.

$$\begin{bmatrix} {}_{g^f} I_f^a \end{bmatrix} = \begin{bmatrix} 0.025 & 0 & 0 \\ 0 & 0.45 & 0 \\ 0 & 0 & 0.45 \end{bmatrix} \quad \begin{array}{l} l_f = 0.5553 \text{ m} \\ r_f = 0.056 \text{ m} \\ m_f = 16.0 \text{ kg} \end{array} \quad (6.38)$$

$$\begin{bmatrix} \kappa_{g_n} I_n^n \end{bmatrix} = \begin{bmatrix} 0.0002 & 0 & 0 \\ 0 & 0.002 & 0 \\ 0 & 0 & 0.002 \end{bmatrix} \quad \begin{array}{l} l_n = 0.18326 \text{ m} \\ r_n = 0.025 \text{ m} \\ m_n = 0.65 \text{ m} \end{array} \quad (6.39)$$

The mass moment of inertia of the propeller is approximated by a straight bar with a rectangular cross section shown in Figure 6.13. Using the dimensions given in this figure, the inertia components about X_n axis can be obtained by integration as follows.

$$\begin{aligned} c_g I_{bar_x} &= \int_{-R}^R (y^2 + z^2) dm \approx \int_{-R}^R r^2 dm = \int_{-R}^R r^2 (\rho_{CM} C t dr) \\ &= \rho_{CM} C t D \cdot \frac{D^2}{12} = m_p \frac{D^2}{12} \end{aligned} \quad (6.40)$$

The inertia components about Y_n axis varies when propeller rotates. Its maximum value can be calculated by

$$c_g I_{bar_y} = \int_{-R}^R (x^2 + z^2) dm \approx \int_{-R}^R r^2 dm = c_g I_{bar_x} \quad (6.41)$$

and its minimum value is,

$$c_g I_{bar_y} \approx 0.0 \quad (6.42)$$

hence, an average value is considered as follows.

$$c_g I_{bar_y} = \frac{c_g I_{bar_x}}{2} = m_p \frac{D^2}{24} \quad (6.43)$$

also

$$c_g I_{bar_z} = c_g I_{bar_y} \quad (6.44)$$

and

$$c_g I_{bar_y} = c_g I_{bar_z} = c_g I_{bar_x} \quad (6.45)$$

Substitution of the propeller mass and diameter in the obtained equations gives

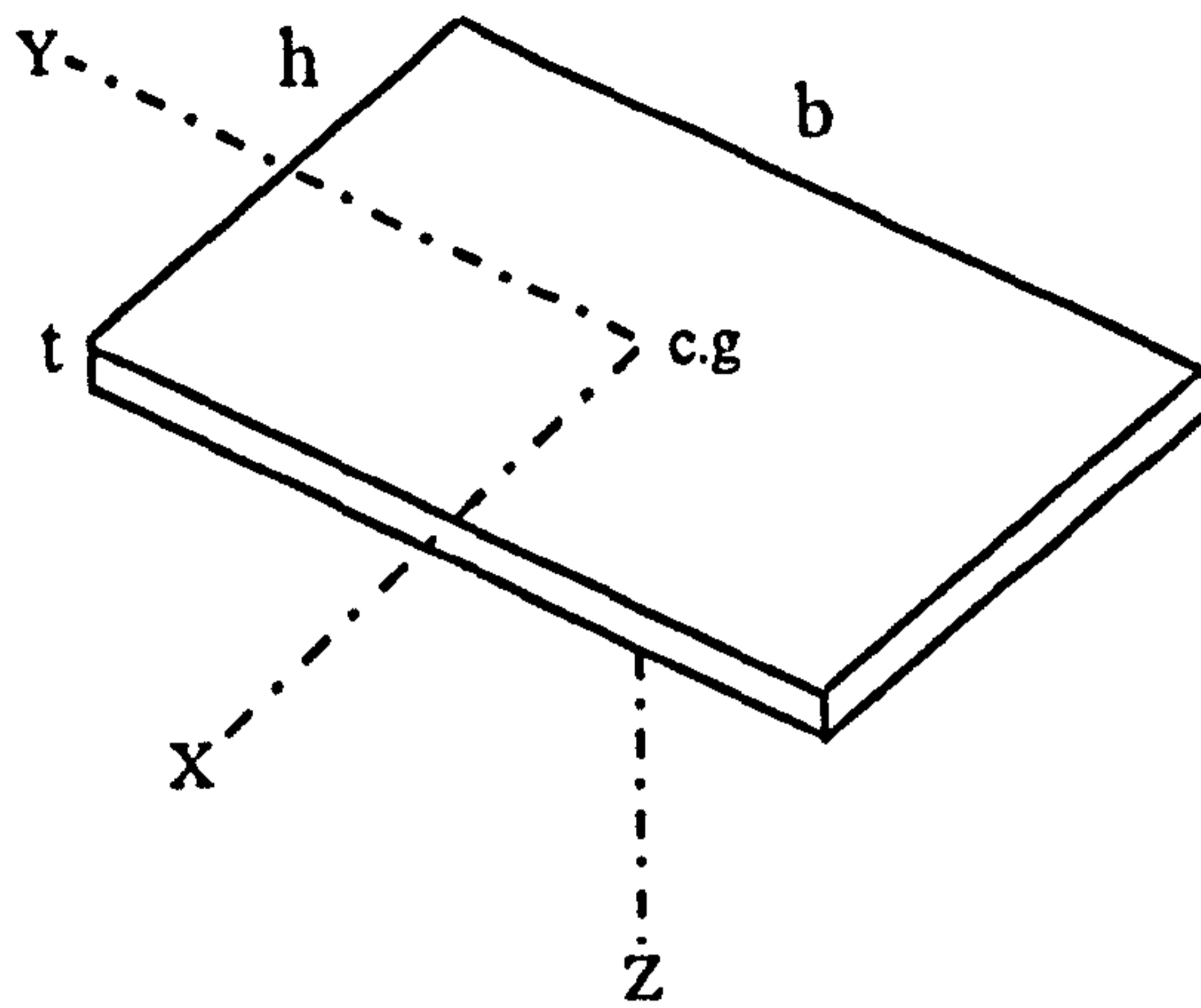


Fig. (6.11): The rectangular plate used to estimate the mass moment of inertia of an airfoil

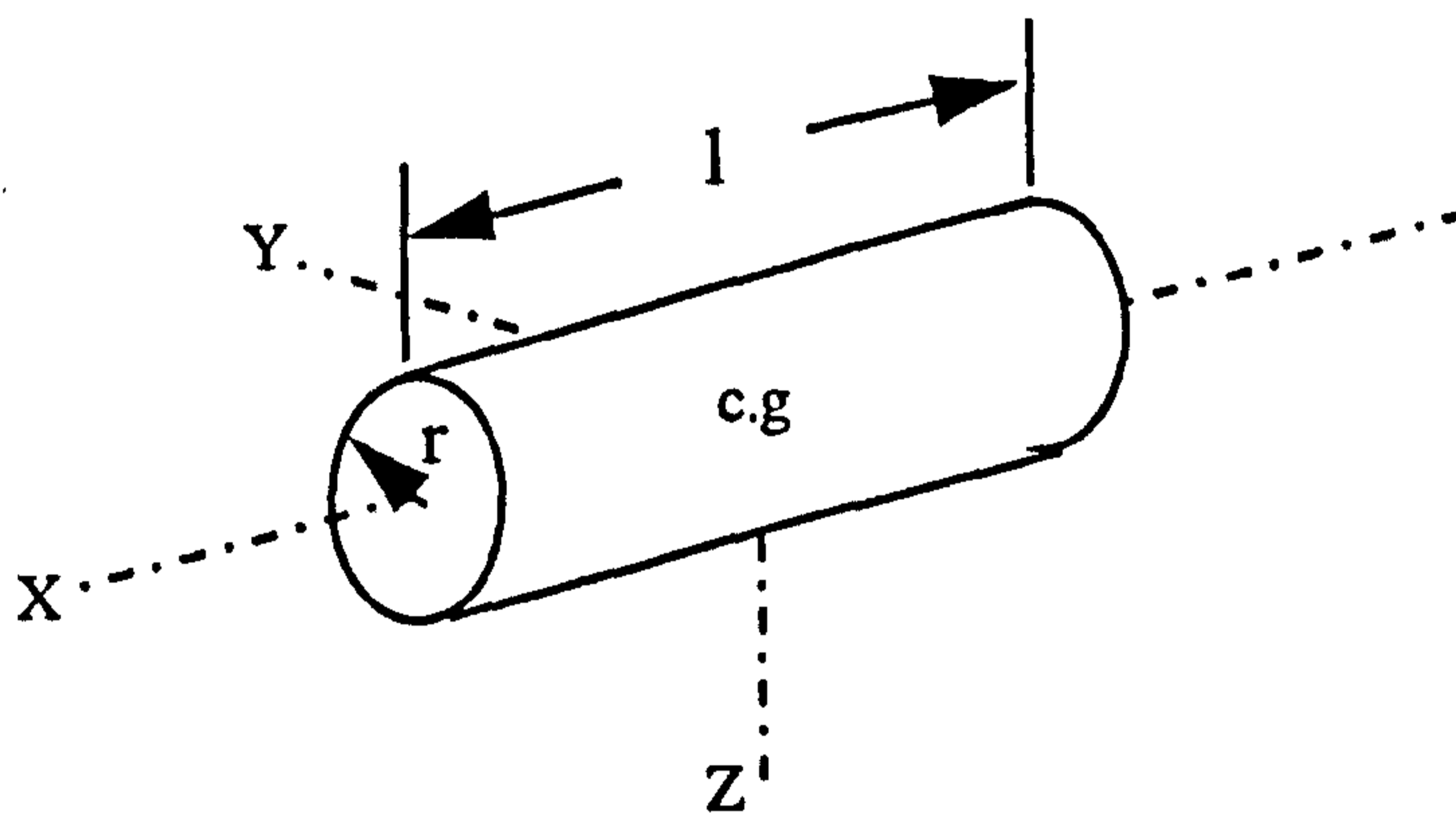


Fig. (6.12): The circular cylinder used to estimate the mass moment of inertia of a streamline body

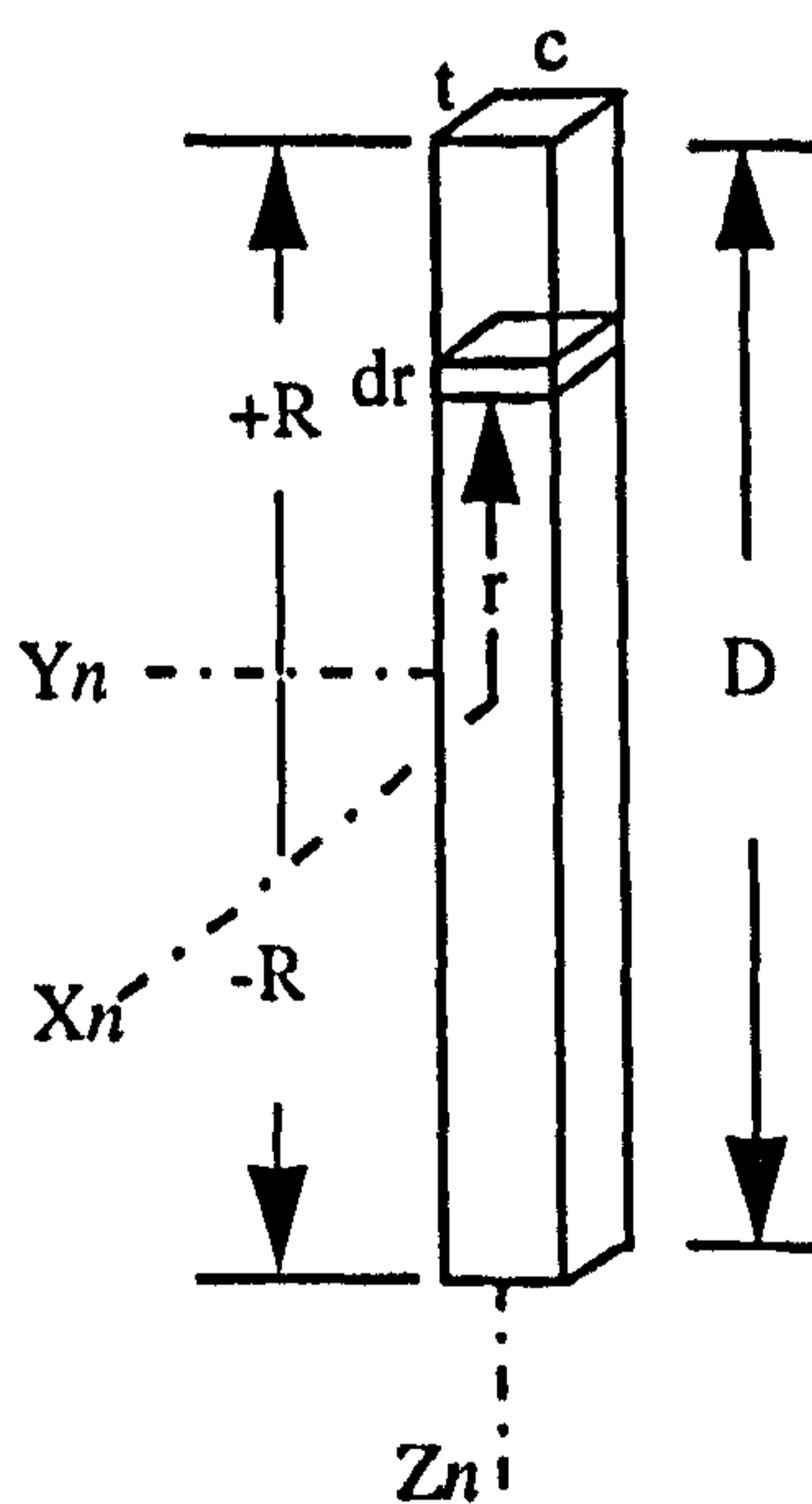


Fig. (6.13): The straight bar used to estimate the mass moment of inertia of a propeller

$$\begin{bmatrix} 0.0018 & 0 & 0 \\ 0 & 0.00091 & 0 \\ 0 & 0 & 0.00091 \end{bmatrix} \quad \begin{array}{l} D = 0.522 \text{ m} \\ m_p = 0.08 \text{ kg} \end{array} \quad (6.46)$$

CHAPTER SEVEN COMPUTER PROGRAMMING

7.1 INTRODUCTION

All the aspects of mathematical modelling and data collection were discussed in previous chapters. In this chapter, it is assumed that modelling is complete and attention is going to be focused on programming the resulting equations on a computer. This is an important phase of computer simulation, especially when the mathematical model is so complicated. The degree of versatility, applicability and reliability of the simulation model is highly dependent on how it is programmed and tested. Therefore, the present chapter is devoted to the programming related discussions. The result of this phase will be a verified executable computer program. Using simulation results obtained from this program, the model credibility will be investigated in the following chapter.

7.2 SUPPORT LANGUAGES FOR MODEL SIMULATION

It was recognised during the early years of the development of electronic digital computer, that the programming and coding of each such computers would be inordinately difficult and error-prone without the availability of programming aids. As a result, a hierarchy of languages and software packages, all designed to facilitate the

programming efforts gradually emerged [43]. In this section, it is attempted to quickly review the different levels of this hierarchy in order to emphasize the importance of using the special purpose computer languages in a simulation work.

7.2.1 General Purpose Languages

At the lowest level of the language hierarchy is the machine language, reflecting the command structure and detail design of the computer. This is in fact the only language which a computer can recognise directly, and requires that all instructions be provided as strings of *ones* and *zeros* and that all memory addresses likewise be provided in binary form. At the next level of the language hierarchy the so-called assemblers are located. Assembly languages permit a more compact and easily recognised abbreviation of each command, and are available for virtually every commercial digital computer [43].

As far as most computer users are concerned, the most important programming aids are found at the third level of hierarchy, the so-called programming languages. These include the scientific programming languages which facilitate the preparation of a program in a compact manner, using expression and statements (syntax) that are relatively easy to learn and understand by scientifically oriented programmers. Languages falling down into this category include BASIC, FORTRAN, PASCAL and COBOL etc. Compilers are available for each of these languages to translate the program prepared by the programmer into the assembly or machine language of the digital computer.

7.2.2 Languages Inadequate Facilities

Development of a complete simulation program by using one of the mentioned high level languages still involves a considerable amount of work, particularly when a useful range of facilities should be provided with the simulation, for example the capability of changing simulation parameters from run to run or system analysis. It is very inconvenient if the original source has to be edited and recompiled for a small change in the program. In addition, configuration control of the simulation software becomes very difficult. Alternatively, all the program data can be held in a file. This file can then be edited and read into the compiled program at run time. However, it is still quite a hard task and may result in many large data files having to be held as part of the documentation of the computer runs. A better system is a run time interpreter that does

modifications to selected data values in a standard data base and also keeps a record of the run time transaction for each computer run. This however represent a considerable amount of extra code that has to be written for the simulation [46].

In addition, graphs are usually required at the end of each computer run in order to analyse the computed behaviour of the system. Again, it is useful if the variable and scaling of these graphs are not fixed at compile time but are selectable at run time.

Another desirable feature is to be able to call up standard mathematical sub models that are used regularly in simulations, especially ones involving discontinuities such as dead space, limiting etc.

The above features point to the advantages of having a special language or program for writing simulation models so that it provides the above facilities as standard. In this way one can concentrate on the definition of the mathematical model and leave the provision of run time facilities to the computer. This kind of special languages will be discussed in the following section.

7.2.3 Simulation Languages

This class of languages are located at the fourth level of the software hierarchy which is called simulation languages [71]. A number of such simulation languages have been developed which permit the user to formulate the problem in a more convenient and direct form than is possible in high-level language such as FORTRAN. They permit the user to make statements which are particularly convenient for the solution of the mathematical expressions in a very compact form. They therefore facilitate programming, particularly by inexperienced programmers, and thereby greatly reduce the time actually spent in programming and debugging.

Simulation languages are also compiler oriented, similar to high-level programming languages, but are specifically used for simulation application. Most simulation languages require less programming time, moreover, it is simpler to change a model once it has been written. It is also easier to debug such programs. A unique feature of simulation languages is their standard functional blocks such as first- and second-order transfer

functions in addition to nonlinear functions (dead space, hysteresis, saturation, and so on).

Today's simulation languages provide one of the most powerful tools for modelling and simulation activities in an interactive mode. The *interactive* environment of simulation permits the simulation process on the computer be interrupted for the purpose of asking, or reporting to, the user (modular, programmer, or decision maker). Based on the information available from the computer (output), the human partner decides on what is to be modified or executed next. This capability is very useful in the interactive process of model building, as well as in validation studies.

Many simulation languages are now available on a wide range of machines. The readers is referred to References [43,71] for further information about simulation languages and packages. One of the most popular and widely available one is the *Advanced Continuous Simulation Languages* or *ACSL*. In the present work this simulation language (version window/PC 10.1) has been used for computer programming of the mathematical model. In the following section a complete description of ACSL will be presented

7.3 ADVANCED CONTINUOUS SIMULATION LANGUAGE - ACSL

The Advanced Continuous Simulation Language (ACSL) was originally designed for the digital simulation of aircraft type dynamic problems although it has a number of features which make it suitable for the study of a wide range of dynamic topics. The ACSL is a FORTRAN based system that compiles, links and executes code in an environment uniquely created for simulation roles. ACSL has been developed for the purpose of modelling and evaluation of continuous systems described by time dependent, nonlinear differential equations and/or transfer function. The ACSL program is intended to provide a simple method of representing mathematical models on a digital computer.

An ACSL simulation consists of two sections, a model definition and the run time commands. Using this structure, a continuous system is mathematically modelled with ACSL statements in model definition section, then model is analysed under the control of instructions interpreted in the run time command section. The advantage of this structure

is that once the model is defined, it can be saved on file and analysed indefinitely with any run time commands specified interactively and/or in batch mode.

A program written in ACSL is initially translated into FORTRAN. The FORTRAN code is then compiled, linked with the ACSL run-time library, and executed. At this point run time command can be entered interactively, by reading from a command file or in a batch process:

7.3.1 Choice of ACSL

Choice of ACSL as the simulation language in the present work seems natural. ACSL is a high level language conceived especially for simulation purposes. One of the important feature of ACSL is its sorting of continuous model equations, in contrast to general purpose programming languages such as FORTRAN where program execution depends critically on statement order. A program written in ACSL is already structured in terms of the Initial, Dynamic and Terminal region. In other languages this structure has to be constructed manually with the use of logical flags and branching. In addition, ACSL provides its own integration algorithms, a graph plotting routine, integration of user generated tables, calculation of the system Jacobian matrix, eigenvalue and associated eigenvector. Using these facilities, the programmer can concentrate on the specification of the model and its analysis. Also, being a FORTRAN based language ACSL offers the facility of accepting subroutines written in that language to complement the main program features if required. The reader is referred to the Reference [60] for complete description of the ACSL capabilities.

7.3.2 ACSL Explicit Structure

The ACSL explicit structure, Figure 7.1, is built up of three regions devoted as the *Initial Region*, the *Dynamic Region* (with embedded *Derivative* and *Discrete Section*) and the *Terminal Region*. The Initial region encompasses all those calculations, operations and initialising procedures that must be performed prior to a simulation run. In other words, every variable whose value never changes throughout the simulation is computed. The Dynamic region is that portion of the simulation that solves the simulation equations at each user-defined value of time.

The basic time interval represented by each pass through the Dynamic region, is termed communication interval. This time interval is determined solely by the accuracy requirements on communication with the outside world i.e. the user or in the case of real time simulation any external hardware or operations connected to the simulation. The Dynamic region performs its task by using an integration routine integrating over a period of the time step using the code embedded within the Derivative region. The interval at which the integration is updated can be smaller than the communication interval. This calculation interval is determined strictly by the accuracy requirements of the integration. Discrete section is only executed periodically. This section is intended primarily for modelling digital sampled data controllers where the communication to and from the continuous world occurs at fixed time known in advance. Only the code within the Derivative or Discrete section can be sorted by ACSL.

The Terminal region receives control from the Dynamic region and returns control to the simulation entry. Calculations and input/output necessary to properly terminate a single simulation run is performed before control is returned to the simulation entry.

Once back to the run time entry point, ACSL will plot variables previously declared to be prepared before the simulation is commenced. In this way, time histories can be produced. Similarly, variables may be displaced whilst a simulation run is taking place. The procedure of the simulation programming with ACSL is shown in Figure 7.2.

7.3.3 ACSL Inconveniences

In spite of many useful features of ACSL, It however should be pointed out that some major inconveniences have been experienced during programming with ACSL. The first one was the need for the whole program to be compiled and linked as a single unit, preventing the separate development, debugging and implementation of program sub-units which would then be linked to the main program at compilation time.

The second difficulty was associated with the FORTRAN compiler. The current version of the FORTRAN compiler (FORTRAN 5.1) places the code from each module (compiled source file) in its own segment (blocks in memory). Since the maximum size of each segment is 64K, the compiled code in each module can not exceed 64K. Therefore, if the size of the translated FORTRAN program code is bigger than 64K, the

Fig.(7.1): ACSL explicit structure [60]

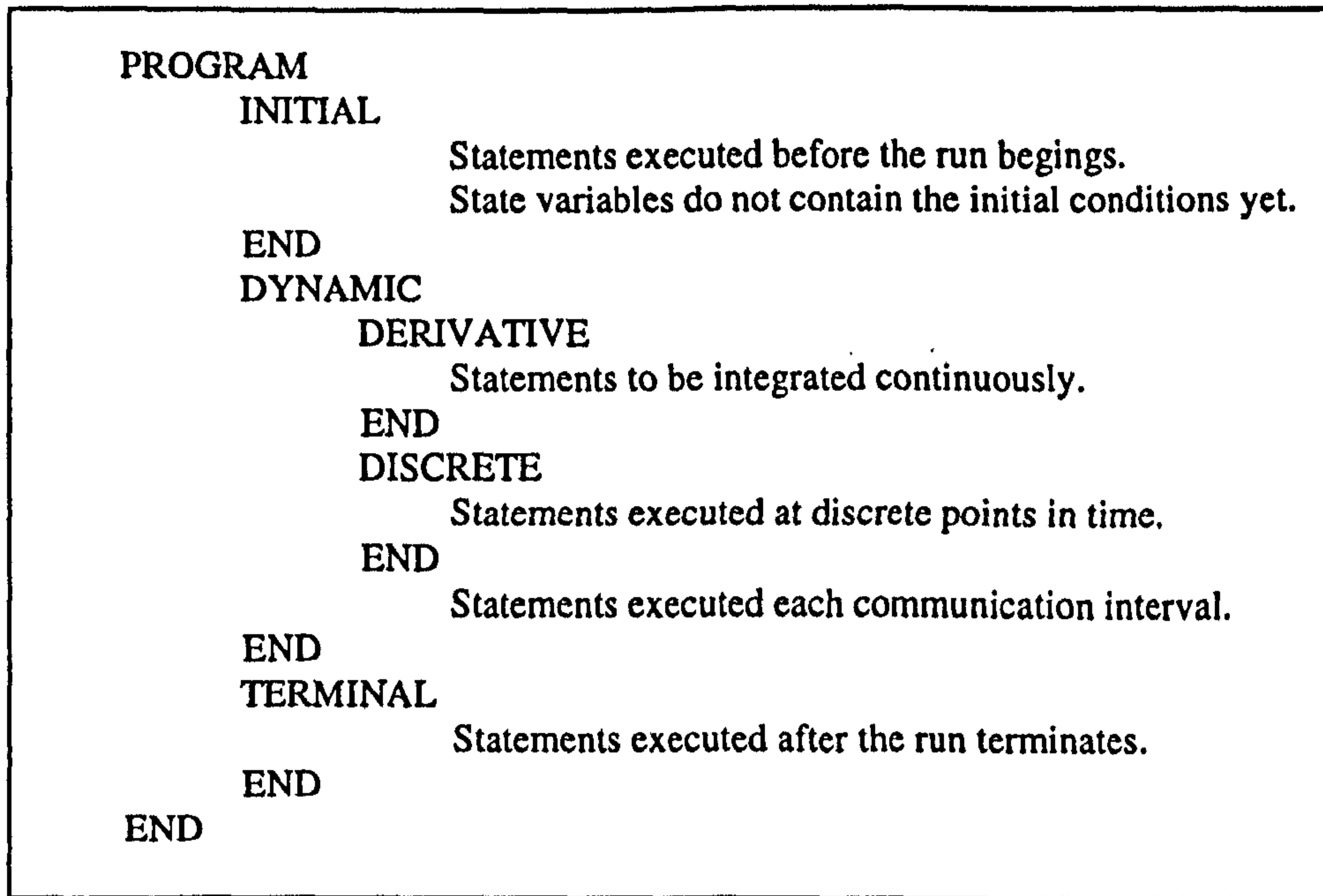
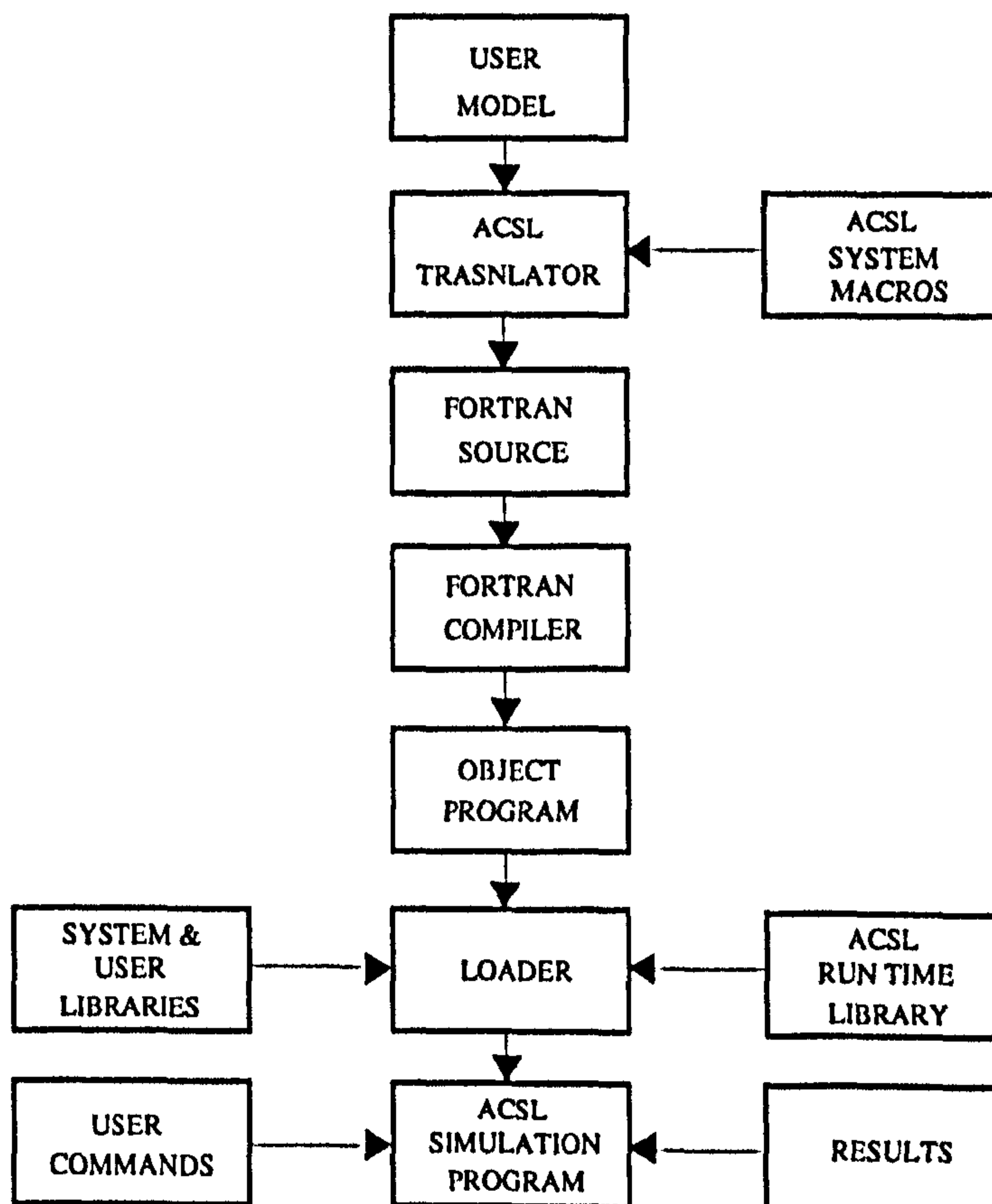


Fig.(7.2): Simulation program procedure [46]



only way is to divide the program into a main ACSL program and some FORTRAN subroutines which are called by the main program. The ACSL will then translate the main program and compile its FORTRAN version plus other associated FORTRAN subroutines, subjected to that none of them has exceeded the code-size limit. Since, ACSL statements and facilities can not be used in FORTRAN subroutines, they become useless in this way. Also, those variables used in subroutines are not defined in the common block, and so can not be recognised by the main ACSL program. Therefore, their values can not be traced, recorded, set or plotted during simulation by ACSL commands. This is a drawback of the current version of ACSL associated with large program size and can be a major inconvenience for the user.

Due to the size of the current program, such a problem was encountered during programming of the mathematical model in ACSL, consequently, the source program was broken down into a main ACSL program and six associated FORTRAN subroutines. Inside subroutines, some of the interpolation functions that had already been defined by TABLE statement in main program, had to be used. However, these functions could not be called in the FORTRAN subprograms. Therefore, the ACSL one variable interpolation subroutine ZZF1 [60] was directly employed. It should be pointed out that the latest version of ACSL removes these problems but it was not available in time for this work.

The third difficulty was that the error reporting messages produced by ACSL were not as direct and explicit as those found in other languages, which made error identification and tracing a rather time consuming process.

The fourth inconvenience was that the ACSL system was not able to combine the results of more than one run in a single plot. For example, when a program was run for a period of time and then terminated and again run for some extra time, the ACSL was only able to plot the results of the second period at the end of the simulation. Therefore, it was not possible to have a single plot of the results from the beginning to the end of the simulation.

7.4 PROGRAM DEVELOPMENT

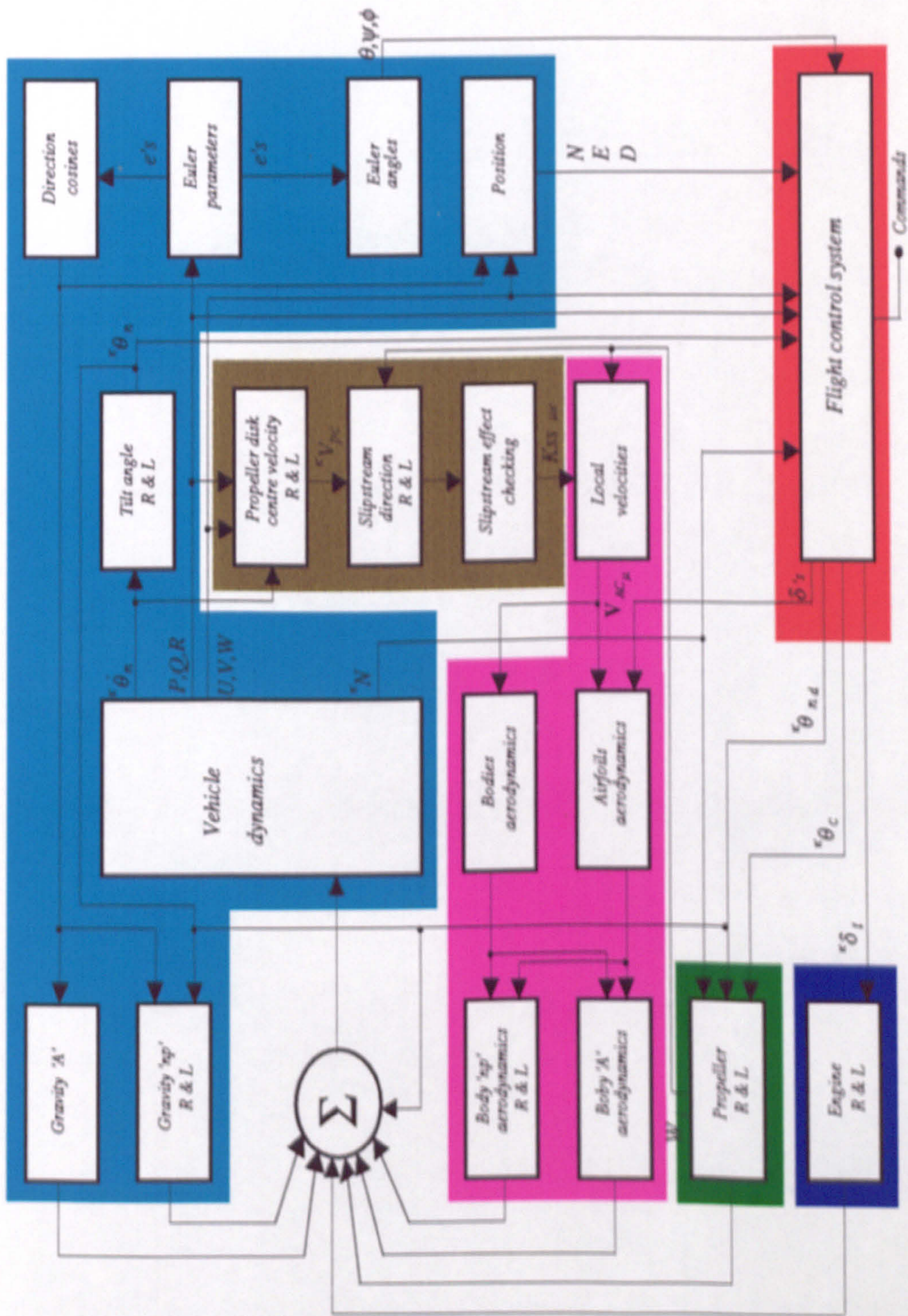
Having chosen the programming language, the next goal was to develop a well-documented, reliable, easy to use, flexible and correct program. Similar to the development of the mathematical model, it was intended to establish the simulation program on a modular basis.

In Figure 7.3, the data flow diagram of the simulation model is presented, summarising the way in which the simulation actually works. This diagram illustrates the major modules, the flow of numerical information and the general structure of the simulation. As shown in the figure, each of the six modules, gravity A, gravity np, aerodynamic A, aerodynamic np, propeller and engine feeds information into the state summer to form the force vector and receives information from the other modules. All together, there are eighteen modules in which the one called *Vehicle Dynamics* is the core of the system and includes the system equations of motion. These modules are also grouped in six subsystems known as, *Vehicle Projectile Like Dynamics*, *Airframe Aerodynamics*, *Slipstream Effect Checking*, *Propeller*, *Engine* and *Flight Control System*, shown in different colours.

Due to the model complexity, a systematic approach with a number of defined steps was undertaken to establish the computer model. In the first step of this approach, it was attempted to gain a good understanding of what the computer program is going to do and what makes it easy to use, regarding some possible future extensions. Having grasped such an understanding, a set of requirements and model enhancements was defined in the second step. This step was then ended up by establishing some guidelines, conventions and procedures that had to be followed throughout the computer programming development. In the fourth step, the general structure of the program was constructed. Using this structure, the model was then implemented in the final step.

This step-by-step approach was quite helpful for the assessment of the progress during program development and to improve the quality of the final computer program. It should however be pointed out that keeping the program development exactly based on such an orderly sequential manner was very difficult. In practice, most of the time, it was needed to work on all the steps simultaneously. Therefore, in the following some of the

Fig.(7.3): The data flow diagram of the simulation model



program specifications will be described rather than trying to express what was exactly done in each individual step.

7.4.1 Simulation Program

The Vertical Take Off and Landing UnManned Aircraft flight dynamics simulation program (VTOLUMA) was developed in ACSL, based on the mathematical model presented in the previous chapters. Due to the problems associated with possible numerical singularities at the pitch angles near 90 deg., two versions of the program, one with Euler angles and the other with Euler parameters (quaternions), have been prepared. In its final form, the program is composed of a main ACSL program and six associated FORTRAN subroutines, all together have nearly 4000 lines of programming code. A copy of the program is available in the Flight Dynamics group at the College of Aeronautics.

The building of the program in ACSL, including translation, compilation and linking took approximately one hour to be accomplished on a PC/486 computer. This time could be reduced to 15-20 minutes by using the command SMARTDRV in DOS prompt before starting to build the program in ACSL environment. The long time of the program building process plus the already mentioned error reporting difficulties associated with ACSL were naturally discouraging the introduction of more sophisticated refinements. However, the program enhancement was carried out wherever it was necessary, regardless of the mentioned associated difficulties.

The simulation run time of the program depends on the choice of integration control parameters, including the integration algorithm and integration time step. A typical simulation of 1.0 sec. with Runge-Kutta fourth order and time step 0.1 sec. would take approximately 3.0 minutes to be accomplished. This gives a ratio approximately 3.0 between simulation time and real time.

As a requirement for a research tool, the program is easy to use, modify and as flexible as possible. The input data to the program are in the simplest possible form. All the calculations that could possibly be done by hand and then implemented, have been left to the computer. The configuration type can easily be selected by setting the code *CONF1* (introduced in Chapter 3), at the beginning of the execution or while it is running so that

it is even possible to take off in Tilt-nacelle configuration and then land as a Tilt-wing aircraft by changing the configuration code during flight. Moreover, using a code called *ENGONOFF*, the engines can be switched off and on anytime during flight. The rotational direction of each propeller can also be chosen by the code *RPMrdc*, presented in Chapter 5 . Another code called *LOCK* has been considered to specify the locked and unlocked situation of the tilting parts.

Due to the requirement of running the program in two different modes, *With* and *Without* feedback control, a facility has been provided in the program by using a code called *CONT*. Using this code, the user is able to activate or deactivate the feedback control system in order to compare the aircraft dynamics in these two flight modes.

7.4.2 Programming Style

In this section some of the programming guidelines that have been followed to make the program more readable, which led to fewer errors and better documentation, are listed. In general, program layout, units, naming conventions and speed enhancement have been taken into attention.

- Readability of the program has been enhanced by trying to have a neat and consistent layout with columnar organisation and spaces.
- A brief statement of the purpose and general structure of the program has been given to help the reader quickly identify the program.
- The program structure keywords (PROGRAM, INITIAL, DYNAMIC, DERIVATIVE, DISCRETE, TERMINAL, and their matching END) have been stated in column 1 where they can be easily found. Appending comment to the END statements have been used to track of them.
- Assignment statements start in column 5. To help scanning the listing, the equal signs have been lined up in column 14 (unless pushed to the right by an oversized variable name). Spaces proceed and follow the equal signs.

- Spaces have been used in both sides of operators (including logical operators), except multiplication, division and exponentiation. No space has been used beside the internal side of parentheses.
- A statement is continued onto another line by putting an ampersand (&) at the end of each confined line, using column 72.
- A combination of dashed and dotted lines have been used to help the eyes in finding comments easily.
- A combination of uppercase and lowercase letters have been used in the program to distinguish language elements from user variables. Program structure keywords, ACSL and FORTRAN subroutines, function, and operator names are typed by uppercase letters. Also, uppercase letters have been used in user variables to highlight the key part of the name.
- The SI units has been used throughout the simulation program. However, if it was necessary to enter an input in another unit and convert it within the program, a unique name with a suffix indicating converted value, has been used.
- The names of variables are the same as those in the mathematical model accompanied with their descriptive superscript and subscript. The key part of variable names have been given in uppercase letters and the rest are in lowercase letters.
- Program speed enhancing was undertaken by extracting dependent variables that need only be calculated once out of the derivative section. Also, multiple calls to the same trigonometric functions have been eliminated by creating new variables. This all aids in the reduction of non-read to real time ratio.
- ACSL's explicit structure is clearly visible, as individual parts with titles. Program comments have been included to aid the reader in understanding the coding.

Manual program sorting has been observed as far as possible during implementation of the code in ACSL, in order that if it was necessary, a program language without sorting facility could also be used as environment to generate the simulation program.

7.4.3 Program Hierarchical Structure

In this section, it is intended to explain the program hierarchical structure which represent the organisation of the program components. It does not represent the procedural aspects of the program.

As stated previously, the specific structure of ACSL has been followed to generate an explicitly structured program. Within this framework, the VTOLUMA simulation program was developed in a Top-down design manner [72], i.e. the program's elements were initially specified only in broad outline, and then during the multi-phased development, they are successively refined in greater detail, until the required coded stages were attained.

The complete program hierarchical structure may be divided into seven levels, including ACSL explicit structure, Figure 7.4. The whole program is considered as the level one of the hierarchy. The ACSL's Regions and Sections are then located in levels two and three, respectively. In Figure 7.4, the ACSL explicit structure keywords are stated by using highlighted uppercase letters. In the levels four, five and six of the program hierarchy, the user defined areas, sub-areas and sub-sub-areas are located and titled by normal uppercase letters. The FORTRAN subroutines are considered as the seventh level and are distinguished by grey shaded areas.

The hierarchy of the complete program consists of 78 ACSL main program functional blocks distributed on the first six levels plus 26 FORTRAN functional blocks distributed in different subroutines. These functional blocks are denoted by their titles which are given in lowercase letters. Each functional block has a well defined task so that it can be tested individually. In Figure 7.4, functional blocks are marked by the same colour as their associated sub-systems in Figure 7.3.

It should be pointed out that for better demonstration of the program's sub-systems in the derivative section, all functional blocks associated with sub-system *Vehicle projectile like dynamics* are brought together in the same area and title in Figure 7.4. However, in the actual program, for the reason mentioned in the last comment of the Section 7.4.2, some of these functional blocks are located somewhere else in the derivative section. To be referred, the actual hierarchical structure of the program is provided in Appendix C.

Fig. (7.4): The VTOLUMA simulation program hierarchical structure

PROGRAM	
INITIAL	
	INPUT DATA
	Set up constants
	TABLE DEFINITION
	PROPELLER
	Thrust coefficient vs pitch angle and advanced ratio
	Propeller power coefficient vs pitch angle and advance ratio
	ENGINE
	Engine power vs throttle setting and rpm
	AIRFOIL
	Airfoil CL vs angle of attack
	Airfoil CD vs angle of attack
	Airfoil CM vs angle of attack
	Airfoil CLdelta vs angle attack
	Airfoil CMDelta vs angle attack
	STREAMLINE BODY
	Streamline body CM vs angle of attack
	Streamline body CDwet
	Streamline body COD11fu
	INITIALIZING
	Untitled calculations
	Set up reference inputs, states and control gains
	CALL SETCONT
	Initialization of reference inputs and reference states
	Read Gainp
	Substitution the Gainp matrix into the Gainf matrix
	Transformation of some position vectors
	Mass calculations
	Weight calculations
	Calculation of the c.g. co-ords of the hvf assembly in a-axes related to O
	Calculation of the position vector of the different parts of hvf assembly related to gb
	Calculation of the c.g. co-ords of the bodies np in n-axes related to J
	Calculation of the c.g. co-ords of the body A in a-axes related to O
	Set up the fuselage inertia matrix in a-axes about gb
	Set up the horizontal stabilizer inertia matrices in a-axes about gn
	Set up the horizontal stabilizer inertia matrices in a-axes about gb
	Set up the vertical stabilizer inertia matrices in a-axes about gv
	Set up the vertical stabilizer inertia matrices in a-axes about gb
	Set up the hvf assembly inertia matrix in a-axes about gb
	Set up the nacelle inertia matrices in n-axes about J
	Set up the propeller inertia matrix in n-axes about J
	Set up the wing inertia matrices in n-axes about gw
	Set up the wing inertia matrices in n-axes about J
	Set up the body np inertia matrices in n-axes about J
	set up the hvf assembly inertia matrix in a-axes about O
	Set up the wing inertia matrices in a-axes about gw
	Set up the wing inertia matrices in a-axes about O
	Set up the body A inertia matrix in a-axes about O
	Set up the propeller inertia in n-axes gp
	Zeroise matrices
	Calculation of initial E parameters
END INITIAL	

Continue

DYNAMIC		
Untitled calculations		
DERIVATIVE		
FLIGHT CONTROL SYSTEM		
Calculation of control inputs		
CALL CONTROL		
Calculation of control inputs		
PROPELLER		
Calculation of the ALPHAm and PSI _m		
Propeller model		
Propeller total force components in m-axes		
Propeller total moment components in m-axes		
Transformation to n-axes		
Calculation of the moment generated by the propeller total force about J in n-axes		
Propeller total moment about gp in n-axes		
Calculation of the moment generated by the propeller total force about gp in n-axes		
ENGINE		
Engine model		
SLIPSTREAM EFFECT CHECKING		
Calculation of the slipstream velocity and THETAs		
Set up the slipstream influence codes		
CALL INFL		
Set up the slipstream influence codes for the right horizontal stabilizer		
Set up the slipstream influence codes for the left horizontal stabilizer		
Set up the slipstream influence codes for the upper vertical stabilizer		
Set up the slipstream influence codes for the lower vertical stabilizer		
Set up the slipstream influence codes for the right wing (Tilt-rotor conf.)		
Set up the slipstream influence codes for the left wing (Tilt-rotor conf.)		
Set up the slipstream influence codes for the right nacelle		
Set up the slipstream influence codes for the left nacelle		
Set up the slipstream influence code for the right wing (Tilt-wing conf.)		
Set up the slipstream influence code for the left wing (Tilt-wing conf.)		
AIRFRAME AERODYNAMICS		
Calculation of the aerodynamic forces and moments of the body A		
CALL AEROHVF _W		
Cal. of the aerod. forces and moments of the right horizontal stab.		
Cal. of the aerod. forces and moments of the left horizontal stab.		
Cal. of the aerod. forces and moments of the upper vertical stab.		
Cal. of the aerod. forces and moments of the lower vertical stab.		
Cal. of the aerod. forces and moments of the right wing (Tilt-rotor)		
Cal. of the aerod. forces and moments of the left wing (Tilt-rotor)		
Cal. of the aerod. forces and moments of the fuselage		
Calculation of the aerodynamic forces and moments of the hvfw assembly		
Calculation of the aero. fors. and moms. of the elements of the body n at right and left		
CALL AERONW		
Calculation of the aerodynamic forces and moments of the right nacelle		
Calculation of the aerodynamic forces and moments of the left nacelle		
Cal. of the aerod. forces and moments of the right wing (Tilt-wing)		
Cal. of the aerod. forces and moments of the left wing (Tilt-wing)		
Calculation of the aerodynamic forces and moments of the right and left propellers		
Calculation of the aerodynamic forces and moments of the right and left bodies np		

Continue

VEHICLE PROJECTILE LIKE DYNAMICS		
		Untitled calculations
		Direction cosine matrix from aircraft to inertial axis
		Direction cosine matrix from inertial to aircraft axis
		Calculation of the absolute angular velocity of the body np
		Calculation of the absolute velocity of the joint
		Actuator model
		Transformation of the weight of the body np to n-axes
		Calculation of the moment generated by the weight of the body np about J in n-axes
		The moment of the propeller weight about gp in n-axes
		Transformation of the weight of the body A from i-axes to a-axes
		Calculation of the moment generated by the weight of the body A about O in a-axes
		Cal. of the vectors and matrices required to build up the mass matrix and total for. vec
		Calculation of the mass matrix
		Invert mass matrix
		CALL INVERT
		Calculation of inverse mass matrix
		Dynamic vector
		Total force vector
		Acceleration vector
		Rate of change of E parameters
		Velocity vector in i-axes
		Integration
		Aircraft attitude
		END DERIVATIVE
		DISCRETE
		END DISCRETE
		Termination calculations
		END DYNAMIC
		TERMINAL
		END TERMINAL
		END PROGRAM

In practice, due to the available sorting facility in ACSL, there is no difference between these structures.

The major advantage of this structured programming approach is that consistency between various parts of the whole program is maintained throughout all the stages of development. Also, it provides a systematic way of deriving the code for a block, and thus the program is more comprehensive and communicative. Since, programming errors can be easily detected and corrected, program modification and development is accelerated.

7.5 PROGRAM TESTING

In any simulation, it is of the utmost importance that the model yields results which are representation of the physical system being studied. Therefore, the process of verification and validation introduced in Chapter (1) are considered as the very important parts in the development of an accurate and useful computer simulation. If a model is not verified and validated, then any conclusion derived from the model will be of doubtful value.

To satisfy the objectives of verification and validation process, it is necessary to define a test procedure which ensure that results of the simulation are reliable and the decisions made with the model will be similar to those that would be made by actual physical system. The testing method must be comprehensive in order that any anomalies may be detected and corrected.

In the following, in the first place it is attempted to provide a general view of testing process, strategies and techniques applied in the present work. Having introduced the selected methods, further details of the program testing will be provided in the second place.

7.5.1 The Testing Process

It is obvious that a complex simulation should not be tested as a single unit, i.e. write all the code and then test the full model. Such an approach would make it extremely difficult to find the errors. The more sensible approach is to break the code down into simpler,

discrete blocks and test them individually. In this way, the final program will be a collection of well-tested components, which may now be compared against the known behaviour of the full physical model.

As mentioned previously, during the program development phase, the system was well-decomposed into sub-systems, modules and functional blocks. This well-organised structure was then used to apply testing process introduced in Reference [73]. Using this method, the testing process proceeded in five stages, grouped in three activities shown in Figure 7.5.

In general, the sequence of testing activities was component testing, integration testing and then acceptance testing. However, as defects were discovered at any one stage, they required program modifications to correct them. This might require other stages in the testing process to be repeated. The process was therefore an iterative one with information fed back from later stages to earlier part of the process.

7.5.2 Testing strategies

There are various testing strategies which can be adopted to test a program. Two of the most important ones are Bottom-up and Top-down testing [72-74].

In the first approach, testing is started from low-level parts which are then integrated and coupled with parts at the next higher level. The components thus obtained is tested next. In top-down testing, the top-level parts are tested first, and are gradually integrated with lower-level parts.

In Bottom-up testing, the environment in which the part being tested is to be integrated, has to be simulated. Such an environment is called a test driver [72,73]. In Top-down testing the opposite is true, the lower-level parts, have to be simulated through so-called test stubs. Stubs are simple components which have the same interface as that of the part. [73]

Both methods have their advantages and disadvantages. For instance, in Top-down testing, unnoticed programming structural design errors may be detected at an early stage in the testing process. Early error detection means that extensive redesign and implementation may be avoided. Top-down testing has also the advantage that a limited

working system is available at an early stage in the development. This is psychologically encouraging because it demonstrates the feasibility of the system at the beginning. The disadvantage of Top-down testing is the requirement that program stubs, simulating lower level of the system, must be produced. Producing stubs can be laborious and time consuming.

Bottom-up testing does not require producing stubs. However, test drivers must be written to exercise the lower level components. In addition, it may be difficult to get a sound impression of the final system during the early stages of testing because whilst the top-level parts are not integrated, there is no system, there are only individual elements.

In this work, a combination of both methods was used at different stages of the testing process. As mentioned previously, the program has been developed in a Top-down design manner. Therefore, in some testing stages Top-down development was combined with bottom-up testing strategy. This required that all parts of the program to be implemented before testing could begin. In Figure 7.5, the testing strategy used for each testing stage is presented in testing methods section of the table.

Whatever strategy is adopted, testing can be carried out either incrementally [73] or non-incrementally. In non-incremental approach each part is tested separately and finally they will be integrated and whole system will be tested again. In incremental approach, the system is tested incrementally. Figure 7.6 shows a test sequence corresponding to an incremental approach. In this approach part A is tested first. Part B is then integrated and the system composed of the parts A and B is tested. Then part C is integrated and the whole system is tested. The process will continue until all parts have been integrated into a complete system. When a part is introduced at some stage in this process, tests, which were previously unsuccessful, may now detect defects. These defects are probably due to the introduction of the new part. The source of the problem is localised, thus defect location and repair is simplified.

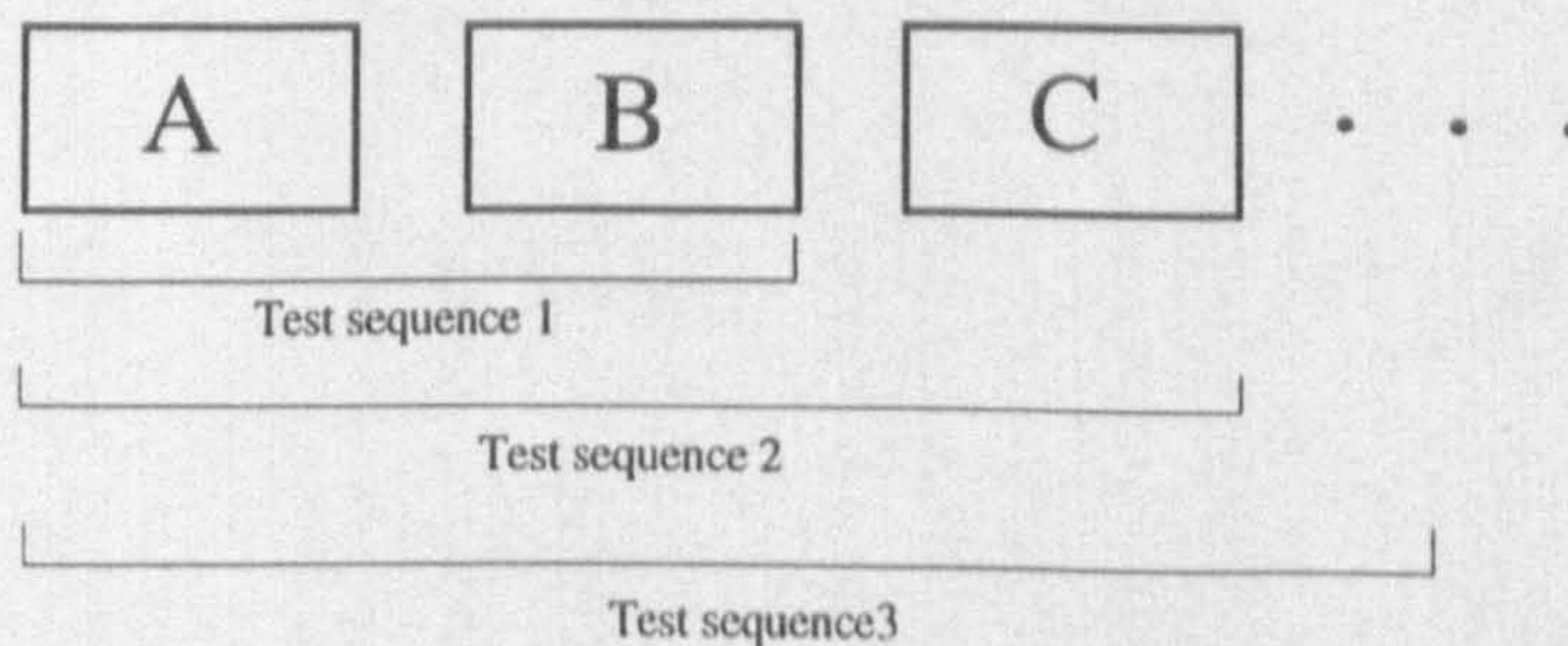
In general, incremental approach is recommended. However, it can be very time consuming. Therefore, this approach was used only in integration testing stage where it is well-matched with the top-down strategy method, Figure 7.5.

Fig.(7.5): Testing process, strategies and techniques

ACTIVITIES	User testing	Integration testing		Component testing				
	Acceptance testing	System testing	Sub-system testing	Module testing	Functional block testing			
T E S T I N G S T A G E S	S y s t e m	S y s t e m	Vehicle projectile like dynamics	1	1,2,3,			
				2	1,2,3,			
				3	1,2,3,			
				4	1,2,3,			
				5	1,2,3,			
				6	1,2,3,			
				7	1,2,3,			
				8	1,2,3,			
			Airframe aerodynamics	1	1,2,3,			
				2	1,2,3,			
				3	1,2,3,			
				4	1,2,3,			
				5	1,2,3,			
			Slipstream effect checking	1	1,2,3,			
				2	1,2,3,			
				3	1,2,3,			
			Propeller	1	1,2,3,			
			Engine	1	1,2,3,			
			Flight control system	1	1,2,3,			
			TESTING METHODS	Output analysis	Top-down Incremental All static* All dynamic*		Bottom-up Non-incremental All static Some dynamic*	

- * All static : All components are tested statically
- * All dynamic : All components are tested dynamically
- * Some dynamic : Some of the components are tested dynamically

Fig.(7.6): Incremental testing



7.5.3. Test Techniques

Test techniques can be separated into static and dynamic analysis techniques. Static techniques are concerned with the analysis of the system representations such as the requirements, design and program listing, they are applied at all stages of the process through structural review. During static techniques, the program is generally not executed. Static techniques can only check the correspondence between a program and its specifications (verifications), they can not demonstrate that the program is operationally useful. Static techniques include Reading, Walkthrough and inspection, etc. [72]. A large part of the static analysis is nowadays done by the language compiler.

Dynamic techniques or test involve exercising an implementation. During dynamic analysis, the program is executed. With this form of testing the program is given some input, and the results of the execution are compared with the expected results. The reader is referred to Reference [72] for further information about the subject.

In this work, a combination of both methods was used at different stages of the testing process. In Figure 7.5, the method used for each stage is specified.

7.5.4 Component testing

The component testing including functional block and module testing was carried out to make sure that individual components of the program operate correctly. The same procedure was undertaken in component testing stage of all sub-systems. As shown in Figure 7.5, since the functional blocks and modules are relatively simple and shorter programs, a bottom-up and non-incremental strategy was used for the sake of saving time. In other words, each component was considered as a stand-alone entity and then tested statically, and also, for some of them, dynamically. The components are then integrated to build up their associated sub-systems. As mentioned previously, a test driver had to be prepared for each dynamically tested component. For example, simple programs were written to exercise each of the functional blocks containing a look up table and plot the data. A range of the independent variables were chosen to ensure that interpolation and extrapolation were performed correctly.

7.5.5 Integration testing

Integration testing was carried out in two phases. The first phase, i.e. sub-system testing, involved with testing collection of modules which had been integrated into sub-systems. The sub-systems were then integrated to make up the entire system in the second phase. In this phase, the testing process was concerned with finding errors which normally result from unanticipated interactions between the sub-systems. As shown in Figure 7.5, a Top-down and incremental testing strategy have been used.

As a first step of incremental testing, the sub-system *Vehicle Projectile Like Dynamics* was tested. In this step, test stubs were used to replace all other sub-systems. In other words, airframe aerodynamic and propeller forces and moments, engine power and feedback gain were equated to zero, and slipstream effect checking was disactivated by setting all the slipstream influence codes equal to zero.

The sub-system *Vehicle Projectile Like Dynamics* is the core of the system which consists of the equations of motion of an articulated flying object plus all other necessary parts of the program by which the simulation of the vehicle dynamics only under the influence of gravity can be carried.

Since the aircraft equations of motion had originally been derived in this thesis, Chapter 4, their validity had to be proved via a number of sufficient and convincing tests. According to Newton's second law, a projectile like dynamics was expected to observe from the motion of the vehicle under gravitational force effect. A number of tests were then designed and carried out in order to confirm such an observation. Figures 7.7-7.20 are devoted to graphically demonstrate the results of these tests.

On the Top left hand side of each figure, the initial conditions associated with each test are given in a table. In this table the more important items which should be taken into attention are shaded. On the top right hand side, it is tried to exhibit the vehicle conditions at the beginning of each test in a simple way. Using the given aircraft views, the reader can simply and quickly understand which test the presented results are associated with.

In Test 1, the vehicle was given an initial vertical velocity of -10.0 m/s. As seen in Figure 7.7, it exhibits a parabolic height variation with time. The vertical velocity in inertial axes increases linearly from -10.0 m/s at zero height to 0.0 at maximum height. It continues to increase until it reaches the same value as the initial vertical velocity but in opposite direction (10.0 m/s) at the time of crash. The slope of this line is equal to 9.81 m/s² which is exactly equal to the gravitational acceleration. The vehicle centre of gravity moves on a vertical straight line. The time to reach the maximum height is exactly half of the time to crash. All these results are confirmed qualitatively and quantitatively by application of Newton's second law.

In Test 2, the vehicle was also given a horizontal velocity of 10.0 m/s. As expected, in vertical motion, the same behaviour as in Test 1 was observed. A parabolic trajectory with a correct range was also obtained in this test.

In Test 3, a two dimensional motion in YZ plane was examined. The same result as in the Test 2 associated with a projectile like motion has been obtained. The time to crash is equal to those in the two previous tests.

In Test 4, the aircraft was given an initial vertical velocity of -10.0 m/s plus an initial pitch spin velocity of 1000.0 deg/s. The initial height was chosen to be 10.0 m in this test. As seen in Figure 7.10, pitch spin has not affected the linear vertical motion of the aircraft and its expected parabolic trajectory under the constant gravitational acceleration. The pitch spin velocity has remained constant during flight. The pitch angle has constantly increased, however, since the quaternion version of the program has been used in which the pitch angle is defined between -90.0 to 90.0 deg., a periodic pitch angle variation is seen in Figure 7.10. Due to the rotation of the body axes, a periodic variation in velocity components U and W is also observed. Both U and W are zero at maximum height where the vertical velocity in inertial axes and in turn its components become zero.

In Test 5, Test 4 has been repeated by adding a horizontal velocity of 10.0 m/s. As seen in Figure 7.11, the aircraft trajectory is now parabolic, however, the time to crash is the same as before. The pitch rate and pitch angle have the same behaviour because the added horizontal velocity has not affected the aircraft rotational motion. The variations of the U and W components have the same frequency as before. However, as expected,

Fig.(7.7): Vehicle projectile like dynamics, Test 1

Uic=0.0	PSIic=0.0	THnicrd=90.0	Tstop=4.0
Vic=0.0	THETAic=0.0	THnicld=90.0	Conf1=0.0
Wic=-10.0	PHIic=0.0	THndicrd=0.0	
Picd=0.0	NORTHic=0.0	THndicld=0.0	
Qicd=0.0	EASTic=0.0	LOCK1r=0.0	
Ricd=0.0	HEIGHTic=0.0	LOCK1l=0.0	Axes at c.g.

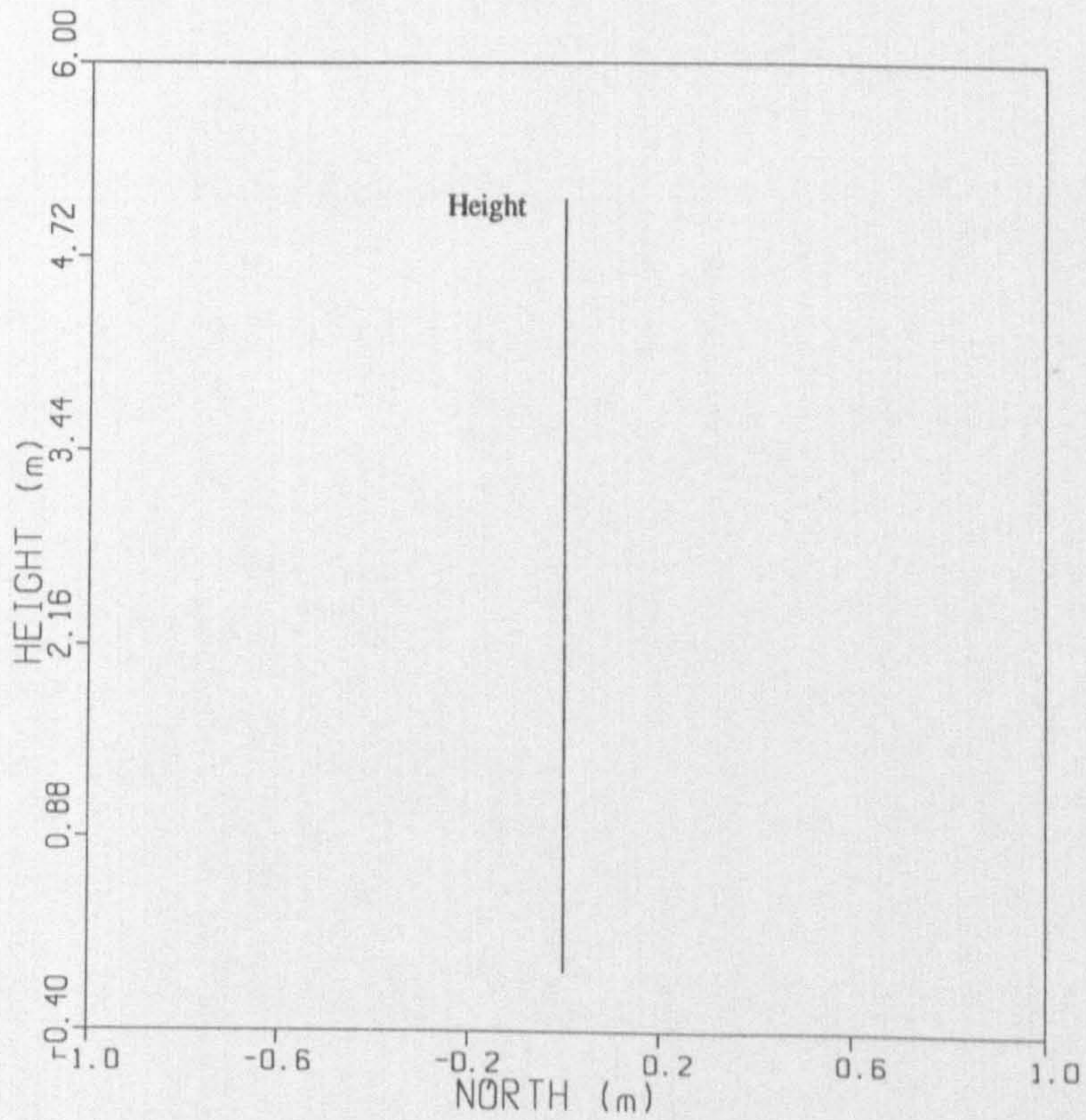
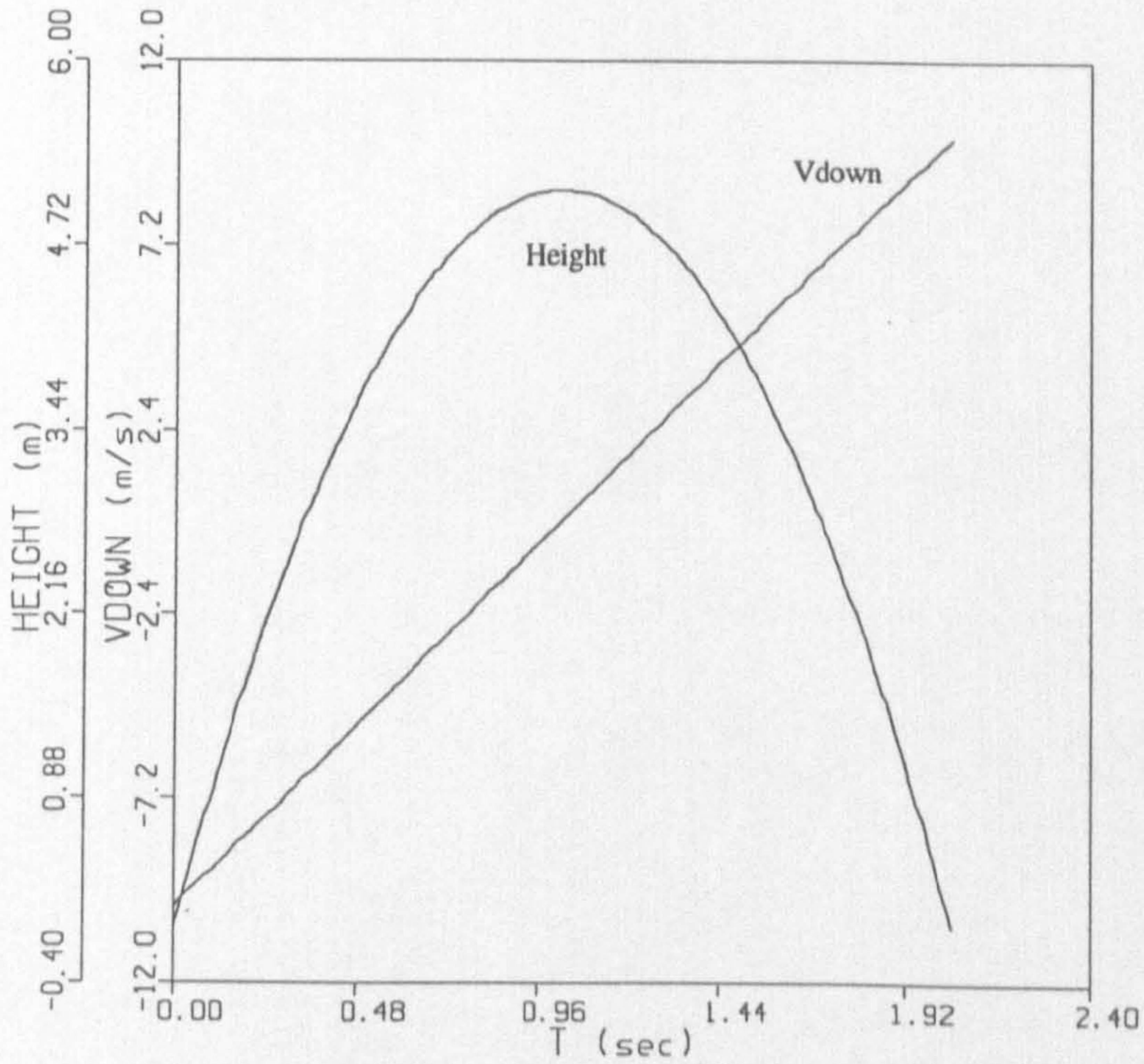
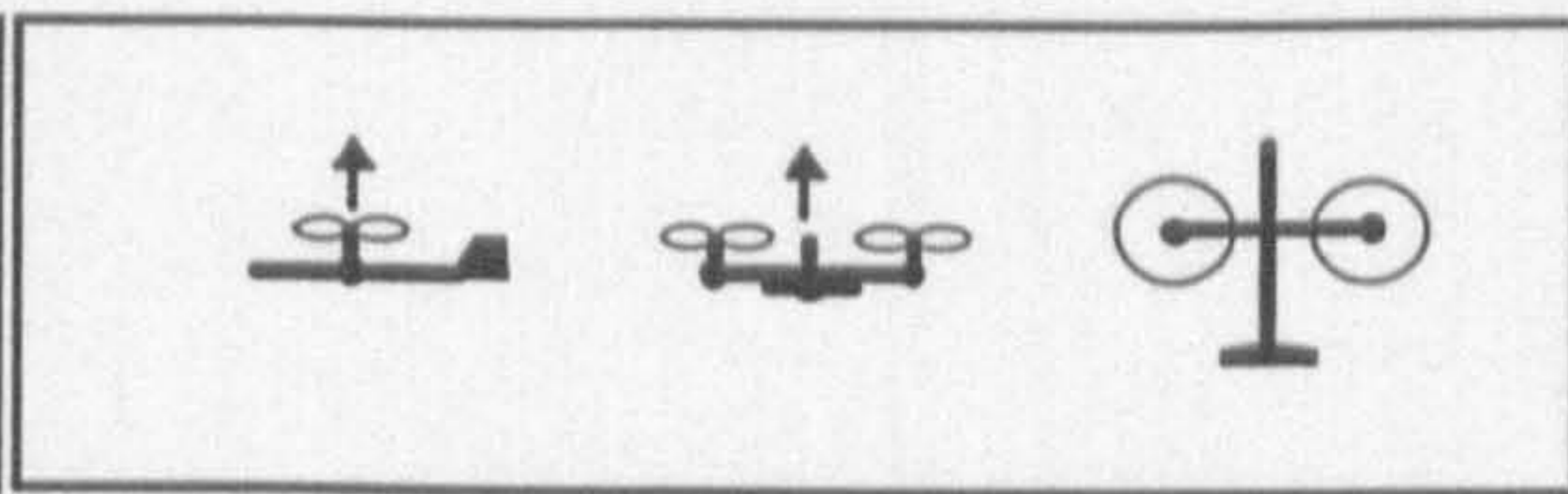


Fig.(7.8): Vehicle projectile like dynamics, Test 2

Uic=10.0	PSlic=0.0	THnicrd=90.0	Tstop=4.0	
Vic=0.0	THETAic=0.0	THnicld=90.0	Conf1=0.0	
Wic=-10.0	PHlic=0.0	THndicrd=0.0		
Picd=0.0	NORTHic=0.0	THndicld=0.0		
Qicd=0.0	EASTic=0.0	LOCK1r=0.0		
Ricd=0.0	HEIGHTic=0.0	LOCK1l=0.0	Axes at c.g.	

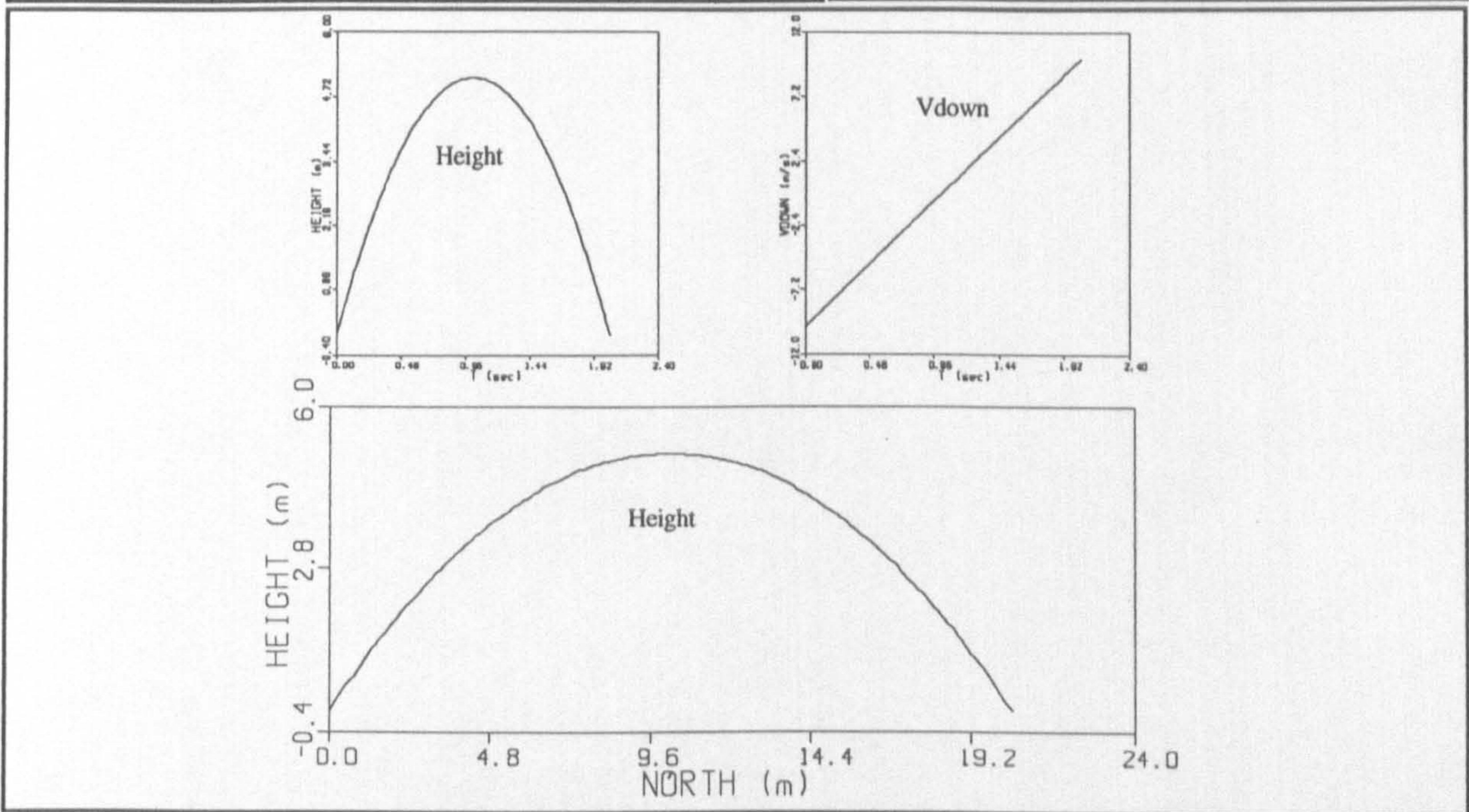


Fig.(7.9): Vehicle projectile like dynamics, Test 3

Uic=0.0	PSlic=0.0	THnicrd=90.0	Tstop=4.0	
Vic=10.0	THETAic=0.0	THnicld=90.0	Conf1=0.0	
Wic=-10.0	PHlic=0.0	THndicrd=0.0		
Picd=0.0	NORTHic=0.0	THndicld=0.0		
Qicd=0.0	EASTic=0.0	LOCK1r=0.0		
Ricd=0.0	HEIGHTic=0.0	LOCK1l=0.0	Axes at c.g.	

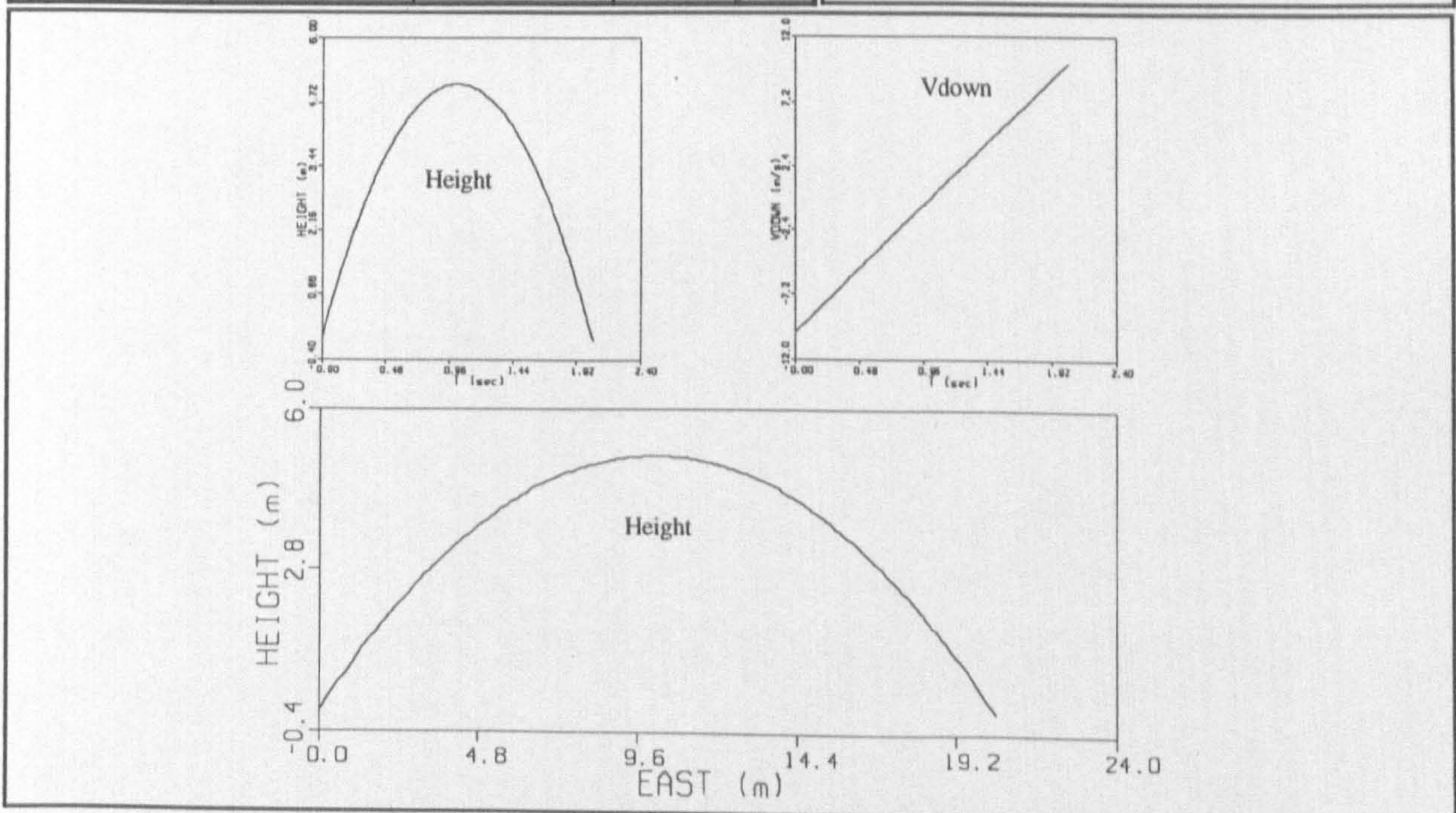


Fig.(7.10): Vehicle projectile like dynamics, Test 4

Uic=0.0	PSlic=0.0	THnicrd=90.0	Tstop=4.0
Vic=0.0	THETAic=0.0	THnicld=90.0	Conf1=0.0
Wic=-10.0	PHlic=0.0	THndicrd=0.0	
Picd=0.0	NORTHic=0.0	THndicld=0.0	
Qicd=1000.0	EASTic=0.0	LOCK1r=0.0	
Ricd=0.0	HEIGHTic=10.	LOCK1l=0.0	Axes at c.g.

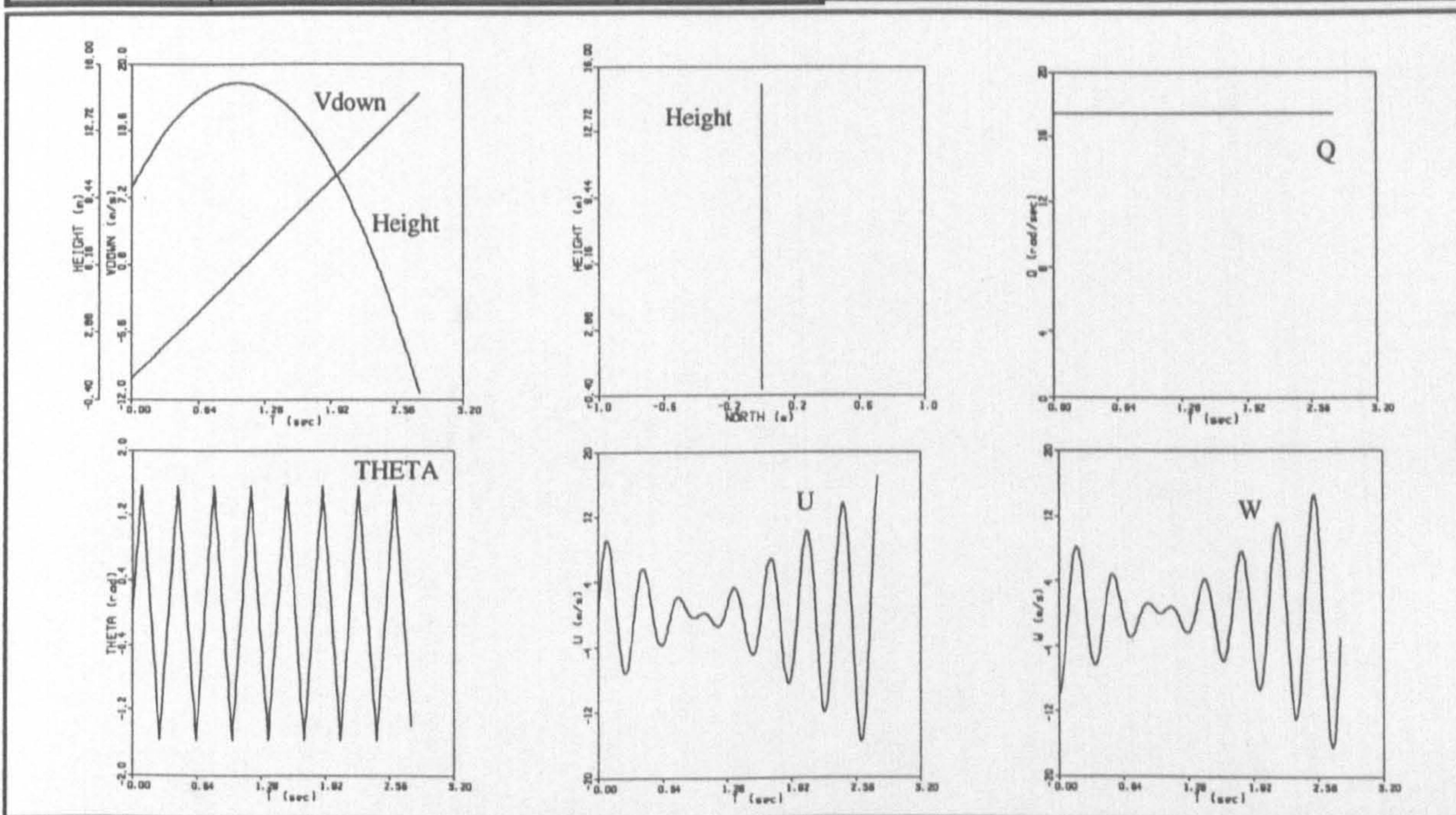
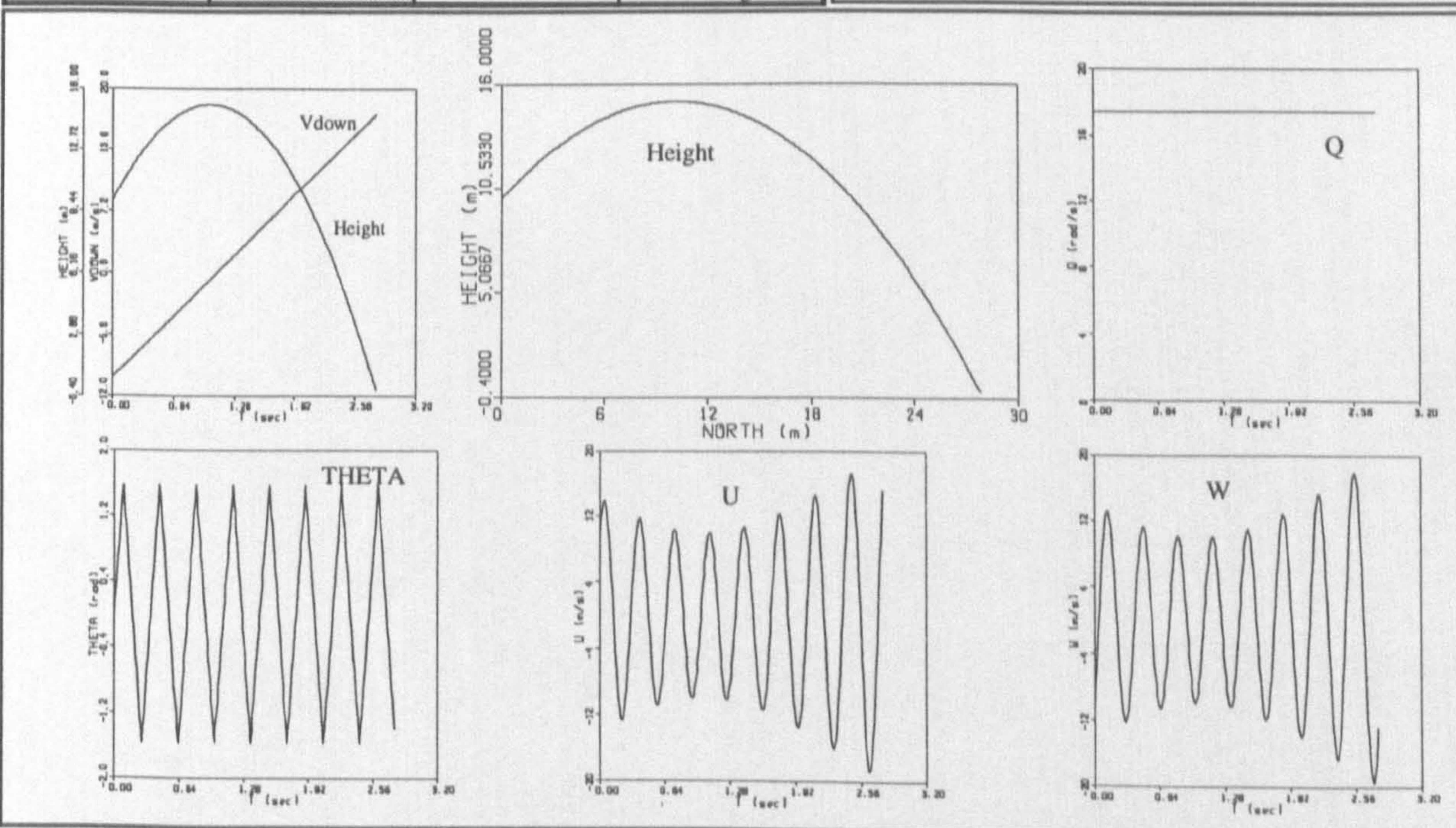


Fig.(7.11): Vehicle projectile like dynamics, Test 5

Uic=10.0	PSlic=0.0	THnicrd=90.0	Tstop=4.0
Vic=0.0	THETAic=0.0	THnicld=90.0	Conf1=0.0
Wic=-10.0	PHlic=0.0	THndicrd=0.0	
Picd=0.0	NORTHic=0.0	THndicld=0.0	
Qicd=1000.0	EASTic=0.0	LOCK1r=0.0	
Ricd=0.0	HEIGHTic=10.	LOCK1l=0.0	Axes at c.g.



at maximum height the vector summation of U and W is equal to the initial horizontal velocity.

In Test 6, the body axes was located at the nose of the aircraft in order to check that the location of the body axes does not affect the aircraft dynamics when the conditions are the same as those in the Test 5. As seen in Figure 7.12, the height vs time and height vs north curves have an oscillatory motion around an overall parabolic path. Also, Vdown oscillates around an average linear path. The oscillatory motion associated with these curves were expected. In fact, in these curves the position and the velocity of the aircraft nose are shown which vary periodically with the aircraft rotation around the pitch axis.

The time to crash is less than its corresponding value in Test 5. This is due to the fact that these tests were not really similar. In Test 5, the aircraft centre of gravity was given a vertical initial velocity of -10.0 m/s, however, in Test 6, nose was given a vertical initial velocity of -10.0 m/s and c.g. had a different velocity. To have an initial vertical velocity of -10.0 m/s at c.g. , an initial vertical velocity of -16.10865 (calculated manually, using the relative velocity relation between nose and c.g.) must be given when the body axes is located at nose which was carried out in Test 7.

As mentioned, in test 7, the body was given an initial velocity of -16.10865. The other initial conditions were the same as those in Test 6. As explained earlier, oscillatory motion of the height and Vdown curves are due to the effect of the aircraft rotation on the absolute linear velocity of the aircraft nose. As seen in Figure 7.13, the time to crash and the maximum range are equal to those in test 5. The pitch rate has remained constant and the pitch angle has exactly the same oscillation as in test 5.

In Test 8, a more complicated initial conditions was given including the roll and yaw rate, however the pitch rate was set to zero. The body axes was located at c.g. again. As seen in Figure 7.14, the motion of the aircraft c.g. in space has not been affected by spin motion. However, due to the inertial cross coupling, the roll and yaw spins have produced some pitch spin.

In Test 9, the aircraft was launched in XZ plane with the same vertical and horizontal velocity as before. However, tilting parts were allowed to rotate with an initial relative angular velocity of -45.0 deg/s. No internal active moment between the tilting parts and

Fig.(7.12): Vehicle projectile like dynamics, Test 6

Uic=10.0	PSlic=0.0	THnicrd=90.0	Tstop=4.0
Vic=0.0	THETAic=0.0	THnicld=90.0	Confl=0.0
Wic=-10.0	PHlic=0.0	THndicrd=0.0	
Picd=0.0	NORTHic=0.0	THndicld=0.0	
Qicd=1000.0	EASTic=0.0	LOCK1r=0.0	
Ricd=0.0	HEIGHTic=10.	LOCK1l=0.0	Axes at nose

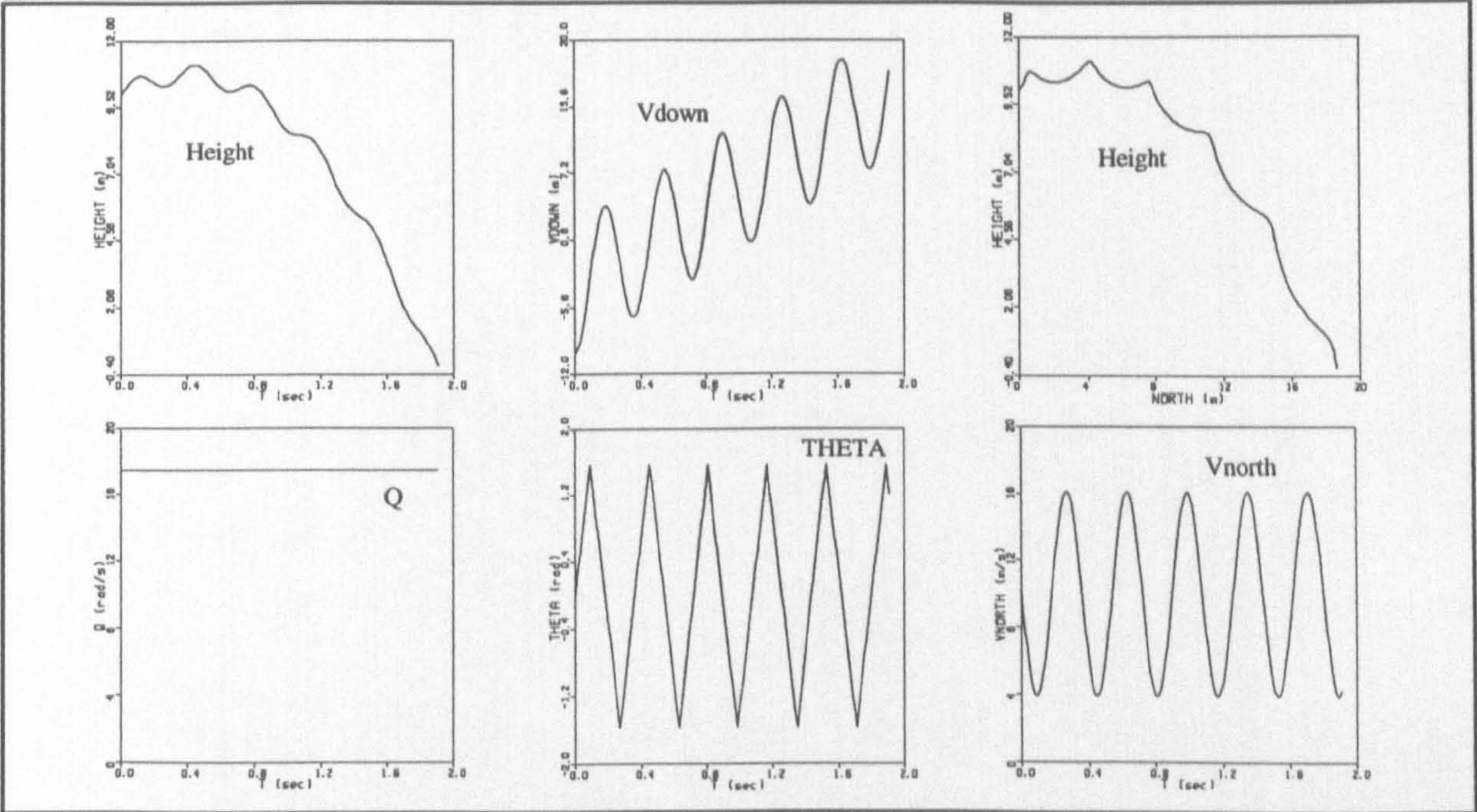


Fig.(7.13): Vehicle projectile like dynamics, Test 7

Uic=10.0	PSlic=0.0	THnicrd=90.0	Tstop=4.0
Vic=0.0	THETAic=0.0	THnicld=90.0	Confl=0.0
Wic=-16.10865	PHlic=0.0	THndicrd=0.0	
Picd=0.0	NORTHic=0.0	THndicld=0.0	
Qicd=1000.0	EASTic=0.0	LOCK1r=0.0	
Ricd=0.0	HEIGHTic=10.	LOCK1l=0.0	Axes at nose

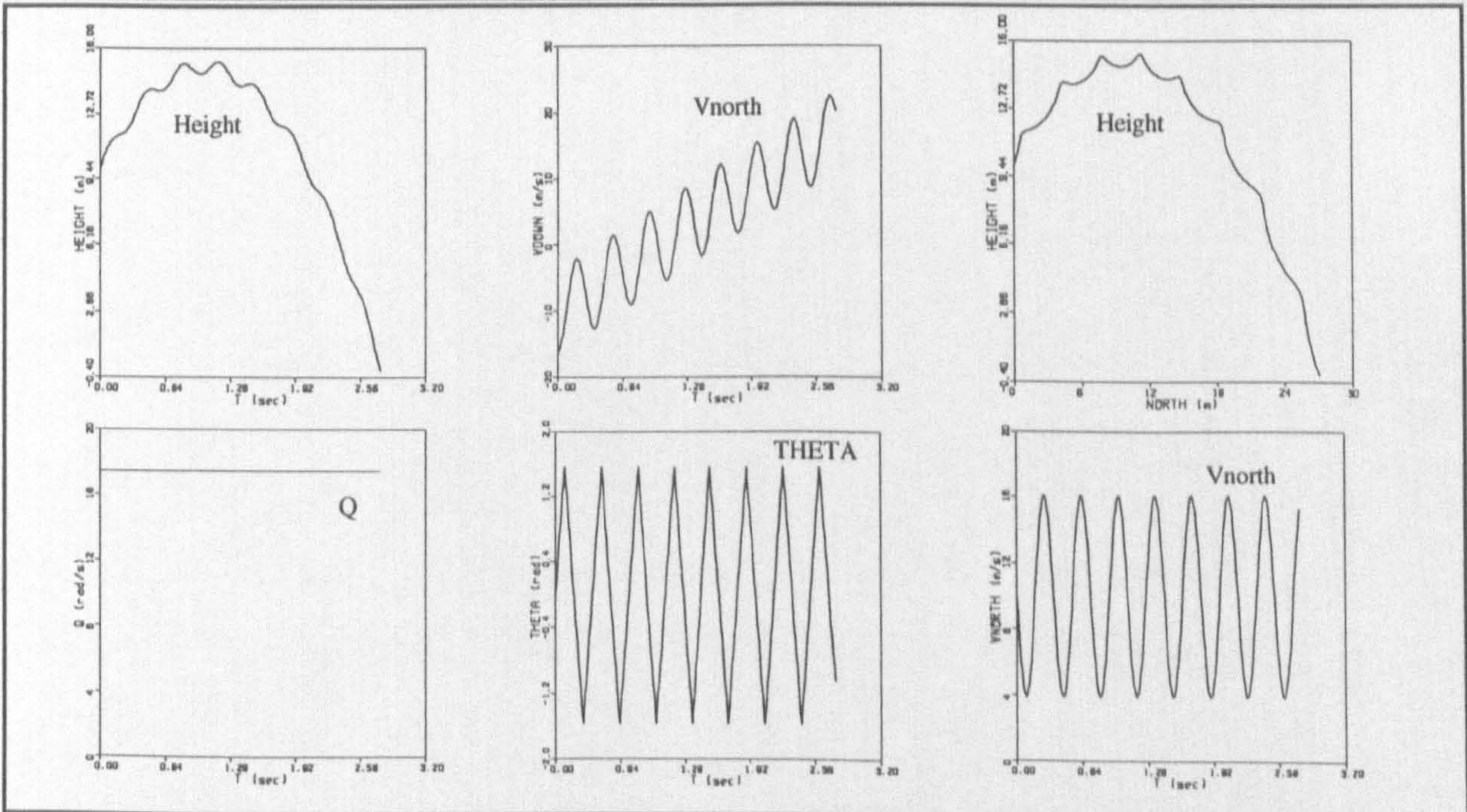
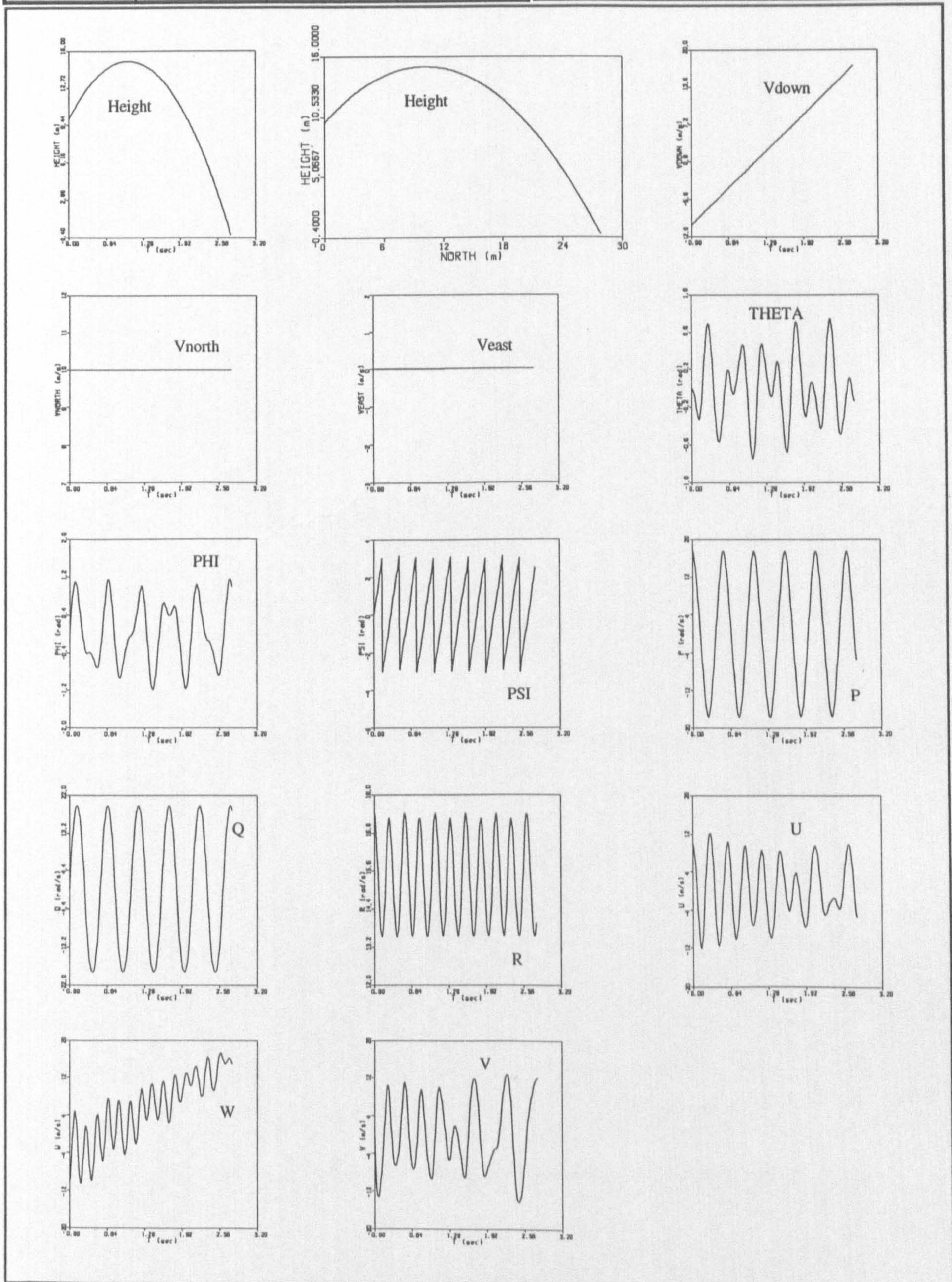
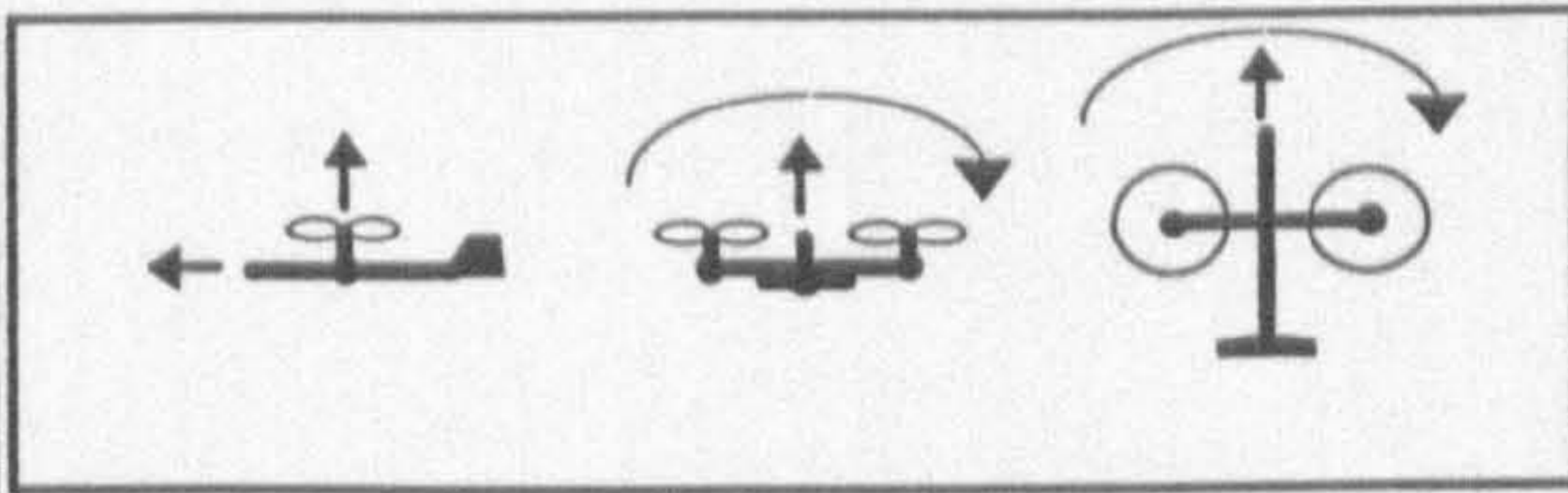


Fig.(7.14): Vehicle projectile like dynamics, Test 8

Uic=10.0	PSlic=0.0	THnicrd=90.0	Tstop=4.0
Vic=0.0	THETAic=0.0	THnicld=90.0	Confl=0.0
Wic=-10.0	PHlic=0.0	THndicrd=0.0	
Picd=1000.0	NORTHic=0.0	THndicld=0.0	
Qicd=0.0	EASTic=0.0	LOCKIr=0.0	
Ricd=1000.0	HEIGHTic=10.	LOCKIl=0.0	Axes at c.g



the main body was imposed, i.e. , zero servomotor output torque and zero friction. As seen in Figure 7.15, the parabolic character of the curves associated with height variation has not been changed. These curves are very smooth, mainly due to the fact that the displacement of the light tilting parts has not significantly changed the aircraft c.g. location. The same maximum height, range, time to crash, and slope of the Vdown curve (gravitational acceleration) have been obtained. As seen in Figure 7.15, the pitch angle (THETA) has changed very slightly from its initial value (zero) in the same direction as the tilt angles (THnr,THnl) have been changed. Since, there is no pitching moment (no aerodynamic and internal active torque in the joints), such behaviour might not be expected. However, as mentioned in Chapter 6, this is due to the fact that the aircraft c.g. does not have exactly the same location as the joints in XZ plane and small distance exists between them, Figure 6.1. Therefore, the centrifugal force generated by the tilting parts during rotating forward has produced a small negative pitching moment. This, in turn, has caused a small negative pitch rate and consequently a small change in pitch angle .

Similarly, in Test 10, the tilting parts were allowed to rotate, however, this time rotation was generated by servomotors with an output torque of -0.1 n.m. The other initial conditions were similar to those in the Test 10. As seen in Figure 7.16, the aircraft behaves as it was expected. Due to the equal and opposite internal active torque, the main body rotates in the opposite direction to the tilting parts. The tilting parts rotate much faster than the main body, because they are much lighter. The oscillatory motion of the pitch rate has been caused by centrifugal forces (right and left) explained in the previous paragraph. Due to the variation in the length of the moment arm with rotation, the pitching moments generated by these centrifugal forces have changed sign periodically. Due to this, an oscillation around an average value in some of the curves is observed. In addition, due to the increase of the tilting rates (Thndr, Thndl) with time, these centrifugal forces have increased. Therefore, an increasing oscillation with time is observed in the curves. The Qdot vs Thnr curve is a good description of what has happened. As seen in this curve, Qdot has an extremum approximately every 180.0 degrees decrease in Thnr at which the lines of action of the centrifugal forces pass through the joints.

Test 11 was started with the same conditions as in the test 10, however, after two second the tilting parts were locked and simulation was carried on until crash happened. As seen

Fig.(7.15): Vehicle projectile like dynamics, Test 9

Uic=10.0	PSlic=0.0	THnicrd=90.0	Tstop=4.0
Vic=0.0	THETAic=0.0	THnicld=90.0	Confl=0.0
Wic=-10.0	PHlic=0.0	THndicrd=-45.0	Gservo=0.0
Picd=0.0	NORTHic=0.0	THndicld=-45.0	THdmndr=0.0
Qicd=0.0	EASTic=0.0	LOCK1r=1.0	THdmndl=0.0
Ricd=0.0	HEIGHTic=10.0	LOCK1l=1.0	Axes at c.g.

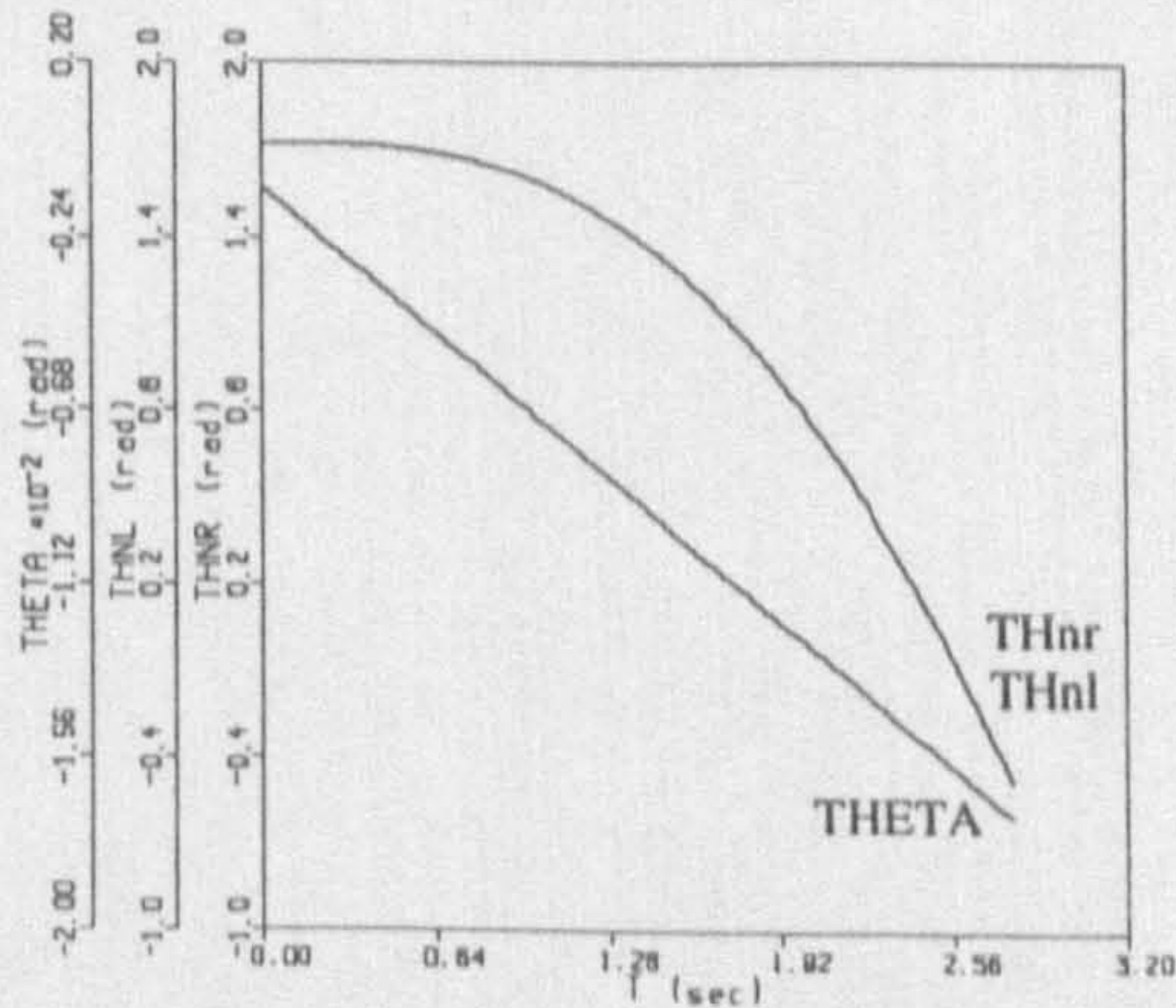
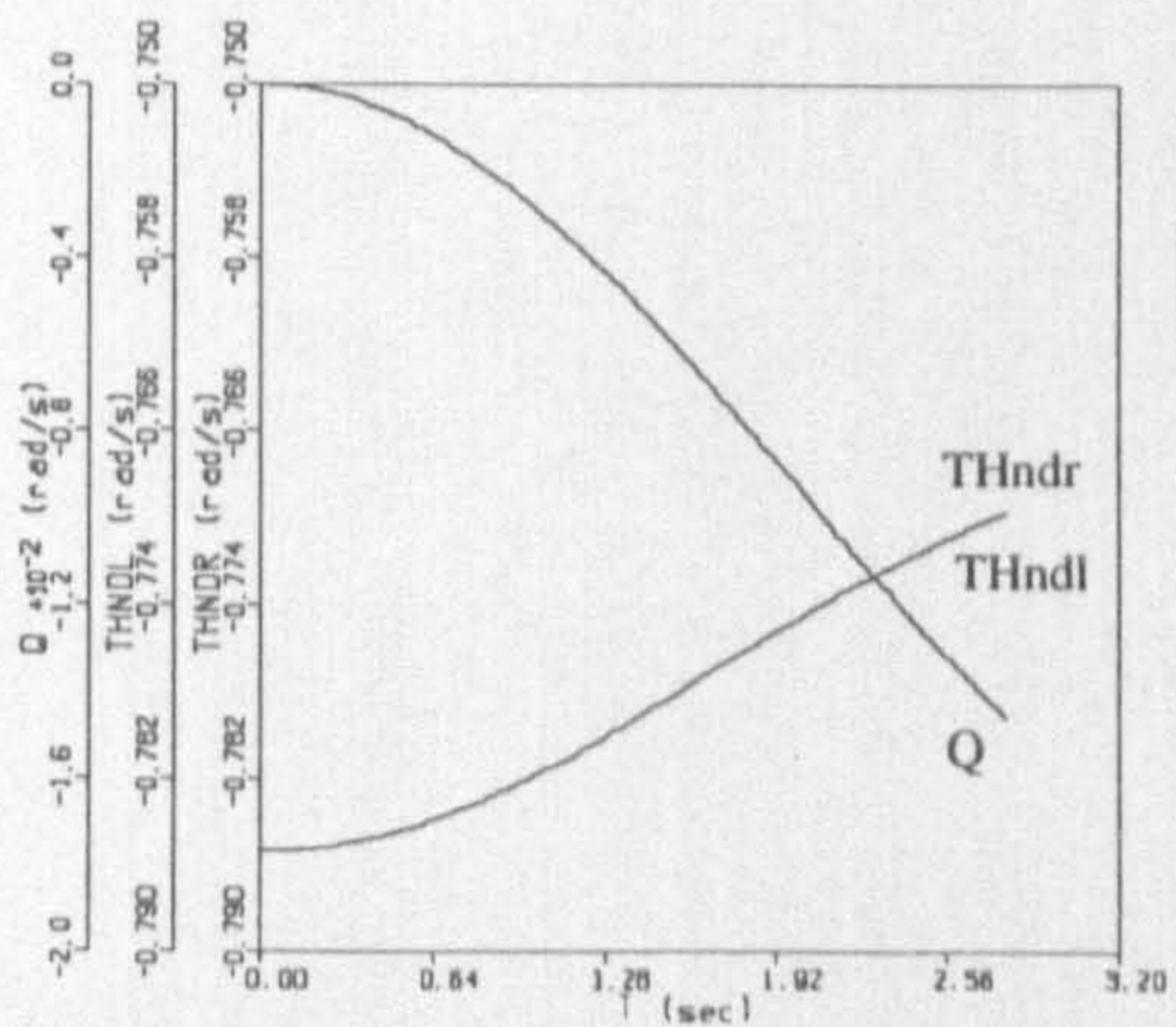
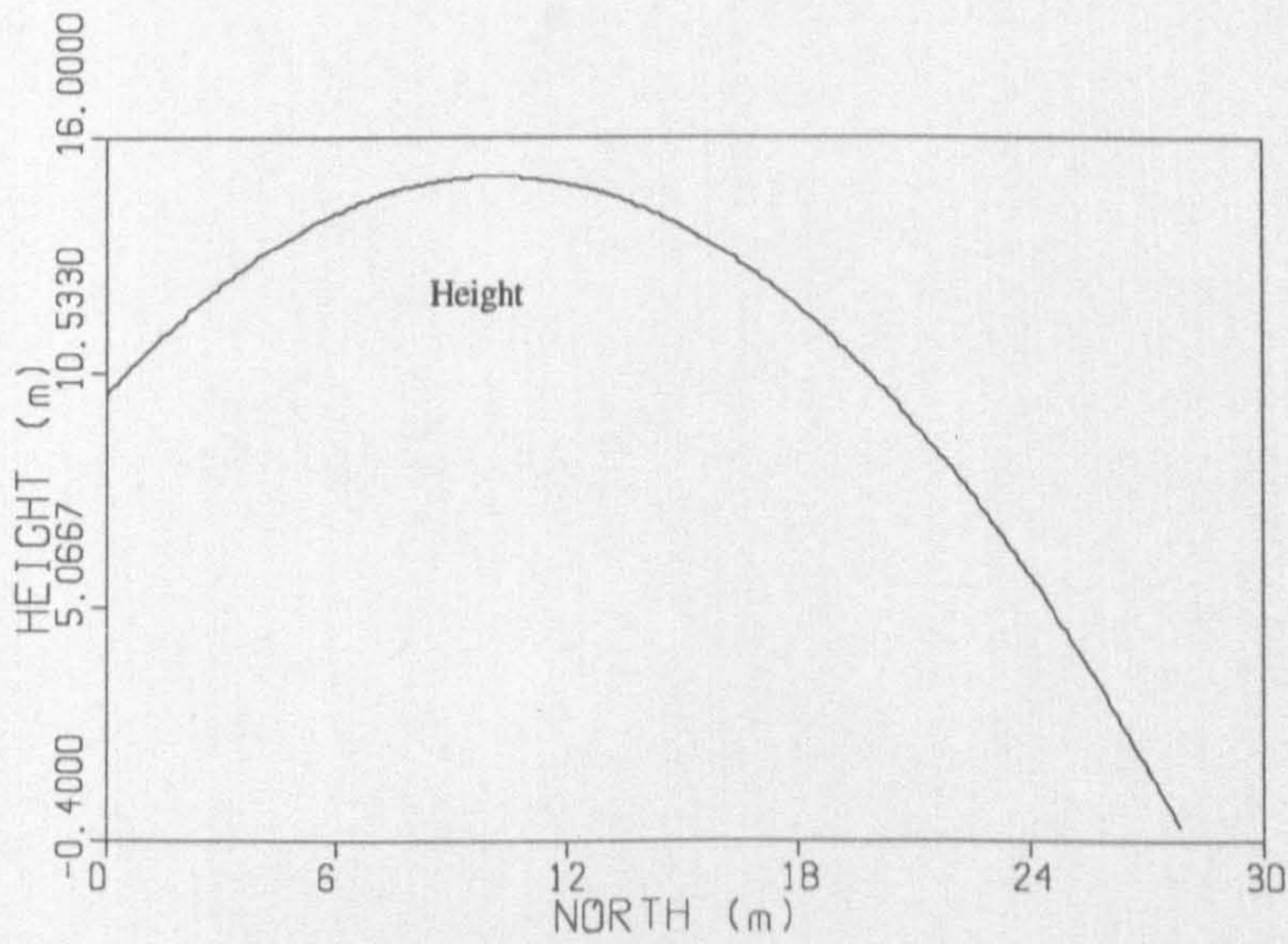
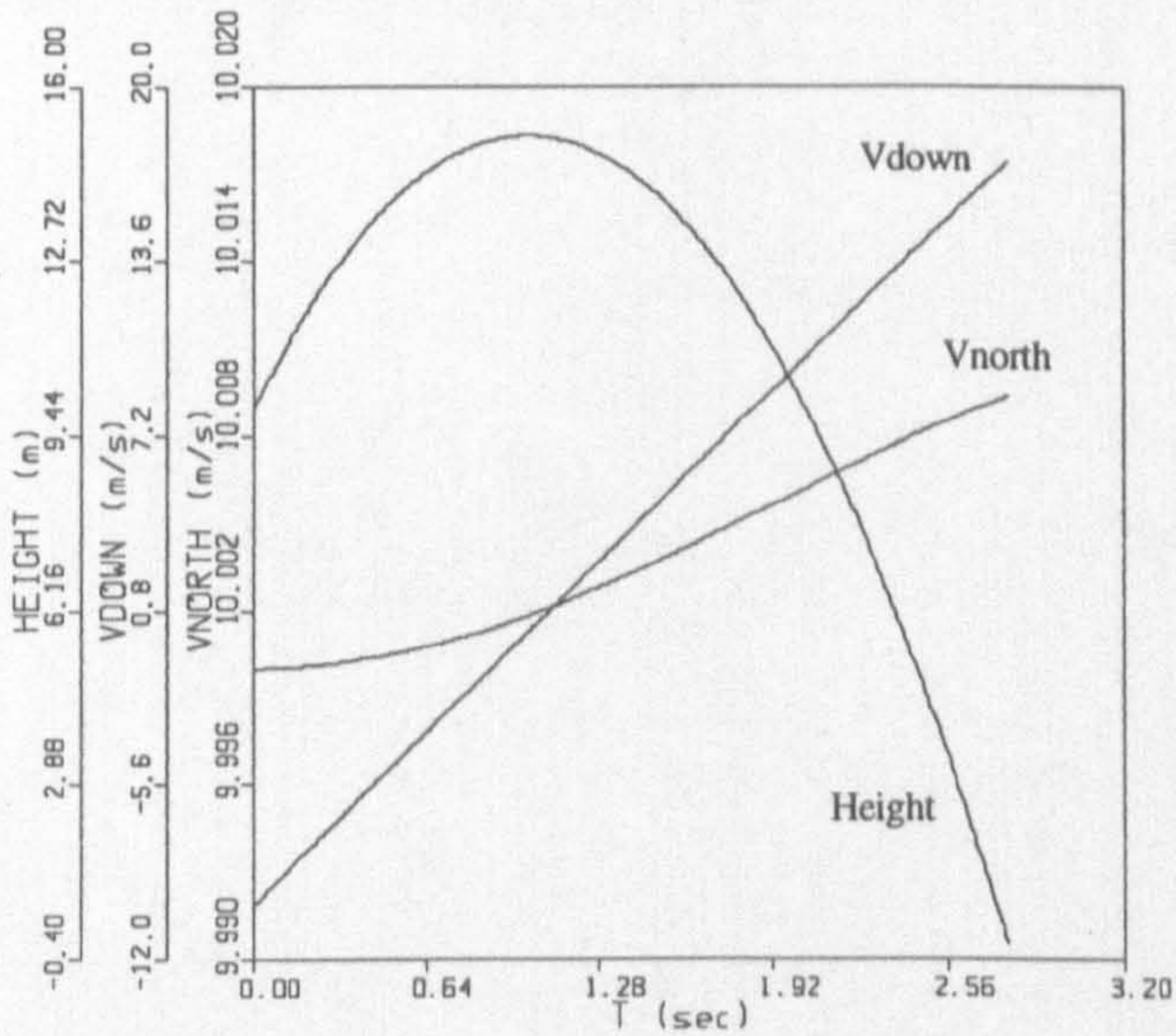
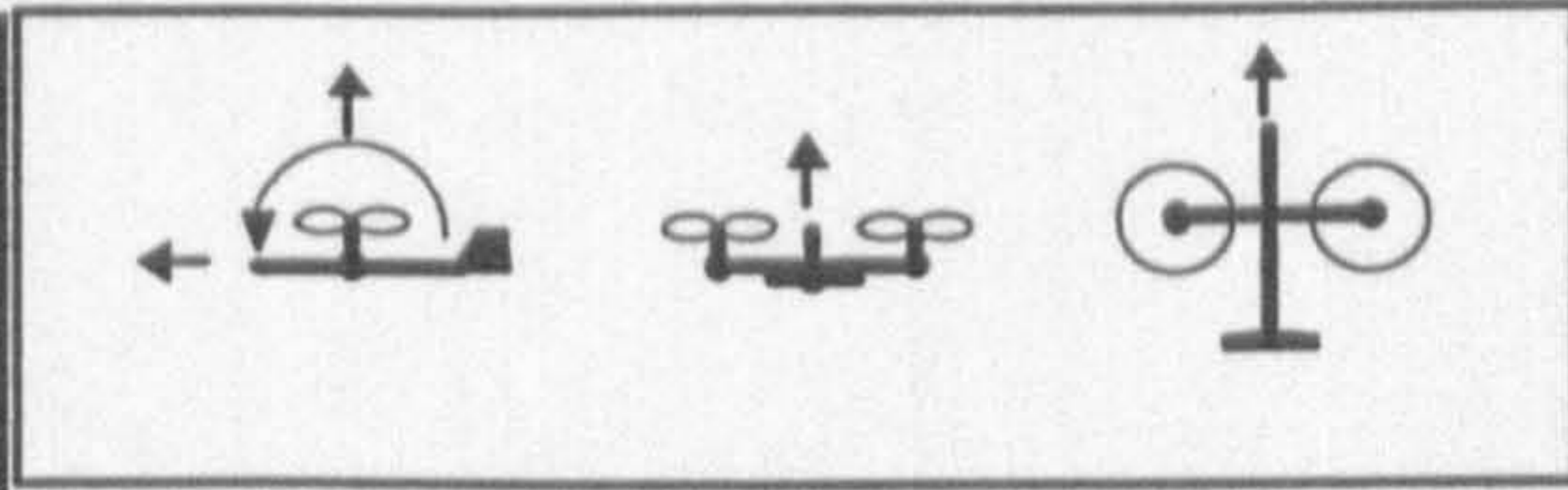
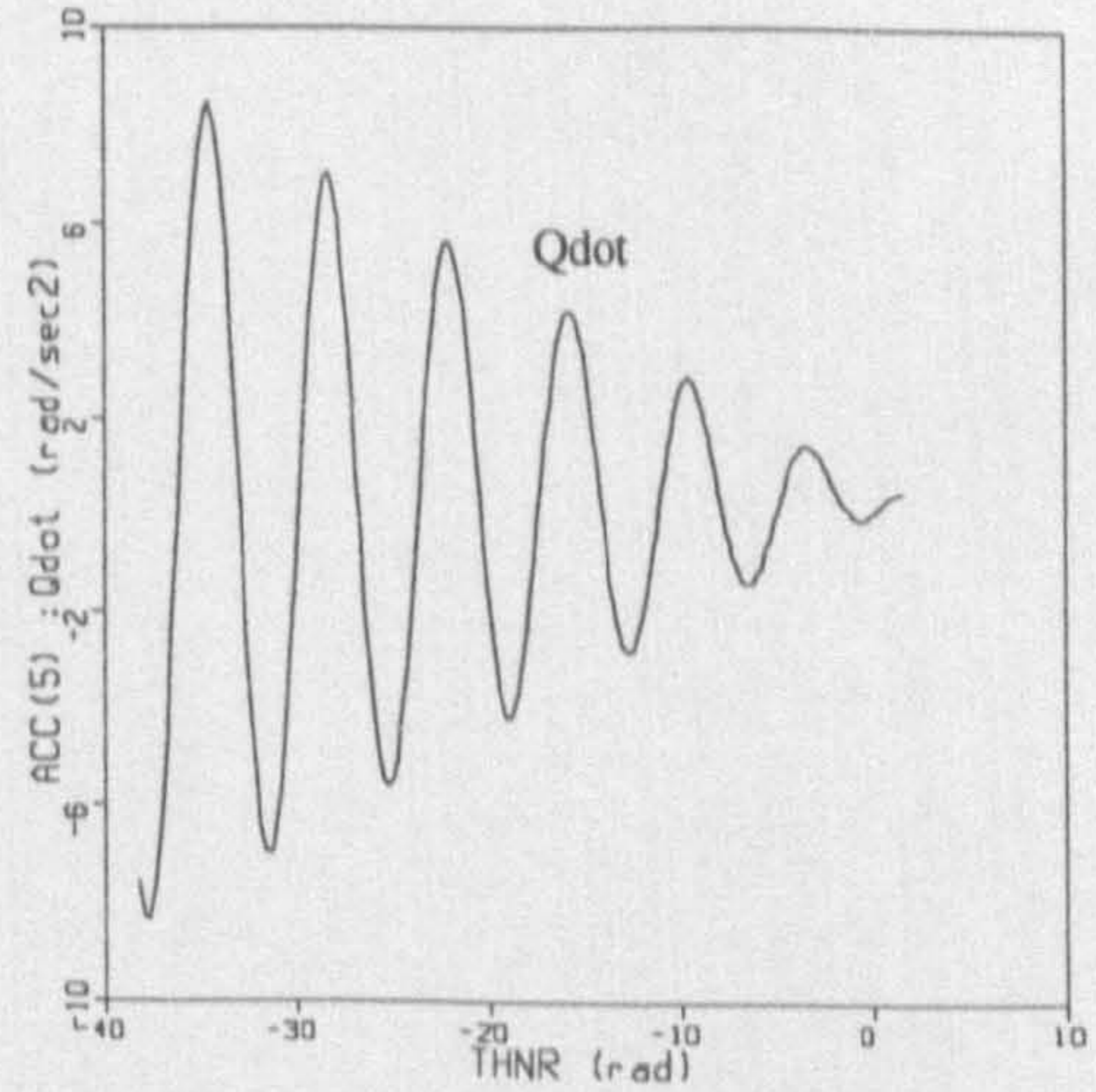
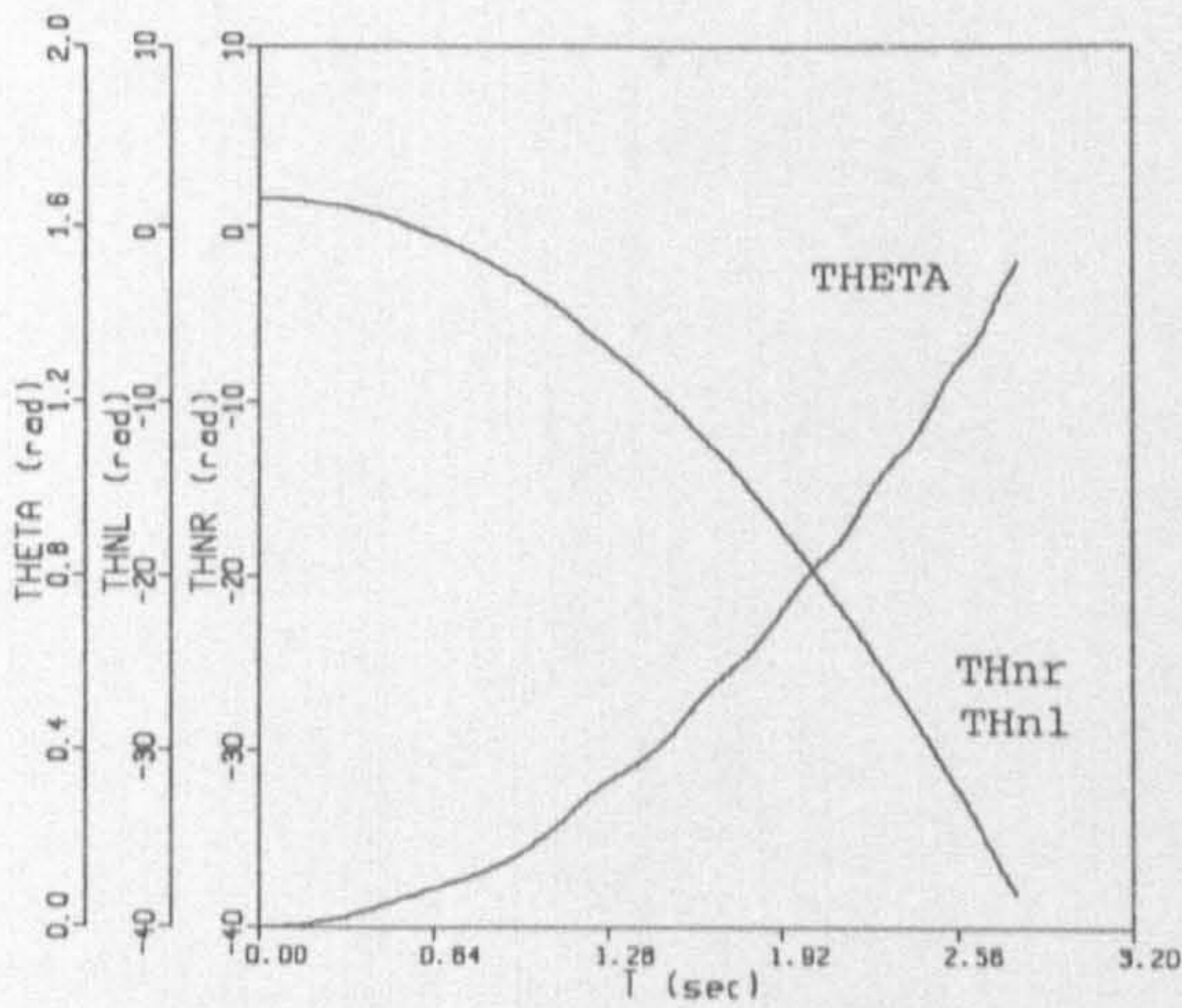
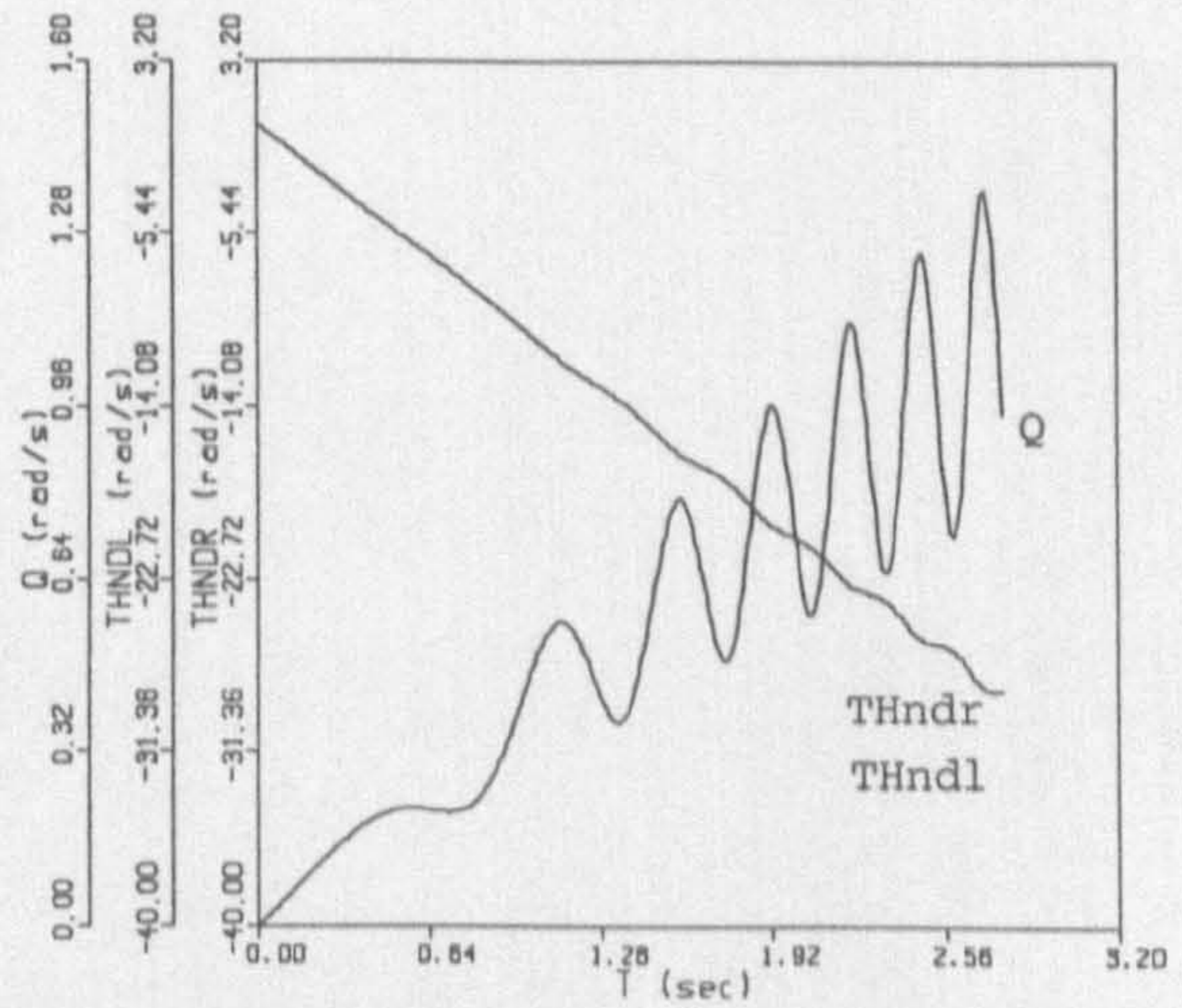
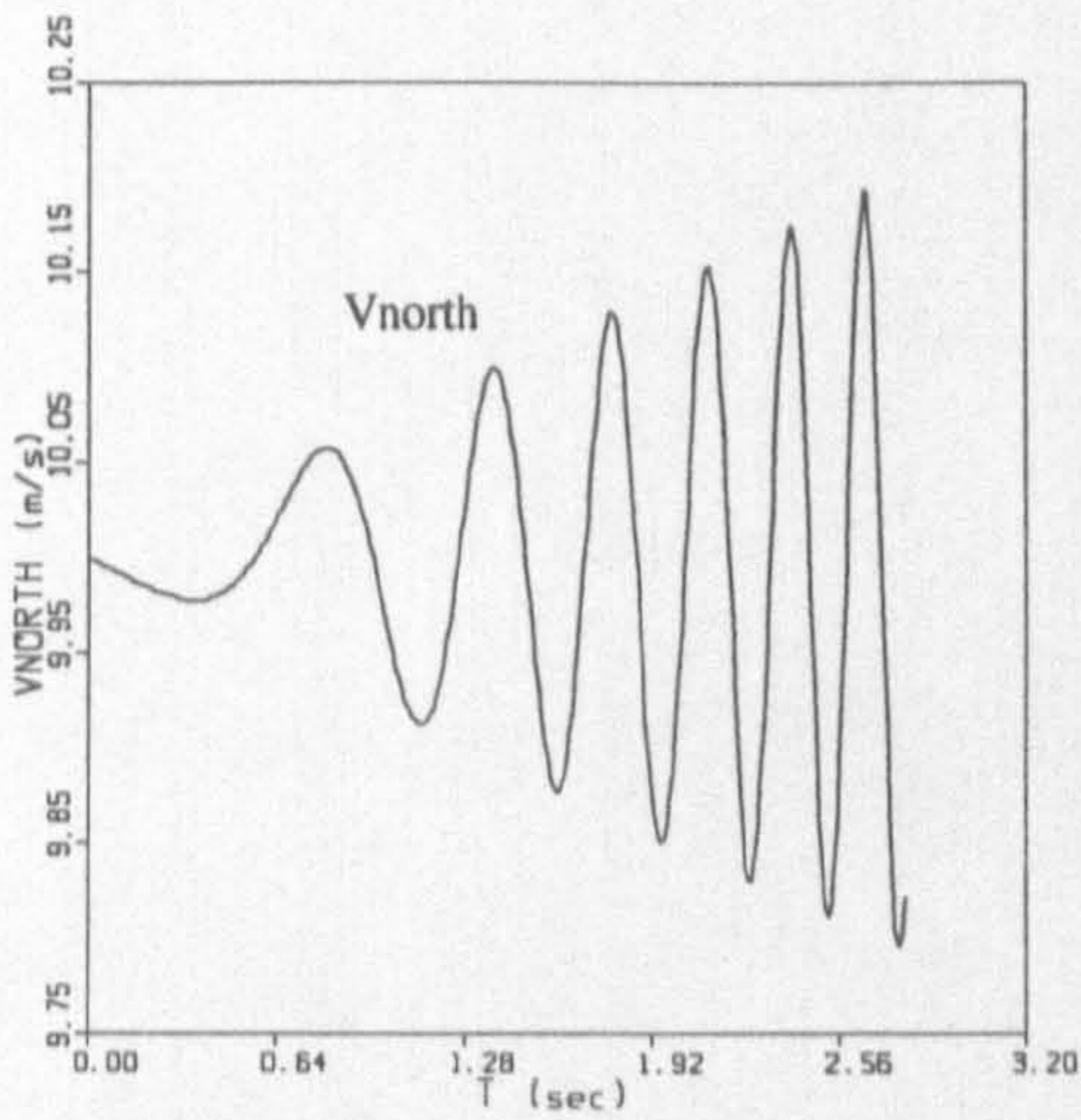
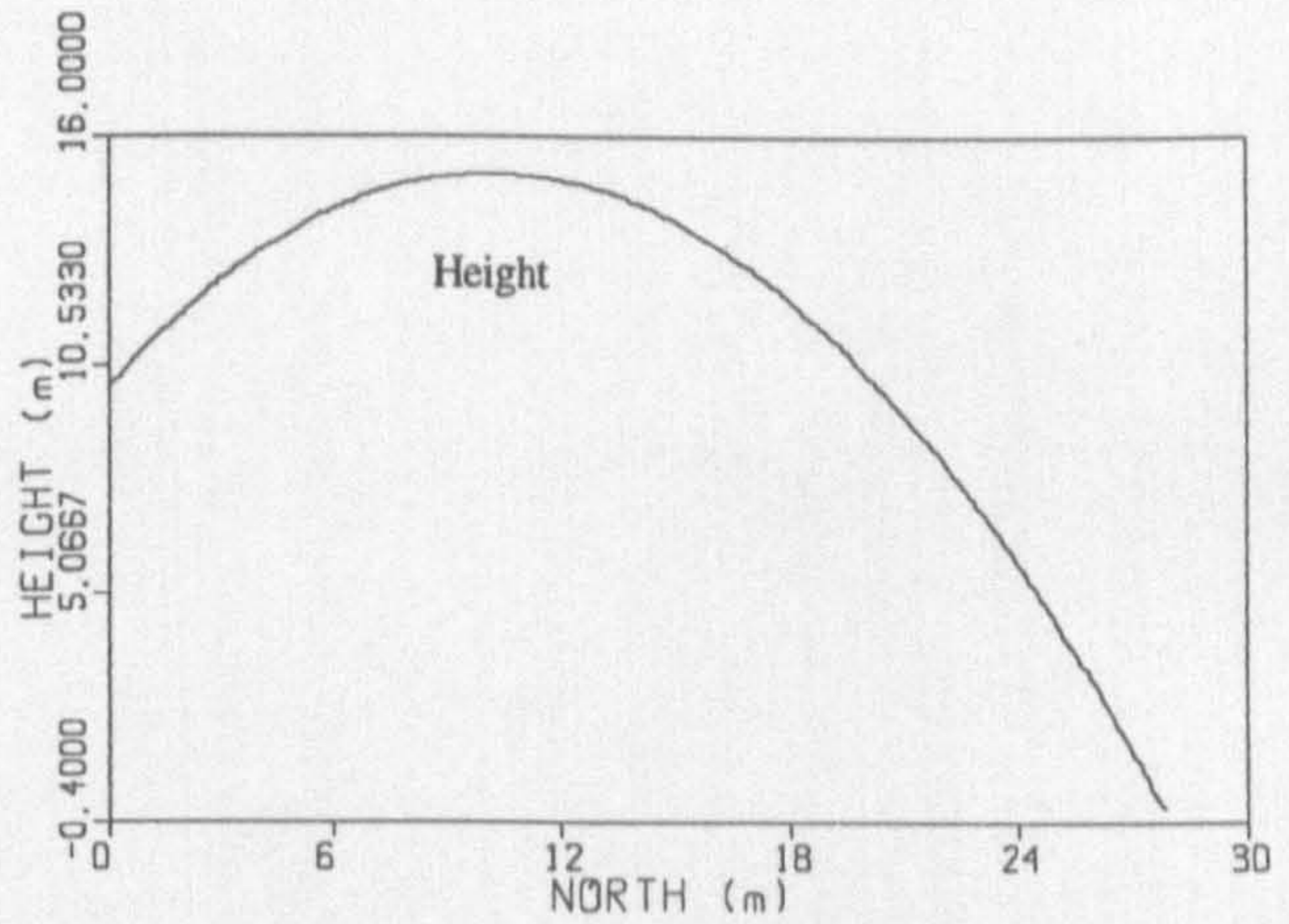
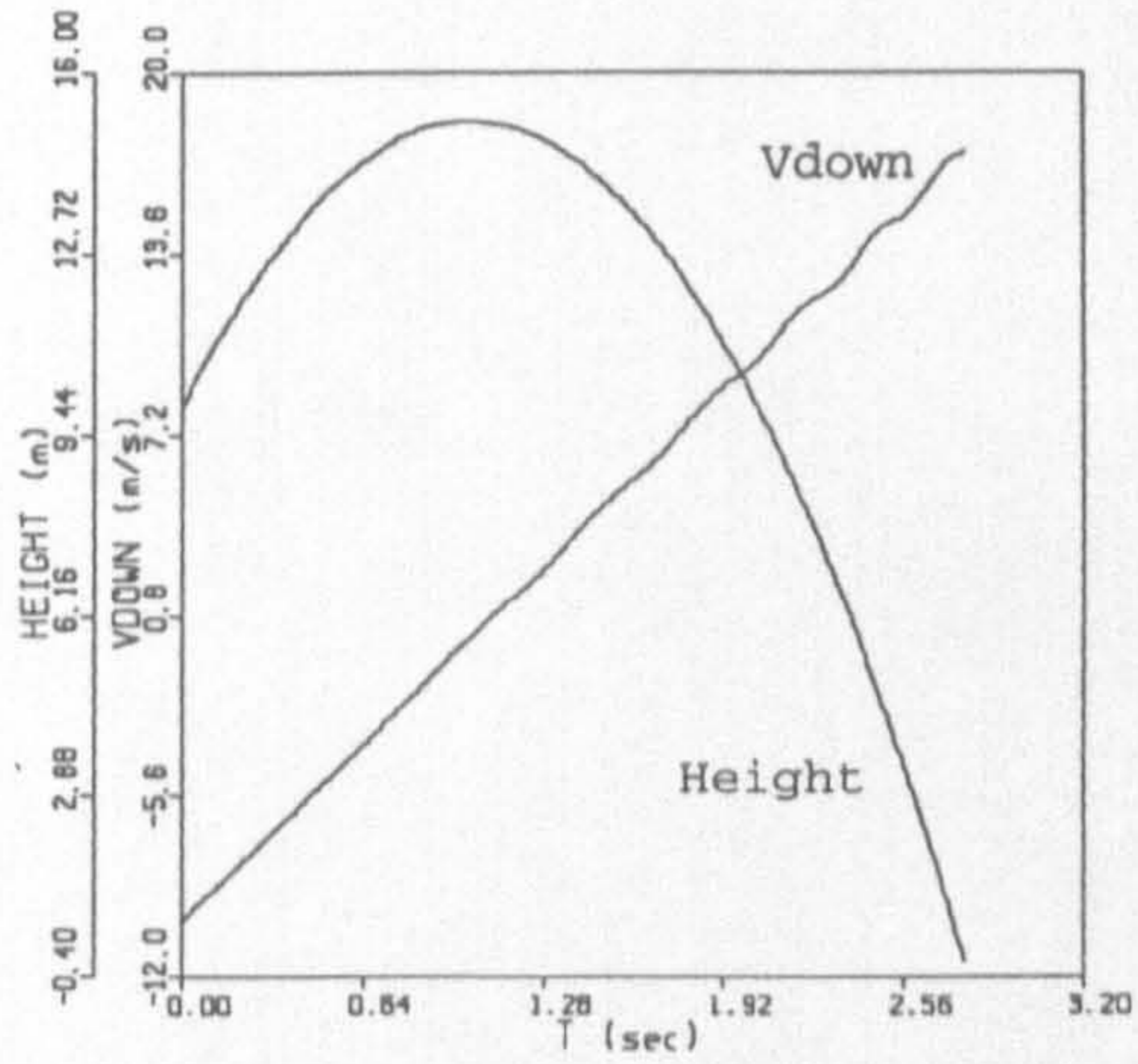


Fig.(7.16): Vehicle projectile like dynamics, Test 10

Uic=10.0	PSlic=0.0	THnicrd=90.0	Tstop=4.0
Vic=0.0	THETAic=0.0	THnicld=90.0	Confl=0.0
Wic=-10.0	PHlic=0.0	THndicrd=0.0	Gservo=1.0
Picd=0.0	NORTHic=0.0	THndicld=0.0	THdmndr=-0.1
Qicd=0.0	EASTic=0.0	LOCKI=1.0	THdmndl=-0.1
Ricd=0.0	HEIGHTic=10.0	LOCKII=1.0	Axes at c.g.



in Figure 7.17, for two seconds everything is exactly similar to the Test 10. After, the tilting parts were locked, the vehicle has continued its motion on an parabolic trajectory with the same specifications as before. The pitch rate has remained constant at its value at $t=2.0$. The tilt rates (THndr,THndl) have suddenly jumped to zero. The pitch angle has continued to increase linearly with a slope equal to Q . The tilt angles have remained constant at their values at $t=2.0$. Since, after locking the tilting parts, there is no internal active moment, $Qdot$ has suddenly jumped to zero. These observations were entirely predictable.

In Test 12, the vehicle was given the same initial conditions as in Test 11. However, this time with the propellers rotating with $rpm=6000.0$. Since, the simulation was carried out with contra-rotating propellers, no difference between the results in this test and those of previous one was observed. The propeller angular velocities (RPMr, RPMl) have remained constant.

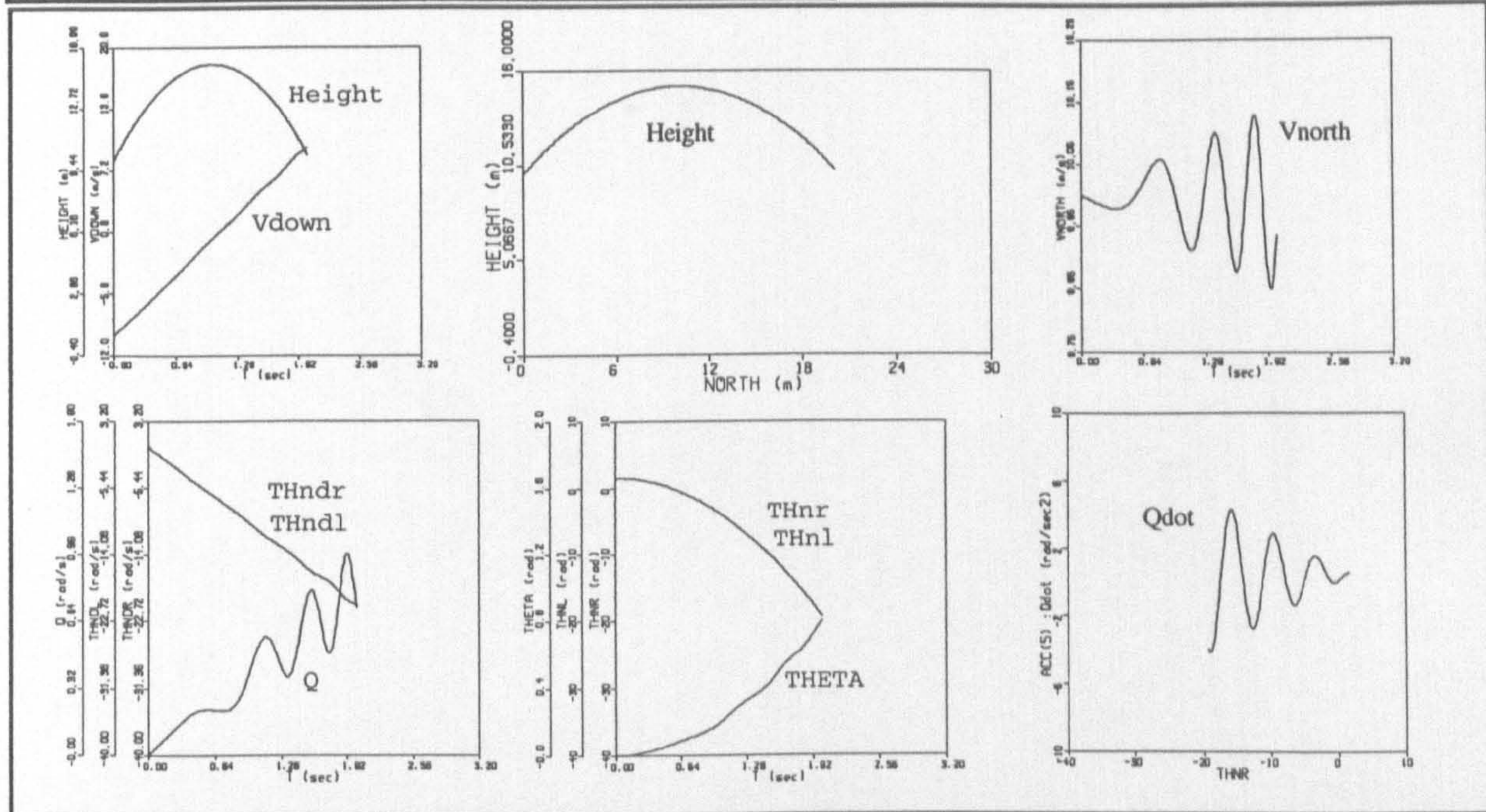
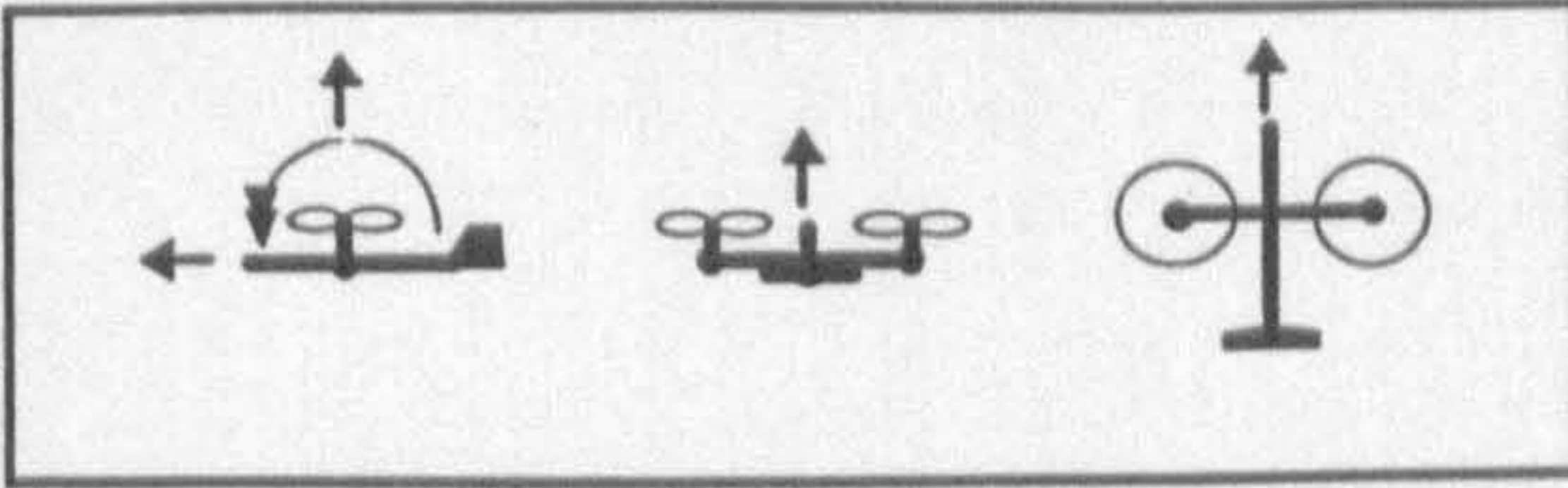
In Test 13, Test 12 was repeated with non-contra-rotating propellers. As seen in Figure 7.19, the vehicle trajectory is exactly the same as before. However, since the propellers have been considered to rotate in the same direction, the generated gyroscopic moments during rotation of the tilting parts have not been cancelled by each other. Due to this, all components of angular velocity have been affected and an unsymmetrical behaviour is observed in Figure 7.19.

In Test 14, Test 12 was repeated, using tilt-wing configuration. As seen in Figure 7.20, the vehicle projectile like dynamics is exactly the same as before. However, due to the change in mass and mass moment of inertia of the tilting parts, different variations were observed in tilt-rate vs time and tilt-angle vs time curves. It needs to be pointed out that due to the numerical issues, even in completely symmetrical cases, like in this test and Test 12, the roll and yaw rates always have a very small non-zero value. Since, the specifications of the tilting parts have been changed in this test, the roll and yaw rates are relatively bigger than those in Test 12. These terms may grow with time and affect the simulation results.

In the second step of incremental testing, the sub-system *Propeller* was added and both sub-systems were tested together. Since, the single module associated with this sub-system had previously been tested in module testing stage, the program was only run to

Fig.(7.17): Vehicle projectile like dynamics, Test 11

Uic=10.0	PSlic=0.0	THnicrd=90.0	Tstop=2.0
Vic=0.0	THETAic=0.0	THnicld=90.0	Confl=0.0
Wic=-10.0	PHlic=0.0	THndicrd=0.0	Gservo=1.0
Picd=0.0	NORTHic=0.0	THndicld=0.0	THdmndr=-0.1
Qicd=0.0	EASTic=0.0	LOCK1r=1.0	THdmndl=-0.1
Ricd=0.0	HEIGHTic=10.	LOCK1l=1.0	Axes at c.g.



Continue: Tilting parts locked

Uic=10.0	PSlic=0.0	THnicrd=90.0	Tstop=4.0
Vic=0.0	THETAic=0.0	THnicld=90.0	Confl=0.0
Wic=-10.0	PHlic=0.0	THndicrd=0.0	Gservo=1.0
Picd=0.0	NORTHic=0.0	THndicld=0.0	THdmndr=-0.1
Qicd=0.0	EASTic=0.0	LOCK1r=0.0	THdmndl=-0.1
Ricd=0.0	HEIGHTic=10.	LOCK1l=0.0	Axes at c.g.

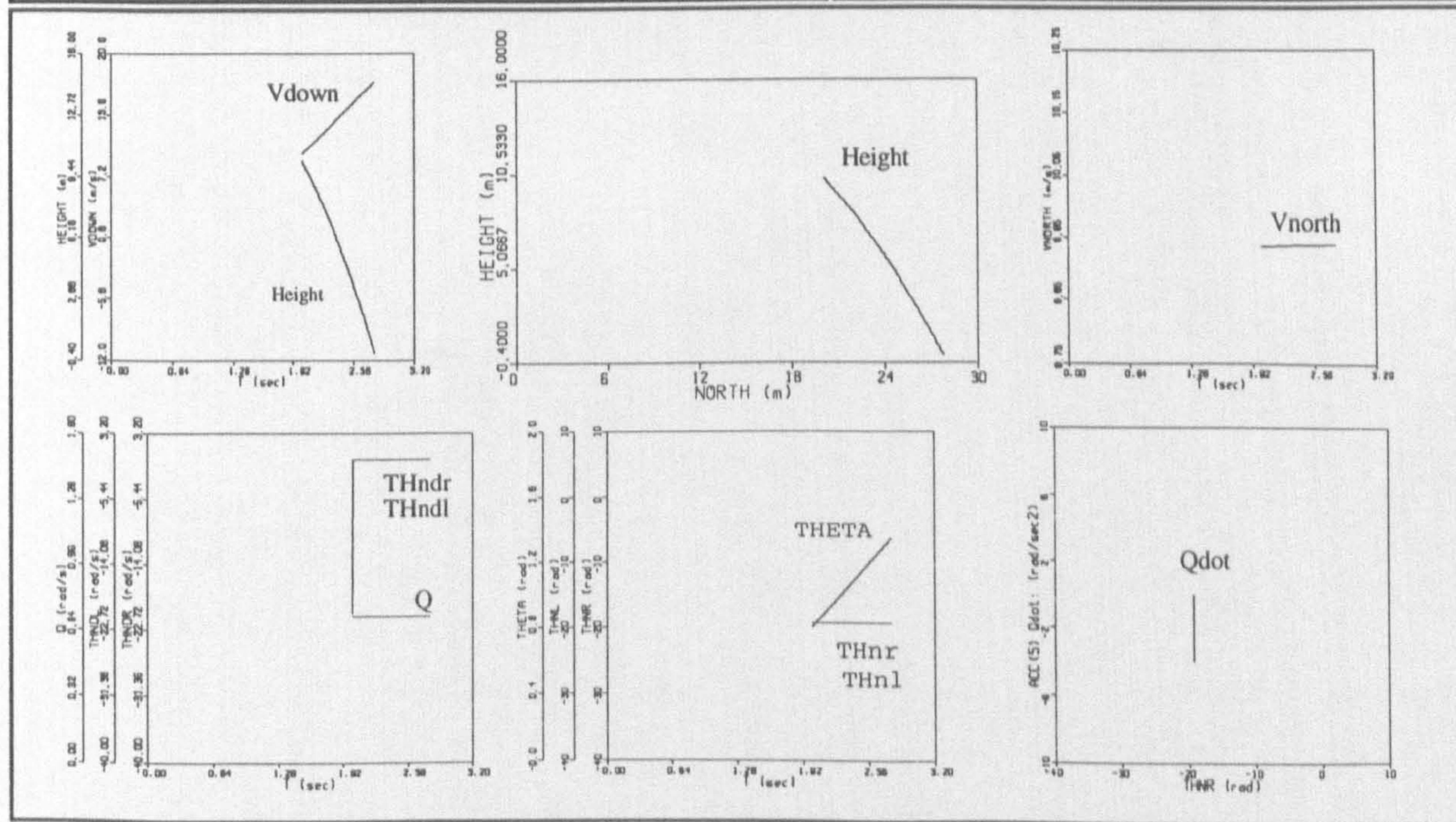
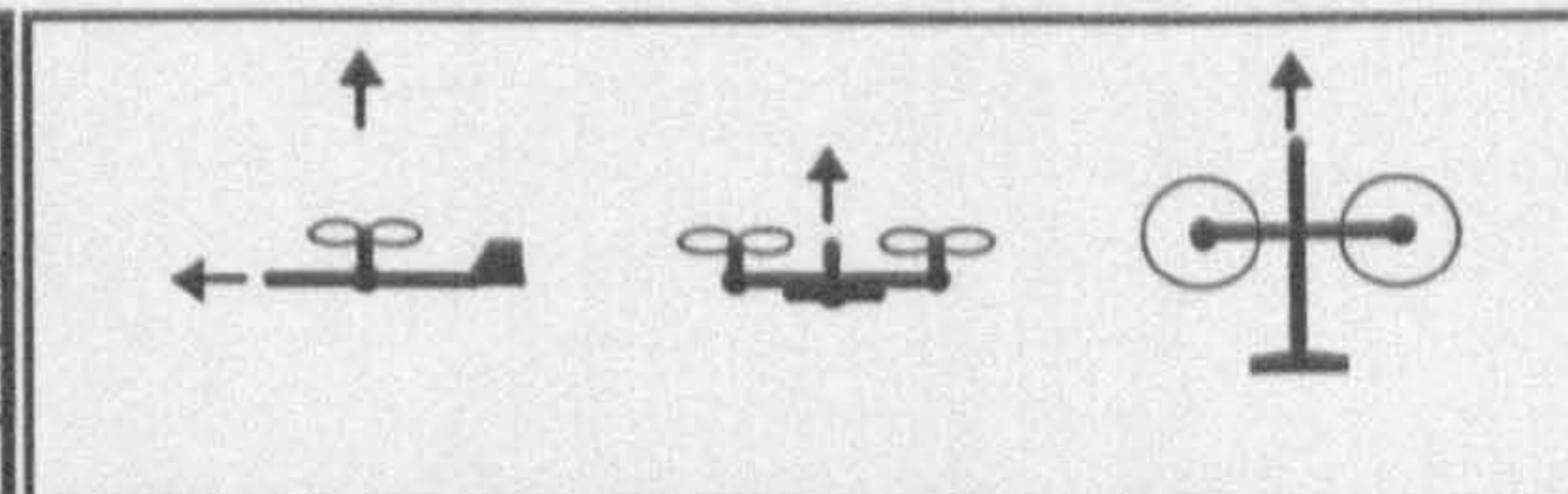


Fig.(7.18): Vehicle projectile like dynamics, Test 12

Uic=10.0	PSlic=0.0	THnicrd=90.0	Tstop=4.0
Vic=0.0	THETAic=0.0	THnicld=90.0	Conf1=0.0
Wic=-10.0	PHlic=0.0	THndicrd=0.0	Gservo=1.0
Picd=0.0	NORTHic=0.0	THndicld=0.0	THdmndr=-0.1
Qicd=0.0	EASTic=0.0	LOCK1r=1.0	THdmndl=-0.1
Ricd=0.0	HEIGHTic=10.	LOCK1l=1.0	Axes at c.g.
RPMrdcr=1	RPMrdcl=-1	RPMr=6000.0	RPMl=6000.0

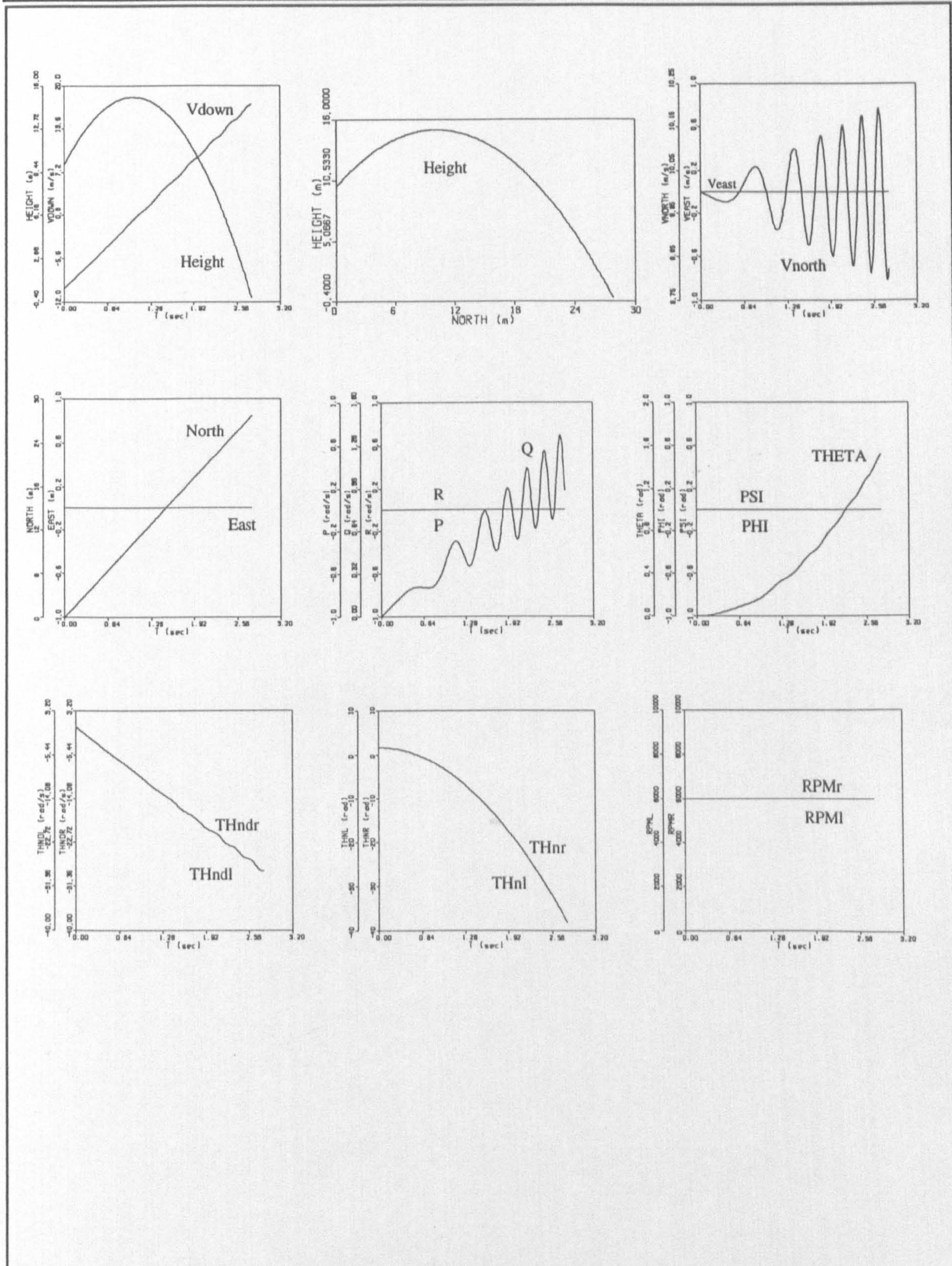
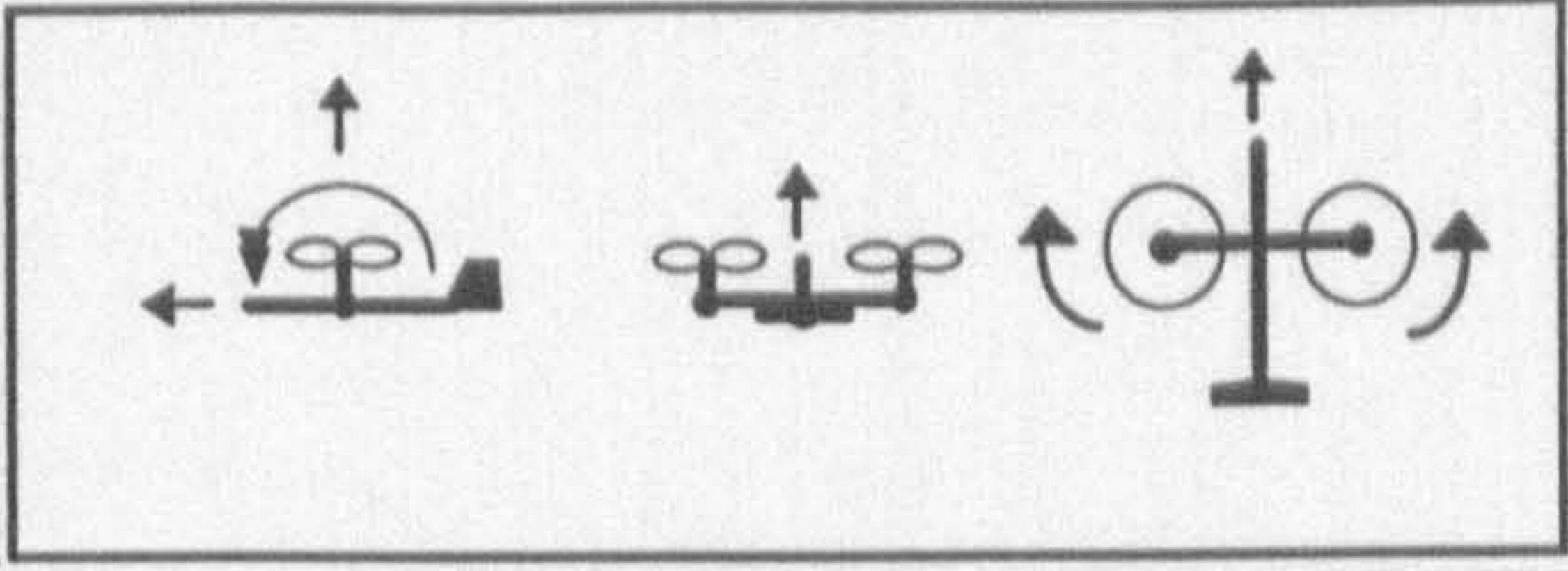


Fig.(7.19): Vehicle projectile like dynamics, Test 13

Uic=10.0	PSlic=0.0	THnicrd=90.0	Tstop=4.0
Vic=0.0	THETAic=0.0	THnicld=90.0	Confl=0.0
Wic=-10.0	PHlic=0.0	THndicrd=0.0	Gservo=1.0
Picd=0.0	NORTHic=0.0	THndicld=0.0	THdmndr=-0.1
Qicd=0.0	EASTic=0.0	LOCKlr=1.0	THdmndl=-0.1
Ricd=0.0	HEIGHTic=10.0	LOCKll=1.0	Axes at c.g.
RPMrdcr=1	RPMrdcl=1	RPMr=6000.0	RPMl=6000.0

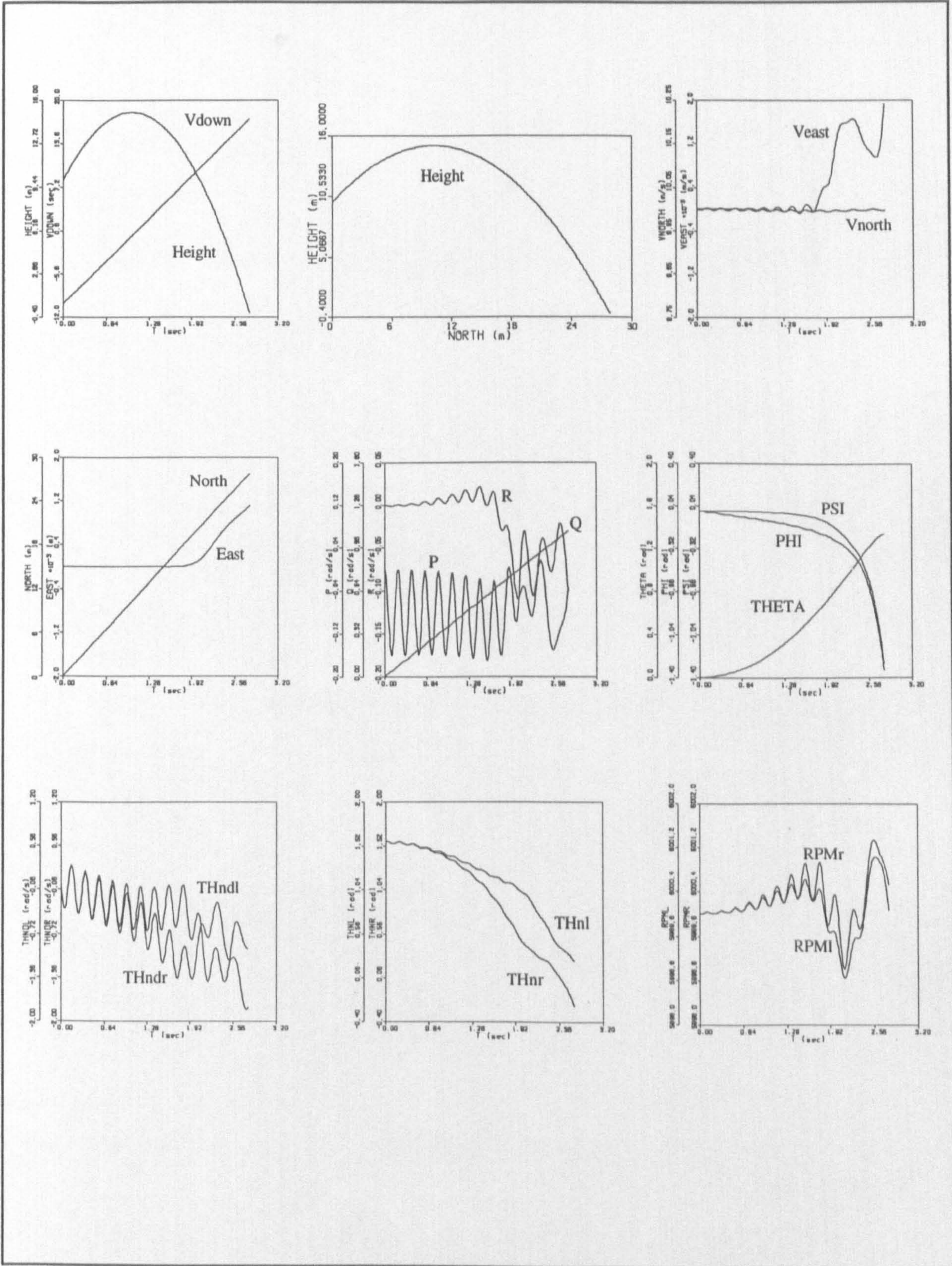
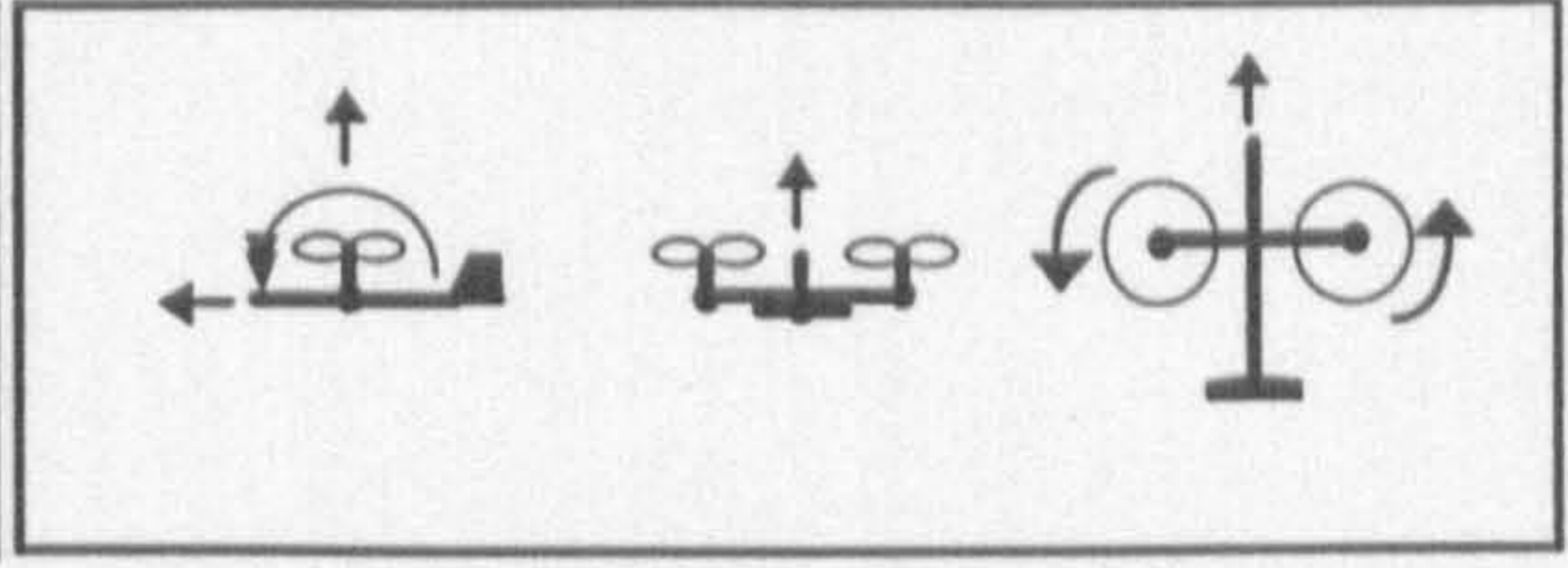
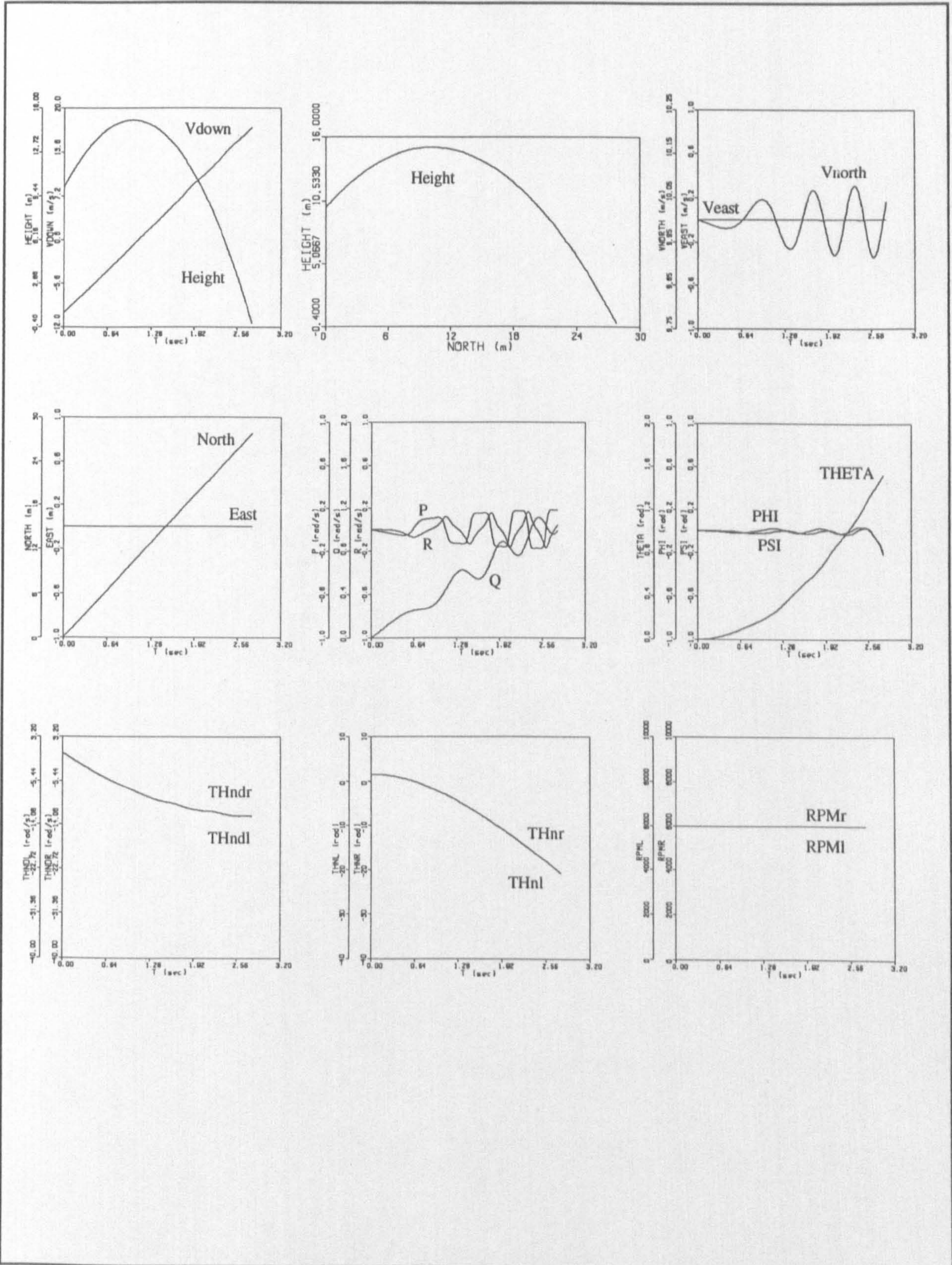
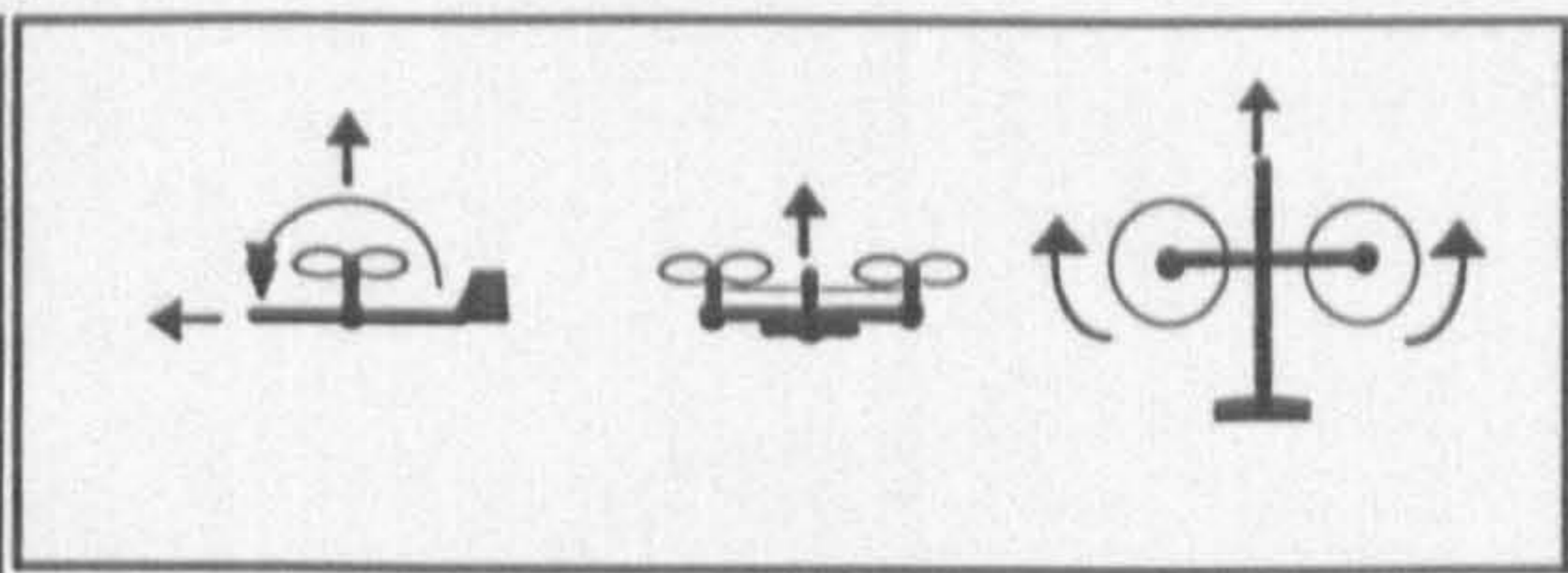


Fig.(7.20): Vehicle projectile like dynamics, Test 14

Uic=10.0	PSlic=0.0	THnicrd=90.0	Tstop=4.0
Vic=0.0	THETAic=0.0	THnicld=90.0	Conf1=1.0
Wic=-10.0	PHlic=0.0	THndicrd=0.0	Gservo=1.0
Picd=0.0	NORTHic=0.0	THndicld=0.0	THdmndr=-0.1
Qicd=0.0	EASTic=0.0	LOCK1r=1.0	THdmndl=-0.1
Ricd=0.0	HEIGHTic=10.	LOCK1l=1.0	Axes at c.g.
RPMrdcr=1	RPMrdcl=-1	RPMr=6000.0	RPMl=6000.0



confirm that the interaction between sub-systems had been appropriately established. Similar to previous case, test stubs were used to replace the rest of sub-systems. The airframe aerodynamic forces and moments, feedback gain and slipstream influence codes were substituted by zero and a constant value was considered for engine power.

In the third step, the sub-system *Engine* was integrated. Similarly, its single module had been tested previously, therefore, only interaction between sub-systems was tested.

The sub-system *Slipstream Effect Checking* was then integrated. Using different combination of tilt angles and velocity components as initial conditions, a variety of the propellers slipstream directions were produced and checking was performed to test whether the program could correctly specify the affected components or not. All tests were successfully passed.

The correctness of the airframe aerodynamic modules had been proved previously in module testing. Therefore, in the next step they were gathered and integrated into the program. Tests were then carried out by giving different velocity components and comparing the calculated forces and moments associated with the individual elements with those were obtained manually.

In the final step of integration testing, the sub-system *Flight control system* was activated by using some typical non-zero gain matrices associated with different combinations of states and controllers. No anomalies have been found.

7.5.6 User Testing

A series of extensive and comprehensive tests have been accomplished during the two last testing activities. The program is now supposed to be free of any anomalies. However, from the operation point of view there is one more testing stage which should be carried out before the program is really accepted for practical use. This stage is called user testing or acceptance testing. Acceptance testing often reveals those system drawbacks that are associated with the anticipated performance and functionality.

In the present work, this part of the testing process has been combined in the process of the credibility investigation which will be carried out in the following chapter by producing some convincing simulation results.

CHAPTER EIGHT SIMULATION RESULTS

8.1 INTRODUCTION

In the previous chapters, a great deal of emphasis on the mathematical modelling and computer programming have been placed. A computer model was developed, and the internal verification criteria were then applied to confirm its internal consistency and algorithmic validity. In this chapter, it is intended to assess the suitability and accuracy of the model in the context of its intended application, the procedure which was defined as external validation in Chapter 2. This stage is categorised as acceptance testing in terms of the testing process described in Chapter 7.

In this acceptance testing, the primary aim is to show the validity of the simulation model in terms of its capabilities to provide a series of reasonable and explainable simulation results for the considered VTOL configurations. In addition, it is shown that the simulation model is sufficiently flexible and applicable to play its role as a research tool to be used for a wide spectrum of the intended applications including initial sizing, performance limitation studies, estimation of the stability derivatives, aircraft trimming, stability and control investigations such as eigenvalue and eigenvector analysis, stability augmentation and autopilot design. Moreover, it is shown that the simulation model is able to predict the aircraft behaviour correctly and has the potential for hypothesis testing, explanation and discovery. However, it should be noted that it is not primarily

aimed to get involved with the synthesis or even analysis of the aircraft dynamics or propose changes in the aircraft estimated parameters for better functionality, although it is not entirely avoided. As will be seen, whenever needed, sufficient description of the aircraft behaviour is provided.

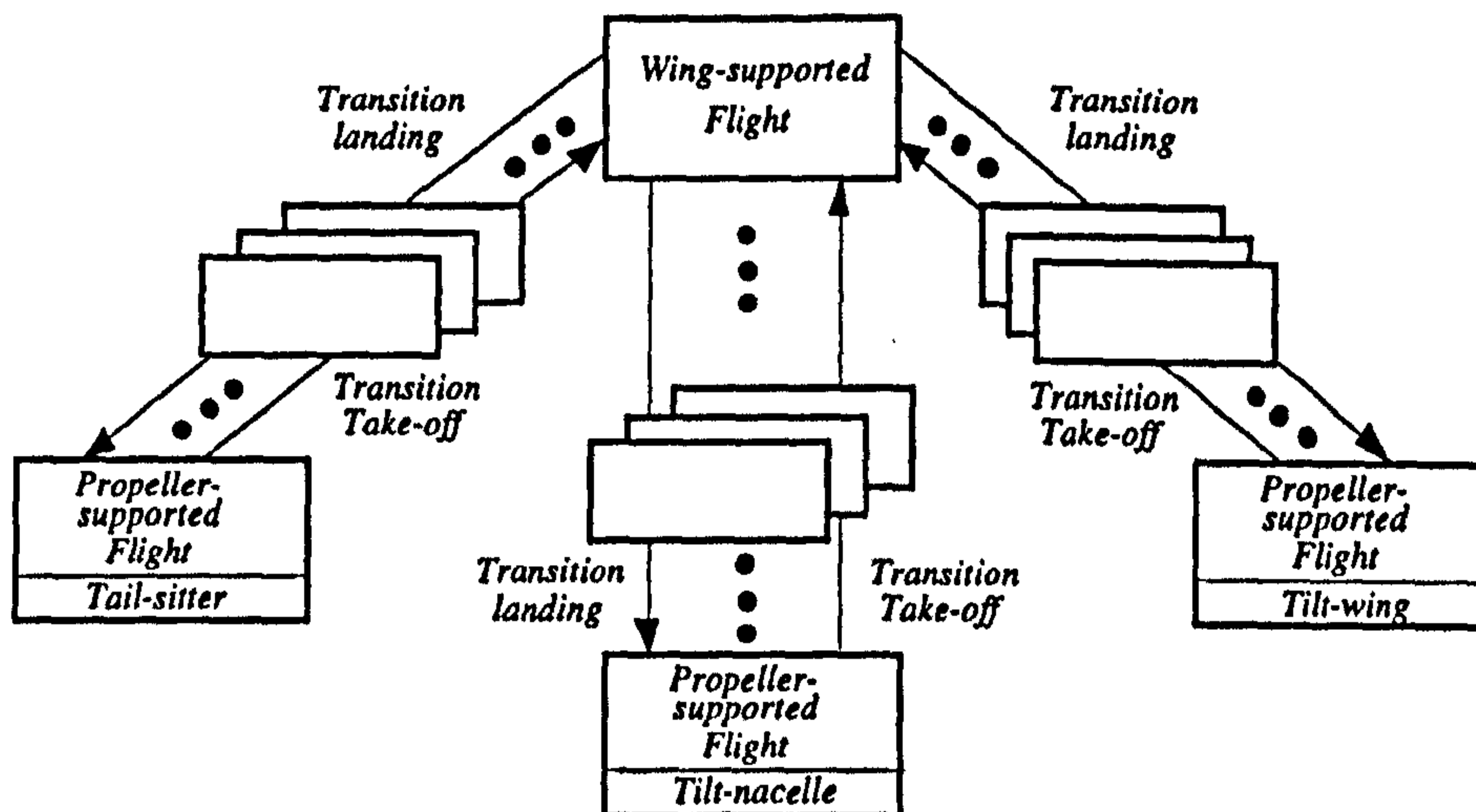
In addition, the empirical validity, in the form of the degree of agreement between the behaviour of the model and the real system is not possible in this work, simply because there is no real system. However, there are some fundamental characteristics associated with the flight of such a combination of airfoils, bodies, propellers and engines in various flight conditions which are expected to be observed. These characteristics are considered as the criteria to be satisfied for empirical validity.

8.2 RESULT PRODUCING STRATEGY

Due to the generality and flexibility aspects of the simulation program, numerous simulation results may be presented for the three considered aircraft configurations at different flight regimes. Figure 8.1 provides an idea about the range of the flight conditions that may be investigated. As shown in this figure, a complete investigation of the aircraft dynamics involves many different cases. However, regardless of the flight condition, an almost similar procedure is applied in order to investigate the aircraft dynamics. Therefore, only a selection of the simulation results seems to be sufficient to satisfy the objectives of this chapter.

As shown in Figure 8.1, the flight envelope of the considered VTOL configurations can be divided into three main flight phases, including the Wing-supported flight (cruising), the Propeller-supported flight (hovering) and Transition in which the flight is supported by a combination of the lift forces generated by the propellers and wings. Whether a VTOL aircraft can successfully accomplish the transition process or not, it is expected to be able to fly in two extreme ends of its flight envelope, i.e. wing-supported flight and propeller-supported flight. For these flight phases, there are some known behaviour of the conventional vehicles such as fixed-wing aircraft and helicopters which can be used for the validation purposes. Therefore, in the following sections, the wing-supported flight as a common flight phase and the propeller-supported flight phase of each aircraft

Fig.(8.1): Different flight conditions of the VTOL aircraft



configuration are considered, and the selected simulation results which covers aircraft trimming, aircraft modes and aircraft control are presented.

8.3 FINAL CONSIDERATIONS

In Chapter 6, some values were estimated for the aircraft dimensions in terms of the available engine and propeller data, and baseline configuration. There are still three angles about which decision must be made based on the aircraft trim conditions in level horizontal wing-supported flight. These are the wing and horizontal stabiliser incidence angles λ_{wa} , λ_{ha} and the angle between each nacelle and its associated wing λ_{nw} .

In a level horizontal flight, sufficient lift is supposed to be generated by the wing to support the aircraft weight. Assuming a zero angle of attack, the generated lift force depends on three factors, wing area, aircraft forward velocity and wing lift coefficient (consequently, wing incidence angle). Since it is desirable to keep the previously fixed value of the aircraft wing area unchanged (Chapter 6), only the aircraft velocity and wing lift coefficient must be finalised.

In general, an increase in lift coefficient results in a decrease in the lowest achievable aircraft speed for a trimmed level horizontal flight. Therefore, to keep the aircraft velocity reasonably low, that is expected for the class of the light unmanned aircraft, it is decided to choose the highest possible lift coefficient. However, it is also necessary to define a safety margin to prevent wing stalling which, in this case, occurs at $C_{L_{max}} = 1.3$. Regarding these facts, the value of $C_L = 1.0$ is finally considered which corresponds to the aircraft velocity of approximately 50.0 m/s and wing incidence angle $\lambda_{wa} = 10.0$ deg.

This wing incidence angle is relatively large in comparison with that of the conventional aircraft. However, it should be noted that for these aircraft, wings are sized in terms of the minimum velocity for a conventional take off and landing. Therefore, they are relatively larger and a smaller wing incidence angle is possible. In addition, as mentioned in Chapter 6, it should not be forgotten that the selected airfoil section may not be a perfect choice in our case.

Having finalised the wing incidence to make an equilibrium condition in vertical direction, the next step is to obtain equilibrium in pitching motion. This can be carried out by calculating an appropriate horizontal tail incidence angle in order to obtain a zero total pitching moment. Using simulation program, this was achieved by giving the horizontal tail a positive incidence of $\lambda_{ha} = 0.427$ deg. As it might be noticed, λ_{ha} is a very small angle. This is due to the fact that the pitching moments generated by thrust and lift forces about aircraft c.g. are small. Therefore, a small upward force in horizontal tail is sufficient to balance the total pitching moment.

Finally, regarding that the wing incidence angle has been fixed on 10.0 deg. , an nacelle-wing angle of $\lambda_{nw} = 10.0$ deg. is automatically considered in order to keep the directions of the thrust lines parallel to the aircraft longitudinal axis in level horizontal wing-supported flight.

8.4 WING-SUPPORTED FLIGHT

In this section, the results obtained from the simulation studies of the aircraft dynamics during a conventional level straight horizontal non-sideslipping wing-supported flight are presented. This flight condition can be defined in terms of the following state variables.

$$\begin{array}{llll}
 U = \text{Const.} & P = 0.0 & \theta = 0.0 & \\
 V = 0.0 & Q = 0.0 & \psi = 0.0 & {}^rN = \text{Const.} \\
 W = 0.0 & R = 0.0 & \varphi = 0.0 & {}^lN = \text{Const.}
 \end{array} \quad (8.1)$$

It can be seen that the overall angle of attack ($\tan^{-1}(W/U)$) is considered to be zero. This implies that the weight of the aircraft is supported only by the lift force generated by the wing. This lift force is directly related to the wing incidence angle (λ_{wa}) which was selected to be 10.0 deg. as mentioned earlier.

Steady-state Trimmed Flight

The simulation program was used to find the set of the non-zero state variables and control inputs for the aircraft in the trimmed flight condition. The aircraft is said to be trimmed when all forces are in balance and there is no resultant moment about any axis.

In other words, it flies in a steady-state condition where all acceleration components are zero:

$$\dot{U}, \dot{V}, \dot{W}, \dot{P}, \dot{Q}, \dot{R}, {}^* \dot{N}, {}^l \dot{N} = 0.0 \quad (8.2)$$

The tilting parts were set in *Locked* position at zero tilt-angle and the aircraft altitude at 10.0 m. The contra-rotating propeller option was selected. The lateral trim was then easily obtained by setting the aileron and rudder at their zero value position and giving the same value to the engine throttles at right and left. However, for longitudinal trim, a process of trial and error was followed by successively running the program at $t=0.0$, trying to drive the heave acceleration (\dot{W}), the forward acceleration (\dot{U}), the propeller rotational accelerations (${}^* \dot{N}$) and pitch acceleration (\dot{Q}) to zero.

In this process, the forward velocity (U) was used to control (\dot{W}). Any change in forward velocity produces a direct change in lift which ultimately results in a change in heave acceleration. Similarly, the forward acceleration (\dot{U}) was controlled by the propeller rotational speeds (${}^* N$). Any change in ${}^* N$ will change the amount of the thrust delivered by the propellers and, consequently, changes the forward acceleration. To control each of the propeller rotational acceleration (${}^* \dot{N}$), its associated engine throttle (${}^* \delta_e$) were used. The engine throttle has a direct influence on the engine output power and torque, and ultimately on the propeller rotational acceleration. For the pitch acceleration (\dot{Q}), as explained in previous section, it was preferred to keep the elevator angle at its zero position, and instead using the horizontal tail incidence angle (λ_{ha}) to drive \dot{Q} to zero. Clearly, changing in (λ_{ha}) will produce a direct change in total pitching moment and consequently in \dot{Q} .

The following values were eventually obtained for the forward velocity, the engine rpms and the throttle settings in the trim condition:

$$\begin{aligned} U &= 49.2787 \text{ m/s} \\ {}^* RPM &= 6108.22 \\ {}^* \delta_e &= 0.167435 \end{aligned} \quad (8.3)$$

It should be pointed out that there is a trim command in ACSL which can be used to find the trim condition of the system. However, since, in our case, this command did not provide satisfactory results, the previously mentioned procedure was undertaken.

Flight Simulation

Using the obtained trim values, the aircraft was then initially set to trimmed flight condition and simulation was carried out for a short and a long period of time. The time histories of the state variables corresponding to the aircraft longitudinal motion are shown in Figures 8.2, 8.3.

As shown in these figures, since the trim condition is not numerically perfect, oscillation in longitudinal variables is observed before the aircraft obtains a new steady-state condition. Two types of motion are demonstrated by the aircraft. The first one is a small damping short period motion manifested in pitch rate and heave velocity. The second one is a moderate damping long-period motion in which all variables are involved. These motions resemble the natural modes of a fixed-wing aircraft known as short-period and phugoid modes. [44,75-83]

Simulated Response to an Elevator Pulse

For better demonstration of these modes, it was intended to excite each mode by using an appropriate input. The short-period motion can be excited by elevator input. Therefore, an elevator doublet pulse, with the value of 2.0 deg. from 0.0 to 0.5 sec. and -2.0 deg. from 0.5 to 1.0 sec. was applied to the trimmed aircraft and simulation was carried out for 5.0 sec. As expected, this input did not affect the lateral-directional states. However, as shown in Figure 8.4, all the longitudinal states are affected. As seen in this figure, the aircraft velocity has approximately remained constant and oscillations in pitch rate, pitch angle and heave velocity are quickly damped. The figure shows that pitch angle and heave velocity vary in unison. It reveals that there is only a small change in flight-path angle. These all are the short-period motion characteristics of an aircraft.

Fig.(8.2): Simulated aircraft in trimmed wing-supported flight-Short time

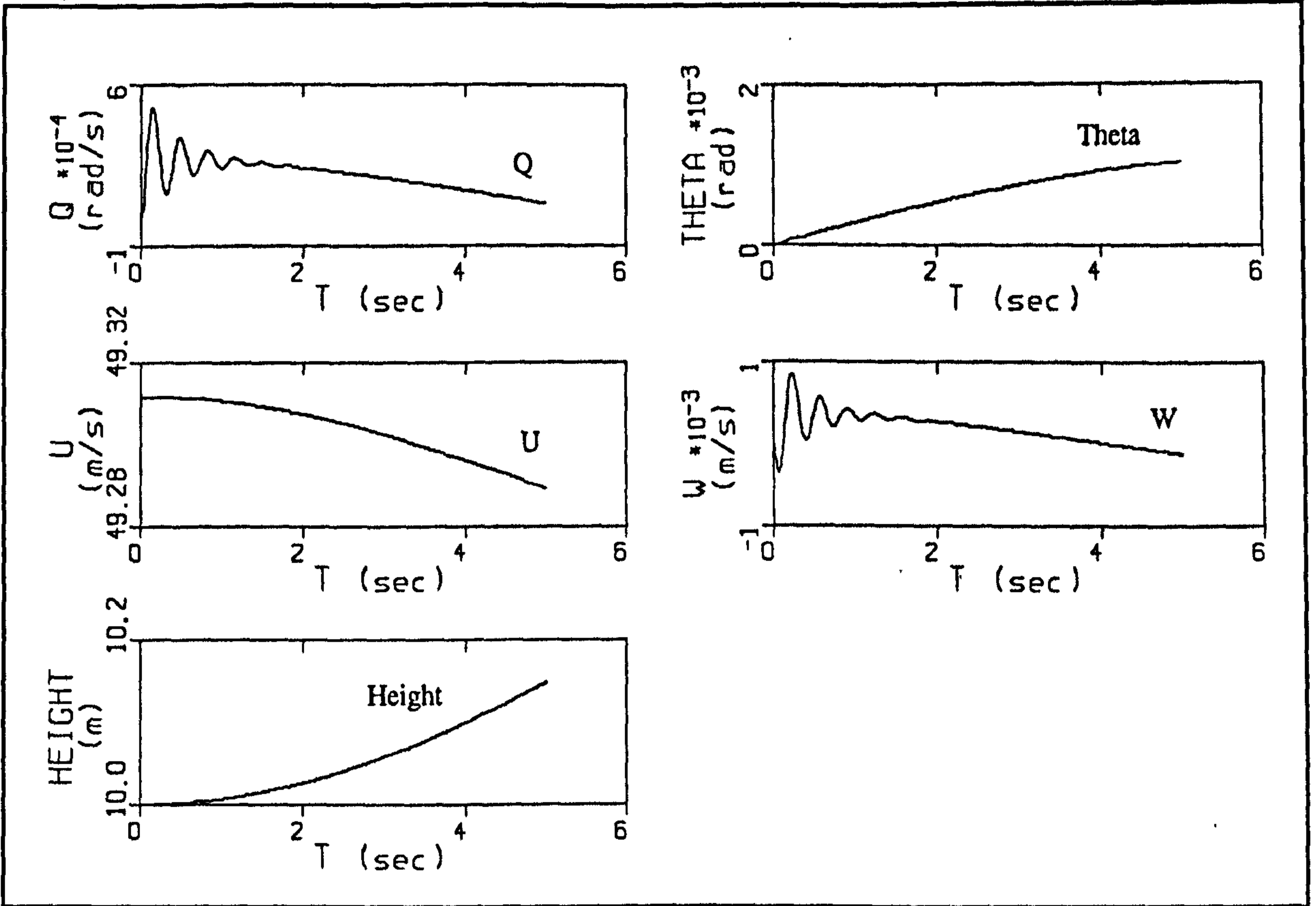
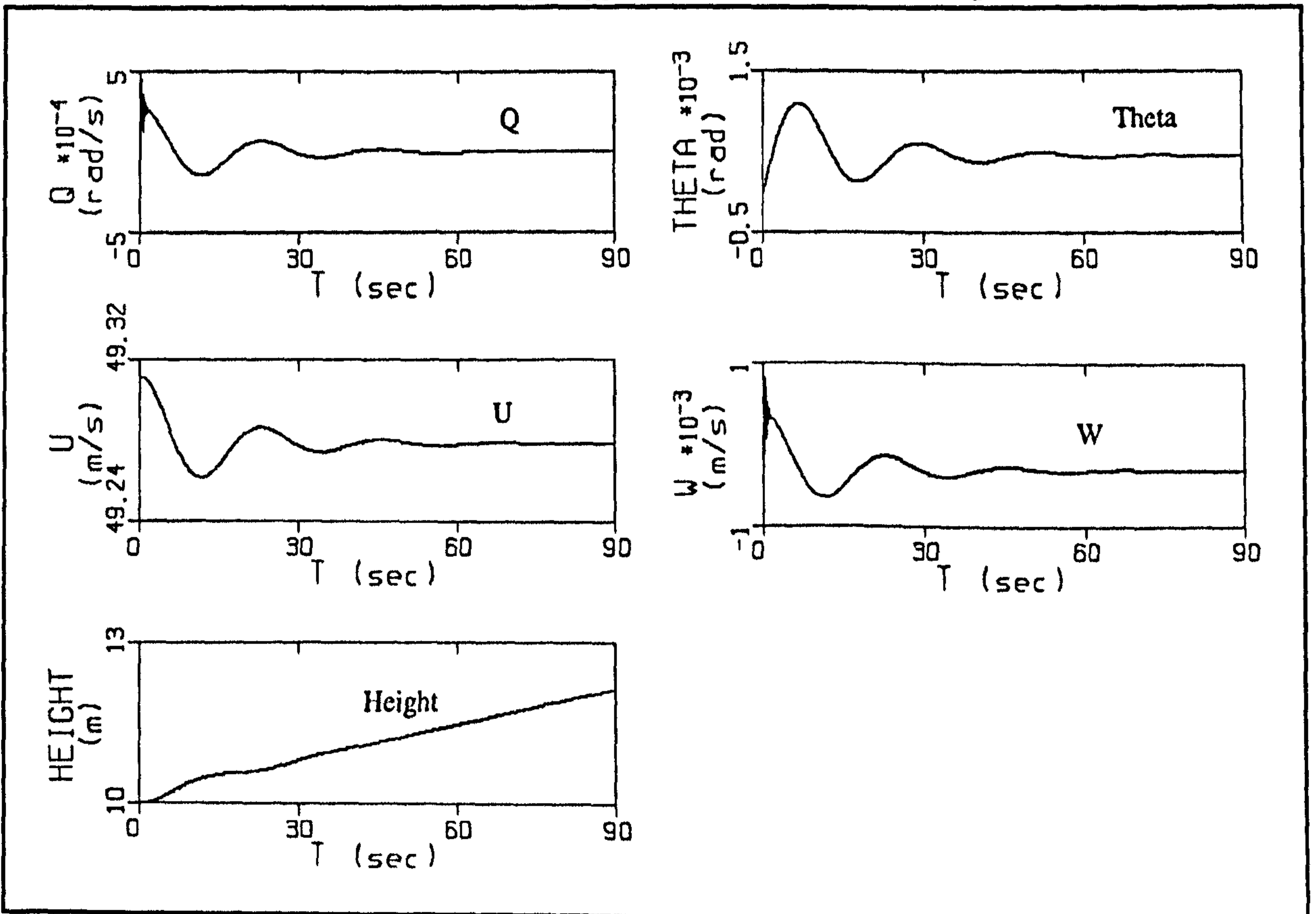


Fig.(8.3): Simulated aircraft in wing-supported trimmed flight-Long time



Simulated Response to a Throttle Pulse

To excite the phugoid mode, the same trim condition was used and a doublet pulse on the steady-state throttle setting was superimposed. The doublet had the value of 0.1 from 0.0 to 2.0 sec. and -0.1 from 2.0 to 4.0 sec. Again, the lateral-directional dynamics was unaffected. Figure 8.5 shows the longitudinal responses where the pitch rate has a small variation and the heave velocity (consequently the angle of attack) is barely affected, but pitch attitude exhibits a very lightly damped oscillation with a long period. Therefore, the flight-path angle changes in phase with pitch attitude. The forward velocity also varies. This is phugoid mode which involves an interchange of potential and kinetic energy as the aircraft climbs and slows down, and then dives and speeds up [44]. The result is a damped sinusoidal flight-path about the datum height, as shown in Figure 8.5. Since the thrust vectors do not exactly pass through the c.g. , the throttle pulse has also excited the short-period mode which is damped too quickly to be clearly seen in Figure 8.5.

Linearisation of the Nonlinear Model

The equations of motion of a rigid-aircraft can be split into two uncoupled sets under the conditions of small perturbations from steady-state wing-level non-sideslipping flight [44]. These are the longitudinal equations that involve the variables forward velocity, heave velocity, pitch attitude, and pitch rate, and lateral-directional equations that involve sideslip velocity, bank angle, and roll & yaw rates.

Using the simulation program and the existing Jacobian command in ACSL, it was intended to demonstrate such a decoupling. Having applied the Jacobian command and by inspection the derived Jacobian matrices, it was found that the position states Height, North, East and the orientation state ψ have no coupling with the other states. Therefore, they were frozen and the new Jacobian matrices were obtained and reordered as shown in Figure 8.6.

The A and B matrices are partitioned in order to separate the longitudinal and lateral states and controls. As it can be seen in Figure 8.6, the expected decoupling between the longitudinal and the lateral motion is observed, although there are specific couplings between both $'N$ and $'N$ with the other state variables. Apart from this fact, it is

Fig.(8.4): The excited short-period mode

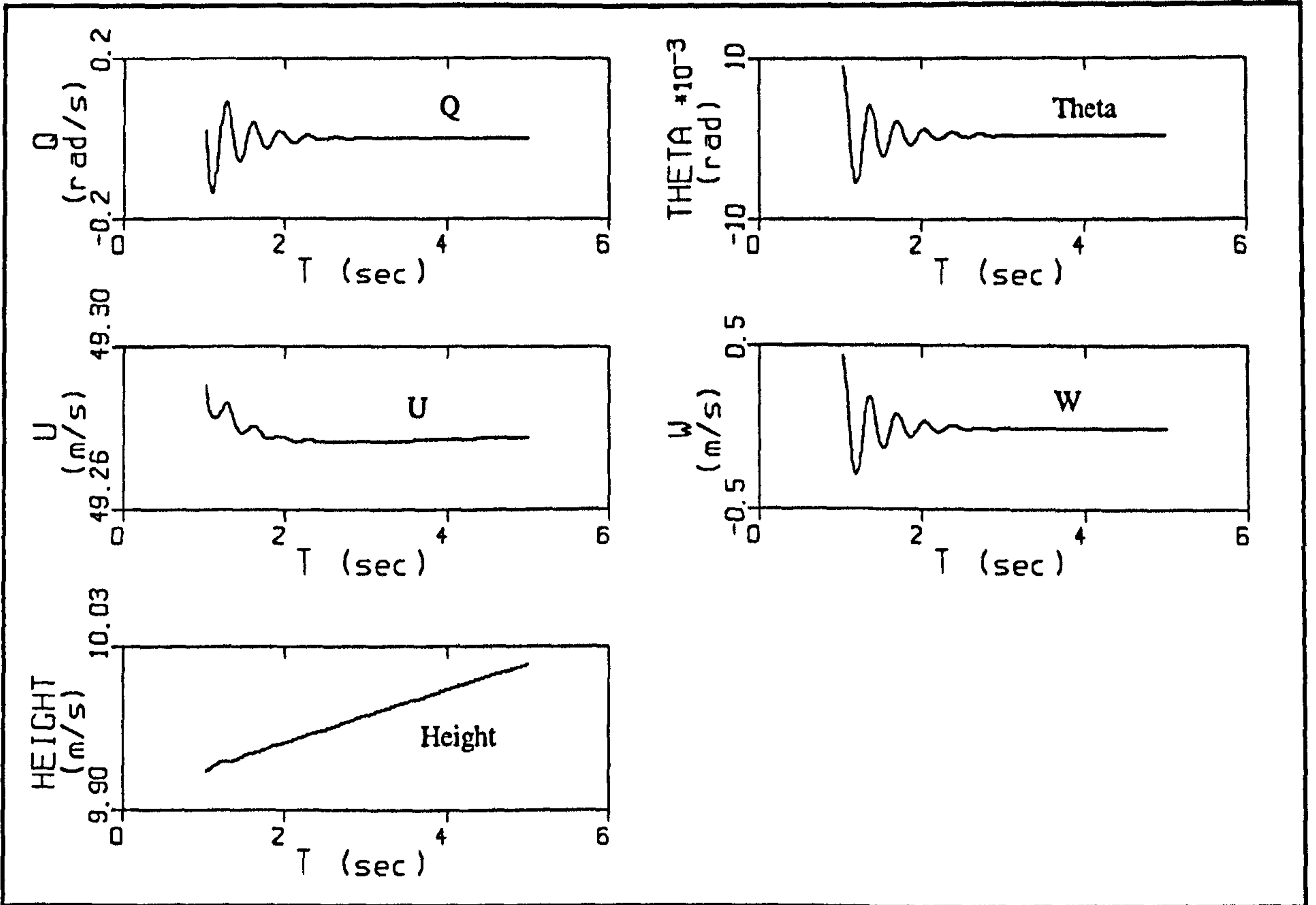
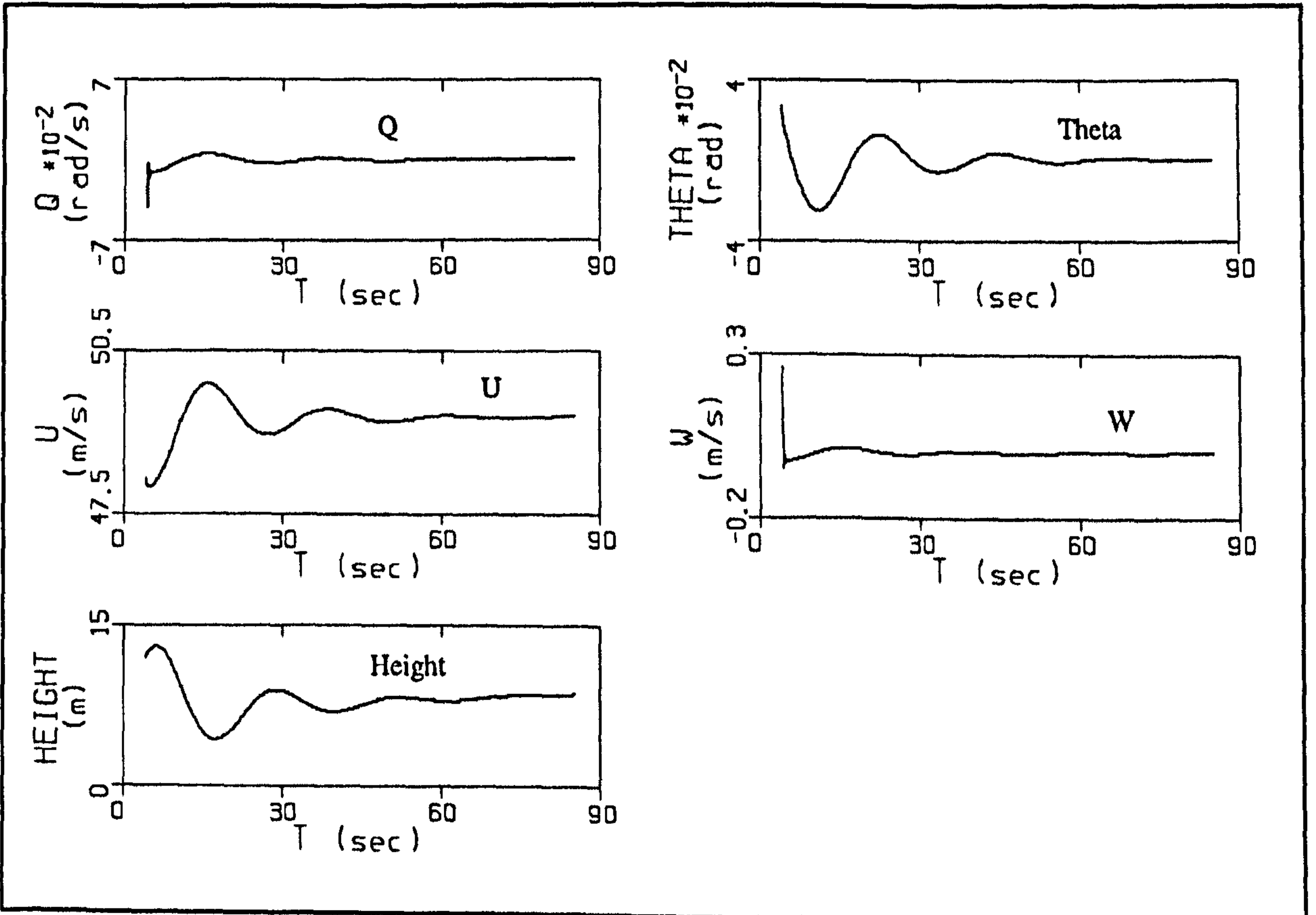


Fig.(8.5): The excited phugoid mode



evident that the expected decoupling between longitudinal and lateral motion does indeed exist. The other expected feature is the appearance of the value of the gravitational acceleration in $A(3,1)$, indicating the change in X-force with respect to θ which should be equal to the gravitational acceleration, [77].

It might be noticed that in matrix B, the longitudinal states are affected by the wing control surfaces, and lateral states by the horizontal stabiliser control surfaces. This is due to the fact that in the present simulation model each control surface is considered as an individual control input. To form the conventional control inputs, i.e. , elevator, rudder and aileron the following constraints must be applied.

$$\begin{aligned}\delta_{wr} &= -\delta_{wl} \\ \delta_{hr} &= \delta_{hl} \\ \delta_{vu} &= \delta_{vl}\end{aligned}\tag{8.4}$$

In matrix B, the coefficients of δ_{wr} and δ_{wl} related to the longitudinal states are equal, and the coefficients of δ_{hr} and δ_{hl} related to the lateral states are equal with opposite sign. Regarding these facts, it is obvious that by imposing the above constraints, (the conventional control surfaces are formed), the effect of δ_w (aileron) on longitudinal motion and δ_h (elevator) on lateral motion will be vanished which, of course, is expected for a conventional aircraft.

Modal Decomposition Applied to the Aircraft Dynamics

Earlier in this section, the classical phugoid and short-period modes of the aircraft in the considered trim condition were illustrated by nonlinear simulation. The complete set of the aircraft modes will now be illustrated by modal decomposition using the linear model derived earlier and shown in Figure 8.6. If propeller states $'N$ and $'N$ are left in matrix A, they will produce two almost equal eigenvalues -12.6 and -12.9. Freezing these states does not considerably affect the basic aircraft modes. As discussed earlier, there is a clear decoupling of the lateral and longitudinal dynamics, therefore the modal decomposition will be demonstrated using two separate reduced order Jacobian matrices.

Longitudinal Modes

The longitudinal dynamics Jacobian matrix is located in the top-left part of the A matrix in Figure 8.6. Selecting the longitudinal states, the ACSL Eigenvalue and Eigenvector commands were then used to produce the results shown in Table 8.1.

As shown in Table 8.1, four longitudinal states give rise to two complex-conjugate pairs of eigenvalues, which correspond to two stable oscillatory modes. The periods of these modes are separated by more than one order of magnitude. Therefore, they are easily identifiable as the short-period and phugoid modes. The periods are also in reasonable agreement with the results of nonlinear simulation, shown in Figures 8.2, 8.3. The corresponding eigenvectors are also given in Table 8.1. As expected, the eigenvectors of short-period mode are dominated by the elements corresponding to pitch rate and heave velocity. These elements are involved relatively weakly in the phugoid mode. The dominant element in the eigenvectors of the phugoid mode is the one corresponding to the forward velocity. These results agree with the conclusion drawn from the nonlinear simulation and general characteristics of an aircraft longitudinal modes.

Lateral-Directional Modes

The Jacobian matrix for the lateral-directional dynamics is shown in the bottom-right part of the A matrix in Figure 8.6. Two real eigenvalues and a complex-conjugate pair associated with lateral-directional motion are given in Table 8.2.

The oscillatory mode involves the yaw rate and sideslip velocity, and produces some bank angle and roll rate effects. This rolling and yawing motion is called Dutch-Roll mode. The eigenvalues show that the Dutch roll period is quite short and the oscillation is very slightly damped.

The second mode is simply a stable exponential mode which involves mostly roll rate. This mode is known as the Roll subsidence. The time constant of $T=0.302$ s associated with this mode indicates a fast roll response.

The third mode is a slightly unstable exponential mode. It is distinguished by a much larger time constant $T=22.03$ s. It involves more bank angle and yaw rate than the roll mode and is known as Spiral mode. The spiral modes of many real aircraft are also slightly unstable.

Altitude Hold Autopilot

In Figure 8.2 and 8.3, it might be noticed that even in trim condition, the aircraft slowly drifts in altitude since trim condition is never perfect. To hold altitude, an altitude hold autopilot must be designed. Therefore, the linearised system matrices A, B, C, and D were found, using all the longitudinal states plus altitude as the fifth state, and horizontal stabiliser control surfaces as inputs. A feedback gain matrix and associated closed-loop eigenvalues were then obtained by using the LQR command in MATLAB with $Q=[I]$ and $R=[I]$ [69], shown in Figure 8.7.

The simulation of the control system with the nonlinear aircraft dynamics which is an essential part of the complete control design process was also performed. Figure 8.8 shows the results obtained from the nonlinear simulation with feedback control system. As shown in this figure, under the control system action, the aircraft initially moves to a steady-state condition with a constant height at approximately $t=4.0$ sec. However, since the selected controllers (δ_{hr}, δ_{hl}) have no direct effect on the forward velocity, this variable is gradually increased, causing some increase in overall lift force and, consequently, a change in altitude at approximately $t=8.0$ sec.

In this simulation the lateral-directional dynamics were left uncontrolled. However, the lateral-directional motion remained unexcited for at least a long period of simulation time, since the lateral-directional states and inputs were accurately initialised with their steady-state values.

As shown in δ_{hr} vs t curve, the control system again starts to act to bring the altitude back to the constant value. By adding throttle inputs, a more precise altitude control can be achieved [52]. It should be noted that the feedback control has also changed the fast short-period oscillation to a smooth and gradually varying behaviour, as shown in Figure 8.8.

A step command on altitude at $t=10.0$ sec was then applied to the aircraft in order to change its height from 10.0 m to 11.0 m. The results are shown in Figure 8.9. As can be seen, some of the variables have a large overshoot at $t=10.0$ sec because of the

Table(8.1): The wing-supported flight longitudinal modes

	Short-priod mode	Phugoid mode
	-2.443+/-18.619 Freq.=18.778 rad/s Damp.=0.130 T=0.337 s	-0.189+/-0.235 Freq.=0.301 rad/s Damp.=0.626 T=26.74 s
Q	-0.307+/-0.179	-0.004-/+0.008
Th	-0.007-/+0.017	0.029+/-0.008
U	-0.006+/-9.98E-4	-0.359-/+0.930
W	-0.434-/+0.828	-0.0252-/+0.066

Table(8.2): The wing-supported flight lateral-directional modes

	Dutch roll mode	Roll mode	Spiral mode
	-1.569+/-15.164 Freq.=15.246 rad/s Damp.=0.102 T=0.414 s	-3.315 T=0.302 s	0.0454 T=22.03 s
P	0.0774-/+0.0633	0.955	0.044
Phi	-0.005-/+0.005	-0.288	0.974
R	-0.15+/-0.253	-0.060	0.193
V	-0.851-/+0.424	-0.031	0.107

Fig.(8.7): The gain matrix and closed-loop eigenvalues of the controlled aircraft in wing-supported flight

Gain matrix

-0.70710678	-1.2171582	-46.909505	-0.17157577	0.35435449
-0.70710678	-1.2171582	-46.909505	-0.17157577	0.35435449

Closed-loop eigenvalues

1. -0.2995
2. -0.7423+/- 0.7667 i
4. -34.0385+/-27.629 i

immediate action of the control inputs. In addition, δ_{hr} (also δ_{hl}) has initially reached to its minimum limit (-20.0 deg. = 0.349 rad.), and the aircraft altitude has finally settled down at approximately 11.0 m after ten seconds..

As a further check, the eigenvalues of the controlled system obtained from nonlinear model by Eigenvalue command in ACSL were compared with those derived by linear model in MATLAB. A very good agreement between these two sets confirmed the correct performance of the controller and aircraft.

8.5 PROPELLER-SUPPORTED FLIGHT

In this section, the results obtained from simulation studies of the aircraft dynamics during the propeller-supported flight condition for the three configurations Tail-sitter, Tilt-nacelle and Tilt-wing are presented.

8.5.1 Tail-sitter configuration

In terms of the state variables, the considered flight condition for the Tail-sitter configuration can be defined as follows.

$$\begin{array}{llll}
 U = 0.0 & P = 0.0 & \theta = \text{Const.} \approx 90.0 \text{ deg.} & {}^1N = \text{Const.} \\
 V = 0.0 & Q = 0.0 & \psi = 0.0 & {}^1N = \text{Const.} \\
 W = 0.0 & R = 0.0 & \varphi = 0.0 & \text{LOCK}_{r,l} = 0.0
 \end{array} \quad (8.5)$$

Steady-state Trimmed Flight

To find the steady-state flight condition, the aircraft altitude was initially set at 10.0 m. The tilting parts were fixed at zero tilt-angle and contra-rotating propeller option was selected. Normally, only wings are affected by the propellers' slipstream in this condition. Having set up the rudder and aileron at their zero value position and using the same value for both throttle settings, the lateral-directional trim had already been achieved. Similar to the previous case, a process of trial and error was then followed at $T=0.0$ s to find the longitudinal trim.

Fig.(8.8): Simulation of the controlled aircraft in wing-supported flight

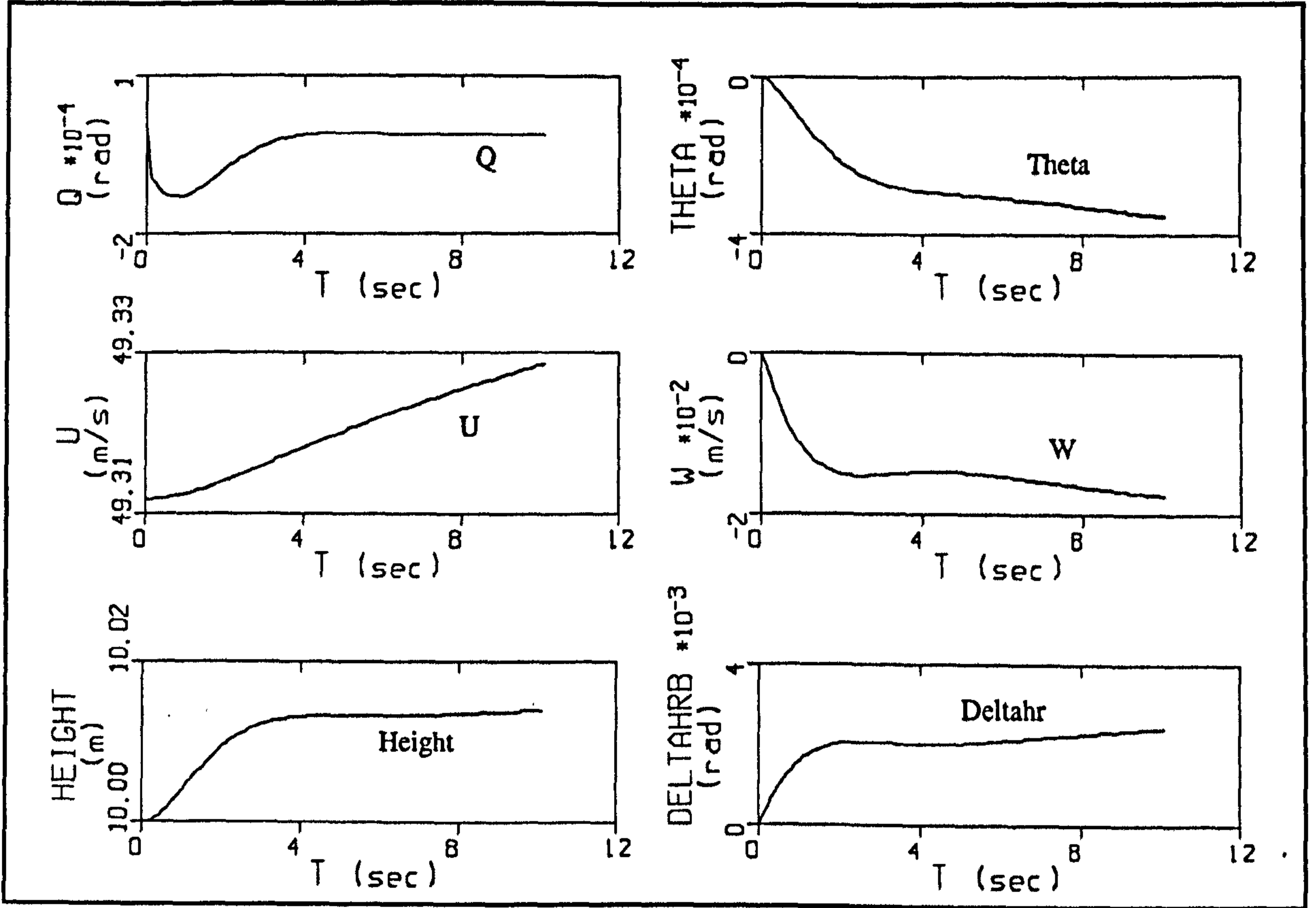
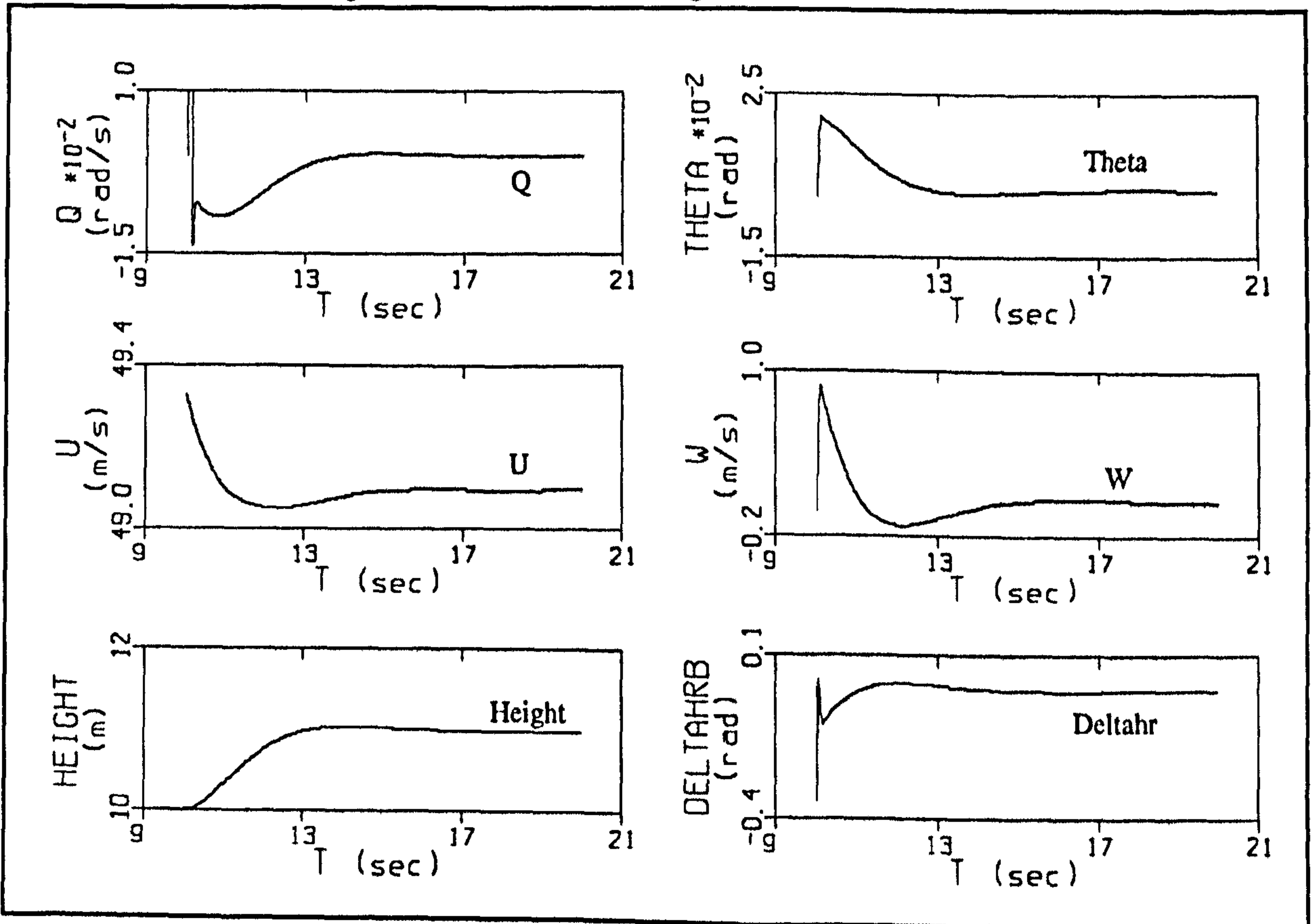


Fig.(8.9): Aircraft response to an altitude change command



In this process, the propeller rotational speeds (*N), the pitch attitude (θ) and the engine throttles (${}^*\delta_e$) were respectively used to drive the forward acceleration (\dot{U}), the heave acceleration (\dot{W}) and the propeller rotational accelerations (${}^*\dot{N}$) to zero. For the pitch acceleration, it was experienced that neither the wing control surfaces nor the horizontal stabiliser control surfaces (if, of course, they are artificially located in the propellers' slipstream by slightly increasing the slipstream diameter by using `Ksscon1`) can produce sufficient moment to balance the thrust force generated pitching moment.

The resultant thrust force is equal to the aircraft weight. This implies that even a small distance between thrust line and the aircraft c.g. may produce a considerable moment. Therefore, it was decided to slightly change the location of the joints in order to achieve a zero value for \dot{Q} . Having experienced this fact, it has been found that powerful control surfaces with high effectiveness value are necessary for a successful control of a Tail-sitter aircraft in hover.

The following values were eventually obtained for the location of the joints, the pitch altitude, the engine rpms and the throttle settings in trim condition.

$$\begin{aligned} {}^*d_z^a &= .0154 \text{ m} \\ \theta &= 85.8100005 \text{ deg} \\ {}^*\delta_e &= 0.703145 \\ {}^*RPM &= 6078.8 \end{aligned} \tag{8.6}$$

Flight Simulation

Using the obtained trim values, the aircraft simulation was then carried out for a few seconds. The time histories of some of the major variables are presented in Fig.(8.10). As seen in this figure, due to the accurate initialisation of the lateral-directional states with their steady-state values, a very small variation is observed in these states. However, in longitudinal motion an unstable oscillation with fairly long period is exhibited by the aircraft. This type of oscillation is very similar to what was reported by NACA for a vertically rising research model aircraft [84], shown in Figure 8.11, . In this figure, the variable Z is equivalent to the variable *North* in our case.

Aircraft Modes

By defining the following state and control vectors

$$\text{State vector: } [Q, \theta, U, W, 'N, 'N, P, \phi, R, V] \quad (8.7)$$

$$\text{Control vector: } [\delta_{wl}, \delta_{wr}, ' \delta_i, ' \delta_i]$$

the linearised system matrices were then obtained by using ACSL Jacobian command and are shown in Figure 8.12. In this figure, it is clearly shown that in constant propeller rotational speeds, the longitudinal and lateral motions are decoupled. The obtained eigenvalues of each separated longitudinal and lateral-directional dynamics are presented in Table 8.3.

The previously mentioned longitudinal oscillation resulted from nonlinear simulation is now well-confirmed by the obtained longitudinal unstable complex-conjugate eigenvalues which have the same period as that observed in nonlinear simulation. In addition, the same lateral-directional divergent oscillatory mode, as predicted in Table 8.3, was observed in nonlinear simulation when this mode was excited by giving some lateral-directional out of the trim initial conditions. However, it is not presented here. Again, similar lateral-directional oscillatory motion is reported in Reference [84].

It should be pointed out that two damped subsidence and a divergent oscillation in longitudinal and lateral-directional motions are the typical modes of helicopters during hover [53-56,83,85]. Therefore, the obtained results confirm the expected similarity between a Tail-sitter aircraft and a conventional helicopter.

Position Hold Autopilot

To enable the aircraft to maintain its position fixed in space a position hold autopilot was designed using the state and control vectors given in relation 8.7, and the LQR method. The simulation of the controlled aircraft was then carried out. The time histories of some of the variables are given in Figure 8.13. As it can be seen, the control system was able to stabilise the aircraft and hold its position (Height, North, East) after approximately 60.0 sec . However, the system had the tendency to be destabilised even with a small position change command, implying that the control system had a poor robustness characteristics. This can be justified by the fact that the wing control surfaces are too

Fig.(8.10): Propeller-supported, Tail-sitter, simulation in trimmed condition

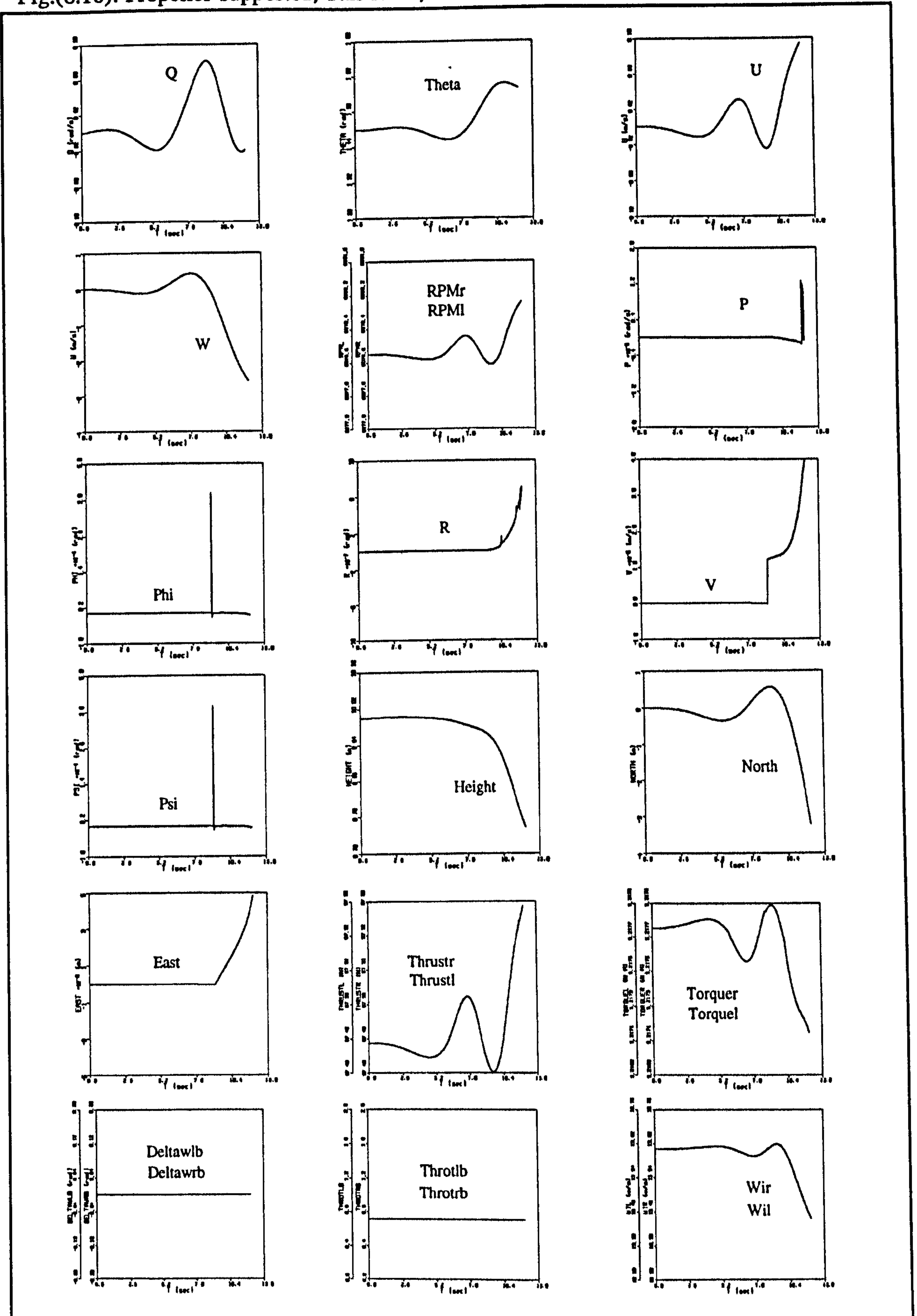


Fig.(8.11): Uncontrolled pitching motion of a vertically-rising model aircraft in hovering flight [84]

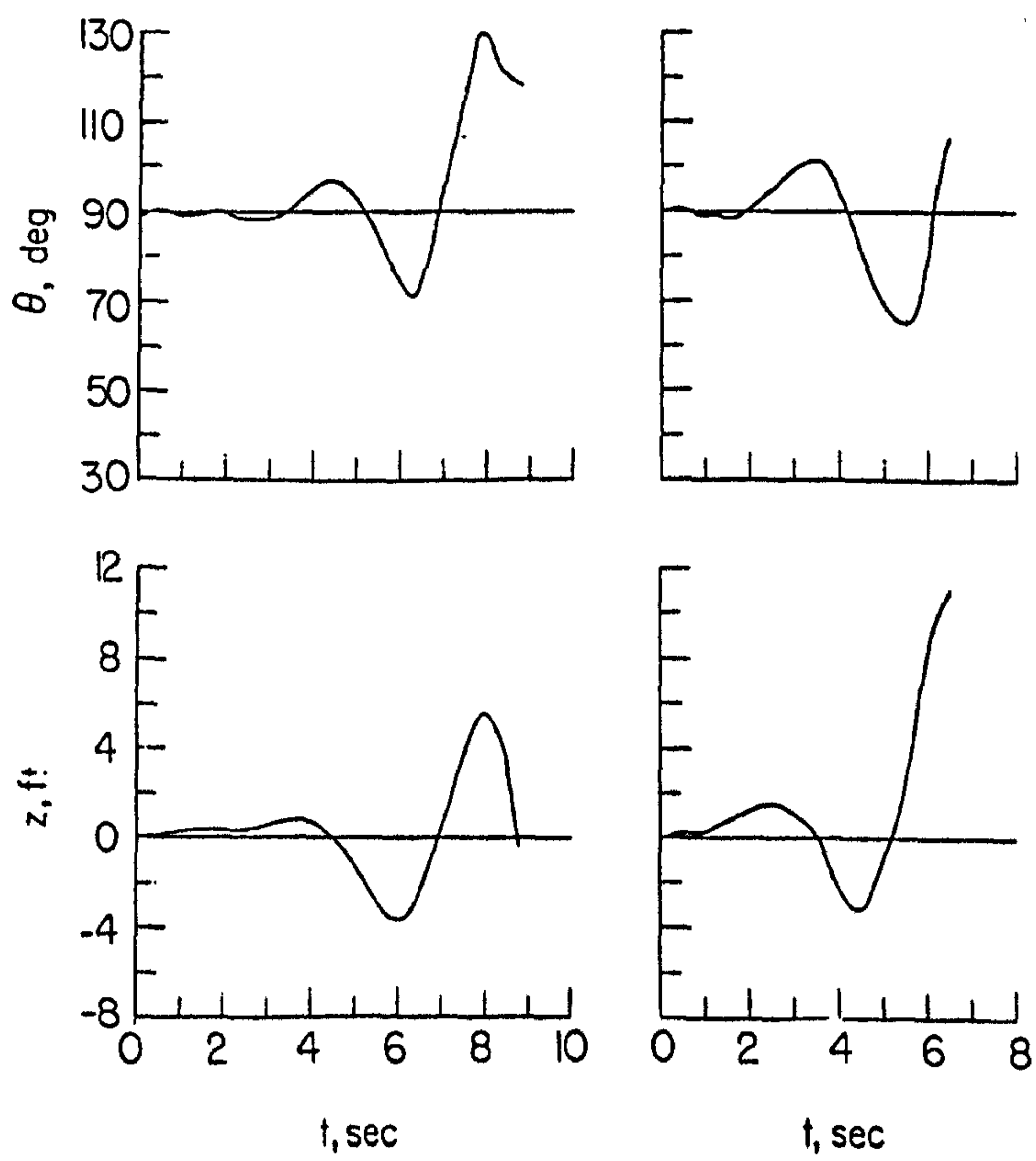


Fig.(8.12): The linearised system matrices for propeller-supported trimmed flight ,Tail-sitter configuration

Matrix A

	Q	Th	U	W	'N	'N	P	Phi	R	V
Qd	-0.003	-0.002	0.037	0.110	-3.455e-5	3.13e-5	3.143e-5	0.0	1.1e-4	0.0
Thd	1.0	0.0	0.0	0.0	0.0	0.0	0.0	0.0	0.0	0.0
Ud	1.620e-4	-0.714	-0.016	-0.023	-0.015	0.015	5.99e-5	0.0	-6.22e-5	0.0
Wd	0.004	-9.784	-0.104	-0.301	0.001	-0.001	2.422e-4	0.0	-2.411e-4	0.0
'Nd	-2.328e-6	-4.994e-5	-17.217	-0.008	-11.263	0.003	0.784	-7.654e-5	-6.895	3.519e-4
'Nd	-2.328e-6	-4.975e-5	17.221	-0.008	0.003	-11.263	0.784	-7.625e-5	-6.895	3.522e-4
Pd	2.328e-6	4.977e-5	-0.002	0.008	-0.003	-0.003	-0.784	7.622e-5	0.272	-3.521e-4
Phid	0.0	0.0	0.0	0.0	0.0	0.0	1.0	0.0	13.650	0.0
Rd	3.748e-4	0.008	-1.921e-4	-4.499e-4	-0.134	-0.134	0.0184	7.662e-7	-0.0149	-0.005
Vd	-2.778e-6	-5.936e-5	-3.125e-5	1.340e-4	9.512e-4	9.530e-4	-0.0127	0.717	0.003	-0.002

Matrix B

	throttlel	throttlr	deltawl	deltawr
Qd	0.0	0.0	0.113	0.113
Thd	0.0	0.0	0.0	0.0
Ud	0.0	0.0	-0.002	-0.002
Wd	0.0	0.0	-0.336	-0.336
'Nd	-1448.12	8.835	-4.411	4.410
'Nd	-8.835	-1448.12	-4.411	4.411
Pd	8.835	-8.835	4.411	-4.411
Phid	0.0	0.0	0.0	0.0
Rd	0.025	-0.020	0.001	-0.010
Vd	0.142	-0.142	0.071	-0.071

Matrix C

	Q	Th	U	W	'N	'N	P	Phi	R	V
Qd	1.0	0.0	0.0	0.0	0.0	0.0	0.0	0.0	0.0	0.0
Thd	0.0	1.0	0.0	0.0	0.0	0.0	0.0	0.0	0.0	0.0
Ud	0.0	0.0	1.0	0.0	0.0	0.0	0.0	0.0	0.0	0.0
Wd	0.0	0.0	0.0	1.0	0.0	0.0	0.0	0.0	0.0	0.0
'Nd	0.0	0.0	0.0	0.0	1.0	0.0	0.0	0.0	0.0	0.0
'Nd	0.0	0.0	0.0	0.0	0.0	1.0	0.0	0.0	0.0	0.0
Pd	0.0	0.0	0.0	0.0	0.0	0.0	1.0	0.0	0.0	0.0
Phid	0.0	0.0	0.0	0.0	0.0	0.0	0.0	1.0	0.0	0.0
Rd	0.0	0.0	0.0	0.0	0.0	0.0	0.0	0.0	1.0	0.0
Vd	0.0	0.0	0.0	0.0	0.0	0.0	0.0	0.0	0.0	1.0

Matrix D

	throttlel	throttlr	deltawl	deltawr
Qd	0.0	0.0	0.0	0.0
Thd	0.0	0.0	0.0	0.0
Ud	0.0	0.0	0.0	0.0
Wd	0.0	0.0	0.0	0.0
'Nd	0.0	0.0	0.0	0.0
'Nd	0.0	0.0	0.0	0.0
Pd	0.0	0.0	0.0	0.0
Phid	0.0	0.0	0.0	0.0
Rd	0.0	0.0	0.0	0.0
Vd	0.0	0.0	0.0	0.0

close to the aircraft c.g., therefore they can only generate a very small controlling moment. This moment was enough to stabilise the aircraft at its trim condition, but it was not enough to sustain the stability after a large disturbing command such as a command for changing its position. This was confirmed when the horizontal stabiliser control surfaces which can produce bigger moments were added as control inputs. The simulation results of the new system are given in Figure 8.14. As expected, the new control system has better characteristics. As can be seen in Figure 8.14, the aircraft has reached the steady-state condition in a fixed position in shorter time. A command was then applied in order to change the aircraft position by one meter in each direction. As shown in Figure 8.15, after an initial overshooting the aircraft has finally taken its new position at $t=90.0$ sec. .

Figure 8.16 shows the trajectory of the aircraft c.g. in three perpendicular planes. As shown the aircraft initially moves in horizontal direction and then starts to gain altitude. This is an expected behaviour, because in general, horizontal movement is much easier than vertical movement during which the gravitational force must be overcome. The same behaviour was also observed for a Tail-sitter UAV in a video which was accompanied with a paper presented in 11th RPVs conference [86]

The same closed-loop eigenvalues were obtained from nonlinear model in ACSL with those derived by linear model in MATLAB which further confirmed the study.

8.5.2 Tilt-nacelle Configuration

In terms of the state variables, the considered flight condition for the Tilt-nacelle configuration can be defined as follows.

$$\begin{aligned}
 U &= 0.0 & P &= 0.0 & \theta &= 0.0 & {}^iN &= \text{Const.} \\
 V &= 0.0 & Q &= 0.0 & \psi &= 0.0 & {}^iN &= \text{Const.} & {}^k\theta_n &= \text{Const.} \approx 90.0 \text{ deg.} \\
 W &= 0.0 & R &= 0.0 & \varphi &= 0.0 & \text{LOCK}_{r,l} &= 0.0
 \end{aligned} \tag{8.8}$$

Steady-state Trim Condition

Again, an altitude of 10.0 m, *Locked* tilting parts and contra-rotating propeller option were used. Due to the complete symmetry, the lateral-directional trim had already been achieved. To achieve longitudinal trim, the propeller rotational speeds (kN), the tilt

Fig.(8.13): Propeller-supported, Tail-sitter, controlled aircraft without δh

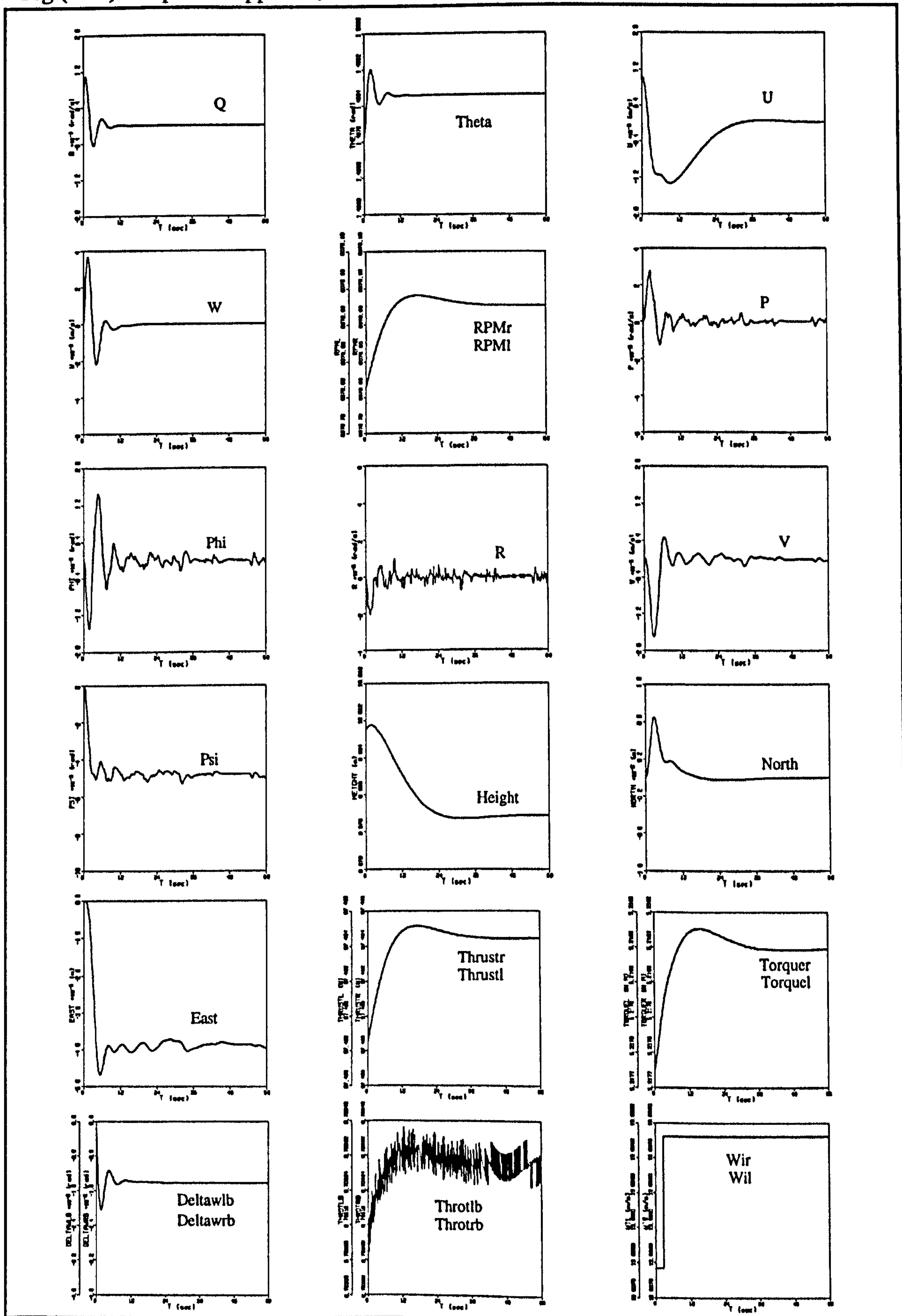


Fig.(8.14): Propeller-supported, Tail-sitter, controlled aircraft with δh

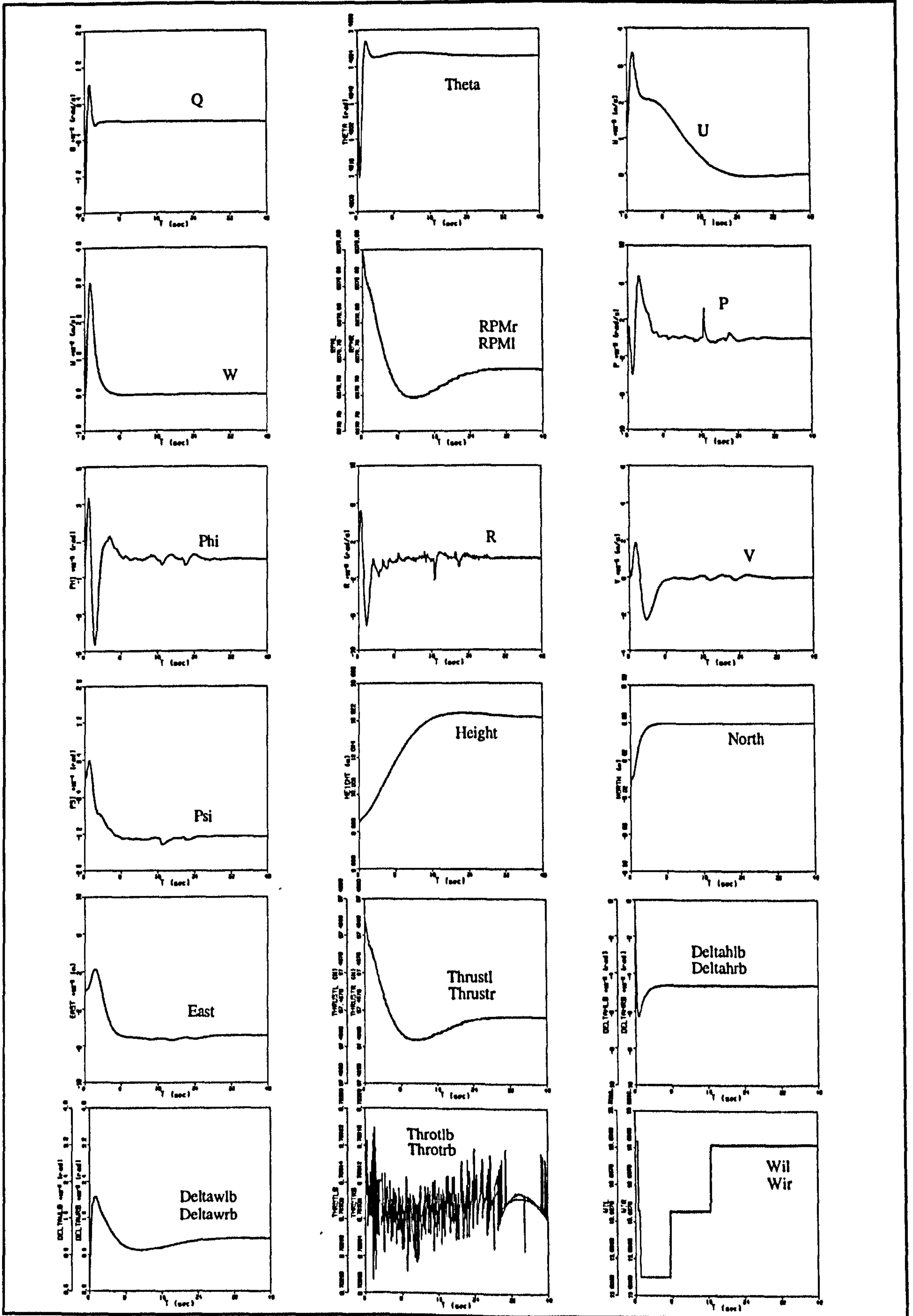


Fig.(8.15): Aircraft response to a position change command

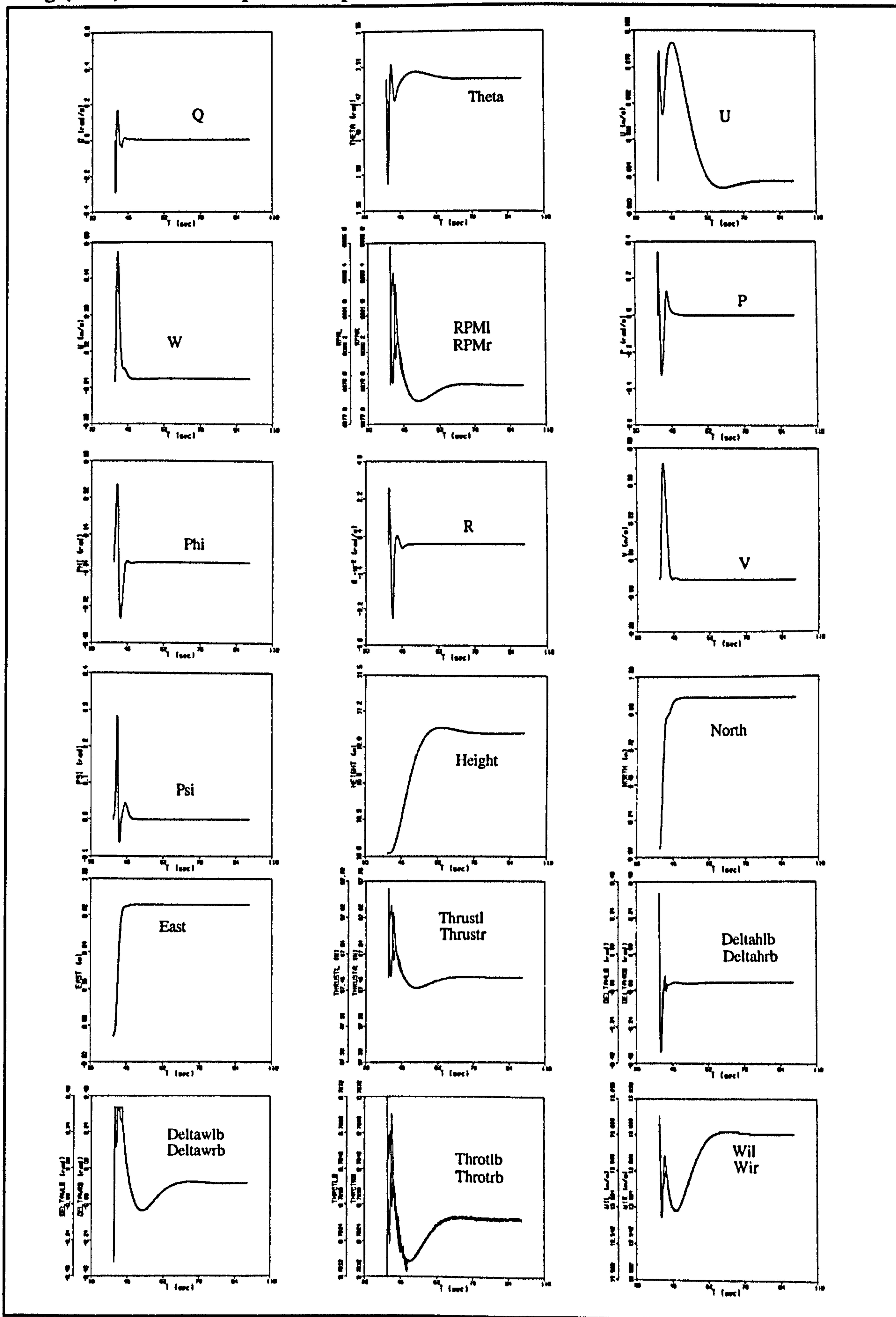
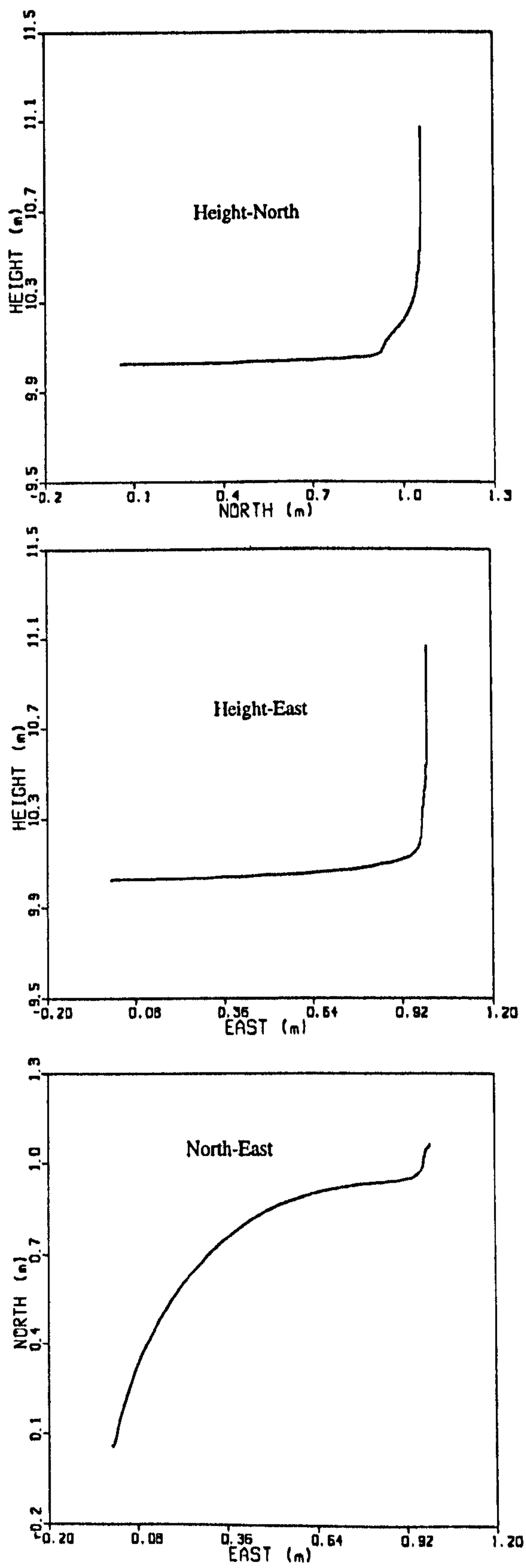


Fig.(8.16): Propeller-supported, Tail-sitter, aircraft trajectory



angles (${}^* \theta_n$) and the throttle settings (${}^* \delta_t$) were respectively used to control the heave acceleration (\dot{W}), the forward acceleration (\dot{U}) and the propeller rotational acceleration (${}^* \dot{N}$). The pitch acceleration was then driven to zero by a small displacement in the location of the Joints.

It needs to be pointed out that due to the considerable aerodynamic download over the wing produced by the propellers' slipstream, a high propeller rotational speed was necessary to generate sufficient thrust and keep the aircraft in trim condition. However, the engines were not able to produce sufficient torque even at maximum throttle to counter balance the reacting aerodynamic torque on the propellers at this condition. This problem was rectified by using a smaller propeller collective pitch (18.0 deg.) as opposed to the default value 20.0 deg.

The following trim values were eventually obtained.

$$\begin{aligned}
 {}^* d_x^a &= -0.00687 m \\
 {}^* \delta_t &= 0.746537 \\
 {}^* RPM &= 6602 \\
 {}^* \theta_n &= 91.64 \text{ deg.} \\
 {}^* \theta_c &= 18.0 \text{ deg.}
 \end{aligned}
 \tag{8.9}$$

Flight Simulation

The simulation results in the form of time histories are given in Figure 8.17. As shown, a sort of limit cycling has happened. To explain this kind of behaviour, the second and the third graphs of Figure 8.17 must be taken into attention. As seen in these curves, due to the existence of a longitudinal unstable subsidence mode (will be derived later) which is dominated by the forward velocity, the aircraft exhibits an unstable divergent motion during the first few seconds. Accordingly, the aircraft nose comes down and the aircraft forward velocity is increased rapidly. As a consequence, the horizontal tail becomes effective and the divergent pitch motion is controlled and damped. However, the forward velocity continues to increase, changing the direction of the propellers' slipstream until the wing goes out of them. As seen in the second graph of Figure 8.17, the value of the slipstream influence code, K_{sswr} (also K_{sswl}) jumps to zero at approximately $t=16.0$ s. This causes a rapid change in the angle of attack and dynamic pressure over the wing. Consequently, the aircraft nose comes up and the forward velocity decreases. The wing

is again affected by the propellers' slipstream and pitch motion is damped, however, this time at a different pitch angle. At this moment, the pitch altitude starts to decrease gradually. This is ended up by second increase in forward velocity and the same cycle is repeated.

Aircraft Modes

Considering the same state and control vectors as shown in relation 8.7, the linearised system matrices presented in Figure 8.18 were obtained. Decoupling between the longitudinal and lateral motion is also observed in this case. The obtained eigenvalues of each separated longitudinal and lateral-directional dynamics are presented in Table 8.4. As can be seen, an unstable oscillatory mode in lateral-directional motion is also observed for the Tilt-nacelle configuration. However, the longitudinal unstable oscillatory mode of the Tail-sitter configuration has been replaced by an unstable subsidence mode. Also, one of the longitudinal stable real roots has been changed to a complex-conjugate stable mode.

Position Hold Autopilot

In order to stabilise the aircraft in both longitudinal and lateral directional, and also to keep it in station, the LQR method was used in order to design a position hold autopilot. In Figure 8.19, the results obtained from the nonlinear simulation are presented. As shown, the feedback control system was able to stabilise the aircraft and hold its position after approximately 100.0 sec.

The response of the aircraft to a position change command was also checked. The trajectory of the aircraft c.g. during the course of changing position in different planes are given in Figure 8.20. The same discussion as that provided in the case of Tail-sitter is also valid about the shape of the trajectory.

The controlled system eigenvalues obtained by linear and nonlinear models were also compared and a very good agreement were found.

8.5.3 Tilt-wing Configuration

The considered flight condition for Tilt-wing configuration can be defined as follows:

Fig.(8.17): Propeller-supported, Tilt-nacelle, simulation in trimmed condition

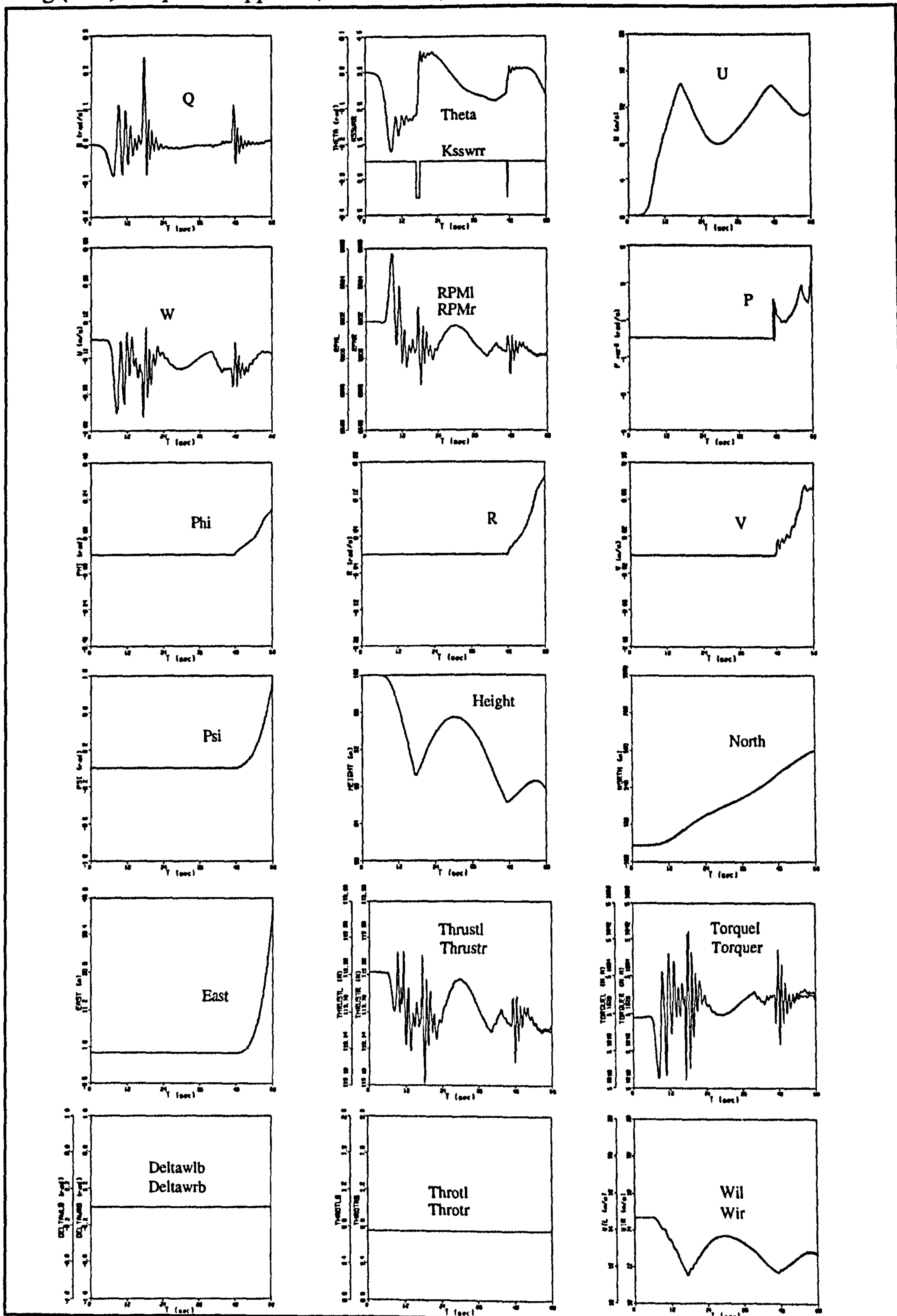


Fig.(8.18): The linearised system matrices for propeller-supported trimmed flight
,Tilt-nacelle configuration

Matrix A

	Q	Th	U	W	'N	'N	P	Phi	R	V
Qd	0.003	-4.156e-4	-0.079	-0.2577	-1.977e-4	1.915e-4	0.001	0.0	0.0	0.0
Thd	1.0	0.0	0.0	0.0	0.0	0.0	0.0	0.0	0.0	0.0
Ud	0.0013	-9.81	-0.009	-0.046	-3.508e-5	3.403e-5	1.209e-4	0.0	0.0	0.0
Wd	-9.721e-4	-0.002	0.002	-0.271	0.014	-0.014	9.662e-4	0.0	0.0	0.0
'Nd	0.001	0.0	2.640e-4	9.272	-9.797	-0.0123	-2.632	-6.321e-4	-0.0134	-4.619e-4
'Nd	0.001	0.0	2.640e-4	-9.271	-0.0123	-9.792	-2.632	-6.318e-4	-0.0134	-4.619e-4
Pd	0.057	0.0	-0.0036	-0.0036	-0.315	-0.315	-0.853	0.054	-0.136	-0.0126
Phid	0.0	0.0	0.0	0.0	0.0	0.0	1.0	0.0	0.0	0.0
Rd	-4.87e-4	0.0	3.667e-4	7.511e-4	-0.0033	-0.0033	0.0415	-0.0022	-0.0095	-1.027e-4
Vd	-5.15e-7	0.0	5.101e-7	1.056e-6	-5.63e-6	-5.62e-6	-0.00137	9.81	1.009e-5	-0.0018

Matrix B

	throttlel	throttlr	deltawl	deltawr
Qd	0.0	0.0	0.024	0.025
Thd	0.0	0.0	0.0	0.0
Ud	0.0	0.0	-0.0186	-0.0186
Wd	0.0	0.0	9.334e-4	9.319e-4
'Nd	-1852.35	4.2976	-0.0921	0.0921
'Nd	-4.2977	1852.35	-0.0921	0.0921
Pd	-0.3356	0.3356	-0.008	0.008
Phid	0.0	0.0	0.0	0.0
Rd	-4.2898	4.2898	-0.0919	0.0919
Vd	0.0	0.0	-1.306e-4	1.306e-4

Matrix C

	Q	Th	U	W	'N	'N	P	Phi	R	V
Qd	1.0	0.0	0.0	0.0	0.0	0.0	0.0	0.0	0.0	0.0
Thd	0.0	1.0	0.0	0.0	0.0	0.0	0.0	0.0	0.0	0.0
Ud	0.0	0.0	1.0	0.0	0.0	0.0	0.0	0.0	0.0	0.0
Wd	0.0	0.0	0.0	1.0	0.0	0.0	0.0	0.0	0.0	0.0
'Nd	0.0	0.0	0.0	0.0	1.0	0.0	0.0	0.0	0.0	0.0
'Nd	0.0	0.0	0.0	0.0	0.0	1.0	0.0	0.0	0.0	0.0
Pd	0.0	0.0	0.0	0.0	0.0	0.0	1.0	0.0	0.0	0.0
Phid	0.0	0.0	0.0	0.0	0.0	0.0	0.0	1.0	0.0	0.0
Rd	0.0	0.0	0.0	0.0	0.0	0.0	0.0	0.0	1.0	0.0
Vd	0.0	0.0	0.0	0.0	0.0	0.0	0.0	0.0	0.0	1.0

Matrix D

	throttlel	throttlr	deltawl	deltawr
Qd	0.0	0.0	0.0	0.0
Thd	0.0	0.0	0.0	0.0
Ud	0.0	0.0	0.0	0.0
Wd	0.0	0.0	0.0	0.0
'Nd	0.0	0.0	0.0	0.0
'Nd	0.0	0.0	0.0	0.0
Pd	0.0	0.0	0.0	0.0
Phid	0.0	0.0	0.0	0.0
Rd	0.0	0.0	0.0	0.0
Vd	0.0	0.0	0.0	0.0

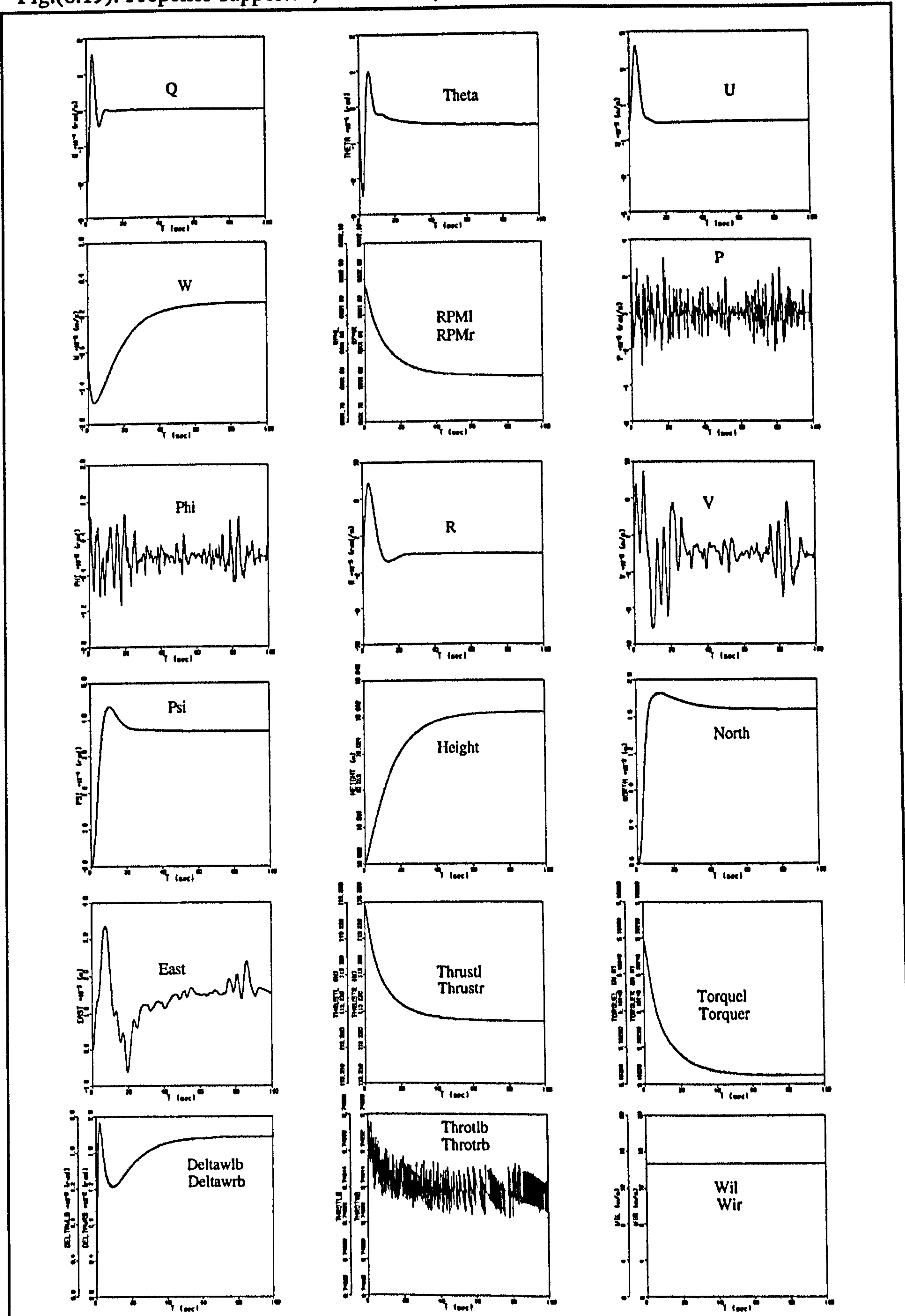
Table(8.3): Propeller-supported, Tail-sitter, aircraft modes

Longitudinal			
0.426+/-0.901i	Freq.=0.996 rad/s	Damp=-0.427	T=6.974 s
-0.007464		T=134.0 s	
-1.16474		T=0.859 s	
Lateral-directional			
0.214+/-0.375i	Freq.=0.431 rad/s	Damp=-0.495	T=16.755 s
-0.497		T=2.012 s	
-0.792		T=1.263 s	

Table(8.4): Propeller-supported, Tilt-nacelle, aircraft modes

Longitudinal			
0.922		T=1.085 s	
-0.249		T=4.016 s	
-0.460+/-0.799	Freq.=0.922 rad/s	Damp.=0.499	T=7.93 s
Lateral-directional			
0.103 +/- 0.355I	Freq.=0.369 rad/s	Damp.=-0.279	T=17.7 s
-0.0084		T=119.05 s	
-0.880		T=1.136 s	

Fig.(8.19): Propeller-supported, Tilt-nacelle, controlled aircraft



$$\begin{array}{llll}
 U = 0.0 & P = 0.0 & \theta = 0.0 & {}^rN = \text{Const.} \\
 V = 0.0 & Q = 0.0 & \psi = 0.0 & {}^lN = \text{Const.} \\
 W = 0.0 & R = 0.0 & \varphi = 0.0 & \text{LOCK}_{r,l} = 1.0
 \end{array}
 \quad
 \begin{array}{l}
 {}^n\theta = \text{Const.} \approx 90.0 \text{ deg.} \\
 {}^n\dot{\theta} = 0.0
 \end{array}
 \quad (8.10)$$

The same procedure as mentioned in previous section for Tilt-nacelle configuration was used to find the trim condition. Since, the *Unlocked* tilting parts option had been selected, the tilting part relative angular accelerations (${}^n\ddot{\theta}$) also had to be driven to zero. This was carried out by using the output torque of the servomotors. The following trim values were finally obtained.

$$\begin{array}{l}
 {}^n d_x^a = -0.00085m \\
 {}^n \delta_1 = 0.703719 \\
 {}^n RPM = 6079.5 \\
 {}^n \theta_d = -0.0602n.m \\
 {}^n \theta_n = 85.9 \text{ deg.}
 \end{array}
 \quad (8.11)$$

Using the obtained trim values, the aircraft simulation was then carried out, and the results are presented in Figure 8.21. An unstable oscillatory behaviour is exhibited by the aircraft which is similar to what observed for the Tail-sitter configuration. These two configurations are principally similar in that the thrust line and the wing chord are in the same direction in both, whereas in Tilt-nacelle configuration they are perpendicular. Using the following state and control vectors, a feedback control gain was then obtained by using LQR method.

$$\begin{array}{l}
 \text{State vector: } [Q, \theta, U, W, {}^lN, {}^rN, {}^l\theta, {}^r\theta, {}^l\dot{\theta}, {}^r\dot{\theta}, \varphi, R, V] \\
 \text{Control vector: } [{}^l\theta_d, {}^r\theta_d, {}^l\delta_1, {}^r\delta_1]
 \end{array}
 \quad (8.12)$$

The result of the nonlinear simulation of the controlled aircraft and the aircraft response to a position change command are shown in Figures 8.22, 8.23. As can be seen, the control system has been able to stabilise the aircraft and keep its position. The open-loop and closed-loop eigenvalues are also provided for comparison reason in Table 8.5.

Fig.(8.20): Propeller-supported, Tilt-nacelle, aircraft trajectory

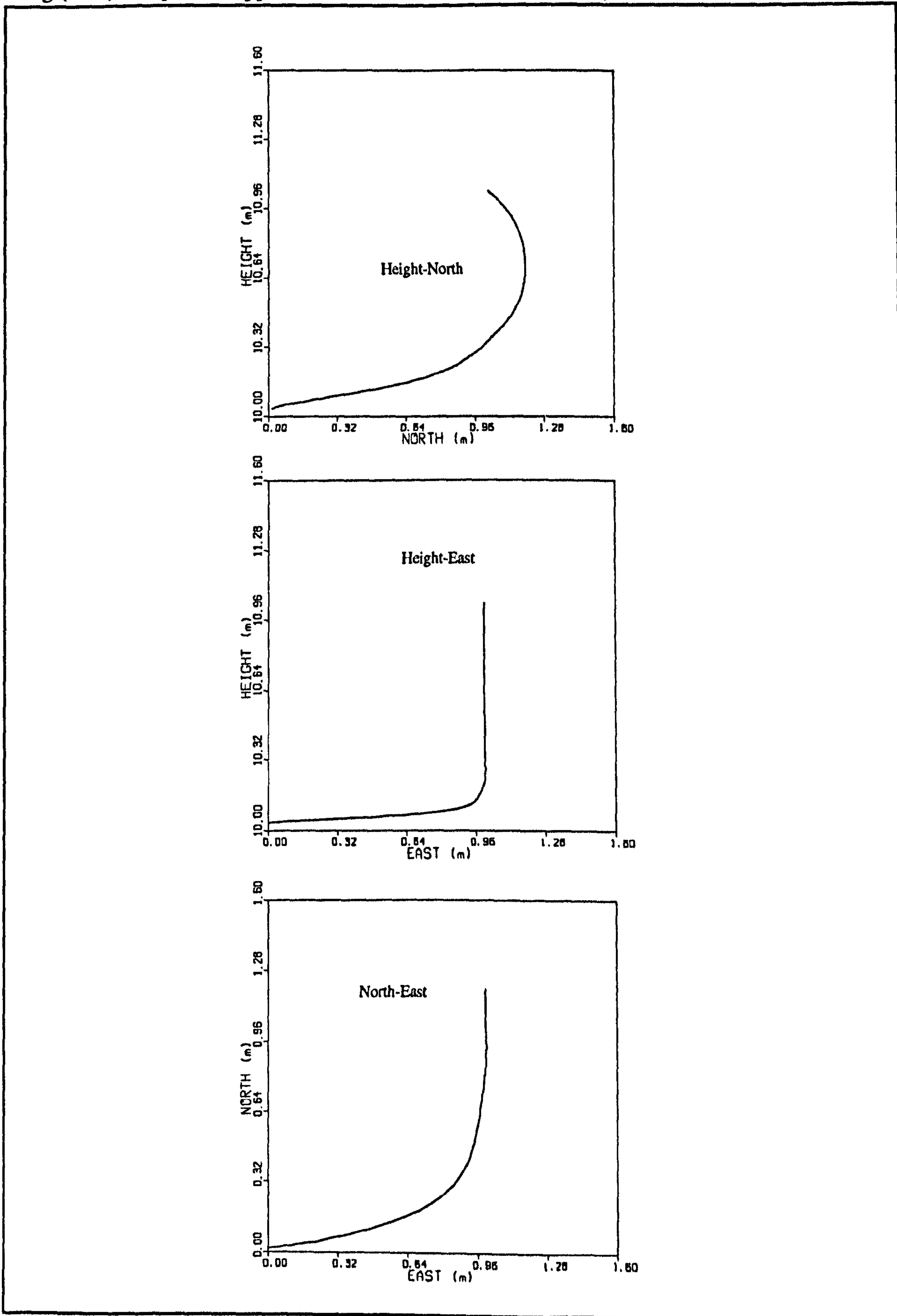


Fig.(8.21): Propeller-supported, Tilt-wing, simulation in trimmed condition

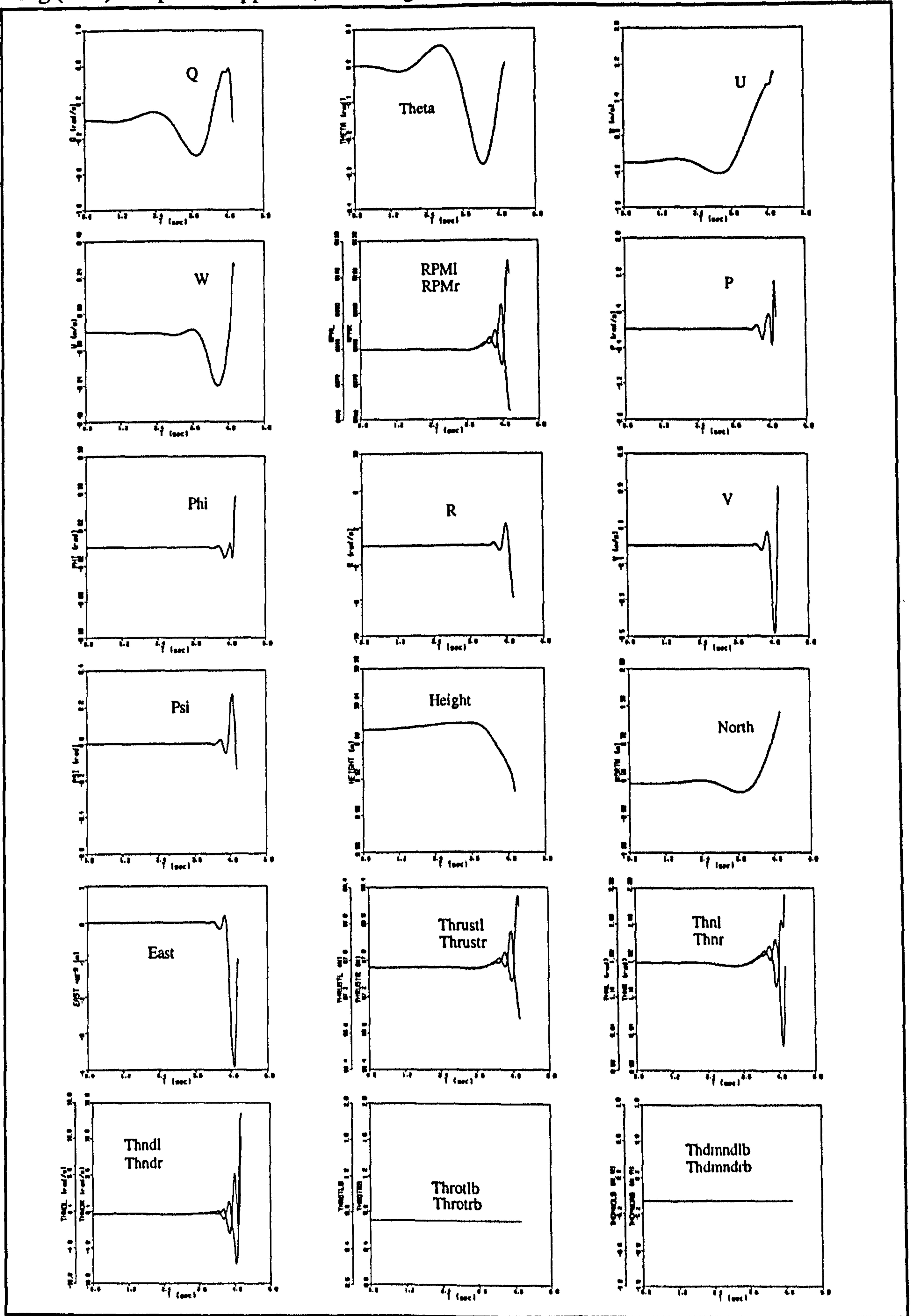


Fig.(8.22): Propeller-supported, Tilt-wing, controlled aircraft

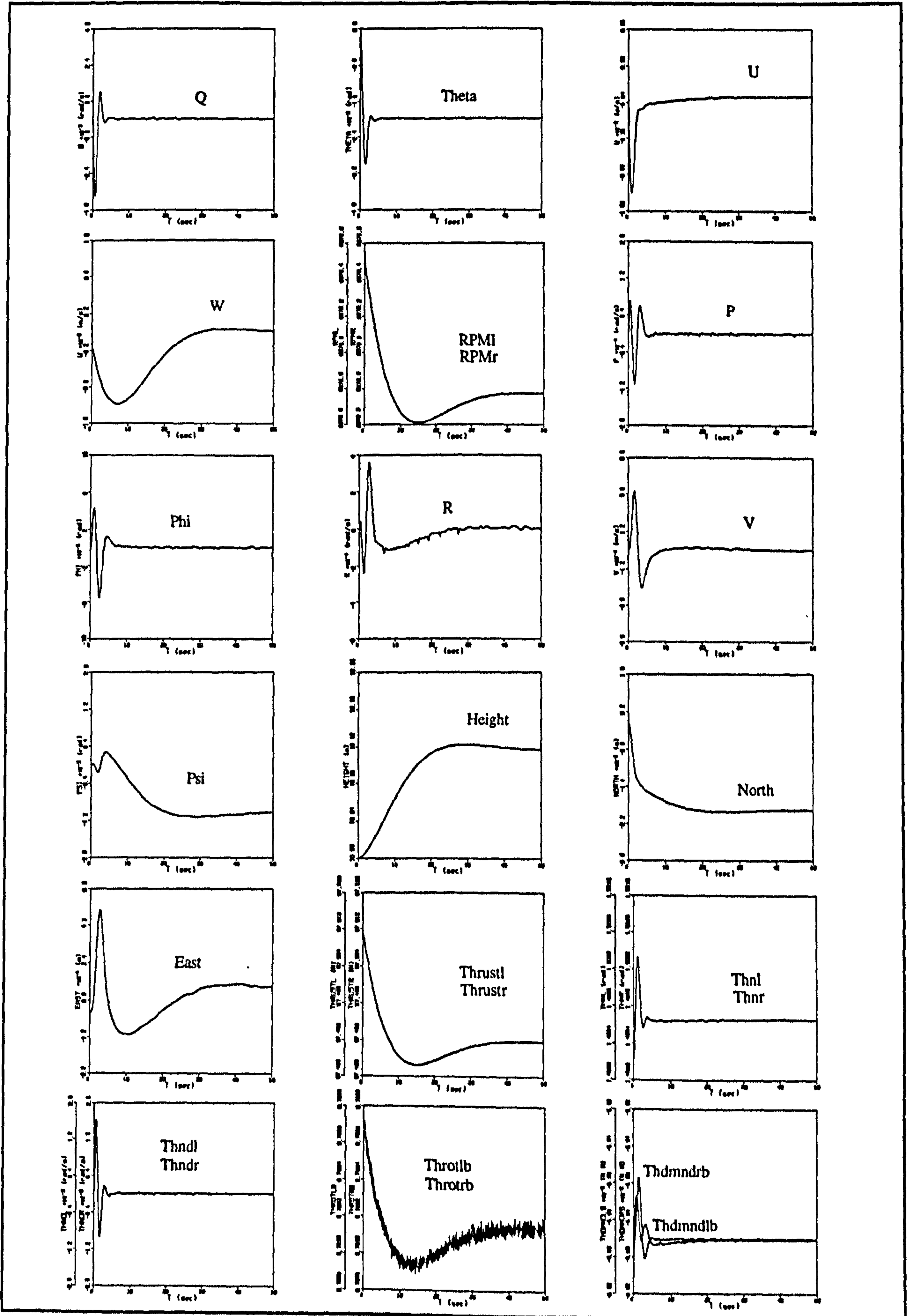


Fig.(8.23): Propeller-supported, Tilt-wing, aircraft trajectory

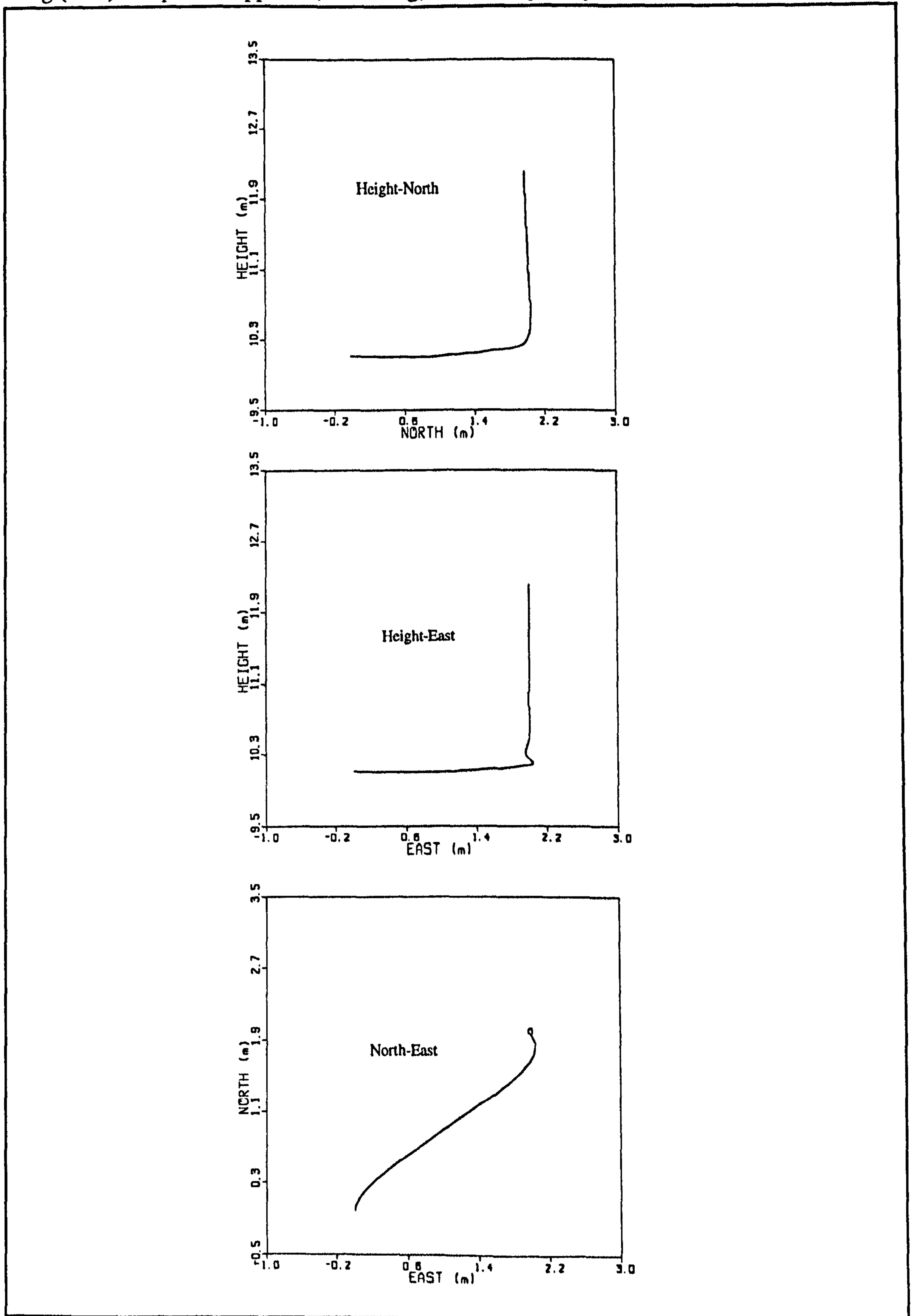


Table (8.5): Propeller-supported, Tilt-wing, open-loop and closed-loop eigenvalues

Open-loop
5.14+/-15.18i
0.098+/-4.38i
1.094+/-2.24i
0.05+/-0.235i
0.0358
0.0
-0.478
-2.75
-7.63
-11.31
-14.373
Closed-loop
-0.211
-1.217+/-0.282i
-1.35+/-1.746i
-0.946+/-2.79i
-3.77+/-2.51i
-6.335+/-5.97i
-81.8437
-81.53
-1439.63
-1447.48

CHAPTER 9

CONCLUSIONS AND FURTHER WORKS

9.1 CONCLUSIONS

The primary objective of this research work, i.e. development of a simulation model for flight dynamics and control investigations of the considered VTOL configurations and feasibility study of the proposed concept, has been achieved. The following points may be highlighted in this respect.

- The obtained results provide confidence in the validity of the mathematical model upon which the simulation is based. No logical contradiction and inconsistency in the mathematical modelling has been observed.
- The object-based approach has proved to be an applicable method for the simulation of an aircraft when there is little data available and, when at the same time, a general knowledge of the aircraft dynamics is required.
- Using the object-based approach, the amount and the variety of the required aerodynamic data has been considerably reduced.
- The simulation results confirm the capability of the object-based approach of predicting the fundamental characteristics of VTOL flight, even though the aircraft aerodynamics are not perfectly modelled in this approach, as discussed in Chapter 3.

- The equations of motion of the aircraft multibody system have been originally derived in this thesis. Using separated objects, the derivation of these equations has been carried out in a straightforward manner without explicitly dealing with the rate of change of inertia and centre of gravity position. The validity of these equations have been proved through a number of sufficient and convincing tests.
- The geometric and kinematic similarities between components and configurations have been used to maintain the simplicity and modularity of the simulation model. The modularity simplifies modification tasks so that model improvement may be carried out easily and quickly without having concern for loss of integrity.
- Using the Object-based approach, the requirements of generality, flexibility and singleness (one simulation model for three different configurations) for the simulation model have been achieved. This technique allows the user a larger amount of freedom in specifying the components' geometry and aerodynamics.
- The propeller's slipstream effect model developed in Chapter 5 has been found sufficiently effective for continuous tracing the slipstream direction and calculating the effect of the propeller induced velocity on the affected components.
- The ability of the simulation model to provide invaluable insight of the aircraft stability and control characteristics has been demonstrated. This ability can be used to obtain the most suitable control strategies together with optimum sizing of the aircraft at early stage in the design process. In addition, it is shown that the simulation model is sufficiently flexible and accurate to play its role as a research tool and has the potential for hypothesis testing, explanation and discovery.
- The simulation model has been able to demonstrate the natural longitudinal and lateral-directional modes of aircraft during conventional wing-supported flight, including Short-period, Phugoid, Dutch-Roll, Roll subsidence and Spiral mode. In addition, the expected decoupling between longitudinal and lateral-directional motions has been observed.

- The period of unstable oscillatory modes of the aircraft obtained by nonlinear simulation in hover flight are generally long and could be easily controlled by an experienced pilot.
- Unstable oscillatory behaviour were exhibited by both the Tail-sitter and Tilt-wing configurations, indicating the expected principal similarity in that the thrust line and the wing chord are in the same direction in both of them, whereas in Tilt-nacelle they are perpendicular.
- Two damped subsidence and a divergent oscillation in longitudinal and lateral-directional motion which are the typical modes of helicopters during hover, have been observed for the Tail-sitter configuration, confirming the expected similarity between two vehicles in hover. Similar divergent oscillations have been reported for a tail-sitter model aircraft by NACA [84].
- Although the majority of the input data have been estimated in this work, using completely different sources, the simulation results are surprisingly reasonable and encouraging. This indicates that a careful data preparation has been carried out.
- No contradiction has been found in connection with the proposed control concept during the aircraft simulation. However, it is quite clear that a comprehensive investigation must be carried out before a decisive comment can be given.
- The LQR method used to find the feedback gain matrices has been found a powerful method. In all the cases, the feedback control systems designed by LQR method were able to stabilise the aircraft, at least in the vicinity of the trim condition. It should however be pointed out that a practical control system for such aircraft needs to be elaborately designed, considering real factors and restrictions.
- In general, the obtained simulation results indicate that the mathematical model is highly nonlinear in nature, so that even a small change in aircraft condition may lead to completely different behaviour.
- The results obtained by the linearised model have always confirmed the nonlinear simulation results, indicating the validity of the ACSL linearization routine.

- An interesting limit cycling phenomenon has been observed and explained for the Tilt-nacelle configuration which proves the ability of the simulation model to discover the unknown nonlinear behaviours and to describe them.
- The Advanced Continuous Simulation Language (ACSL) has been found a suitable language with sufficient facilities for the purpose of modelling and evaluation of non-real-time nonlinear systems, although some inconveniences have been experienced during the course of working with this language.
- Using structured programming approach, the consistency between various parts of the whole program was maintained throughout all the stages of the development. Also, it provided a systematic way of deriving the code for the functional blocks. In addition, since programming errors could be easily detected and corrected, program modification and development were accelerated.

9.2 FURTHER WORK

The following suggestions are presented for further development and applications of the simulation model and the applied methodology.

- Clearly, the next step in the research work is to use the developed simulation program for the analysis of flight dynamics and control of the aircraft in different regimes, in particular the transition phase. This task can be started by trying to optimise the aircraft sizing in order to obtain the best possible functionality.
- In the present simulation model, no dihedral angle has been considered for lifting surfaces e.g. wings. With suitable assumptions, this angle may also be incorporated in the simulation model.
- The aircraft trim conditions presented in this thesis have been obtained by hand and through a process of trial and error. However, using an appropriate trim routine, steady-state conditions may be obtained in a faster and more accurate way.

- As previously concluded, the methodology used in this work is a suitable method to be used when a general knowledge about the flight dynamics of an unconventional aircraft is required and there is little data available. Therefore, this methodology can be applied for the other alternative VTOL concepts such as the Freewing and Tilt-body, shown in Figures 9.1-9.4, or the derivatives of the considered concepts such as U-tail Tilt-rotor aircraft, shown in Figure 9.5. The strange looking of these aircraft and their conversion process indicate that even an initial investigation of their flight dynamics must be started by wind tunnel tests. Therefore, the application of the methodology in these cases is well justified.
- The object-oriented simulation is a recognised and appreciated method in the field of discrete event and discrete time systems [87]. However, to the knowledge of the author, no effort has been made so far to extend the application of this method for continuous systems. The present work might be regarded as an initial attempt and a basis for the future work by those who think it may be possible.

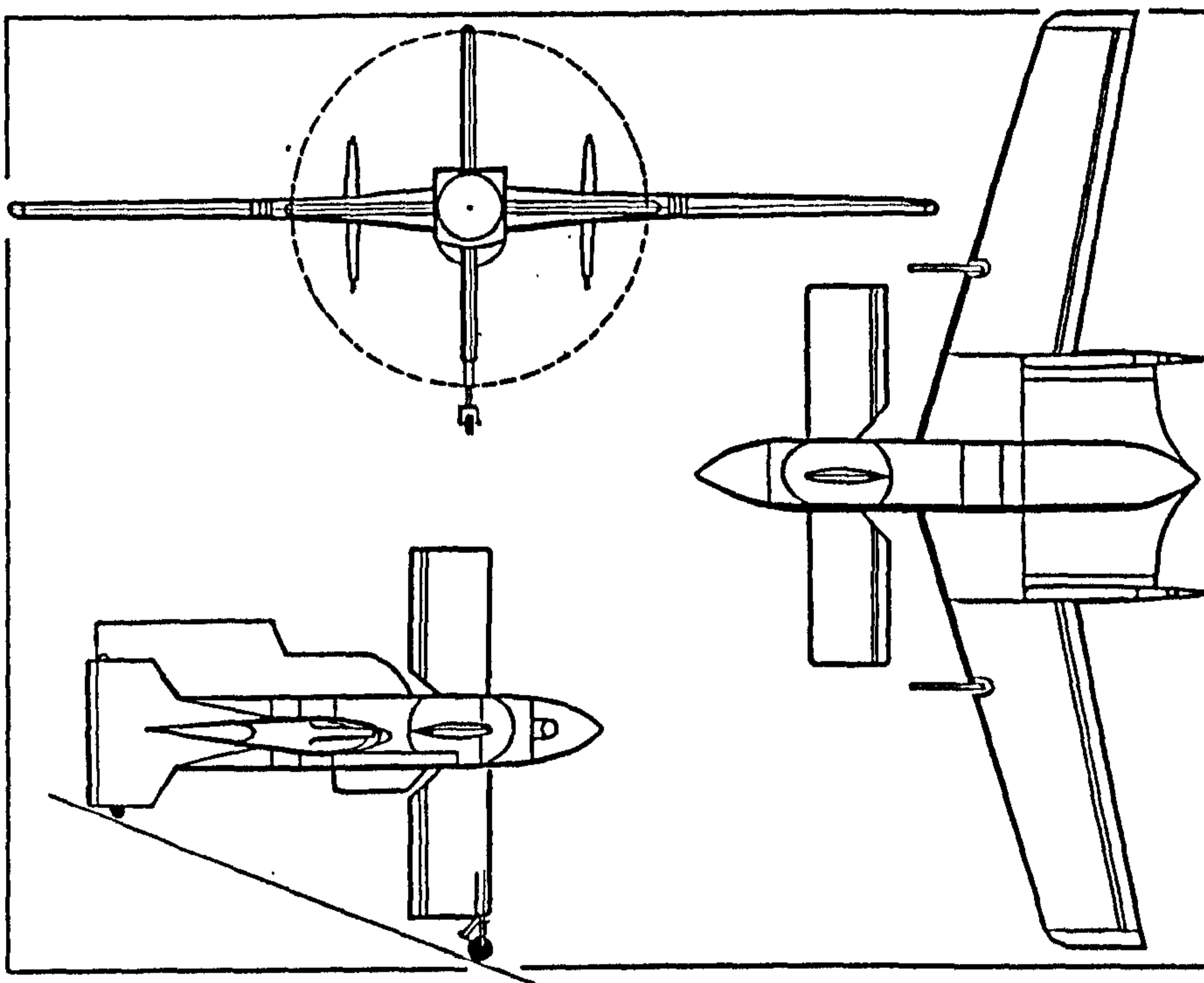


Fig.(9.1): Daedalus STF-9A demonstrator [38]

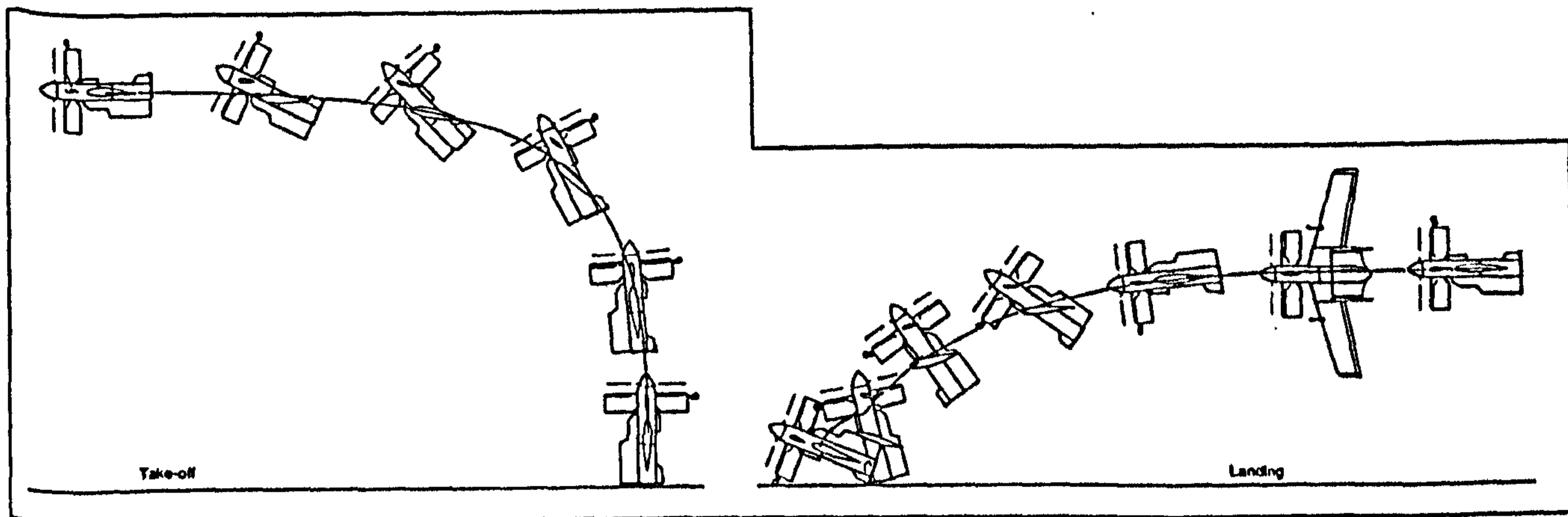


Fig.(9.2): Slaved tandem freewing take off and landing sequences [38]

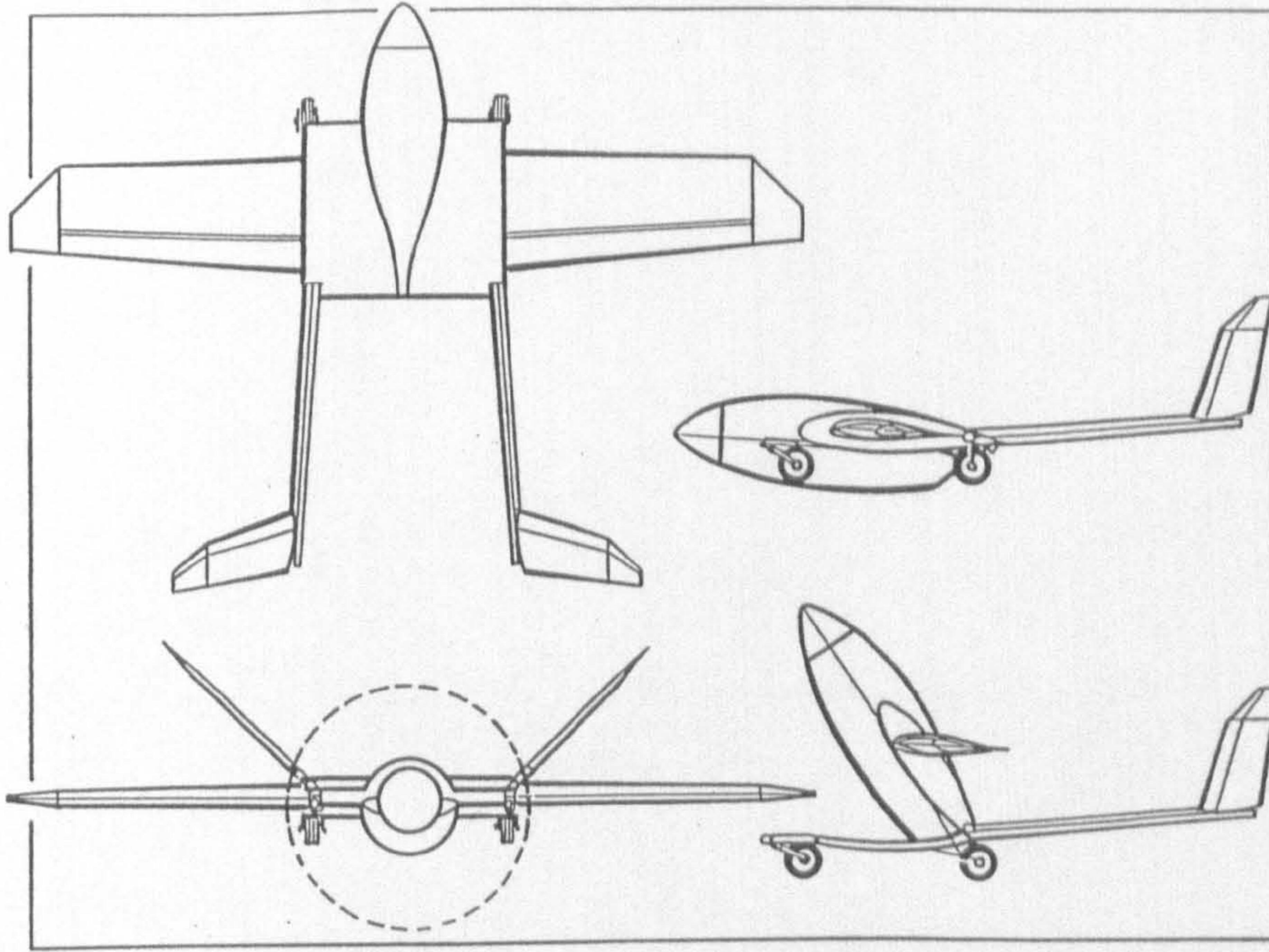


Fig.(9.3): Freewing Scorpion Tilt-body UAV [38]

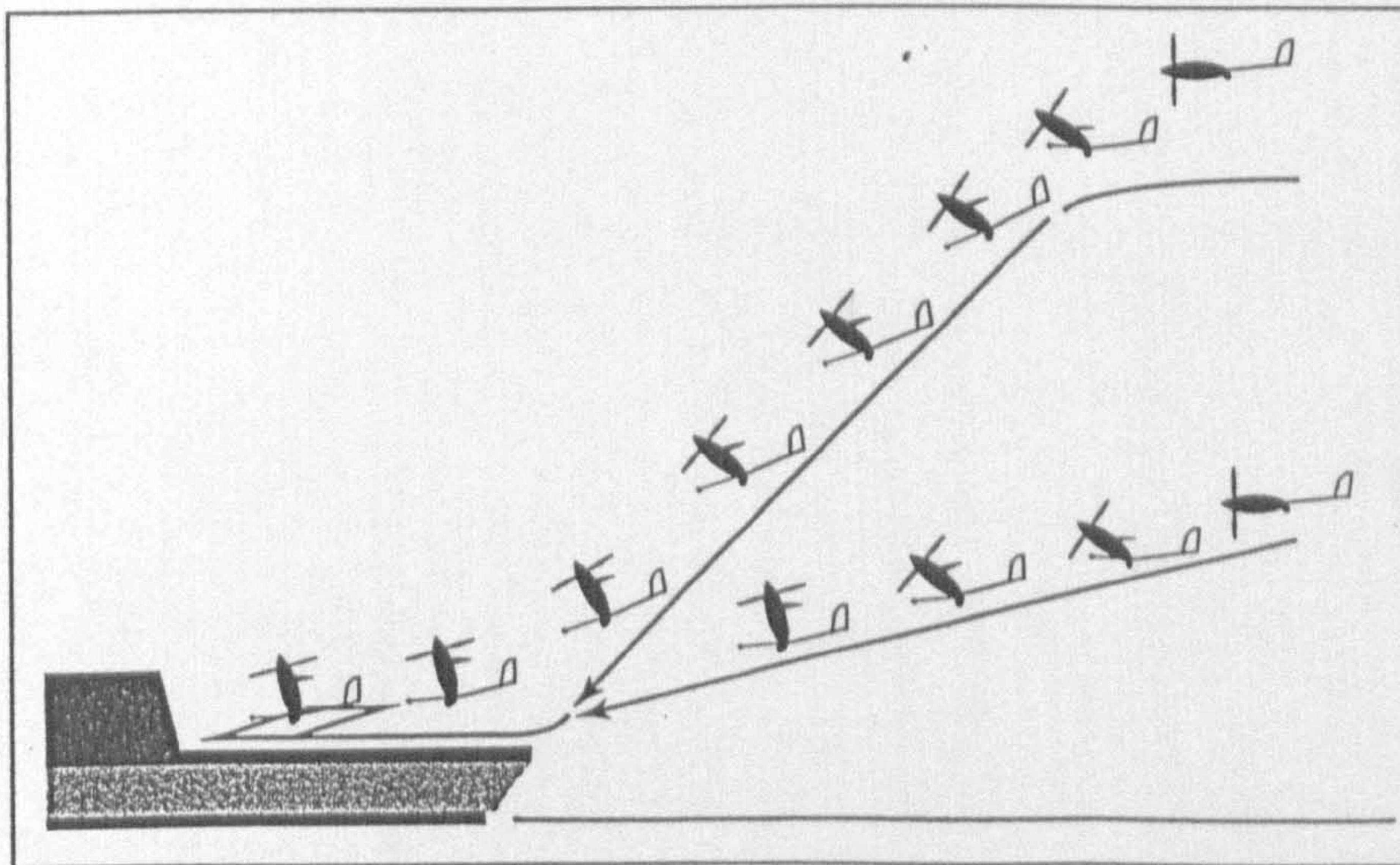


Fig.(9.4): Alternative Tilt-body deck landing sequences [38]

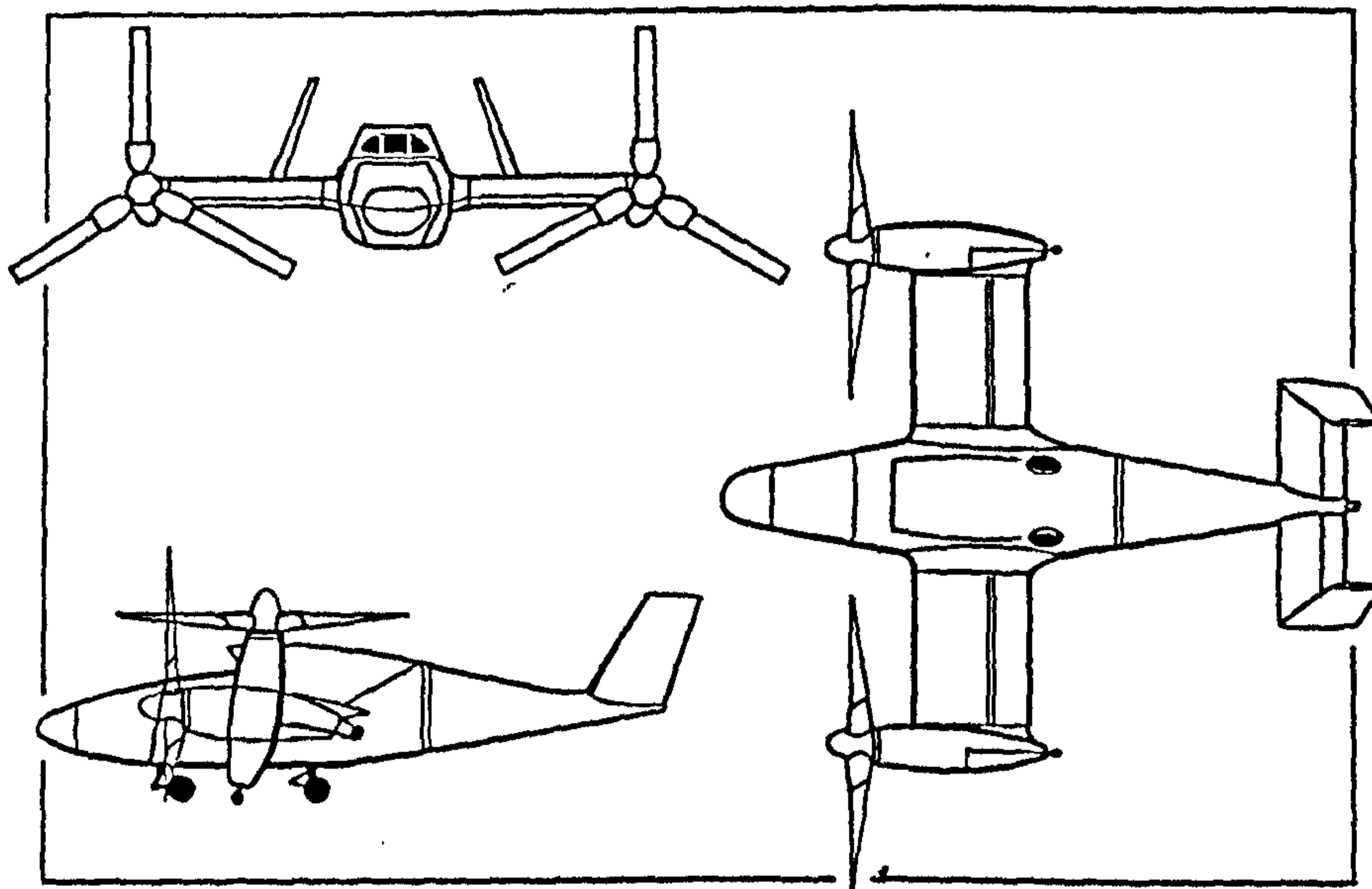


Fig.(9.5): Bell Eagle Eye tilt-rotor UAV [38]

REFERENCES

1. Siuru, B. , *Planes Without Pilots , Advances in Unmanned Flight* , TAB/AERO Books, 1991
2. Robert, A. C., Lyne, J. D., Wheeler, T. G., *RPV Recovery Systems* , 1th RPV's International Conference, Bristol, UK, 3-5 Sept. 1979
3. Lichten, R. L., Gradam, L. M., Wernicke, K. G., *A Survey of Low-Disc-Loading VTOL Aircraft Designs* , AIAA 65-756
4. McCormick, B. W., *Aeronautics of V/STOL Flight*, Academic Press Inc. , 1967
5. Jonkers, R. P., *Conceptual Design of an Exective Tiltrotor Aircraft*, M.Sc Thesis, College of Aeronautics, Cranfield University, 1991
6. Chana, I. F., Sullivan, T. M., *The Tilt-wing Advantage - for High Speed VSTOL Aircraft*, SAE Technical paper series 921911
7. Schneider, J., Wilkerson J., *Advanced Rotorcraft V/STOL Technology Needs for the High Speed Rotorcraft*, AIAA 90-3298
8. Lynn, R. R., *The Rebirth of the Tiltrotor - The 1992 Alexander A. Nikolsky Lecture*, American Helicopter Society's 48th Annual Forum and Technology Display, Washington D. C., June 1992
9. Schaeffer, J., Alwang, R., *V-22 Thrust Power Management Control Law Development*, 47th Forum of the American Helicopter Society, Phoenix, Arizona , 1991
10. Rutherford, J., Bass, S., *Advanced Technology Tilt Wing Study* , AIAA 92-4237

11. Rutherford, J., Bass, S., Lovenguth, M., *A Concept Mission Sensitivity Study of Several Medium to High-Speed V/STOL Aircraft* , AIAA 91-3096
12. O'Rourke, M., Rutherford, J., *Methods to Determine Limits to Tiltwing Conversion* , AIAA 91-3143
13. Marr, R. L., Churchill, G. B., *Piloted Simulation in the Development of the XV-15 Tilt-rotor Research Aircraft* , AGARD Conference Proceedings No. 408, Flight Simulation
14. Clark, D. R., McVeigh, M. A., *Analysis of the wake Dynamics of a Typical Tilt-rotor Configuration in Transition Flight* , 11th European Rotorcraft Forum, Paper No. 28, London, England, Sept. 1985
15. McManns, B. L., *V-22 Tilt-rotor Fly-by-wire Flight Control System* , 11th European Rotorcraft Forum, London, England, Paper 57, Sept. 1985
16. Poisson-Quinton, Ph., Cook, W. L., *A Summary of Wind-Tunnel Research on Tilt-rotors from Hover to Cruise Flight* ,
17. O'heron, P. J., Kunz, D., Nikraves, P., Arabyan, A., *A Multi-Body Approach to Modelling Rotorcraft Dynamics* , AIAA 92-0487
18. Lebacqz, J. V., Decker, W. A., Alderete, T. S., Scott, B. C., Harper, P. J. G., Chung W. W., *Ground-Simulation Investigations of VTOL Airworthiness Criteria for Terminal-Aera Operations* , The Royal Aeronautics Society, Progress in Helicopter and V/STOL Aircraft Simulation, May 1990
19. Tishchenko, M. N., *Helicopter or Tilt-rotor , A Soviet View* , Vertiflite , Sept/Oct 1990, Vol. 36, No. 5
20. Schaefer, J. H., Spivey, R. F., Barbour, D. J., Atkins C. D., *Tiltrotor Evolution Leads to Effectiveness Revolution* , 43th Annual Forum Proceedings V1 Pub1 by American Helicopter Society, Alexandria, VA, USA P11-124

21. McVicar, J. S. G., *A Generic Tilt-rotor Simulation Model With Parallel Implementation* , Ph.D Thesis University of Glassgow, Feb. 1993
22. Paisley, D. J., *Rotor Aeronautic Optimization for High Speed Tiltrotors* , 43th Annual Forum of the American Helicopter Society, St. Louis , Mo , May 1987
23. Harendra, P. B., Jaglekar, M. M., Gaffey, T. M., Marr, R. L., *A Mathematical Model for Real Time Flight Simulation of the Bell Model 301 Tilt-rotor Research Aircraft*, NASA CR-114614
24. Ishida, T., Nakatani, I., *TW-68 Tilt Wing High Speed Commercial VTOL* , Vertiflite , Jan/Feb 1990 , Vol. 36 No. 1
25. Humpherson, D. V., *Possible Rotorcraft Configurations for Unmanned Aircraft*, 8th RPV's International Conference, Bristol, UK, 1990
26. Lindenbaum, B., *VTOL RPVs - A Technology Assessment* , Journal of American Helicopter Society, Vol. 21, Oct. 1976
27. Kenneth M., *World Unmanned Aircraft* , Jane's Publishing Company Limited, 1988
28. *Watcher in the Sky* , Flight International , 14-20 April , 1993
29. Sheffield, R. E., *An Analysis Tool for UAV Effectiveness Evaluation* , Vertiflite May/June 1992 Vol. 36, No. 5
30. Tharp, W., Morgan, R., Magee, J. P., *Design of A Tiltrotor Unamnned Vehicle for Maritime Applications* , Bell Helicopter Textron Inc., AIAA 93-1040
31. Rondey, K., *The Pointer - A New Concept for RPV Air Vehicles* , Bell Helicopter Textron Inc. , 7th RPV's International Conference, Bristol, UK, 1988
32. Austin, R. G., *One Man's View* , 10th RPV's International Conference, Bristol, UK, Sept. 1994

33. Schneiderman, R., *Unmanned Systems Win Unexpected Support* , Microwaves & RF, Sept. 1991, P30-43
34. McClure, R. D., Hall, P. G., *The Pointer - Test and Evaluation of the Tiltrotor UAV* , Bell Helicopter Textron Inc., AHS Annual Textron Inc., Boston, MA, May 22-24 , 1989, P 243-250
35. Brown, B. M., Jacobus, C. H., Hall, P. G., *Tiltrotor UAV - The Next Generation Unmanned System* , Vertiflite, May/June 1992, Vol 38, No 3, P18-24
36. Taylor, R. S., *The Pointer, A Revolutionary Idea to Improve RPV Capabilities* , 44th Forum of American Helicopter Society, Washington D. C. , June 16-18, 1988
37. *Eagle Eye Transitions* , Aviation Week and Space Technology, Feb. 7 , 1994
38. Munson, K., *Jane's, Unmanned Aerial Vehicles and Targets* , Jane's Information Group Limited, 1995
39. *Candidate for UAV Program Debut at Unamnned Aerial Vehicle Meeting* , Aviation Week & Space Technology, August 26, 1991
40. *Boeing Unveils Heliwing UAV* , Aviation Week & Space Technology, April 1994
41. *Matra Buys Option on Rutan UAV Design* , Aviation Week and Space Technology , August 8 , 1994
42. Rolfe, J. M., Staples, K. J., *Flight Simulation*, Cambridge, 1986
43. Spriet, J. A., Ghislain, C. V., *Computer-Aided Modelling and Simulation*, Academic Press Inc. , 1982
44. Stevens, B. L., Lewis, F. L., *Aircraft Control and Simulation*, John Wiley & Sons, 1992
45. Etkin, B., *Dynamics of Atmospheric Flight*, John Wiley & Sons Inc., 1994

46. Thomasson P. G., *Computer Modelling of Aerospace Vehicles*, Lecture Notes, College of Aeronautics, Cranfield University, 1995
47. Franklin, G. F., Powel, D. J., Emami-Naeini, A., *Feedback Control of Dynamic Systems*, Addison-Wesley Publishing Company, 1994
48. Murray-smith, D. J., *Problems and Prospects in the Validation of Dynamic Models*, Computational System Analysis, 1992
49. Roberson, R. E., Schwertassek, R., *Dynamics of Multibody Systems*, Springer-Verlag, 1988
50. Hughes, P. G., *Spacecraft Attitude Dynamics*, John Wiley & Sons, 1986
51. Von mises, R., *Theory of Flight*, Dover Publication Inc., 1959
52. Saghafi, F., *Author's Private Notes*
53. Bramwell, A. R. S., *Helicopter Dynamics*, Edward Arnold Ltd, 1976
54. Johnson, W., *Helicopter Theory*, Princeton University Press, 1980
55. Newman, S., *The Foundations of Helicopter Flight*, Simon Newman, 1994
56. Prouty, R. W., *Helicopter Performance, Stability and Control*, PWS Publishers, 1986
57. Wood, K. D., *Technical Aerodynamics*, McGraw-Hill Inc., 1955
58. Thomasson, P. G., From RPVs to UMA, Aerogram, College of Aeronautics, Cranfield University, Vol. 7, No. 3, Nov. 1993
59. Trebble, W. J. G., *The Aerodynamic Performance of Propellers Suitable for Unmanned Aircraft (UMAs)*, Royal Aircraft Establishment, Tech. Memo Aero 2094, Jan. 1987
60. Mitchell & Gaitheir Associates (MGA) Inc., *ACSL Users Manual*, Version 10., 200 Baker Avenue, Concord MA 01742-2100, USA
61. Thomasson, P. G., Cranfield University, College of Aeronautics, Private Communication
62. Critzos, C. C., Heyson, H. H., Boswinkle, R. W., *Aerodynamic Characteristics of NACA 0012 Airfoil Section at Angles of Attack from 0 to 180 deg.*, NACA TN-3361

63. Harendra, P. B., Jaglekar, M. M., Gaffey, T. M., Marr, R. L., *A Mathematical Model for Real Time Flight Simulation of the Bell Model 301 Tilt-rotor Research Aircraft*, NASA CR-114614, 1980
64. Hoerner, S. F., Borst, H. V., *Fluid-Dynamic Lift*, Published by Mrs. Liselotte A. Hoerner, 1975
65. Hoerner, S. F., *Fluid-Dynamic Drag*, Published by Author, 1965
66. Turbull, A., *Development of Preliminary Sizing Method for Unmanned Aircraft*, M.Sc Thesis, College of Aeronautics, Cranfield University, 1988
67. Milonidis, E., *The Development of the Mathematical Model of a Remotely Piloted Vehicle and an Investigation on the use of an Extended Kalman Filter for Aerodynamic Derivatives*, M.Phil Thesis, College of Aeronautics, Cranfield University, 1987
68. Turbull, A., *A Preliminary Sizing Method for Unmanned Aircraft Using Multi-variable Optimization*, Ph.D Thesis, College of Aeronautics, Cranfield University, 1991
69. MATLAB user,s guide, The Mathwork Inc., 1990
70. Meriyam, J. L., Kraige, L. G., *Engineering Mechanics, Dynamics*, Volume two, Third Edition, John wiley & Sons, 1993
71. Kheir, N. A., *Systems Modelling and Computer Simulation*, Second Edition, Marcel Dekker, 1996
72. Valiet H. Van., *Software Engineering*, John wiley & Sons Ltd., 1993
73. Sommerville, I., *Software Engineering, Principle and Practice*, Addison-Wesley Publishers Ltd., 1992
74. Pressman, R. S., *Sofetware Engineering, A Practitioner's Approach*, McGraw-Hill Book Company Europe, 1992
75. Stepniewski, W. Z., Keys, C. N., *Rotary-wing Aerodynamics*, General Publishing Company Ltd, 1984
76. Etkin, B., Reid, L. D., *Dynamics of Flight, Stability and Control*, Third Edition, John Wiley & Sons Inc., 1996
77. Blakelock, J., *Automatic Control of Aircraft and Missiles*, Second Edition, John Wiley & Sons Inc., 1996

78. Nelson, R. C., *Flight Stability and Automatic Control*, McGraw-Hill, 1989
79. Hancock, G. J., *An Introduction to the Flight Dynamics of Rigid Aeroplanes*, Ellis Limited, 1995
80. McLean, D., *Automatic Flight Control Systems*, Prentice Hall International (UK) Ltd, 1990
81. Roskam, J., *Airplane Flight Dynamics and Automatic Flight Controls*, Published by Author, 1979
82. Babister, A. W., *Aircraft Dynamic, Stability and Response*, 1980
83. Bryson, E., *Control of Spacecraft and Aircraft*, Princeton University Press, 1994
84. Kirby, R. H., *Flight Investigation of the Stability and Control Characteristics of a Vertically Rising Airplane Research Model with Swept or Unswept Wings*, NACA TN 3812, 1956
85. Stepniewski, W. Z., Keys C. N., *Rotary-wing Aerodynamics*, General Publishing Company Ltd, 1984
86. Ohno, M., Sinagawa, T., *Hover Control For Tail-sitter UAVs*, 11th RPVs International Conference, Bristol, UK, 12-14 Sept. 1994
87. Arons, H. D. S., *Object Orientation in Simulation*, European Simulation Symposium, Istanbul, 1994

BIBLIOGRAPHY

1. Sedgwick, H. J., Haydon T. F., *Launch and Recovery Techniques For RPVs*, 3th International Conference on RPV's, 1982
2. Shannon, R. E., *Systems Simulation, The Art and Science*, Prentice-Hall Inc., 1975
3. Craig, J. J., *Introduction to Robotics Mechanics and Control*, Second Edition, Addison-Wesley Publishing Company, 1989
4. Shabana, A. A., *Dynamics of Multibody Systems*, John Wiley & Sons Inc., 1989
5. Ginsberg, J. H., *Advanced Engineering Dynamics*, Harper & Row Inc., 1988
6. Huston, R. L., *Multibody Dynamics*, Butterworth-Heinemann, 1990
7. Thomasson, P. G., *The Development of a PC-based Real Time Simulator for UMA's*, 10th International Conference, Bristol, UK, March 1993
8. Thomasson, P. G., *A Method For the Analysis and Simulation of Discontinuous Systems*, *European Simulation Conference*, Delft, Oct. 25-28, 1993
9. Harris, C. J., *Six Degree of Freedom Simulation of the F-16A*, M.sc Thesis, College of Aeronautics, Cranfield University, 1992
10. Janson, A. H. J., *A Large Amplitude Real-time Simulation of the Hawker Mark 12* M.Sc Thesis, College of Aeronautics, Cranfield University, 1992
11. Khan, S., *Development of a Large Amplitude Six degree of Freedom Simulation of the Jetstream Aircraft*, M.Sc Thesis, College of Aeronautics, Cranfield University, Sept. 1988

12. Mullen, G. J., *The Initial Development of a Helicopter Continuous Simulation For Flight Control Application*, M.Sc Thesis, College of Aeronautics, Cranfield University, 1990
13. Becker, S. I., *The Development of a Helicopter Continuous Simulation*, M.Sc Thesis, College of Aeronautics, Cranfield University, Sept. 1991
14. Theodorsen, T., *Theory of Propellers*, McGraw-Hill Book Company, 1948
15. Glauert, H., *The Elements of Aerofoil and Airscrew Theory*, Second Edition, Cambridge at the University Press, 1959
16. Saunders, G. H., *Dynamics of Helicopter Flight*, John Wiley & Sons, 1975
17. Padfield, G. D., *A Theoretical Model of Helicopter Flight Mechanics For Application to Piloted Simulation*, RAE TR 81048, 1981
18. Gray, G. J., *Development and Validation of Nonlinear Models for Helicopter Dynamics*, Ph.D Thesis, University of Glasgow, 1992
19. Talbot, P. D., Bruce, E. T., Decker, W. A., Chen, R. T. N., *A Mathematical Model of a Single Main Rotor Helicopter For Piloted Simulation*, NASA-TM-84281, Sept. 1982
20. Johnson, W., benton, H. L., Jeffrey, V. B., *Calculated Performance, Stability and Manoeuvrability of High-speed Tilting-prop-rotor Aircraft*, NASA-TM-88349
21. Trebble, W. J. G., *Low speed Wind-Tunnel Tests on the X-RAE 2 Unmanned Aircraft in the RAE Wind Tunnel*, Royal Aircraft Establishment, Tech. Memo Aero 2048
22. Obert, E., *The Effect of Propeller Slipstream on the Static Longitudinal Stability and Control of Multi-Engined Propeller Aircraft*, ICAS-94-7.3.4

23. Klinar, W. J., Wilkes, L. F., *Dynamics Model Investigation of Two Tail-Sitter vertically Rising Airplane to Determine the Altitude Required to Approach Normal-Flight Conditions after Power Failure in Hovering Flight*, NACA RM L56H29a
24. Schade, R. O., *Flight-Test Investigation on the Langley Control-line Facility of a Model of a Propeller-Driven Tail-Sitter-Type Vertical-Take-Off Airplane With Delta Wing Rapid Transitions*, NACA TN 4070, 1957
25. Newsom, W. A., *Effect of Ground Proximity on the Aerodynamic Characteristics of a Four-Engined Vertical-Take-Off-and-Landing Transport-Airplane Model With Tilting Wing and Propellers*, NACA TN 4124, 1957
26. Lovell, P. M., Parlett L. P., *Transition-Flight Tests of a Model of a Low-Wing Transport Vertical-Take-Off Airplane With Tilting Wing and Propellers*, NACA TN 3745, 1956
27. Lovell, P. M., Parlett L. P., *Flight Tests of a Model of a High-Wing Transport Vertical-Take-Off Airplane With Tilting Wing and Propellers and With Jet Control at the Rear of the Fuselage for Pitch and Yaw Control*, NACA TN 3912, 1957
28. McKinney, M. O., Tostl, L. P., Davenport, E. E., *Dynamic Stability and Control Characteristics of a Cascade-Wing Vertically Rising Airplane Model in Take-Offs, Landings and Hovering Flight*, NACA TN 3198, 1954
29. McKinney, M. O., *NACA Research on VTOL and STOL Aeroplanes*, Sixth Anglo-American Aeronautical Conference, 1957
30. Lovell, P. M., Parlett L. P., *Effects of Wing Position and Vertical-Tail Configuration on Stability and Control Characteristics of A Jet-Powered Delta-Wing Vertically Rising Airplane Model*, NACA TN 3899, 1957
31. Banks, J., Gerstein, D. M., Searles S. P., *Verification and Validation of Large Scale Simulation Models*, Proceedings of UKSC Conference on Computer Simulation, Brighton, 5-7th Sept. 1990

32. Carson, E. R., Flood, R. L., *Model Validation: Philosophy, Methodology and Examples*, Transactions of the Institute of Measurement and Control, Vol. 12, No. 4, 1990
33. Bradley, R., Padfield G. D., *Validation of Helicopter Mathematical Models*, Transactions of the Institute of Measurement and Control, Vol. 12, No. 4, 1990
34. Gawthrop, P. J., Mirab, H., Li, X, *Robot Model Validation*, Transactions of the Institute of Measurement and Control, Vol. 12, No. 4, 1990

APPENDIX A1

The general form of the Newton's second law for translational and angular rotation of the body A , can be written as follows:[50]

$$\mathbf{F}_a^a = \frac{d}{dt}(\mathbf{P}_a^a) \quad (\text{A1.1})$$

$${}_o\mathbf{M}_a^a = \frac{d}{dt}({}_o\mathbf{H}_a^a) + \mathbf{V}_o^a \times \mathbf{P}_a^a \quad (\text{A1.2})$$

The total linear momentum of the body A can be expressed as follows:

$$\mathbf{P}_a^a = m_a \mathbf{V}_{ga}^a \quad (\text{A1.3})$$

where

$$\mathbf{V}_{ga}^a = \mathbf{V}_o^a + \boldsymbol{\Omega}_{ai}^a \times \mathbf{b}^a \quad (\text{A1.4})$$

substituting \mathbf{V}_{ga}^a in Equation (A1.3), then:

$$\mathbf{P}_a^a = m_a \mathbf{V}_o^a + m_a \boldsymbol{\Omega}_{ai}^a \times \mathbf{b}^a \quad (\text{A1.5})$$

Now, Equation (A1.1) can be written in the following form:

$$\mathbf{F}_a^a = \frac{d}{dt}(m_a \mathbf{V}_o^a + m_a \boldsymbol{\Omega}_{ai}^a \times \mathbf{b}^a) \quad (\text{A1.6})$$

Similarly, the total angular momentum of the body A about O can be expressed as follows:

$${}_o\mathbf{H}_a^a = {}_{g^a}\mathbf{H}_a^a + \mathbf{b}^a \times \mathbf{P}_a^a \quad (\text{A1.7})$$

where

$${}_{g^a}\mathbf{H}_a^a = [{}_{g^a}\mathbf{I}_a^a] \boldsymbol{\Omega}_{ai}^a \quad (\text{A1.8})$$

using Equations (A1.5) and (A1.8) and after simplification we have:

$${}_o\mathbf{H}_a^a = [{}_{g^a}\mathbf{I}_a^a] \boldsymbol{\Omega}_{ai}^a + m_a \mathbf{b}^a \times (\boldsymbol{\Omega}_{ai}^a \times \mathbf{b}^a) + m_a \mathbf{b}^a \times \mathbf{V}_o^a \quad (\text{A1.9})$$

According to parallel axis theorem [46]:

$$[{}_o\mathbf{I}_a^a] \boldsymbol{\Omega}_{ai}^a = [{}_{g^a}\mathbf{I}_a^a] \boldsymbol{\Omega}_{ai}^a + m_a \mathbf{b}^a \times (\boldsymbol{\Omega}_{ai}^a \times \mathbf{b}^a) \quad (\text{A1.10})$$

Now, using Equation (A1.10), Equation (A1.9) can be written as follows:

$${}_o\mathbf{H}_a^a = [{}_o\mathbf{I}_a^a] \boldsymbol{\Omega}_{ai}^a + m_a \mathbf{b}^a \times \mathbf{V}_o^a \quad (\text{A1.11})$$

Substituting ${}_o\mathbf{H}_a^a$ and \mathbf{P}_a^a from Equations (A1.11) and (A1.5) into Equation (A1.2), then:

$$\begin{aligned} {}_o\mathbf{M}_a^a &= \frac{d}{dt} \{ [{}_o\mathbf{I}_a^a] \boldsymbol{\Omega}_{ai}^a \} + \frac{d}{dt} (m_a \mathbf{b}^a \times \mathbf{V}_o^a) \\ &\quad + \mathbf{V}_o^a \times (m_a \mathbf{V}_o^a + m_a \boldsymbol{\Omega}_{ai}^a \times \mathbf{b}^a) \end{aligned} \quad (\text{A1.12})$$

$$\begin{aligned} &= \frac{d}{dt} \{ [{}_o\mathbf{I}_a^a] \boldsymbol{\Omega}_{ai}^a \} + m_a \frac{d}{dt} (\mathbf{b}^a) \times \mathbf{V}_o^a + m_a \mathbf{b}^a \times \frac{d}{dt} (\mathbf{V}_o^a) \\ &\quad + m_a \mathbf{V}_o^a \times \mathbf{V}_o^a + m_a \mathbf{V}_o^a \times (\boldsymbol{\Omega}_{ai}^a \times \mathbf{b}^a) \end{aligned} \quad (\text{A1.13})$$

where

$$m_a \mathbf{V}_o^a \times \mathbf{V}_o^a = 0 \quad (\text{A1.14})$$

and

$$\frac{d}{dt}(\mathbf{b}^a) = \dot{\mathbf{b}}^a + \boldsymbol{\Omega}_{ai}^a \times \mathbf{b}^a \quad (\text{A4.1.15})$$

The vector \mathbf{b}^a is fixed in the $X_a Y_a Z_a$ axes system, thus the time derivative of this vector w.r.t. this system (denoted by \bullet) is zero. Therefore

$$\frac{d}{dt}(\mathbf{b}^a) = \boldsymbol{\Omega}_{ai}^a \times \mathbf{b}^a \quad (\text{A1.16})$$

substituting the associated terms in Equation (A1.13) and note that:

$$(\boldsymbol{\Omega}_{ai}^a \times \mathbf{b}^a) \times \mathbf{V}_o^a = -\mathbf{V}_o^a \times (\boldsymbol{\Omega}_{ai}^a \times \mathbf{b}^a) \quad (\text{A1.17})$$

then,

$${}_o\mathbf{M}_a^a = \frac{d}{dt} \left\{ [{}_o\mathbf{I}_a^a] \boldsymbol{\Omega}_{ai}^a \right\} + m_a \mathbf{b}^a \times \frac{d}{dt}(\mathbf{V}_o^a) \quad (\text{A1.18})$$

The Equations (A1.6) and (A1.18) are used as starting point for the derivation of the equations of the motion of the body A in chapter four.

APPENDIX A2

The general form of the Newton's second law for translational and angular motion of the body ${}^{\kappa}r_p$ can be written as follows:[50]

$${}^{\kappa}\mathbf{F}_{np}^n = \frac{d}{dt}({}^{\kappa}\mathbf{P}_{np}^n) \quad (\text{A2.1})$$

$${}^{\kappa}\mathbf{M}_{J_2}^n = \frac{d}{dt}({}^{\kappa}\mathbf{H}_{np}^n) + {}^{\kappa}\mathbf{V}_{J_2}^n \times {}^{\kappa}\mathbf{P}_{np}^n \quad (\text{A2.2})$$

The total linear momentum of the body ${}^{\kappa}r_p$ is given by:

$${}^{\kappa}\mathbf{P}_{np}^n = {}^{\kappa}\mathbf{P}_n^n + {}^{\kappa}\mathbf{P}_p^n \quad (\text{A2.3})$$

where

$${}^{\kappa}\mathbf{P}_n^n = m_n {}^{\kappa}\mathbf{V}_{gn}^n \quad (\text{A2.4})$$

$${}^{\kappa}\mathbf{P}_p^n = m_p {}^{\kappa}\mathbf{V}_{gp}^n \quad (\text{A2.5})$$

$${}^{\kappa}\mathbf{V}_{gn}^n = {}^{\kappa}\mathbf{V}_{J_2}^n + {}^{\kappa}\boldsymbol{\Omega}_{ni}^n \times {}^{\kappa}\mathbf{k}_1^n \quad (\text{A2.6})$$

$${}^{\kappa}\mathbf{V}_{gp}^n = {}^{\kappa}\mathbf{V}_{J_2}^n + {}^{\kappa}\boldsymbol{\Omega}_{ni}^n \times {}^{\kappa}\mathbf{f}^n \quad (\text{A2.7})$$

Using Equations (A2.4), (A2.5), (A2.6) and (A2.7) and after simplification, the Equation (A2.3) can be expressed in following form:

$${}^{\kappa}\mathbf{P}_{np}^n = (m_n + m_p) {}^{\kappa}\mathbf{V}_{J_2}^n + {}^{\kappa}\boldsymbol{\Omega}_{ni}^n \times (m_n {}^{\kappa}\mathbf{k}_1^n + m_p {}^{\kappa}\mathbf{f}^n) \quad (\text{A2.8})$$

Now, using the relation:

$$m_n {}^{\kappa} \mathbf{k}_1^n + m_p {}^{\kappa} \mathbf{f}^n = m_{np} {}^{\kappa} \mathbf{e}^n \quad (\text{A2.9})$$

where

$$m_{np} = m_n + m_p \quad (\text{A2.10})$$

then

$${}^{\kappa} \mathbf{P}_{np}^n = m_{np} {}^{\kappa} \mathbf{V}_{J_1}^n + m_{np} {}^{\kappa} \boldsymbol{\Omega}_{ni}^n \times {}^{\kappa} \mathbf{e}^n \quad (\text{A2.11})$$

Substituting in Equation (A2.1) yields:

$${}^{\kappa} \mathbf{F}_{np}^n = \frac{d}{dt} (m_{np} {}^{\kappa} \mathbf{V}_{J_1}^n + m_{np} {}^{\kappa} \boldsymbol{\Omega}_{ni}^n \times {}^{\kappa} \mathbf{e}^n) \quad (\text{A2.12})$$

Similarly, the total angular momentum of the body ${}^{\kappa} np$ about J_2 can be expressed as follows:

$${}^{\kappa} \mathbf{H}_{np}^n = {}^{\kappa} \mathbf{H}_n^n + {}^{\kappa} \mathbf{H}_p^n \quad (\text{A2.13})$$

where

$${}^{\kappa} \mathbf{H}_n^n = {}^{\kappa} \mathbf{H}_{gn}^n + {}^{\kappa} \mathbf{k}_1^n \times {}^{\kappa} \mathbf{P}_n^n \quad (\text{A2.14})$$

$${}^{\kappa} \mathbf{H}_p^n = {}^{\kappa} \mathbf{H}_{gp}^n + {}^{\kappa} \mathbf{f}^n \times {}^{\kappa} \mathbf{P}_p^n \quad (\text{A2.15})$$

$${}^{\kappa} \mathbf{H}_{gn}^n = [{}^{\kappa} \mathbf{I}_n^n] {}^{\kappa} \boldsymbol{\Omega}_{ni}^n \quad (\text{A2.16})$$

$${}^{\kappa} \mathbf{H}_{gp}^n = [{}^{\kappa} \mathbf{I}_p^n] ({}^{\kappa} \boldsymbol{\Omega}_{ni}^n + {}^{\kappa} \boldsymbol{\Omega}_{pn}^n) \quad (\text{A2.17})$$

Using Equation (A2.4), (A2.5), (A2.6), (A2.7), (A2.14), (A2.15), (A2.16), (A2.17), and after simplification, Equation (A2.13) takes the following form:

$$\begin{aligned}
{}^{\kappa}H_{np}^n &= [{}^{\kappa}I_{gn}^n]{}^{\kappa}\Omega_{ni}^n + m_n {}^{\kappa}k1^n \times ({}^{\kappa}\Omega_{ni}^n \times {}^{\kappa}k1^n) \\
&+ [{}^{\kappa}I_{gp}^n]{}^{\kappa}\Omega_{ni}^n + m_p {}^{\kappa}f^n \times ({}^{\kappa}\Omega_{ni}^n \times {}^{\kappa}f^n) \\
&+ [{}^{\kappa}I_{gp}^n]{}^{\kappa}\Omega_{pn}^n + (m_n {}^{\kappa}k1^n + m_p {}^{\kappa}f^n) \times {}^{\kappa}V_{J_i}^n
\end{aligned} \tag{A2.18}$$

According to parallel axis theorem [46]:

$$[{}^{\kappa}I_{J_i}^n]{}^{\kappa}\Omega_{ni}^n = [{}^{\kappa}I_{gn}^n]{}^{\kappa}\Omega_{ni}^n + m_n {}^{\kappa}k1^n \times ({}^{\kappa}\Omega_{ni}^n \times {}^{\kappa}k1^n) \tag{A2.19}$$

$$[{}^{\kappa}I_{J_i}^n]{}^{\kappa}\Omega_{ni}^n = [{}^{\kappa}I_{gp}^n]{}^{\kappa}\Omega_{ni}^n + m_p {}^{\kappa}f^n \times ({}^{\kappa}\Omega_{ni}^n \times {}^{\kappa}f^n) \tag{A2.20}$$

Now, using Equations (A2.19), (A2.20) and (A2.9), Equation (A2.18) can be expressed as follows:

$${}^{\kappa}H_{np}^n = [{}^{\kappa}I_{J_i}^n]{}^{\kappa}\Omega_{ni}^n + [{}^{\kappa}I_{gp}^n]{}^{\kappa}\Omega_{pn}^n + m_{np} {}^{\kappa}e^n \times {}^{\kappa}V_{J_i}^n \tag{A2.21}$$

where

$$[{}^{\kappa}I_{J_i}^n] = [{}^{\kappa}I_{J_i}^n] + [{}^{\kappa}I_{J_i}^n] \tag{A2.22}$$

Using Equations (A2.21), (A2.11), Equation (A2.2) can be expressed in following form:

$$\begin{aligned}
{}^{\kappa}M_{np}^n &= \frac{d}{dt} \left\{ [{}^{\kappa}I_{J_i}^n]{}^{\kappa}\Omega_{ni}^n + [{}^{\kappa}I_{gp}^n]{}^{\kappa}\Omega_{pn}^n \right\} \\
&+ \frac{d}{dt} \left\{ m_{np} {}^{\kappa}e^n \times {}^{\kappa}V_{J_i}^n \right\}
\end{aligned} \tag{A2.23}$$

$$\begin{aligned}
&+ {}^{\kappa}V_{J_i}^n \times \left\{ m_{np} {}^{\kappa}V_{J_i}^n + m_{np} {}^{\kappa}\Omega_{ni}^n \times {}^{\kappa}e^n \right\} \\
&= \frac{d}{dt} \left\{ [{}^{\kappa}I_{J_i}^n]{}^{\kappa}\Omega_{ni}^n + [{}^{\kappa}I_{gp}^n]{}^{\kappa}\Omega_{pn}^n \right\} \\
&+ m_{np} \frac{d}{dt} ({}^{\kappa}e^n) \times {}^{\kappa}V_{J_i}^n + m_{np} {}^{\kappa}e^n \times \frac{d}{dt} ({}^{\kappa}V_{J_i}^n) \\
&+ m_{np} {}^{\kappa}V_{J_i}^n \times {}^{\kappa}V_{J_i}^n + m_{np} {}^{\kappa}V_{J_i}^n \times ({}^{\kappa}\Omega_{ni}^n \times {}^{\kappa}e^n)
\end{aligned} \tag{A2.24}$$

where

$$m_{np} {}^{\kappa} \mathbf{V}_{J_1}^n \times {}^{\kappa} \mathbf{V}_{J_1}^n = \mathbf{0} \quad (\text{A2.25})$$

and

$$\frac{d}{dt} ({}^{\kappa} \mathbf{e}^n) = {}^{\kappa} \dot{\mathbf{e}}^n + {}^{\kappa} \boldsymbol{\Omega}_{ni}^n \times {}^{\kappa} \mathbf{e}^n \quad (\text{A2.26})$$

The vector ${}^{\kappa} \mathbf{e}^n$ is fixed in the ${}^{\kappa} X_n {}^{\kappa} Y_n {}^{\kappa} Z_n$ axes system, thus the time derivative of this vector w.r.t. this system (denoted by \circ) is zero. Therefore:

$$\frac{d}{dt} ({}^{\kappa} \mathbf{e}^n) = {}^{\kappa} \boldsymbol{\Omega}_{ni}^n \times {}^{\kappa} \mathbf{e}^n \quad (\text{A2.27})$$

Substituting the associated terms in Equation (A2.24) and note that:

$$({}^{\kappa} \boldsymbol{\Omega}_{ni}^n \times {}^{\kappa} \mathbf{e}^n) \times {}^{\kappa} \mathbf{V}_{J_1}^n = -{}^{\kappa} \mathbf{V}_{J_1}^n \times ({}^{\kappa} \boldsymbol{\Omega}_{ni}^n \times {}^{\kappa} \mathbf{e}^n) \quad (\text{A2.28})$$

we have:

$$\begin{aligned} {}^{\kappa} \mathbf{M}_{J_1}^n = & \frac{d}{dt} \left\{ [{}^{\kappa} I_{np}^n] {}^{\kappa} \boldsymbol{\Omega}_{ni}^n + [{}^{\kappa} I_p^n] {}^{\kappa} \boldsymbol{\Omega}_{pn}^n \right\} \\ & + m_{np} {}^{\kappa} \mathbf{e}^n \times \frac{d}{dt} ({}^{\kappa} \mathbf{V}_{J_1}^n) \end{aligned} \quad (\text{A2.29})$$

The Equations (A2.12) and (A2.29) are used as starting point for the derivation of the equations of motion of the body ${}^{\kappa} np$ in chapter four.

APPENDIX A3

The general form of the Newton's second law for angular motion of the body ${}^{\kappa}p$ can be written as follows:[50]

$${}^{\kappa}M_{sp}^n = \frac{d}{dt}({}^{\kappa}H_p^n) \quad (\text{A3.1})$$

where

$${}^{\kappa}H_p^n = [{}^{\kappa}I_p^n]({}^{\kappa}\Omega_{ni}^n + {}^{\kappa}\Omega_{pn}^n) \quad (\text{A3.2})$$

Thus Equation (A3.1) can be expressed in the following form:

$${}^{\kappa}M_{sp}^n = \frac{d}{dt} \left\{ [{}^{\kappa}I_p^n]({}^{\kappa}\Omega_{ni}^n + {}^{\kappa}\Omega_{pn}^n) \right\} \quad (\text{A3.3})$$

APPENDIX A4

In this appendix, it is attempted to present the derivation of the aircraft equations of motion in complete detail so that they will always be available for the readers who wish to follow the equations in more detail. Before starting with the kinetic of the system some kinematic relationships must be derived.

A4.1 KINEMATIC RELATIONS

The absolute angular velocity of the ${}^{\kappa}X_n {}^{\kappa}Y_n {}^{\kappa}Z_n$ axes system can be expressed in terms of absolute angular velocity of the $X_a Y_a Z_a$ axes system and relative angular velocity of the axes system ${}^{\kappa}X_n {}^{\kappa}Y_n {}^{\kappa}Z_n$ w.r.t. $X_a Y_a Z_a$ axes system as follows:

$${}^{\kappa}\Omega_{ni}^n = {}^{\kappa}\Omega_{ai}^n + {}^{\kappa}\Omega_{na}^n \quad (\text{A4.1})$$

$$= {}^{\kappa}[DCM]^{na} \Omega_{ai}^a + {}^{\kappa}\Omega_{na}^a \quad (\text{A4.2})$$

then

$${}^{\kappa}\dot{\Omega}_{ni}^n = {}^{\kappa}\dot{\Omega}_{ai}^n + {}^{\kappa}\dot{\Omega}_{na}^n \quad (\text{A4.3})$$

$$= \left({}^{\kappa}[DCM]^{na} \dot{\Omega}_{ai}^a \right) + {}^{\kappa}\dot{\Omega}_{na}^a \quad (\text{A4.4})$$

Now, performing differentiation presented in Equation (4.6b)

$${}^{\kappa}\dot{\Omega}_{ni}^n = {}^{\kappa}[DCM]^{na} \dot{\Omega}_{ai}^a + {}^{\kappa}[DCM]^{na} \dot{\Omega}_{ai}^a + {}^{\kappa}\dot{\Omega}_{na}^n \quad (A4.5)$$

and using relation (4.5b), then:

$${}^{\kappa}\dot{\Omega}_{ni}^n = {}^{\kappa}C1 + {}^{\kappa}[DCM]^{na} \dot{\Omega}_{ai}^a + {}^{\kappa}\dot{\Omega}_{na}^n \quad (A4.6)$$

where

$${}^{\kappa}C1 = -[{}^{\kappa}\Omega_{na}^n] [{}^{\kappa}DCM]^{na} \Omega_{ai}^a \quad (A4.7)$$

Similarly,

$${}^{\kappa}V_{ji}^n = {}^{\kappa}V_{ji}^n = {}^{\kappa}[DCM]^{na} {}^{\kappa}V_{ji}^a \quad (A4.8)$$

where

$${}^{\kappa}V_{ji}^a = V_o^a + \Omega_{ai}^a \times {}^{\kappa}d^a \quad (A4.9)$$

therefore,

$${}^{\kappa}V_{ji}^n = {}^{\kappa}V_{ji}^n = {}^{\kappa}[DCM]^{na} V_o^a + {}^{\kappa}[DCM]^{na} [\Omega_{ai}^a] {}^{\kappa}d^a \quad (A4.10)$$

Differentiation of Equation (A4.8) according to relation (4.6b) gives:

$${}^{\kappa}\dot{V}_{ji}^n = {}^{\kappa}\dot{V}_{ji}^n = ({}^{\kappa}\dot{[DCM]}^{na} {}^{\kappa}V_{ji}^a) \quad (A4.11)$$

$$= {}^{\kappa}\dot{[DCM]}^{na} {}^{\kappa}V_{ji}^a + {}^{\kappa}[DCM]^{na} \dot{V}_{ji}^a \quad (A4.12)$$

using relation (4.5b) and (A4.9), then:

$${}^{\kappa}\dot{V}_{ji}^n = {}^{\kappa}\dot{V}_{ji}^n = {}^{\kappa}C2 + {}^{\kappa}[DCM]^{na} \dot{V}_o^a - {}^{\kappa}[DCM]^{na} [{}^{\kappa}d^a] \dot{\Omega}_{ai}^a \quad (A4.13)$$

where

$${}^{\kappa}C2 = -[{}^{\kappa}\Omega_{na}^n] [{}^{\kappa}DCM]^{na} {}^{\kappa}V_{ji}^a \quad (A4.14)$$

A4.2 EQUATIONS OF MOTION OF THE BODY A

Starting with the Equations (A1.6) and (A1.18), we have:

$$\mathbf{F}_a^a = \frac{d}{dt}(m_a \mathbf{V}_o^a + m_a \boldsymbol{\Omega}_{ai}^a \times \mathbf{b}^a) \quad (\text{A4.15})$$

$${}_o\mathbf{M}_a^a = \frac{d}{dt} \left\{ [{}_o\mathbf{I}_a^a] \boldsymbol{\Omega}_{ai}^a \right\} + m_a \mathbf{b}^a \times \frac{d}{dt}(\mathbf{V}_o^a) \quad (\text{A4.16})$$

then, expanding the derivatives by using (4.6a) we have:

$$\begin{aligned} \mathbf{F}_a^a &= m_a \dot{\mathbf{V}}_o^a + m_a \boldsymbol{\Omega}_{ai}^a \times \mathbf{V}_o^a + m_a (\dot{\boldsymbol{\Omega}}_{ai}^a \times \mathbf{b}^a + \boldsymbol{\Omega}_{ai}^a \times \dot{\mathbf{b}}^a) \\ &+ m_a \boldsymbol{\Omega}_{ai}^a \times (\boldsymbol{\Omega}_{ai}^a \times \mathbf{b}^a) \end{aligned} \quad (\text{A4.17})$$

$$\begin{aligned} {}_o\mathbf{M}_a^a &= [{}_o\mathbf{I}_a^a] \dot{\boldsymbol{\Omega}}_{ai}^a + \boldsymbol{\Omega}_{ai}^a \times ([{}_o\mathbf{I}_a^a] \boldsymbol{\Omega}_{ai}^a) + m_a \mathbf{b}^a \times \dot{\mathbf{V}}_o^a \\ &+ m_a \mathbf{b}^a \times (\boldsymbol{\Omega}_{ai}^a \times \mathbf{V}_o^a) \end{aligned} \quad (\text{A4.18})$$

Considering the fact that $\dot{\mathbf{b}}^a = \mathbf{0}$ and by expressing the \mathbf{F}_a^a and ${}_o\mathbf{M}_a^a$ in terms of their components :

$$\mathbf{F}_a^a = \mathbf{W}_a^a + \mathbf{A}_a^a - {}^r\mathbf{F}_{J_i}^a - {}^l\mathbf{F}_{J_i}^a \quad (\text{A4.19})$$

$${}_o\mathbf{M}_a^a = {}_o\mathbf{M}_{W_a}^a + {}_o\mathbf{M}_{A_a}^a - {}^r\mathbf{M}_{J_i}^a - {}^l\mathbf{M}_{J_i}^a - {}^r\mathbf{d}^a \times {}^r\mathbf{F}_{J_i}^a - {}^l\mathbf{d}^a \times {}^l\mathbf{F}_{J_i}^a \quad (\text{A4.20})$$

and substituting in the Equations (A4.17) and (A4.18) then the main body equations of motion take the following forms:

$$\begin{aligned} \mathbf{W}_a^a + \mathbf{A}_a^a - {}^r\mathbf{F}_{J_i}^a - {}^l\mathbf{F}_{J_i}^a &= m_a \dot{\mathbf{V}}_o^a + m_a \boldsymbol{\Omega}_{ai}^a \times \mathbf{V}_o^a \\ &+ m_a \dot{\boldsymbol{\Omega}}_{ai}^a \times \mathbf{b}^a + m_a \boldsymbol{\Omega}_{ai}^a \times (\boldsymbol{\Omega}_{ai}^a \times \mathbf{b}^a) \end{aligned} \quad (\text{A4.21})$$

$$\begin{aligned} {}_o\mathbf{M}_{W_a}^a + {}_o\mathbf{M}_{A_a}^a - {}^r\mathbf{M}_{J_i}^a - {}^l\mathbf{M}_{J_i}^a - {}^r\mathbf{d}^a \times {}^r\mathbf{F}_{J_i}^a - {}^l\mathbf{d}^a \times {}^l\mathbf{F}_{J_i}^a &= \\ [{}_o\mathbf{I}_a^a] \dot{\boldsymbol{\Omega}}_{ai}^a + \boldsymbol{\Omega}_{ai}^a \times ([{}_o\mathbf{I}_a^a] \boldsymbol{\Omega}_{ai}^a) &+ m_a \mathbf{b}^a \times \dot{\mathbf{V}}_o^a + m_a \mathbf{b}^a \times (\boldsymbol{\Omega}_{ai}^a \times \mathbf{V}_o^a) \end{aligned} \quad (\text{A4.22})$$

Using the matrix form of the cross-product expressed in (4.3), Equations (A4.21) and (A4.22) can be expressed as follows:

$$\begin{aligned} W_a^a + A_a^a - {}^r F_{J_1}^a - {}^l F_{J_1}^a = m_a \dot{V}_o^a - m_a [b^a] \dot{\Omega}_{ai}^a \\ + m_a [\Omega_{ai}^a] V_o^a + m_a [\Omega_{ai}^a] [\Omega_{ai}^a] b^a \end{aligned} \quad (A4.23)$$

$$\begin{aligned} {}_o M_{W_a}^a + {}_o M_{A_a}^a - {}^r M_{J_1}^a - {}^l M_{J_1}^a - [{}^r d^a] {}^r F_{J_1}^a - [{}^l d^a] {}^l F_{J_1}^a = \\ [{}_o I_a^a] \dot{\Omega}_{ai}^a + m_a [b^a] \dot{V}_o^a + [\Omega_{ai}^a] [{}_o I_a^a] \Omega_{ai}^a + m_a [b^a] [\Omega_{ai}^a] V_o^a \end{aligned} \quad (A4.24)$$

A4.3 EQUATIONS OF MOTION OF THE BODY ${}^k np$

For the body ${}^k np$ starting with Equations (A2.12) and (A2.29), we have:

$${}^k F_{np}^n = \frac{d}{dt} (m_{np} {}^k V_{J_2}^n + m_{np} {}^k \Omega_{ni}^n \times {}^k e^n) \quad (A4.25)$$

$$\begin{aligned} {}_{J_2}^k M_{np}^n = \frac{d}{dt} \left\{ [{}_{J_2}^k I_{np}^n] {}^k \Omega_{ni}^n + [{}_{gp}^k I_p^n] {}^k \Omega_{pn}^n \right\} \\ + m_{np} {}^k e^n \times \frac{d}{dt} ({}^k V_{J_2}^n) \end{aligned} \quad (A4.26)$$

Expanding time derivatives by using Equation 4.6b yields:

$$\begin{aligned} {}^k F_{np}^n = m_{np} {}^k \dot{V}_{J_2}^n + m_{np} {}^k \Omega_{ni}^n \times {}^k V_{J_2}^n + m_{np} ({}^k \dot{\Omega}_{ni}^n \times {}^k e^n + {}^k \Omega_{ni}^n \times {}^k \dot{e}^n) \\ + m_{np} {}^k \Omega_{ni}^n \times ({}^k \Omega_{ni}^n \times {}^k e^n) \end{aligned} \quad (A4.27)$$

$$\begin{aligned} {}_{J_2}^k M_{np}^n = [{}_{J_2}^k I_{np}^n] {}^k \dot{\Omega}_{ni}^n + [{}_{gp}^k I_p^n] {}^k \dot{\Omega}_{pn}^n + {}^k \Omega_{ni}^n \times ([{}_{J_2}^k I_{np}^n] {}^k \Omega_{ni}^n) + {}^k \Omega_{ni}^n \times ([{}_{gp}^k I_p^n] {}^k \Omega_{pn}^n) \\ + m_{np} {}^k e^n \times ({}^k \dot{V}_{J_2}^n + {}^k \Omega_{ni}^n \times {}^k V_{J_2}^n) \end{aligned} \quad (A4.28)$$

Considering the fact that ${}^k \dot{e}^n = 0$ and by expressing the ${}^k F_{np}^n$ and ${}_{J_2}^k M_{np}^n$ in terms of components

$${}^k F_{np}^n = {}^k T^n + {}^k W_{np}^n + {}^k \Lambda_{np}^n + {}^k F_{J_1}^n \quad (A4.29)$$

$${}^{\kappa}M_{np}^n = {}^{\kappa}M_{pc}^n + {}^{\kappa}M_T^n + {}^{\kappa}M_{W_{wp}}^n + {}^{\kappa}M_{A_{wp}}^n + {}^{\kappa}M_{J_1}^n \quad (\text{A4.30})$$

and substituting in the Equations (A4.27) and (A4.28), the equations of motion of the body ${}^{\kappa}np$ take the following form:

$$\begin{aligned} {}^{\kappa}F_{J_1}^n &= m_{np} {}^{\kappa}\dot{V}_{J_1}^n + m_{np} {}^{\kappa}\Omega_{ni}^n \times {}^{\kappa}V_{J_1}^n + m_{np} {}^{\kappa}\dot{\Omega}_{ni}^n \times {}^{\kappa}e^n \\ &+ m_{np} {}^{\kappa}\Omega_{ni}^n \times ({}^{\kappa}\Omega_{ni}^n \times {}^{\kappa}e^n) - {}^{\kappa}T^n - {}^{\kappa}W_{np}^n - {}^{\kappa}A_{np}^n \end{aligned} \quad (\text{A4.31})$$

$$\begin{aligned} {}^{\kappa}M_{J_1}^n &= [{}^{\kappa}I_{np}^n] {}^{\kappa}\dot{\Omega}_{ni}^n + [{}^{\kappa}I_p^n] {}^{\kappa}\dot{\Omega}_{pn}^n + {}^{\kappa}\Omega_{ni}^n \times ([{}^{\kappa}I_{np}^n] {}^{\kappa}\Omega_{ni}^n) + {}^{\kappa}\Omega_{ni}^n \times ([{}^{\kappa}I_p^n] {}^{\kappa}\Omega_{pn}^n) \\ &+ m_{np} {}^{\kappa}e^n \times {}^{\kappa}\dot{V}_{J_1}^n + m_{np} {}^{\kappa}e^n \times ({}^{\kappa}\Omega_{ni}^n \times {}^{\kappa}V_{J_1}^n) - {}^{\kappa}M_{pc}^n - {}^{\kappa}M_T^n - {}^{\kappa}M_{W_{wp}}^n - {}^{\kappa}M_{A_{wp}}^n \end{aligned} \quad (\text{A4.32})$$

Using the matrix form of the cross-product expressed in (4.3), Equations (A4.27) and (A4.28) can be expressed as follows:

$$\begin{aligned} {}^{\kappa}F_{J_1}^n &= m_{np} {}^{\kappa}\dot{V}_{J_1}^n - m_{np} [{}^{\kappa}e^n] {}^{\kappa}\dot{\Omega}_{ni}^n + m_{np} [{}^{\kappa}\Omega_{ni}^n] {}^{\kappa}V_{J_1}^n \\ &+ m_{np} [{}^{\kappa}\Omega_{ni}^n] [{}^{\kappa}\Omega_{ni}^n] {}^{\kappa}e^n - {}^{\kappa}T^n - {}^{\kappa}W_{np}^n - {}^{\kappa}A_{np}^n \end{aligned} \quad (\text{A4.33})$$

$$\begin{aligned} {}^{\kappa}M_{J_1}^n &= [{}^{\kappa}I_{np}^n] {}^{\kappa}\dot{\Omega}_{ni}^n + [{}^{\kappa}I_p^n] {}^{\kappa}\dot{\Omega}_{pn}^n + m_{np} [{}^{\kappa}e^n] {}^{\kappa}\dot{V}_{J_1}^n + [{}^{\kappa}\Omega_{ni}^n] [{}^{\kappa}I_{np}^n] {}^{\kappa}\Omega_{ni}^n + [{}^{\kappa}\Omega_{ni}^n] [{}^{\kappa}I_p^n] {}^{\kappa}\Omega_{pn}^n \\ &+ m_{np} [{}^{\kappa}e^n] [{}^{\kappa}\Omega_{ni}^n] {}^{\kappa}V_{J_1}^n - {}^{\kappa}M_{pc}^n - {}^{\kappa}M_T^n - {}^{\kappa}M_{W_{wp}}^n - {}^{\kappa}M_{A_{wp}}^n \end{aligned} \quad (\text{A4.34})$$

Now, by defining

$${}^{\kappa}C3 = m_{np} [{}^{\kappa}\Omega_{ni}^n] {}^{\kappa}V_{J_1}^n + m_{np} [{}^{\kappa}\Omega_{ni}^n] [{}^{\kappa}\Omega_{ni}^n] {}^{\kappa}e^n - {}^{\kappa}T^n - {}^{\kappa}W_{np}^n - {}^{\kappa}A_{np}^n \quad (\text{A4.35})$$

$$\begin{aligned} {}^{\kappa}C4 &= [{}^{\kappa}\Omega_{ni}^n] [{}^{\kappa}I_{np}^n] {}^{\kappa}\Omega_{ni}^n + [{}^{\kappa}\Omega_{ni}^n] [{}^{\kappa}I_p^n] {}^{\kappa}\Omega_{pn}^n \\ &+ m_{np} [{}^{\kappa}e^n] [{}^{\kappa}\Omega_{ni}^n] {}^{\kappa}V_{J_1}^n - {}^{\kappa}M_{pc}^n - {}^{\kappa}M_T^n - {}^{\kappa}M_{W_{wp}}^n - {}^{\kappa}M_{A_{wp}}^n \end{aligned} \quad (\text{A4.36})$$

Equation (A4.33) and (A4.34) can be written as follows:

$${}^{\kappa}F_{J_i}^n = m_{np} {}^{\kappa}\dot{V}_{J_i}^n - m_{np} [{}^{\kappa}e^n] {}^{\kappa}\dot{\Omega}_{ni}^n + {}^{\kappa}C3 \quad (A4.37)$$

$${}^{\kappa}M_{J_i}^n = [{}^{\kappa}I_{J_i np}^n] {}^{\kappa}\dot{\Omega}_{ni}^n + [{}^{\kappa}I_{gp}^n] {}^{\kappa}\dot{\Omega}_{pn}^n + m_{np} [{}^{\kappa}e^n] {}^{\kappa}\dot{V}_{J_i}^n + {}^{\kappa}C4 \quad (A4.38)$$

Substituting the ${}^{\kappa}\dot{\Omega}_{ni}^n$ and ${}^{\kappa}\dot{V}_{J_i}^n$ from Equations (A4.6) and (A4.13) in Equation (A4.37), then :

$${}^{\kappa}F_{J_i}^n = {}^{\kappa}C5 + [{}^{\kappa}C6] \dot{V}_o^a + [{}^{\kappa}C7] \dot{\Omega}_{ai}^a + [{}^{\kappa}C8] {}^{\kappa}\dot{\Omega}_{na}^n \quad (A4.39)$$

where

$${}^{\kappa}C5 = m_{np} {}^{\kappa}C2 - m_{np} [{}^{\kappa}e^n] {}^{\kappa}C1 + {}^{\kappa}C3 \quad (A4.40)$$

$$[{}^{\kappa}C6] = m_{np} {}^{\kappa}[DCM]^{na} \quad (A4.41)$$

$$\begin{aligned} [{}^{\kappa}C7] &= -m_{np} {}^{\kappa}[DCM]^{na} [{}^{\kappa}d^a] - m_{np} [{}^{\kappa}e^n] {}^{\kappa}[DCM]^{na} \\ &= -[{}^{\kappa}C6][{}^{\kappa}d^a] - [{}^{\kappa}e^n] [{}^{\kappa}C6] \end{aligned} \quad (A4.42)$$

$$[{}^{\kappa}C8] = -m_{np} [{}^{\kappa}e^n] \quad (A4.43)$$

Similarly, using Equations (A4.6) and (A4.13), then Equation (A4.38) can be written in the following form:

$${}^{\kappa}M_{J_i}^n = {}^{\kappa}C9 + [{}^{\kappa}C10] \dot{V}_o^a + [{}^{\kappa}C11] \dot{\Omega}_{ai}^a + [{}^{\kappa}I_{J_i np}^n] {}^{\kappa}\dot{\Omega}_{na}^n + [{}^{\kappa}I_{gp}^n] {}^{\kappa}\dot{\Omega}_{pn}^n \quad (A4.44)$$

where

$$\begin{aligned} {}^{\kappa}C9 &= [{}^{\kappa}I_{J_i np}^n] {}^{\kappa}C1 + m_{np} [{}^{\kappa}e^n] {}^{\kappa}C2 + {}^{\kappa}C4 \\ &= [{}^{\kappa}I_{J_i np}^n] {}^{\kappa}C1 - [{}^{\kappa}C8] {}^{\kappa}C2 + {}^{\kappa}C4 \end{aligned} \quad (A4.45)$$

$${}^{\kappa}C10 = m_{np} [{}^{\kappa}e^n] {}^{\kappa}[DCM]^{na} = [{}^{\kappa}e^n] [{}^{\kappa}C6] \quad (A4.46)$$

$$\begin{aligned} {}^{\kappa}C11 &= [{}^{\kappa}I_{np}^n] {}^{\kappa}[DCM]^{na} - m_{np} [{}^{\kappa}e^n] {}^{\kappa}[DCM]^{na} [{}^{\kappa}d^a] \\ &= [{}^{\kappa}I_{np}^n] {}^{\kappa}[DCM]^{na} - [{}^{\kappa}e^n] [{}^{\kappa}C6] [{}^{\kappa}d^a] \end{aligned} \quad (A4.47)$$

Now, using the following relationships

$${}^{\kappa}F_{j_i}^a = {}^{\kappa}[DCM]^{na} {}^{\kappa}F_{j_i}^n \quad (A4.48)$$

$${}^{\kappa}M_{j_i}^a = {}^{\kappa}[DCM]^{na} {}^{\kappa}M_{j_i}^n \quad (A4.49)$$

Equations (A4.39) and (A4.44) can be written as follows:

$${}^{\kappa}F_{j_i}^a = {}^{\kappa}C12 + [{}^{\kappa}C13] \dot{V}_o^a + [{}^{\kappa}C14] \dot{\Omega}_{ai}^a + [{}^{\kappa}C15] {}^{\kappa} \dot{\Omega}_{na}^n \quad (A4.50)$$

$${}^{\kappa}M_{j_i}^a = {}^{\kappa}C16 + [{}^{\kappa}C17] \dot{V}_o^a + [{}^{\kappa}C18] \dot{\Omega}_{ai}^a + [{}^{\kappa}C19] {}^{\kappa} \dot{\Omega}_{na}^n + [{}^{\kappa}C20] {}^{\kappa} \dot{\Omega}_{pn}^n \quad (A4.51)$$

where

$${}^{\kappa}C12 = {}^{\kappa}[DCM]^{na} {}^{\kappa}C5$$

$$[{}^{\kappa}C13] = {}^{\kappa}[DCM]^{na} [{}^{\kappa}C6]$$

(A4.52)

$$[{}^{\kappa}C14] = {}^{\kappa}[DCM]^{na} [{}^{\kappa}C7]$$

$$[{}^{\kappa}C15] = {}^{\kappa}[DCM]^{na} [{}^{\kappa}C8]$$

$${}^{\kappa}C16 = {}^{\kappa}[DCM]^{pn} {}^{\kappa}C9$$

$$[{}^{\kappa}C17] = {}^{\kappa}[DCM]^{an} [{}^{\kappa}C10]$$

$$[{}^{\kappa}C18] = {}^{\kappa}[DCM]^{an} [{}^{\kappa}C11] \quad (A4.53)$$

$$[{}^{\kappa}C19] = {}^{\kappa}[DCM]^{an} [{}^{\kappa}I_{J_i}^n]$$

$$[{}^{\kappa}C20] = {}^{\kappa}[DCM]^{an} [{}^{\kappa}I_{sp}^n]$$

Using Equation (A4.50) the term $[{}^{\kappa}d^a] {}^{\kappa}F_{J_i}^a$ in Equation (A4.24) can be expressed in the following form:

$$[{}^{\kappa}d^a] {}^{\kappa}F_{J_i}^a = {}^{\kappa}C21 + [{}^{\kappa}C22] \dot{V}_o^a + [{}^{\kappa}C23] \dot{\Omega}_{ai}^a + [{}^{\kappa}C24] {}^{\kappa}\dot{\Omega}_{na}^n \quad (A4.54)$$

$${}^{\kappa}C21 = [{}^{\kappa}d^a] {}^{\kappa}C12$$

$$[{}^{\kappa}C22] = [{}^{\kappa}d^a] [{}^{\kappa}C13]$$

$$[{}^{\kappa}C23] = [{}^{\kappa}d^a] [{}^{\kappa}C14]$$

$$[{}^{\kappa}C24] = [{}^{\kappa}d^a] [{}^{\kappa}C15]$$

(A4.55)

Now, using Equations (A4.50), (A4.51) and (A4.54) to substitute the associated terms in Equations (A4.23) and (A4.24), then:

$$\begin{aligned} W_a^a + A_a^a - {}^rC12 - [{}^rC13] \dot{V}_o^a - [{}^rC14] \dot{\Omega}_{ai}^a - [{}^rC15] {}^r\dot{\Omega}_{na}^n \\ - {}^lC12 - [{}^lC13] \dot{V}_o^a - [{}^lC14] \dot{\Omega}_{ai}^a - [{}^lC15] {}^l\dot{\Omega}_{na}^n = m_a \dot{V}_o^a - m_a [b^a] \dot{\Omega}_{ai}^a + C25 \end{aligned}$$

(A4.56)

$$\begin{aligned}
& {}_oM_{W_o}^a + {}_oM_{A_o}^a - {}^rC16 - [{}^rC17]\dot{V}_o^a - [{}^rC18]\dot{\Omega}_{ai}^a - [{}^rC19]{}^r\dot{\Omega}_{na}^n - [{}^rC20]{}^r\dot{\Omega}_{pn}^n \\
& - {}^lC16 - [{}^lC17]\dot{V}_o^a - [{}^lC18]\dot{\Omega}_{ai}^a - [{}^lC19]{}^l\dot{\Omega}_{na}^n - [{}^lC20]{}^l\dot{\Omega}_{pn}^n \\
& - {}^rC21 - [{}^rC22]\dot{V}_o^a - [{}^rC23]\dot{\Omega}_{ai}^a - [{}^rC24]{}^r\dot{\Omega}_{na}^n \\
& - {}^lC21 - [{}^lC22]\dot{V}_o^a - [{}^lC23]\dot{\Omega}_{ai}^a - [{}^lC24]{}^l\dot{\Omega}_{na}^n \\
& = [{}_oI_a^a]\dot{\Omega}_{ai}^a + m_a[b^a]\dot{V}_o^a + C26
\end{aligned} \tag{A4.57}$$

where

$$C25 = m_a[\Omega_{ai}^a]V_o^a + m_a[\Omega_{ai}^a][\Omega_{ai}^a]b^a \tag{A4.58}$$

$$C26 = [\Omega_{ai}^a][{}_oI_a^a]\dot{\Omega}_{ai}^a + m_a[b^a][\Omega_{ai}^a]V_o^a \tag{A4.59}$$

In more simplified form the Equations (A4.56) and (A4.57) can be expressed in terms of the selected state variables as follows:

$$[C27]\dot{V}_o^a + [C28]\dot{\Omega}_{ai}^a + [{}^rC15]{}^r\dot{\Omega}_{na}^n + [{}^lC15]{}^l\dot{\Omega}_{na}^n = C29 \tag{A4.60}$$

$$[C30]\dot{V}_o^a + [C31]\dot{\Omega}_{ai}^a + [{}^rC32]{}^r\dot{\Omega}_{na}^n + [{}^lC32]{}^l\dot{\Omega}_{na}^n + [{}^rC20]{}^r\dot{\Omega}_{pn}^n + [{}^lC20]{}^l\dot{\Omega}_{pn}^n = C33 \tag{A4.61}$$

where

$$\begin{aligned}
[C27] &= m[1] + [{}^rC13] + [{}^lC13] \\
[C28] &= -m_a[b^a] + [{}^rC14] + [{}^lC14]
\end{aligned} \tag{A4.62}$$

$$C29 = W_a^a + A_a^a - {}^rC12 - {}^lC12 - C25$$

$$[C30] = m_a [b^a] + [{}^r C22] + [{}^l C22] + [{}^r C17] + [{}^l C17]$$

$$[C31] = [{}^o I_a^a] + [{}^r C23] + [{}^l C23] + [{}^r C18] + [{}^l C18]$$

(A4.63)

$$[{}^k C32] = [{}^k C24] + [{}^k C19]$$

$$C33 = {}^o M_{W_a}^a + {}^o M_{A_a}^a - {}^r C16 - {}^l C16 - {}^r C21 - {}^l C21 - C26$$

A4.4 EQUATIONS OF MOTION OF THE BODY ${}^k P$

For the body ${}^k P$, we only need the angular equations of motion. Therefore, starting with Equation (A3.3) we have:

$${}^k M_P^n = \frac{d}{dt} \left\{ [{}^k I_P^n] ({}^k \Omega_{ni}^n + {}^k \Omega_{pn}^n) \right\} \quad (A4.64)$$

Expanding the derivatives by using Equation (4.6a) and using matrix representation of cross-product, Equation (A4.64) will take the following form:

$${}^k M_P^n = [{}^k I_P^n] {}^k \dot{\Omega}_{ni}^n + [{}^k I_P^n] {}^k \dot{\Omega}_{pn}^n + [{}^k \Omega_{ni}^n] [{}^k I_P^n] {}^k \Omega_{ni}^n + [{}^k \Omega_{ni}^n] [{}^k I_P^n] {}^k \Omega_{pn}^n \quad (A4.65)$$

${}^k M_P^n$ can be expressed in terms of components as follows:

$${}^k M_P^n = {}^k M_{PC}^n + {}^k M_J^n + {}^k M_{W_p}^n + {}^k M_{A_p}^n + {}^k M_{J_i}^n \quad (A4.66)$$

substituting in Equation (A4.65) yields:

$${}^k M_{J_i}^n = [{}^k I_P^n] {}^k \dot{\Omega}_{ni}^n + [{}^k I_P^n] {}^k \dot{\Omega}_{pn}^n + C34 \quad (A4.67)$$

where

$$C34 = \left[{}^{\kappa} \Omega_{ni}^n \right] \left[{}^{\kappa} I_p^n \right] \left({}^{\kappa} \Omega_{ni}^n + {}^{\kappa} \Omega_{pn}^n \right) - {}^{\kappa} M_{pc}^n - {}^{\kappa} M_T^n - {}^{\kappa} M_{W_p}^n - {}^{\kappa} M_{A_p}^n \quad (A4.68)$$

Now, using Equation (A4.6) to substitute for ${}^{\kappa} \dot{\Omega}_{ni}^n$ in Equation (A4.67), then:

$${}^{\kappa} M_{j_i}^n = {}^{\kappa} C35 + [{}^{\kappa} C36] \dot{\Omega}_{ai}^a + [{}^{\kappa} I_p^n] {}^{\kappa} \dot{\Omega}_{na}^n + [{}^{\kappa} I_p^n] {}^{\kappa} \dot{\Omega}_{pn}^n \quad (A4.69)$$

where

$${}^{\kappa} C35 = [{}^{\kappa} I_p^n] {}^{\kappa} C1 + {}^{\kappa} C34 \quad (A4.70)$$

$$[{}^{\kappa} C36] = [{}^{\kappa} I_p^n] [DCM]^{na}$$

A4.5 EQUATIONS OF MOTION OF THE AIRCRAFT MULTIBODY SYSTEM

Using Equations (A4.60), (A4.61), (A4.44) for right and left side and (A4.69) for right and left side, the general equations of motion of the aircraft multibody system can be expressed in matrix form as follows:

$$\begin{bmatrix} [C27] & [C28] & [{}^r C15] & [{}^l C15] & [0] & [0] \\ [C30] & [C31] & [{}^r C32] & [{}^l C32] & [{}^r C20] & [{}^l C20] \\ [{}^r C10] & [{}^r C11] & [{}^r I_{np}^n] & [0] & [{}^r I_p^n] & [0] \\ [{}^l C10] & [{}^l C11] & [0] & [{}^l I_{np}^n] & [0] & [{}^l I_p^n] \\ [0] & [{}^r C36] & [{}^r I_p^n] & [0] & [{}^r I_p^n] & [0] \\ [0] & [{}^l C36] & [0] & [{}^l I_p^n] & [0] & [{}^l I_p^n] \end{bmatrix} \begin{bmatrix} \dot{V}_o^a \\ \dot{\Omega}_{ai}^a \\ \dot{\Omega}_{na}^n \\ \dot{\Omega}_{na}^n \\ \dot{\Omega}_{pn}^n \\ \dot{\Omega}_{pn}^n \end{bmatrix} = \begin{bmatrix} C29 \\ C33 \\ -{}^r C9 + {}^r M_{j_i}^n \\ -{}^l C9 + {}^l M_{j_i}^n \\ -{}^r C35 + {}^r M_{j_i}^n \\ -{}^l C35 + {}^l M_{j_i}^n \end{bmatrix} \quad (A4.71)$$

In conventional form for dynamics systems the above equation can be represented by the following form:

$$MS'' = F \quad (A4.72)$$

where, M is the mass matrix, S' is the state vector and F is the force vector.

Proof of the mass matrix symmetry

Some of the useful relationships that will be used to prove the mass matrix symmetry are as follows:

For a skew-symmetric matrix S

$$\begin{aligned} [S]^T &= -[S] \\ [S] &= -[S]^T \end{aligned} \quad (A4.73)$$

For Direction Cosine Matrix

$$\begin{aligned} ([DCM]^{nn})^T &= [DCM]^{na} \\ ([DCM]^{na})^{-T} &= ([DCM]^{na})^T = [DCM]^{nn} \end{aligned} \quad (A4.74)$$

Now,

$$[{}^k C15] = {}^k [DCM]^{nn} [{}^k C8] = {}^k [DCM]^{nn} (-m_{np}) [{}^k e^n] = -m_{np} {}^k [DCM]^{nn} [{}^k e^n] \quad (A4.75)$$

and

$$\begin{aligned} [{}^k C10] &= m_{np} [{}^k e^n] {}^k [DCM]^{na} = m_{np} (-[{}^k e^n]^T) ({}^k [DCM]^{nn})^T \\ &= (-m_{np} {}^k [DCM]^{nn} [{}^k e^n])^T \end{aligned} \quad (A4.76)$$

Comparing (A4.75) and (A4.76), then:

$$[{}^k C10] = [{}^k C15]^T \quad (\text{A4.77})$$

Also,

$$\begin{aligned} [C28] &= -m_a [b^a] + [{}^r C14] + [{}^l C14] \\ &= -m_a [b^a] + [{}^r DCM]^{nn} [{}^r C7] + [{}^l DCM]^{nn} [{}^l C7] \\ &= -m_a [b^a] + [{}^r DCM]^{nn} (-m_{np} [{}^r DCM]^{na} [{}^r d^a] - m_{np} [{}^r e^n] [{}^r DCM]^{na}) \\ &\quad + [{}^l DCM]^{nn} (-m_{np} [{}^l DCM]^{na} [{}^l d^a] - m_{np} [{}^l e^n] [{}^l DCM]^{na}) \\ &= -m_a [b^a] - m_{np} [{}^r d^a] - m_{np} [{}^r DCM]^{nn} [{}^r e^n] [{}^r DCM]^{na} \\ &\quad - m_{np} [{}^l d^a] - m_{np} [{}^l DCM]^{nn} [{}^l e^n] [{}^l DCM]^{na} \end{aligned} \quad (\text{A4.78})$$

and

$$\begin{aligned} [C30] &= m_a [b^a] + [{}^r d^a] [{}^r C13] + [{}^l d^a] [{}^l C13] + [{}^r DCM]^{nn} [{}^r C10] + [{}^l DCM]^{nn} [{}^l C10] \\ &= m_a [b^a] + [{}^r d^a] [{}^r DCM]^{nn} [{}^r C6] + [{}^l d^a] [{}^l DCM]^{nn} [{}^l C6] \\ &\quad + [{}^r DCM]^{nn} (m_{np}) [{}^r e^n] [{}^r DCM]^{na} + [{}^l DCM]^{nn} (m_{np}) [{}^l e^n] [{}^l DCM]^{na} \\ &= -m_a [b^a]^T - m_{np} [{}^r d^a]^T - m_{np} [{}^l d^a]^T \\ &\quad + m_{np} ({}^r [{}^r DCM]^{na})^T (-[{}^r e^n]^T) ({}^r [{}^r DCM]^{nn})^T + m_{np} ({}^l [{}^l DCM]^{na})^T (-[{}^l e^n]^T) ({}^l [{}^l DCM]^{nn})^T \\ &= -m_a [b^a]^T - m_{np} [{}^r d^a]^T - m_{np} [{}^l d^a]^T \\ &\quad - (m_{np} ({}^r [{}^r DCM]^{nn}) ([{}^r e^n]) ({}^r [{}^r DCM]^{na}))^T - (m_{np} ({}^l [{}^l DCM]^{nn}) ([{}^l e^n]) ({}^l [{}^l DCM]^{na}))^T \end{aligned} \quad (\text{A4.79})$$

Comparing (A4.78) and (A4.79), then:

$$[C30] = [C28]^T \quad (\text{A4.80})$$

Also,

$$\begin{aligned}
 [{}^{\kappa}C32] &= [{}^{\kappa}C24][{}^{\kappa}C19] = [{}^{\kappa}d^a][{}^{\kappa}C15] + {}^{\kappa}[DCM]^{nn} [{}_{j_i}^{\kappa}I_{np}^n] \\
 &= [{}^{\kappa}d^a] {}^{\kappa}[DCM]^{nn} [{}^{\kappa}C8] + {}^{\kappa}[DCM]^{nn} [{}_{j_i}^{\kappa}I_{np}^n] \\
 &= [{}^{\kappa}d^a] {}^{\kappa}[DCM]^{nn} (-m_{np}) [{}^{\kappa}e^n] + {}^{\kappa}[DCM]^{nn} [{}_{j_i}^{\kappa}I_{np}^n] \\
 &= -m_{np} [{}^{\kappa}d^a] {}^{\kappa}[DCM]^{nn} [{}^{\kappa}e^n] + {}^{\kappa}[DCM]^{nn} [{}_{j_i}^{\kappa}I_{np}^n]
 \end{aligned} \tag{A4.81}$$

and

$$\begin{aligned}
 [{}^{\kappa}C11] &= -m_{np} [{}^{\kappa}e^n][{}^{\kappa}d^a] {}^{\kappa}[DCM]^{na} [{}^{\kappa}d^a] + [{}_{j_i}^{\kappa}I_{np}^n] {}^{\kappa}[DCM]^{na} \\
 &= m_{np} ([{}^{\kappa}e^n]^T) ({}^{\kappa}[DCM]^{nn})^T (-[{}^{\kappa}d^a]^T) + ([{}_{j_i}^{\kappa}I_{np}^n]^T) ({}^{\kappa}[DCM]^{nn})^T \\
 &= (-m_{np} [{}^{\kappa}d^a] {}^{\kappa}[DCM]^{nn} [{}^{\kappa}e^n])^T + ({}^{\kappa}[DCM]^{nn} [{}_{j_i}^{\kappa}I_{np}^n])^T
 \end{aligned} \tag{A4.82}$$

Comparing (A4.81) and (A4.82), then:

$$[{}^{\kappa}C11] = [{}^{\kappa}C32]^T \tag{A4.83}$$

Also,

$$[{}^{\kappa}C20] = {}^{\kappa}[DCM]^{nn} [{}_{sp}^{\kappa}I_p^n] \tag{A4.84}$$

and

$$[{}^{\kappa}C36] = [{}_{sp}^{\kappa}I_p^n] {}^{\kappa}[DCM]^{na} = ([{}_{sp}^{\kappa}I_p^n])^T ({}^{\kappa}[DCM]^{nn})^T = ({}^{\kappa}[DCM]^{nn} [{}_{sp}^{\kappa}I_p^n])^T \tag{A4.85}$$

Comparing (A4.84) and (A4.85), then:

$$[{}^{\kappa}C36] = [{}^{\kappa}C20]^T \tag{A4.86}$$

Also,

$$[C27] = m_a [I] + [{}^rC13] + [{}^lC13] \tag{A4.87}$$

since

$$m_a[I] \quad \text{Symmetric} \quad (\text{A4.88})$$

and

$$\begin{aligned} [{}^{\kappa}C13] &= {}^{\kappa}[DCM]^{nn} [{}^{\kappa}C6] = {}^{\kappa}[DCM]^{nn} m_{np} {}^{\kappa}[DCM]^{na} \\ &= m_a[I] \quad \text{Symmetric} \end{aligned} \quad (\text{A4.89})$$

$$[C27] \quad \text{Symmetric} \quad (\text{A4.90})$$

Also,

$$[C31] = [{}_oI_a^a] + [{}^{\prime}C23] + [{}^{\prime}C23] + [{}^{\prime}C18] + [{}^{\prime}C18] \quad (\text{A4.91})$$

since

$$[{}_oI_a^a] \quad \text{Symmetric} \quad (\text{A4.92})$$

and

$$\begin{aligned} [{}^{\kappa}C23] &= [{}^{\kappa}d^a] [{}^{\kappa}C14] = [{}^{\kappa}d^a] {}^{\kappa}[DCM]^{nn} [{}^{\kappa}C7] \\ &= [{}^{\kappa}d^a] {}^{\kappa}[DCM]^{nn} (-m_{np} {}^{\kappa}[DCM]^{na} [{}^{\kappa}d^a] - m_{np} [{}^{\kappa}e^n] {}^{\kappa}[DCM]^{na}) \\ &= -m_{np} [{}^{\kappa}d^a] [{}^{\kappa}d^a] - m_{np} [{}^{\kappa}d^a] {}^{\kappa}[DCM]^{nn} [{}^{\kappa}e^n] {}^{\kappa}[DCM]^{na} \\ &= -m_{np} [{}^{\kappa}d^a] [{}^{\kappa}d^a] - m_{np} [{}^{\kappa}d^a] [{}^{\kappa}e^a] \end{aligned} \quad (\text{A4.93})$$

$$\begin{aligned} [{}^{\kappa}C18] &= {}^{\kappa}[DCM]^{nn} [{}^{\kappa}C11] \\ &= {}^{\kappa}[DCM]^{nn} ([{}^{\kappa}_j I_{np}^n] {}^{\kappa}[DCM]^{na} - m_{np} [{}^{\kappa}e^n] {}^{\kappa}[DCM]^{na} [{}^{\kappa}d^a]) \\ &= [{}^{\kappa}_j I_{np}^n] - m_{np} [{}^{\kappa}e^a] [{}^{\kappa}d^a] \end{aligned} \quad (\text{A4.94})$$

the terms $-m_{np} [{}^{\kappa}d^a] [{}^{\kappa}d^a]$ and $[{}^{\kappa}_j I_{np}^n]$ in Equations (A4.93) and (A4.94) are symmetric.

Also, summation of the terms $-m_{np} [{}^{\kappa}d^a] [{}^{\kappa}e^a]$ and $-m_{np} [{}^{\kappa}e^a] [{}^{\kappa}d^a]$ is symmetric.

Therefore

$$[C31] \quad \text{Symmetric} \quad (\text{A4.95})$$

The obtained results from previous calculations can be summarised as follows:

$$\left. \begin{array}{l} [C27] \\ [C31] \\ \left[\begin{array}{c} \kappa I_{np}^n \\ J_i \end{array} \right] \\ \left[\begin{array}{c} \kappa I_p^n \\ g_p \end{array} \right] \end{array} \right\} : \text{Symmetric} \quad (A4.96)$$

$$\begin{aligned} [C30] &= [C28]^T \\ \left[\begin{array}{c} \kappa C10 \\ \kappa C11 \end{array} \right] &= \left[\begin{array}{c} \kappa C15 \\ \kappa C32 \end{array} \right]^T \\ \left[\begin{array}{c} \kappa C36 \\ \kappa C20 \end{array} \right] &= \left[\begin{array}{c} \kappa C20 \\ \kappa C36 \end{array} \right]^T \end{aligned}$$

The above conditions are exactly the necessary requirement for the matrix M to be symmetric. Therefore, the symmetry of mass matrix is proved.

Final form

Considering the constraints mentioned in Section 4.5.6 and defining the following vectors:

$$\dot{\Omega}_{ai}^a = \begin{Bmatrix} \dot{P} \\ \dot{Q} \\ \dot{R} \end{Bmatrix} ; \dot{V}_o^a = \begin{Bmatrix} \dot{U} \\ \dot{V} \\ \dot{W} \end{Bmatrix}$$

$${}^o\Omega_{na}^n = \begin{Bmatrix} 0 \\ \infty \\ {}^r\theta_n \\ 0 \end{Bmatrix} ; {}^l\Omega_{na}^n = \begin{Bmatrix} 0 \\ \infty \\ {}^l\theta_n \\ 0 \end{Bmatrix} ; {}^r\Omega_{pn}^n = \begin{Bmatrix} {}^oN \\ 0 \\ 0 \end{Bmatrix} ; {}^l\Omega_{pn}^n = \begin{Bmatrix} {}^lN \\ 0 \\ 0 \end{Bmatrix} \quad (A4.97)$$

the final expanded, tenth order system of equations can be expressed as shown in Equation (A4.97).

In this equation

$${}^{\kappa}M_{J_y}^n = {}^{\kappa}M_S \quad (\text{A4.99})$$

$${}^{\kappa}M_{J_x}^n = {}^{\kappa}M_E \quad (\text{A4.100})$$

$${}^{\kappa}M_E = \frac{{}^{\kappa}P_E}{{}^{\kappa}N} \quad (\text{A4.101})$$

The right side of the Equation (A4.98) can be broken down into the two parts as follows:

$$\begin{bmatrix} C29_x \\ C29_y \\ C29_z \\ C33_x \\ C33_y \\ C33_z \\ -{}^rC9_y + {}^rM_{J_y}^n \\ -{}^lC9_y + {}^lM_{J_y}^n \\ -{}^rC35_x + {}^rM_{J_x}^n \\ -{}^lC35_x + {}^lM_{J_x}^n \end{bmatrix} = \begin{bmatrix} C29A_x \\ C29A_y \\ C29A_z \\ C33A_x \\ C33A_y \\ C33A_z \\ -{}^rC9A_y \\ -{}^lC9A_y \\ -{}^rC35A_x \\ -{}^lC35A_x \end{bmatrix} + \begin{bmatrix} C29B_x \\ C29B_y \\ C29B_z \\ C33B_x \\ C33B_y \\ C33B_z \\ -{}^rC9B_y + {}^rM_{J_y}^n \\ -{}^lC9B_y + {}^lM_{J_y}^n \\ -{}^rC35B_x + {}^rM_{J_x}^n \\ -{}^lC35B_x + {}^lM_{J_x}^n \end{bmatrix} \quad (\text{A4.102})$$

The first term in the right hand side of the Equation (A4.102) is called the dynamic vector and the second term is the vector summation of all the aerodynamic, gravitational and thrust forces and moments.

APPENDIX B1

In this appendix, the method of calculating the position vector LS and the code K_{SS} , defined in Section 5.2.2, for each individual component is presented.

All the position vectors and axes systems necessary for the following calculation in this appendix are shown in Figure B1.1. The X-axis of a local coordinate frame is parallel with the zero lifting line of the corresponding airfoil or with the axis of symmetry of the corresponding streamline body. In addition, except for X_v, Y_v, Z_v coordinate system, the Y-axis of all other on-board coordinate frames are parallel. Therefore, one angle is sufficient to define the relative rotation between two adjacent frames and the associated Direction Cosine Matrix. These constant angles and associated sign convention are shown in Figure B1.2. The angles λ_{wa} , λ_{ha} are the incidence angles of the wing and the horizontal stabiliser, respectively. It should be noticed that in the following calculations the effect of each propeller on the fuselage and the components of the tilting part ${}^n np$ in the opposite side of the aircraft is neglected. For example, the right propeller does not affect the left wing.

Starting with the necessary transformations, we have:

$$\begin{aligned}
 {}^h L2_h^a &= [DCM]^{hh} {}^h L2_h^h ; & {}^h L2_h^a &= [DCM]^{hh} {}^h L2_h^h \\
 {}^v L2_v^a &= [DCM]^{vv} {}^v L2_v^v ; & {}^v L2_v^a &= [DCM]^{vv} {}^v L2_v^v \\
 {}^w L2_w^a &= [DCM]^{ww} {}^w L2_w^w ; & {}^w L2_w^a &= [DCM]^{ww} {}^w L2_w^w \\
 {}^n L2_n^a &= [DCM]^{nn} {}^n L2_n^n ; & {}^n L2_n^a &= [DCM]^{nn} {}^n L2_n^n
 \end{aligned} \tag{B1.1}$$

where,

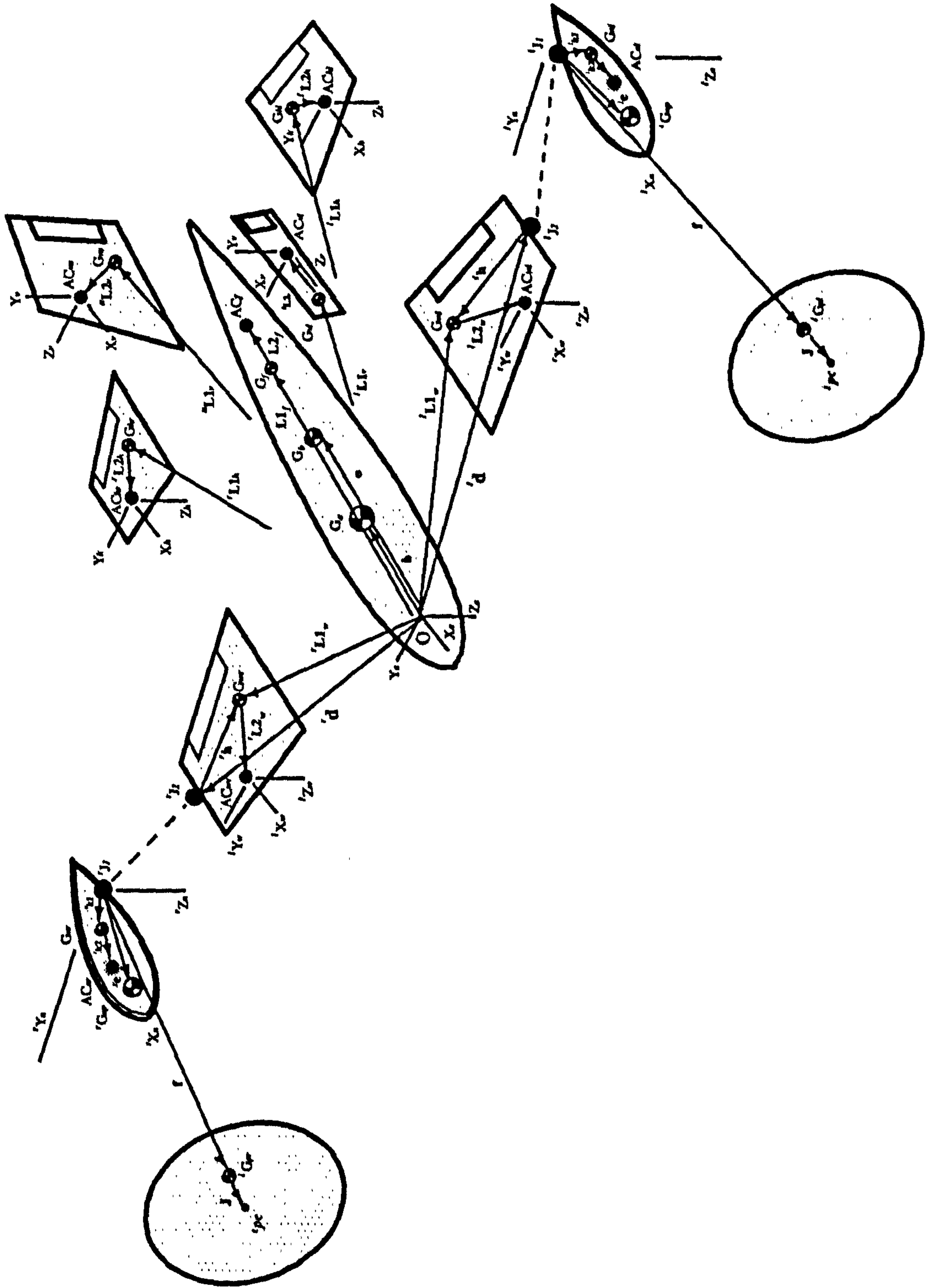


Fig. (B1.1): Definition of all the axes systems and position vectors

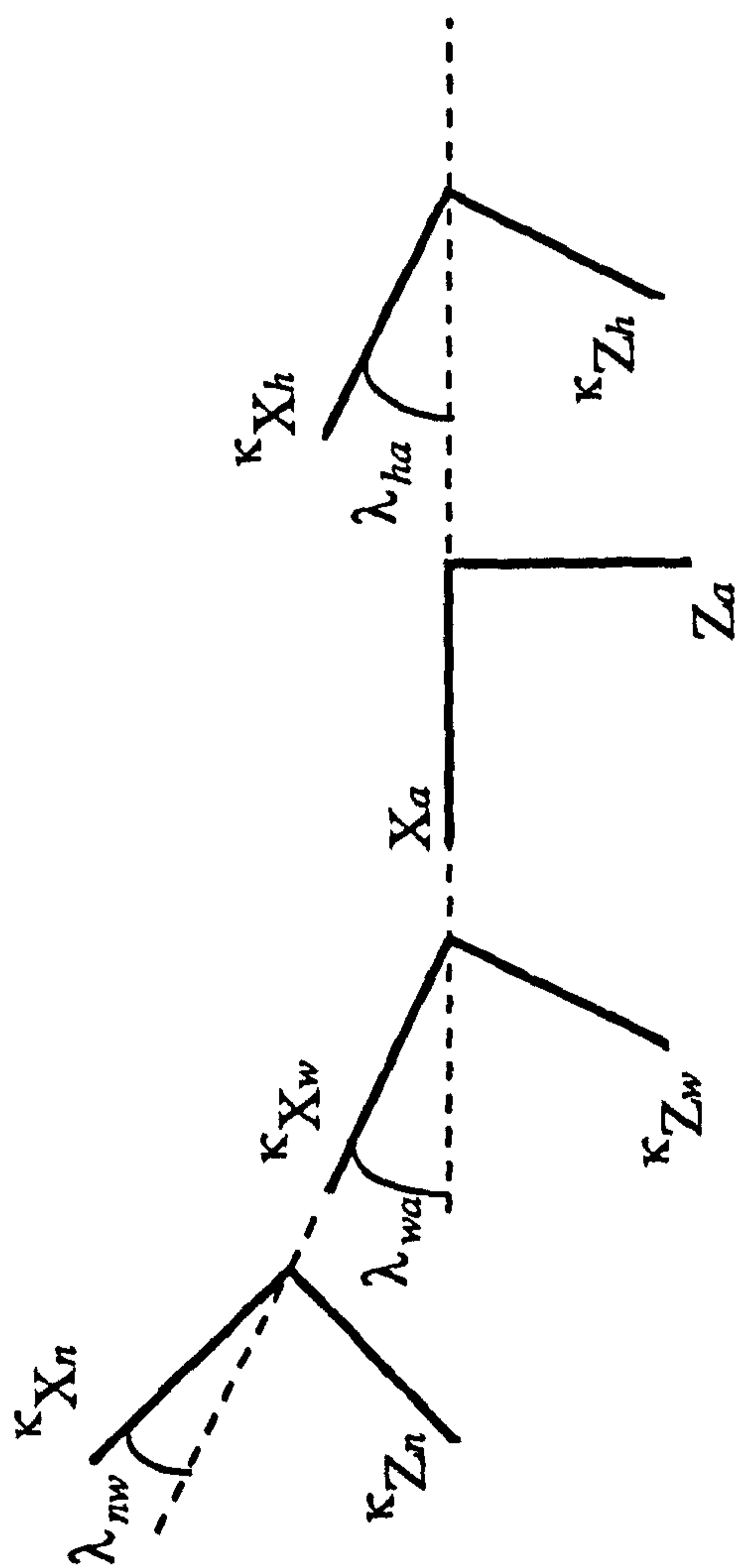


Fig. (B.2): Incidence angles

$$[DCM]^{ah} = \begin{bmatrix} \text{Cos}\lambda_{ha} & 0 & \text{Sin}\lambda_{ha} \\ 0 & 1 & 0 \\ -\text{Sin}\lambda_{ha} & 0 & \text{Cos}\lambda_{ha} \end{bmatrix} \quad (\text{B1.2})$$

$$[DCM]^{xy} = \begin{bmatrix} 1 & 0 & 0 \\ 0 & 0 & 1 \\ 0 & -1 & 0 \end{bmatrix} \quad (\text{B1.3})$$

$$[DCM]^{zw} = \begin{bmatrix} \text{Cos}\lambda_{wa} & 0 & \text{Sin}\lambda_{wa} \\ 0 & 1 & 0 \\ -\text{Sin}\lambda_{wa} & 0 & \text{Cos}\lambda_{wa} \end{bmatrix} \quad (\text{B1.4})$$

$$[DCM]^{nw} = \begin{bmatrix} \text{Cos}\lambda_{nw} & 0 & \text{Sin}\lambda_{nw} \\ 0 & 1 & 0 \\ -\text{Sin}\lambda_{nw} & 0 & \text{Cos}\lambda_{nw} \end{bmatrix} \quad (\text{B1.5})$$

Also

$${}^k[DCM]^{sn} = {}^k[DCM]^{sm} {}^k[DCM]^{mn} \quad (\text{B1.6})$$

where

$${}^k[DCM]^{sm} = \begin{bmatrix} \text{Cos}^k\theta_s & 0 & \text{Sin}^k\theta_s \\ 0 & 1 & 0 \\ -\text{Sin}^k\theta_s & 0 & \text{Cos}^k\theta_s \end{bmatrix} \quad (\text{B1.7})$$

$$[DCM]^{mn} = \begin{bmatrix} 1 & 0 & 0 \\ 0 & \text{Cos}^k\psi_m & -\text{Sin}^k\psi_m \\ 0 & \text{Sin}^k\psi_m & \text{Cos}^k\psi_m \end{bmatrix} \quad (\text{B1.8})$$

Now, for the constituent components of the empennage, we have

$${}^{\kappa}\text{LS}_v^s = {}^{\kappa}[\text{DCM}]^{\kappa} {}^{\kappa}\text{LS}_v^n \quad v = hr, hl, vu, vl \quad (\text{B1.9})$$

where

$$\begin{aligned} {}^r\text{LS}_{hr}^n &= {}^r[\text{DCM}]^{ra} ({}^r\text{L1}_h^a + {}^r\text{L2}_h^a - {}^r\text{d}^a) - (\mathbf{f}^n + \mathbf{j}^n) \\ {}^r\text{LS}_{hl}^n &= {}^r[\text{DCM}]^{ra} ({}^l\text{L1}_h^a + {}^l\text{L2}_h^a - {}^r\text{d}^a) - (\mathbf{f}^n + \mathbf{j}^n) \\ {}^r\text{LS}_{vu}^n &= {}^r[\text{DCM}]^{ra} ({}^u\text{L1}_v^a + {}^u\text{L2}_v^a - {}^r\text{d}^a) - (\mathbf{f}^n + \mathbf{j}^n) \\ {}^r\text{LS}_{vl}^n &= {}^r[\text{DCM}]^{ra} ({}^l\text{L1}_v^a + {}^l\text{L2}_v^a - {}^r\text{d}^a) - (\mathbf{f}^n + \mathbf{j}^n) \end{aligned} \quad (\text{B1.10})$$

$$\begin{aligned} {}^l\text{LS}_{hr}^n &= {}^l[\text{DCM}]^{la} ({}^r\text{L1}_h^a + {}^r\text{L2}_h^a - {}^l\text{d}^a) - (\mathbf{f}^n + \mathbf{j}^n) \\ {}^l\text{LS}_{hl}^n &= {}^l[\text{DCM}]^{la} ({}^l\text{L1}_h^a + {}^l\text{L2}_h^a - {}^l\text{d}^a) - (\mathbf{f}^n + \mathbf{j}^n) \\ {}^l\text{LS}_{vu}^n &= {}^l[\text{DCM}]^{la} ({}^u\text{L1}_v^a + {}^u\text{L2}_v^a - {}^l\text{d}^a) - (\mathbf{f}^n + \mathbf{j}^n) \\ {}^l\text{LS}_{vl}^n &= {}^l[\text{DCM}]^{la} ({}^l\text{L1}_v^a + {}^l\text{L2}_v^a - {}^l\text{d}^a) - (\mathbf{f}^n + \mathbf{j}^n) \end{aligned} \quad (\text{B1.11})$$

Applying the criterion (5.38), then

$$\begin{aligned} \text{If } ({}^{\kappa}\text{LS}_{v,\kappa}^s)^2 (\text{Cos}^{\kappa} \theta_s)^2 + ({}^{\kappa}\text{LS}_{v,\kappa}^s)^2 &\leq 0.25 K_{sscon1} D^2 (\text{Cos}^{\kappa} \theta_s)^2 \\ \text{then } {}^{\kappa}K_{ss_v} &= 1.0 \quad \text{Else } {}^{\kappa}K_{ss_v} = 0.0 \quad ; \kappa = r, l \quad ; v = hr, hl, vu, vl \end{aligned} \quad (\text{B1.12})$$

Similarly, for the constituent components of the tilting body ${}^{\kappa}np$, we obtain

$$\begin{aligned} {}^r\text{LS}_{nr}^s &= {}^r[\text{DCM}]^{rn} {}^r\text{LS}_{nr}^n \\ {}^l\text{LS}_{nl}^s &= {}^l[\text{DCM}]^{ln} {}^l\text{LS}_{nl}^n \\ {}^r\text{LS}_{wr}^s &= {}^r[\text{DCM}]^{rn} {}^r\text{LS}_{wr}^n \\ {}^l\text{LS}_{wr}^s &= {}^l[\text{DCM}]^{ln} {}^l\text{LS}_{wr}^n \end{aligned} \quad (\text{B1.13})$$

where

$$\begin{aligned} {}^r\text{LS}_{nr}^n &= ({}^r\text{k1}^n + {}^r\text{k2}^n) - (\mathbf{f}^n + \mathbf{j}^n) \\ {}^l\text{LS}_{nl}^n &= ({}^l\text{k1}^n + {}^l\text{k2}^n) - (\mathbf{f}^n + \mathbf{j}^n) \end{aligned} \quad (\text{B1.14})$$

Tilt-nacelle

$$\begin{aligned} {}^r\text{LS}_{wr}^n &= {}^r[\text{DCM}]^{na} ({}^r\text{L1}_w^a + {}^r\text{L2}_w^a - {}^r\text{d}^a) - (\mathbf{f}^n + \mathbf{j}^n) \\ {}^l\text{LS}_{wl}^n &= {}^l[\text{DCM}]^{na} ({}^l\text{L1}_w^a + {}^l\text{L2}_w^a - {}^l\text{d}^a) - (\mathbf{f}^n + \mathbf{j}^n) \end{aligned} \quad (\text{B1.15})$$

Tilt-wing

$$\begin{aligned} {}^r\text{LS}_{wr}^n &= ({}^r\text{h}^n + {}^r\text{L2}_w^n) - (\mathbf{f}^n + \mathbf{j}^n) \\ {}^l\text{LS}_{wl}^n &= ({}^l\text{h}^n + {}^l\text{L2}_w^n) - (\mathbf{f}^n + \mathbf{j}^n) \end{aligned} \quad (\text{B1.16})$$

Using criterion (5.38), then

$$\begin{aligned} \text{If } ({}^r\text{LS}_{nr,y}^s)^2 (\text{Cos}^r \theta_s)^2 + ({}^r\text{LS}_{nr,z}^s)^2 &\leq 0.25 \text{ Ksscon1 } D^2 (\text{Cos}^r \theta_s)^2 \\ \text{then } {}^r\text{Kss}_{nr} &= 1.0 \text{ Else } {}^r\text{Kss}_{nr} = 0.0 \end{aligned} \quad (\text{B1.17})$$

$$\begin{aligned} \text{If } ({}^l\text{LS}_{nl,y}^s)^2 (\text{Cos}^l \theta_s)^2 + ({}^l\text{LS}_{nl,z}^s)^2 &\leq 0.25 \text{ Ksscon1 } D^2 (\text{Cos}^l \theta_s)^2 \\ \text{then } {}^l\text{Kss}_{nl} &= 1.0 \text{ Else } {}^l\text{Kss}_{nl} = 0.0 \end{aligned} \quad (\text{B1.18})$$

$$\begin{aligned} \text{If } ({}^r\text{LS}_{wr,y}^s)^2 (\text{Cos}^r \theta_s)^2 + ({}^r\text{LS}_{wr,z}^s)^2 &\leq 0.25 \text{ Ksscon1 } D^2 (\text{Cos}^r \theta_s)^2 \\ \text{then } {}^r\text{Kss}_{wr} &= 1.0 \text{ Else } {}^r\text{Kss}_{wr} = 0.0 \end{aligned} \quad (\text{B1.19})$$

$$\begin{aligned} \text{If } ({}^l\text{LS}_{wl,y}^s)^2 (\text{Cos}^l \theta_s)^2 + ({}^l\text{LS}_{wl,z}^s)^2 &\leq 0.25 \text{ Ksscon1 } D^2 (\text{Cos}^l \theta_s)^2 \\ \text{then } {}^l\text{Kss}_{wl} &= 1.0 \text{ Else } {}^l\text{Kss}_{wl} = 0.0 \end{aligned} \quad (\text{B1.20})$$

APPENDIX B2

In this appendix, the calculation of local velocities and the transformation of the aerodynamic force and moment vector associated with each individual component to the main axes system are presented. All the necessary position vectors are defined in Figure (B1.1).

For the constituents parts of the empennage, we have

$$\begin{aligned} {}^r V_{AC_h}^h &= [DCM]^{hr} V_{AC_h}^a & ; & \quad {}^l V_{AC_h}^h = [DCM]^{hl} V_{AC_h}^a \\ {}^u V_{AC_v}^v &= [DCM]^{vu} V_{AC_v}^a & ; & \quad {}^l V_{AC_v}^v = [DCM]^{vl} V_{AC_v}^a \end{aligned} \quad (B2.1)$$

where

$$\begin{aligned} {}^r V_{AC_h}^a &= V_O^a + \Omega_{ai}^a \times ({}^r L1_h^a + {}^r L2_h^a) - {}^r K_{SS_{hr}} [DCM]^{anr} W_{ind}^n - {}^l K_{SS_{hr}} [DCM]^{anl} W_{ind}^n \\ {}^l V_{AC_h}^a &= V_O^a + \Omega_{ai}^a \times ({}^l L1_h^a + {}^l L2_h^a) - {}^r K_{SS_{hl}} [DCM]^{anr} W_{ind}^n - {}^l K_{SS_{hl}} [DCM]^{anl} W_{ind}^n \\ {}^u V_{AC_v}^a &= V_O^a + \Omega_{ai}^a \times ({}^u L1_v^a + {}^u L2_v^a) - {}^r K_{SS_{vu}} [DCM]^{anr} W_{ind}^n - {}^l K_{SS_{vu}} [DCM]^{anl} W_{ind}^n \\ {}^l V_{AC_v}^a &= V_O^a + \Omega_{ai}^a \times ({}^l L1_v^a + {}^l L2_v^a) - {}^r K_{SS_{vl}} [DCM]^{anr} W_{ind}^n - {}^l K_{SS_{vl}} [DCM]^{anl} W_{ind}^n \end{aligned} \quad (B2.2)$$

Also

$$\begin{aligned} {}^r A_h^a &= [DCM]^{ahr} A_h^h \\ {}^l A_h^a &= [DCM]^{ahl} A_h^h \\ {}^u A_v^a &= [DCM]^{avv} A_v^v \\ {}^l A_v^a &= [DCM]^{avv} A_v^v \end{aligned} \quad (B2.3)$$

and

$$\begin{aligned} {}_{sb}^r M_{A_h}^a &= [DCM]^{ahr} M_{A_h}^h + ({}^r r_h^a + {}^r L2_h^a) \times {}^r A_h^a \\ {}_{sb}^l M_{A_h}^a &= [DCM]^{ahl} M_{A_h}^h + ({}^l r_h^a + {}^l L2_h^a) \times {}^l A_h^a \\ {}_{sb}^u M_{A_v}^a &= [DCM]^{avv} M_{A_v}^v + ({}^u r_v^a + {}^u L2_v^a) \times {}^u A_v^a \\ {}_{sb}^l M_{A_v}^a &= [DCM]^{avv} M_{A_v}^v + ({}^l r_v^a + {}^l L2_v^a) \times {}^l A_v^a \end{aligned} \quad (B2.4)$$

where

$$\begin{aligned} {}^r \mathbf{r}_h^a &= {}^r \mathbf{L1}_h^a - \mathbf{o}^a \\ {}^l \mathbf{r}_h^a &= {}^l \mathbf{L1}_h^a - \mathbf{o}^a \\ {}^u \mathbf{r}_v^a &= {}^u \mathbf{L1}_v^a - \mathbf{o}^a \\ {}^l \mathbf{r}_v^a &= {}^l \mathbf{L1}_v^a - \mathbf{o}^a \end{aligned} \quad (\text{B2.5})$$

For the fuselage

$$\mathbf{V}_{AC_f}^a = \mathbf{V}_O^a + \boldsymbol{\Omega}_{ai}^a \times (\mathbf{L1}_f^a + \mathbf{L2}_f^a) \quad (\text{B2.6})$$

also

$${}_{gb} \mathbf{M}_{A_f}^a = \mathbf{M}_{A_f}^a + (\mathbf{r}_f^a + \mathbf{L2}_f^a) \times \mathbf{A}_f^a \quad (\text{B2.7})$$

where

$$\mathbf{r}_f^a = \mathbf{L1}_f^a - \mathbf{o}^a \quad (\text{B2.8})$$

For the wing in the case of Tilt-nacelle

$$\begin{aligned} {}^r \mathbf{V}_{AC_w}^w &= [\text{DCM}]^{wa} {}^r \mathbf{V}_{AC_w}^a \\ {}^l \mathbf{V}_{AC_w}^w &= [\text{DCM}]^{wa} {}^l \mathbf{V}_{AC_w}^a \end{aligned} \quad (\text{B2.9})$$

where

$$\begin{aligned} {}^r \mathbf{V}_{AC_w}^a &= \mathbf{V}_O^a + \boldsymbol{\Omega}_{ai}^a \times ({}^r \mathbf{L1}_w^a + {}^r \mathbf{L2}_w^a) - {}^r K_{SS_{wr}} [\text{DCM}]^{an} {}^r \mathbf{W}_{ind}^n \\ {}^l \mathbf{V}_{AC_w}^a &= \mathbf{V}_O^a + \boldsymbol{\Omega}_{ai}^a \times ({}^l \mathbf{L1}_w^a + {}^l \mathbf{L2}_w^a) - {}^l K_{SS_{wl}} [\text{DCM}]^{an} {}^l \mathbf{W}_{ind}^n \end{aligned} \quad (\text{B2.10})$$

$${}^x \mathbf{L1}_w^a = {}^x \mathbf{d}^a + [\text{DCM}]^{aw} {}^x \mathbf{h}^w \quad (\text{B2.11})$$

Also

$$\begin{aligned} {}^r \mathbf{A}_w^a &= [\text{DCM}]^{aw} {}^r \mathbf{A}_w^w \\ {}^l \mathbf{A}_w^a &= [\text{DCM}]^{aw} {}^l \mathbf{A}_w^w \end{aligned} \quad (\text{B2.12})$$

and

$$\begin{aligned} {}^o \mathbf{M}_{A_w}^a &= [\text{DCM}]^{aw} {}^r \mathbf{M}_{A_w}^w + ({}^r \mathbf{L1}_w^a + {}^r \mathbf{L2}_w^a) \times {}^r \mathbf{A}_w^a \\ {}^o \mathbf{M}_{A_w}^a &= [\text{DCM}]^{aw} {}^l \mathbf{M}_{A_w}^w + ({}^l \mathbf{L1}_w^a + {}^l \mathbf{L2}_w^a) \times {}^l \mathbf{A}_w^a \end{aligned} \quad (\text{B2.13})$$

and, in the case of Tilt-wing

$$\begin{aligned} {}^r V_{AC_w}^w &= [DCM]^{wn} {}^r V_{AC_w}^n \\ {}^l V_{AC_w}^w &= [DCM]^{wn} {}^l V_{AC_w}^n \end{aligned} \quad (B2.14)$$

where

$$\begin{aligned} {}^r V_{AC_w}^n &= {}^r V_{J_2}^n + {}^r \Omega_{ni}^n \times ({}^r h^n + {}^r L2_w^n) - {}^r K_{SS_{wr}} {}^r W_{ind}^n \\ {}^l V_{AC_w}^n &= {}^l V_{J_2}^n + {}^l \Omega_{ni}^n \times ({}^l h^n + {}^l L2_w^n) - {}^l K_{SS_{wl}} {}^l W_{ind}^n \end{aligned} \quad (B2.15)$$

Also

$$\begin{aligned} {}^r A_w^n &= [DCM]^{nw} {}^r A_w^w \\ {}^l A_w^n &= [DCM]^{nw} {}^l A_w^w \end{aligned} \quad (B2.16)$$

and

$$\begin{aligned} {}^r M_{A_w}^n &= [DCM]^{nw} {}^r M_{A_w}^w + ({}^r h^n + {}^r L2_w^n) \times {}^r A_w^n \\ {}^l M_{A_w}^n &= [DCM]^{nw} {}^l M_{A_w}^w + ({}^l h^n + {}^l L2_w^n) \times {}^l A_w^n \end{aligned} \quad (B2.17)$$

For the nacelles

$$\begin{aligned} {}^r V_{AC_n}^n &= {}^r V_{J_2}^n + {}^r \Omega_{ni}^n \times ({}^r k1^n + {}^r k2^n) - {}^r K_{SS_{nr}} {}^r W_{ind}^n \\ {}^l V_{AC_n}^n &= {}^l V_{J_2}^n + {}^l \Omega_{ni}^n \times ({}^l k1^n + {}^l k2^n) - {}^l K_{SS_{nl}} {}^l W_{ind}^n \end{aligned} \quad (B2.18)$$

Also

$$\begin{aligned} {}^r M_{A_n}^n &= {}^r M_{A_n}^n + ({}^r k1^n + {}^r k2^n) \times {}^r A_n^n \\ {}^l M_{A_n}^n &= {}^l M_{A_n}^n + ({}^l k1^n + {}^l k2^n) \times {}^l A_n^n \end{aligned} \quad (B2.19)$$

and finally for the propellers

$$\begin{aligned} {}^r M_{A_p}^n &= {}^r M_{A_p}^n + f^n \times {}^r A_p^n \\ {}^l M_{A_p}^n &= {}^l M_{A_p}^n + f^n \times {}^l A_p^n \end{aligned} \quad (B2.20)$$

APPENDIX B3

In this appendix, some more detail about the mass moment of inertia calculations presented in Section (5.4) is given.

For the constituent components of the empennage, we have

$$\begin{aligned}
 \begin{bmatrix} r \\ gb \end{bmatrix} I_h^a &= \begin{bmatrix} r \\ gh \end{bmatrix} I_h^a + m_h \{ {}^r \mathbf{r}_h^a \} \\
 \begin{bmatrix} l \\ gb \end{bmatrix} I_h^a &= \begin{bmatrix} l \\ gh \end{bmatrix} I_h^a + m_h \{ {}^l \mathbf{r}_h^a \} \\
 \begin{bmatrix} u \\ gb \end{bmatrix} I_v^a &= \begin{bmatrix} u \\ gv \end{bmatrix} I_v^a + m_{vu} \{ {}^u \mathbf{r}_v^a \} \\
 \begin{bmatrix} l \\ gb \end{bmatrix} I_v^a &= \begin{bmatrix} l \\ gv \end{bmatrix} I_v^a + m_{vl} \{ {}^l \mathbf{r}_v^a \}
 \end{aligned}
 \tag{B3.1}$$

where

$$\begin{aligned}
 \begin{bmatrix} r \\ gh \end{bmatrix} I_h^a &= [DCM]^{ah} \begin{bmatrix} r \\ gh \end{bmatrix} I_h^h [DCM]^{ha} \\
 \begin{bmatrix} l \\ gh \end{bmatrix} I_h^a &= [DCM]^{ah} \begin{bmatrix} l \\ gh \end{bmatrix} I_h^h [DCM]^{ha} \\
 \begin{bmatrix} u \\ gv \end{bmatrix} I_v^a &= [DCM]^{av} \begin{bmatrix} u \\ gv \end{bmatrix} I_v^v [DCM]^{va} \\
 \begin{bmatrix} l \\ gv \end{bmatrix} I_v^a &= [DCM]^{av} \begin{bmatrix} l \\ gv \end{bmatrix} I_v^v [DCM]^{va}
 \end{aligned}
 \tag{B3.2}$$

For the fuselage

$$\begin{bmatrix} gb \\ gf \end{bmatrix} I_f^a = \begin{bmatrix} gb \\ gf \end{bmatrix} I_f^a + m_f \{ \mathbf{r}_f^a \}
 \tag{B3.3}$$

For the wings, in the case of Tilt-nacelle configuration

$$\begin{aligned}
 \begin{bmatrix} r \\ O \end{bmatrix} I_w^a &= \begin{bmatrix} r \\ gw \end{bmatrix} I_w^a + m_w \{ {}^r \mathbf{L}1_w^a \} \\
 \begin{bmatrix} l \\ O \end{bmatrix} I_w^a &= \begin{bmatrix} l \\ gw \end{bmatrix} I_w^a + m_w \{ {}^l \mathbf{L}1_w^a \}
 \end{aligned}
 \tag{B3.4}$$

where

$$\begin{aligned} \left[\begin{matrix} r \\ g^w \end{matrix} I_w^a \right] &= [DCM]^{aw} \left[\begin{matrix} r \\ g^w \end{matrix} I_w^w \right] [DCM]^{wa} \\ \left[\begin{matrix} l \\ g^w \end{matrix} I_w^a \right] &= [DCM]^{aw} \left[\begin{matrix} l \\ g^w \end{matrix} I_w^w \right] [DCM]^{wa} \end{aligned} \quad (B3.5)$$

and, in the case of Tilt-wing configuration

$$\begin{aligned} \left[\begin{matrix} r \\ J_2 \end{matrix} I_w^n \right] &= \left[\begin{matrix} r \\ g^w \end{matrix} I_w^n \right] + m_w \left\{ \begin{matrix} r \\ h^n \end{matrix} \right\} \\ \left[\begin{matrix} l \\ J_2 \end{matrix} I_w^n \right] &= \left[\begin{matrix} l \\ g^w \end{matrix} I_w^n \right] + m_w \left\{ \begin{matrix} l \\ h^n \end{matrix} \right\} \end{aligned} \quad (B3.6)$$

where

$$\begin{aligned} \left[\begin{matrix} r \\ g^w \end{matrix} I_w^n \right] &= [DCM]^{nw} \left[\begin{matrix} r \\ g^w \end{matrix} I_w^w \right] [DCM]^{wn} \\ \left[\begin{matrix} l \\ g^w \end{matrix} I_w^n \right] &= [DCM]^{nw} \left[\begin{matrix} l \\ g^w \end{matrix} I_w^w \right] [DCM]^{wn} \end{aligned} \quad (B3.7)$$

For the nacelles

$$\begin{aligned} \left[\begin{matrix} r \\ J_2 \end{matrix} I_n^n \right] &= \left[\begin{matrix} r \\ g^n \end{matrix} I_n^n \right] + m_n \left\{ \begin{matrix} r \\ k1^n \end{matrix} \right\} \\ \left[\begin{matrix} l \\ J_2 \end{matrix} I_n^n \right] &= \left[\begin{matrix} l \\ g^n \end{matrix} I_n^n \right] + m_n \left\{ \begin{matrix} l \\ k1^n \end{matrix} \right\} \end{aligned} \quad (B3.8)$$

and finally for the propellers

$$\begin{aligned} \left[\begin{matrix} r \\ J_2 \end{matrix} I_p^n \right] &= \left[\begin{matrix} r \\ s^p \end{matrix} I_p^n \right] + m_p \left\{ \begin{matrix} r \\ f^n \end{matrix} \right\} \\ \left[\begin{matrix} l \\ J_2 \end{matrix} I_p^n \right] &= \left[\begin{matrix} l \\ s^p \end{matrix} I_p^n \right] + m_p \left\{ \begin{matrix} l \\ f^n \end{matrix} \right\} \end{aligned} \quad (B3.9)$$

APPENDIX C

Fig. (C.1): The VTOLUMA simulation program hierarchial structure

PROGRAM	
INITIAL	
	INPUT DATA
	Set up constants
	TABLE DEFINITION
	PROPELLER
	Thrust coefficient vs pitch angle and advanced ratio
	Propeller power coefficient vs pitch angle and advance ratio
	ENGINE
	Engine power vs throttle setting and rpm
	AIRFOIL
	Airfoil CL vs angle of attack
	Airfoil CD vs angle of attack
	Airfoil CM vs angle of attack
	Airfoil CLdelta vs angle attack
	Airfoil CMdelta vs angle attack
	STREAMLINE BODY
	Streamline body CM vs angle of attack
	Streamline body CDwet
	Streamline body COD1 Ifu
	INITIALIZING
	Untitled calculations
	Set up reference inputs, states and control gains
	CALL SETCONT
	Initialization of reference inputs and reference states
	Read Gainp
	Substitution the Gainp matrix into the Gainf matrix
	Transformation of some position vectors
	Mass calculations
	Weight calculations
	Calculation of the c.g. co-ords of the hvf assembly in a-axes related to O
	Calculation of the position vector of the different parts of hvf assembly related to gb
	Calculation of the c.g. co-ords of the bodies np in n-axes related to J
	Calculation of the c.g. co-ords of the body A in a-axes related to O
	Set up the fuselage inertia matrix in a-axes about gb
	Set up the horizontal stabilizer inertia matrices in a-axes about gn
	Set up the horizontal stabilizer inertia matrices in a-axes about gb
	Set up the vertical stabilizer inertia matrices in a-axes about gv
	Set up the vertical stabilizer inertia matrices in a-axes about gb
	Set up the hvf assembly inertia matrix in a-axes about gb
	Set up the nacelle inertia matrices in n-axes about J
	Set up the propeller inertia matrix in n-axes about J
	Set up the wing inertia matrices in n-axes about gw
	Set up the wing inertia matrices in n-axes about J
	Set up the body np inertia matrices in n-axes about J
	set up the hvf assembly inertia matrix in a-axes about O
	Set up the wing inertia matrices in a-axes about gw
	Set up the wing inertia matrices in a-axes about O
	Set up the body A inertia matrix in a-axes about O
	Set up the propeller inertia in n-axes gp
	Zeroise matrices
	Calculation of initial E parameters
END INITIAL	

Continue

DYNAMIC			
Untitled calculations			
DERIVATIVE			
Untitled calculations			
FLIGHT CONTROL SYSTEM			
Calculation of control inputs			
CALL CONTROL			
Calculation of control inputs			
Direction cosine matrix from aircraft to inertial axis			
Direction cosine matrix from inertial to aircraft axis			
Calculation of the absolute angular velocity of the body n_p			
Calculation of the absolute velocity of the joint			
PROPELLER			
Calculation of the $ALPHAm$ and $PSIm$			
Propeller model			
Propeller total force components in m-axes			
Propeller total moment components in m-axes			
Transformation to n-axes			
Calculation of the moment generated by the propeller total force about J in n-axes			
Propeller total moment about g_p in n-axes			
Calculation of the moment generated by the propeller total force about g_p in n-axes			
ENGINE			
Engine model			
Actuator model			
Transformation of the weight of the body n_p to n-axes			
Calculation of the moment generated by the weight of the body n_p about J in n-axes			
The moment of the propeller weight about g_p in n-axes			
Transformation of the weight of the body A from i-axes to a-axes			
Calculation of the moment generated by the weight of the body A about O in a-axes			
SLIPSTREAM EFFECT CHECKING			
Calculation of the slipstream velocity and THETAs			
Set up the slipstream influence codes			
CALL INFL			
Set up the slipstream influence codes for the right horizontal stabilizer			
Set up the slipstream influence codes for the left horizontal stabilizer			
Set up the slipstream influence codes for the upper vertical stabilizer			
Set up the slipstream influence codes for the lower vertical stabilizer			
Set up the slipstream influence codes for the right wing (Tilt-rotor conf.)			
Set up the slipstream influence codes for the left wing (Tilt-rotor conf.)			
Set up the slipstream influence codes for the right nacelle			
Set up the slipstream influence codes for the left nacelle			
Set up the slipstream influence code for the right wing (Tilt-wing conf.)			
Set up the slipstream influence code for the left wing (Tilt-wing conf.)			
AIRFRAME AERODYNAMICS			
Calculation of the aerodynamic forces and moments of the body A			
CALL AEROHVFVW			
Cal. of the aerod. forces and moments of the right horizontal stab.			
Cal. of the aerod. forces and moments of the left horizontal stab.			
Cal. of the aerod. forces and moments of the upper vertical stab.			
Cal. of the aerod. forces and moments of the lower vertical stab.			
Cal. of the aerod. forces and moments of the right wing (Tilt-rotor)			
Cal. of the aerod. forces and moments of the left wing (Tilt-rotor)			
Cal. of the aerod. forces and moments of the fuselage			

Continue

			Calculation of the aerodynamic forces and moments of the hvfw assembly
			Calculation of the aero. fors. and moms. of the elements of the body n at right and left
			CALL AERONW
			Calculation of the aerodynamic forces and moments of the right nacelle
			Calculation of the aerodynamic forces and moments of the left nacelle
			Cal. of the aerod. forces and moments of the right wing (Tilt-wing)
			Cal. of the aerod. forces and moments of the left wing (Tilt-wing)
			Calculation of the aerodynamic forces and moments of the right and left propellers
			Calculation of the aerodynamic forces and moments of the right and left bodies np
			Calculation of the vectors and matrices required to build up the mass matrix and total for. vec.
			Calculation of the mass matrix
			Invert mass matrix
			CALL INVERT
			Calculation of inverse mass matrix
			Dynamic vector
			Total force vector
			Acceleration vector
			Rate of change of E parameters
			Velocity vector in i-axes
			Integration
			Aircraft attitude
			END DERIVATIVE
			DISCRETE
			END DISCRETE
			Termination calculations
			END DYNAMIC
			TERMINAL
			END TERMINAL
			END PROGRAM